



Trento Institute for
Fundamental Physics
and Applications



ACTIVITY REPORT 2018



A collaborative centre for translational physics research



While the editing work for this Activity Report was near to completion, we were reached by the shocking news of the sudden death of Graziano Fortuna. Graziano, as the first TIFPA Director, gave an invaluable contribution to the development of this Centre. A rousing attitude towards new undertakings, and an exceptional talent for problem-solving, notably in difficult circumstances, were distinctive features of his unique personality. His untimely demise has left a great void in the TIFPA community, and dedicating this publication to his memory is one of our first acts to remember him.

TIFPA
Activity Report 2018



Trento Institute for Fundamental Physics and Applications

Typeset in the Bitstream Charter typeface using the $\text{\LaTeX} 2_{\epsilon}$ document formatting system and markup language

Editor: Piero Spinnato (TIFPA)

Cover and overall graphics design: Francesca Cuicchio (Ufficio Comunicazione INFN, Rome)

Cover pictures: Left, courtesy of CSES collaboration; Middle, courtesy of V. Pagliarino; Right, courtesy of Baroni and FBK

The INFN Multimedia group and Roberto Giacomelli (INFN Bologna) are warmly acknowledged for the image of G. Fortuna, taken during his presentation of TIFPA at the traditional INFN annual meeting (*Giornate di Studio sul Piano Triennale*) held in Trento in November 2014.

First print, June 2019

Printed and bound at Rotooffset Paganella, Trento

www.rotooffset.it

Contents

Foreword	1	Nuclear Physics	57
TIFPA Staff	2	AEgIS	59
Virtual Labs	3	FOOT	61
Space Research	5	Theoretical Physics	63
Medical Technologies	17	BELL	65
Sensors and Detectors	21	BIOPHYS	67
INFN Experiments	29	FBS	69
Particle Physics	31	FLAG	70
ATLAS	33	MANYBODY	72
FASE2-ATLAS	35	NEMESYS	74
Astroparticle Physics	37	NINPHA	77
AMS	39	TEONGRAV	79
DarkSide	41	Technological Research	81
FISH	43	ARDESIA	83
HUMOR	45	ASAP	85
LIMADOU	47	DEEP_3D	87
LISA Pathfinder and LISA	50	ELOFLEX	89
QUAX	52	IsolpharmAg	91
Virgo	54	KIDS_RD	92
Activities starting in 2019	56	MoVe IT	94
ADHD	56	New Reflections	96
		Redsox2	98

SEED	100	BIRD	115
SICILIA	101	LNS BPS	117
TIMESPOT	103	Microdosimetry	119
XDET	105	MoVe IT-TLD	121
Activities starting in 2019	106	pFDG	123
ARCADIA	106	Prima-RDH-IRPT	125
DRAGON	106	PROMETHEUS	127
ERFNet	107	SEE-GOLD	129
FIRE	107	SINTEF	131
GLARE-X	108	TIFPA Publications	133
NEPTUNE	109	Seminars	151
tHEEOM-RD	110		
Proton Beam-based R&D	111		
ALICE-TOF	113		



Foreword

Giuseppe Battistoni

Direttore,
TIFPA

I have the pleasure to introduce the 2018 Annual Report of the Trento Institute for Fundamental Physics and Applications (TIFPA), a National Research Center of the Italian National Institute for Nuclear Physics (INFN) in cooperation with Trento University (UniTn), Bruno Kessler Foundation (FBK) and the Health-care Agency of Trento (APSS).

I had the honor to succeed to the previous director, Prof. M. Durante, starting from September 2018, inheriting from him the responsibility of the management of a successful Research Center. Actually in 2018, not only all achievements of TIFPA in terms of infrastructures and activity were consolidated, but also the growth of ideas and experimental projects in all areas of INFN interest has steadily increased. In addition also the number of permanent INFN staff members could be enlarged. I really hope that new entries will be possible in the next future.

The relationships among the TIFPA partners, INFN, UniTn, FBK and APSS, are becoming stronger, creating the bases for new possible projects. I wish in particular to put in evidence the important cooperation with the nearby ECT* institute (European Centre of Theoretical Nuclear Physics and Related Areas), which in 2018 celebrated the 25th anniversary of its foundation.

Last, but not least, it has also to be acknowledged the fundamental support which TIFPA has received from the government of Trento Province. Once again it has to be stressed that the merit of all the scientific successes of TIFPA has to be ascribed to the generous commitment of all staff and associates. For this reason I wish to express my sincere gratitude, also on behalf of my predecessor in the direction of TIFPA, to all collaborators, reserving a special thanks to the administrative and technical services: without their precious support and efforts, nothing of what is carried on in this Research Center could be possible. I wish also to add a mention to Dr. Piero Spinnato who edited this publication.

TIFPA Staff

Administration



Marta Perucci

Head of service, Personnel affairs, budget management, purchases, payments, event organization, external funds



Isabella Martire

Business travel support, scientific secretariat, seminars, shipment service



Giuliana Pellizzari

Direction secretariat, scientific associations, Personnel selection procedures, agreements, Personnel training courses, safety matters



Irene Sartini

Assets and inventory, translations, orders. On long-term leave since February 2019

Technical Services



Piero Spinnato

Head of service, general technical management, coordination with UniTN services, IT infrastructure management and development, TIFPA website and publications editor



Christian Manea

Laboratories support, electronics development, technology transfer, Personnel delegate at TIFPA board, Personnel safety delegate



Enrico Verroi

Facility planning for Protontherapy experimental beam-lines, coordination of user support at Protontherapy experimental room

The background consists of several overlapping triangles. A large, dark red triangle occupies the left and bottom-left portions. A bright red triangle is positioned at the top right. A light blue triangle is located at the bottom right. The remaining space is white.

Virtual Labs



Space Research

William Joseph Weber^{1,2}
williamjoseph.weber@unitn.it

with contributions by
William Jerome Burger,^{3,2} Roberto Iuppa^{1,2}

Space research is an area of excellence for our institute as well as a unique point of convergence of the varied scientific expertise, facilities, and research agencies represented in TIFPA.

Space represents an increasingly productive and natural modern laboratory for the biggest questions in fundamental physics, in addition to astronomy and astrophysics. TIFPA researchers have frontline roles in building the “measurement science” bridge that connects the Earth-based techniques that have shaped our knowledge of fundamental interactions – particle accelerators, torsion pendulums, and terrestrial gravitational wave detectors – to orbiting astroparticle and gravitational wave observatories. The challenge of performing precision science from a space platform, to take full advantage of the increased precision allowed by zero-g and the absence of atmosphere but also the need for radiation hardness and miniaturization, naturally leads to new and ambitious development of hardware and techniques with applications for both science and technology. Finally, our society’s increasing dependence on space in the commercial and public sectors spawns new applications, including novel propulsion techniques; radiation safety for future interplanetary astronauts; to cleaning the band of low Earth orbits from space debris; and earth observation in the spectrum of high energy particles and in gravitation.

TIFPA researchers are active in all these as-

pects of space research, in the context of missions for ESA and ASI and in collaborations with top institutes in Europe and abroad, from the US to China. While continuing to analyze and present results from important space missions like the AMS-02 astroparticle observatory and the gravitational wave metrology demonstrator LISA Pathfinder (see dedicated reports at pp. 39 and 50) TIFPA researchers are helping prepare another generation of high impact science missions as well as developing technologies that will enable both fundamental space research and important applications. This brief report summarizes work done in 2018 and some of the next important steps.

DEVELOPMENT OF HARDWARE AND MEASUREMENT TECHNIQUES FOR THE LISA GRAVITATIONAL WAVE OBSERVATORY The LISA orbiting gravitational wave observatory (see p. 50) has formally begun the ESA “phase A” in preparation for the Cosmic vision L3 “large mission” slated for launch in the early 2030s.

The group plays a key role in LISA development with several key responsibilities:

- lead for the Italian (ASI) contribution of the gravitational reference system (GRS), that includes the test mass (TM) and surrounding hardware for electrostatic position sensing and force actuation, TM discharge, and mechanical launch lock and on-orbit release

¹University of Trento, Italy

²INFN TIFPA, Trento, Italy

³FBK, Trento, Italy

- among the coordinating institutes of the “Consortium” of ESA member states that will provide the LISA metrology instrument – the “MOSA” (moving optical sub-assembly, see Fig. 1) that includes the GRS plus an optical bench and telescope used to complete the measurement of relative motion between TM in distant – 2.5 million-km – spacecraft
- metrology experts in the ESA LISA “system engineering office” that leads the mission definition and development, including spacecraft design

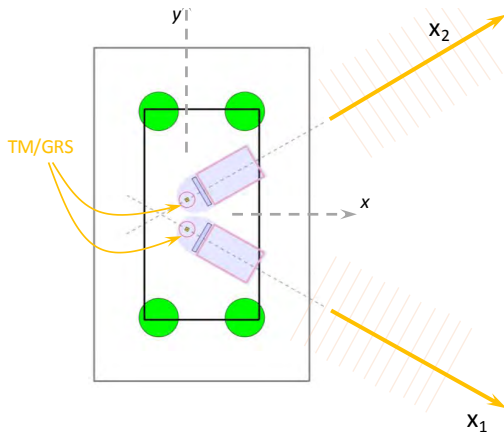


Figure 1: Notional view of one possible spacecraft configuration for LISA, with two “MOSA” instruments in blue, each with a TM and surrounding GRS coupled to a telescope and optical bench. Also visible are cold gas fuel tanks (green), which, along with articulation of the inter-MOSA angle, represent time-varying sources of gravity on the two TM.

The LISA “antenna” is a constellation of orbiting test masses, with a gravitational tidal acceleration resolved against a background noise of accelerations from stray forces. Achieving this constellation of geodesic reference test masses is the unifying theme of the Trento group’s activity for LISA, with a background of experimentation on ground and in space with LISA Pathfinder.¹ This has led to our definition of a comprehensive noise budget for test mass acceleration noise (see Fig. 2) that is guid-

¹Armano, M. et al. (2018), Phys. Rev. Lett. 120, p. 061101.

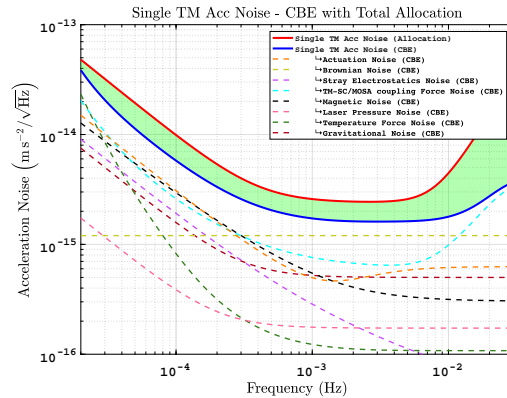


Figure 2: Single test mass acceleration noise budget for the LISA, based largely on the experimental results of LISA Pathfinder.

ing the mission requirements for achieving the observatory low-frequency sensitivity. This brief report describes our specific development activities for LISA around this theme.

Gravitational reference sensor development

The Trento group is leading “ δ -development” of the GRS. Though this has flown on LPF Armano et al. 2018h, several key elements are undergoing redevelopment for LISA. These include:

- **TM charge management**, where a new illumination scheme is being developed for delivering UV light to the TM and surrounding electrode housing surfaces for photoelectric discharge of the TM. A UV LED light source will be used, allowing pulsed modulation at 100 kHz in order to synchronize the illumination with applied electrostatic fields used for capacitive position sensing. Charge transfer between surfaces can be tuned with the phasing of the light relative to the field, resulting in a more efficient, tunable, and reliable discharge. The Trento group is modelling and testing the system, with LPF GRS hardware and the torsion pendulum laboratory, and leading definition of the lightsource requirements.
- **Sensing and actuation performance**, are under review to guarantee the TM and spacecraft control required in the LISA configuration

- **Vacuum**, where improved vacuum and outgassing protocols are being evaluated, along with different possible “vent to space” options to guarantee the μPa pressure environment needed to limit the TM brownian motion and other molecular impact force noise sources
- **Mechanical - thermal interface**, of the GRS to the rest of the MOSA instrument, to guarantee high dimensional stability to the optical metrology system as well as limit temperature fluctuations that couple directly into forces on the TM

Definition of the LISA instrument and spacecraft The LISA spacecraft are an integral part of an apparatus allowing pm-level tracking between distant TM that are in free-fall to within residual accelerations below femto-g. The measurement requires “common mode rejection” of nm-level spacecraft motion, and the angular control of the orbiting spacecraft is part of the overall optical metrology alignment. Relative TM-spacecraft motion also contributes couples into TM acceleration via force gradients. The dynamic control of the TM - spacecraft system is thus a critical part of the LISA measurement, and the group is supporting the system-level development of the control strategies, regarding the use of the GRS as a sensor and actuator but also for requirements to limit coupling to the TM acceleration.

Gravitational balancing represents an additional critical aspect of the LISA spacecraft and instrument design. Any differential DC force on the two TM needs to be balanced with electrostatic forces, which add noise, and any common mode force on the TM will ultimately affect the orbital stability and couples noise spacecraft rotation into acceleration noise. Gravitational balancing, to the level of hundreds of pm/s^2 , is thus a performance-critical technology for LISA. Though this has been tested successfully in LPE, the LISA configuration presents new challenges, with a larger and more complicated spacecraft and important time-varying self-gravity sources, including roughly 200 kg of cold gas fuel that is depleted over the 10 year mission and an annual articulation of up to ± 1 degree between the two MOSA to track the

distant spacecraft in a flexing-triangle orbital configuration. The Trento group is working with ESA and the relevant industrial partners to insure an effective gravitational design as well as gravitational balancing with trim masses inside our GRS.

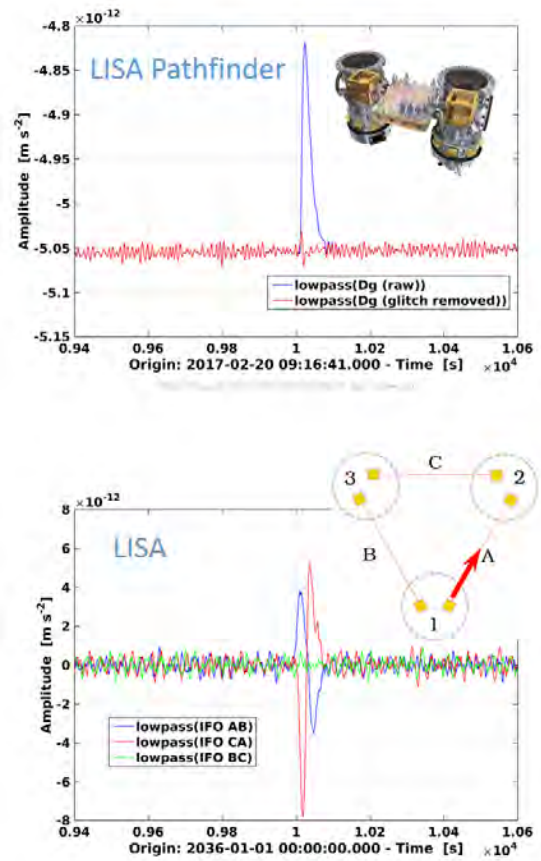


Figure 3: Illustration (top) of a transient glitch in the LISA Pathfinder differential acceleration time series. At bottom is a similar (albeit 10 times larger impulse) glitch force on a single LISA TM reflected in three simplified (first generation) TDI combinations of the measured tidal acceleration on the LISA constellation.

Operations and analysis for LISA The LISA in-flight instrument monitoring and calibrations, plus subsequent data analysis, represent a unique measurement science challenge. The gravitational wave strain data will be dominated by gravitational signals, not instrument noise; the observatory instrument performance can only be understood after removal of thousands of astrophysical signals. Achieving the intrinsic observatory performance will require a series of data corrections, likely including some

subtraction of known forces including coupling to spacecraft motion. We have extensive experience measuring such effects in the two TM LPF system.² However, the “inertial reference” for measuring a force on a specific LISA TM is a TM in another spacecraft 2.5 million km away. Force calibration, and in general mitigation of any force effect, will require the full constellation, including the “time-delay interferometry” (TDI) post-processing techniques needed to synthesize an effectively equal arm interferometer to suppress orders of magnitude of laser frequency noise.

The Trento group is thus working to apply our LPF operations and analysis experience into LISA, to provide analysis and possible experiments to mitigate low frequency force noise and possible transient force effects (see Fig. 3). We are also studying novel combinations of the inter-TM interferometric signals with null or limited sensitivity to gravitational waves, which can help distinguish instrument noise from possible stochastic gravitational wave backgrounds from the early or recent Universe.

DEVELOPMENT OF PARTICLE DETECTORS

In 2018 TIFPA hosted an intense activity of research and development of particle detectors for space applications driven by the project CSES-02, the second satellite of the CSES constellation planned for launch in late 2021. As was the case for the first satellite, launched in 2018, ASI and INFN collaborate with the Chinese National Space Agency (CNSA) and the Chinese Earthquake Agency (CEA) by constructing the High Energy Particle Detector (HEPD), sensitive to electrons and protons from a few MeV to about 200 MeV. The general layout and dimensions of the HEPD-02 will remain unchanged, featuring a tracker to measure the arrival direction of particles, a low-energy detector made of plastic scintillators and a high-energy detector made of LYSO scintillating crystals. All scintillators are readout by photo-multiplier tubes.

The TIFPA team has proposed two important upgrades for the detector:

- (i) the replacement of the two-plane HEPD-01 tracker composed of 300 μm thick Si microstrip sensors, with three layers of 50 μm thick Monolithic Active Pixel Sensors (MAPSs);
- (ii) the addition of redundant scintillator readout by means of Silicon photo-multipliers (SiPMs).

Neither technology has ever been used in space and the success of the TIFPA proposal would mark a milestone in the development of space-grade scientific instrumentation.

Monolithic Active Pixel Sensors The double-sided silicon sensors of the HEPD-01 tracker provide a two-dimensional position measurement; the readout strips on the two-sides of the sensors are oriented in orthogonal directions. An ambiguity is introduced in the y-position measurement, obtained on the n-side of the sensor, since the signals of three strips are daisy-chained to the same readout channel. The ambiguity is resolved by the segmented trigger scintillator plane located behind the tracker.

Pixel sensors have replaced micro-strip sensors for tracking due to their fine segmentation and superior resolution, which are required to cope with the high beam luminosities of the latest generation particle accelerators. In the present context, the considerably thinner silicon pixel tracker has two important advantages: a lower energy detection threshold and the ability to resolve multiple tracks.

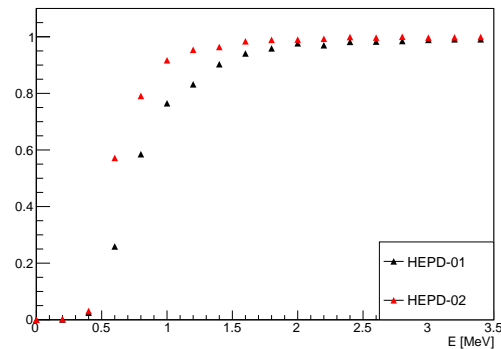


Figure 4: Fraction of electrons traversing the tracker for the HEPD-01 microstrip tracker and the HEPD-02 pixel tracker. Incidence angle 0°.

²Armano, M. et al. (2018), "Phys. Rev. D" 97, p. 122002.

In recent years, CMOS active pixel sensors have been developed for ionising radiation, revolutionising imaging in science as much, if not more, than it has in the consumer arena. Advantages of MAPSs over traditional pixelated detectors are numerous: very high resolution, extremely low noise due to integrated front-end electronics, low cost, ready-to-use digital output. It is not surprising that a number of state-of-the-art experiments both in High Energy Physics and Nuclear Physics based their trackers on MAPSs. The most notable case is probably ALPIDE, developed for the upgrade of the inner tracker of the ALICE experiment at the LHC, to be used in run 3.³

ALPIDE sensors used for ALICE's inner barrel are just 50 μm thick, i.e. 1/6 of a standard double-sided microstrip sensor. For the HEPD this feature is particularly important: the energy threshold can be lowered or the tracker made redundant (three points instead of two) keeping the threshold unchanged. Fig. 4 compares the case of HEPD-01 and that of three planes of ALPIDE sensors à la ALICE inner barrel, HEPD-02 hereafter. The energy thresholds before trigger are 3.0 MeV and 1.7 MeV respectively (99% working point), in spite of HEPD-02 measuring 3 points per track instead of 2.

For low energy electrons like the ones targeted by Limadou, the material budget affects also the angular resolution. Fig. 5 shows the multiple scattering of electrons after the first

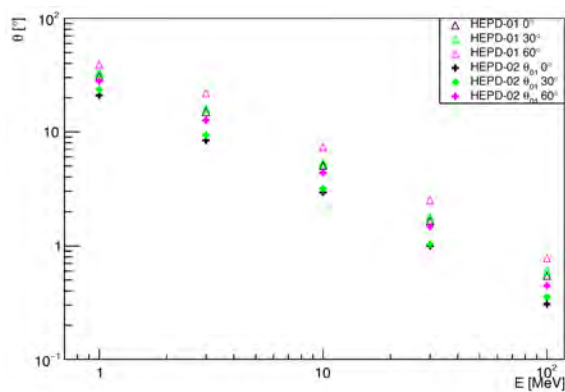


Figure 5: Multiple scattering of 1 – 100 MeV electrons at various incidence angles, for the HEPD-01 microstrip tracker and the HEPD-02 pixel tracker.

³Aglieri Rinella, G. (2017), Nucl. Instrum. Meth. A845, pp. 583–587.

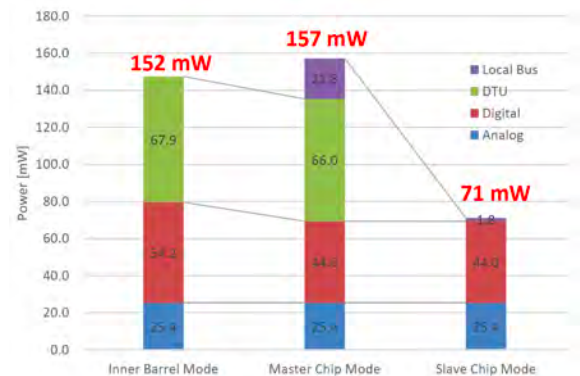


Figure 6: Power consumption of ALPIDE (from Aglieri Rinella 2017).

tracker plane, both for the HEPD-01 and the HEPD-02: from 3 MeV on, the HEPD-02 multiple scattering is half the one of the HEPD-01, independent of the incidence angle. Both the HEPD-01 and HEPD-02 trackers have 0.6° accuracy, a performance that is excessive for HEPD-01, but which turns out to be exploitable for HEPD-02 from energies of 50 MeV and higher.

These improvements motivated the choice of ALPIDE as base sensor for the HEPD-02 tracker, which is a serious technological challenge for a number of reasons.

- (i) ALPIDE was developed for high-speed ground based applications. Its power consumption, yet less than prior MAPSs, is still 20 times larger than microstrip detectors.
- (ii) ALPIDE's output is digital, meaning that no amplitude is available and no particle discrimination on the basis of this observable can be performed.
- (iii) more generally, pixels have been never used in space, and still less MAPSs.

A breakdown of power consumptions of ALPIDE as measured by the ALICE collaboration is reported in Fig. 6. To minimise the load on HEPD-02 power suppliers:

- the “slow” 40 Mbps control line will be used for readout;
- sensors will be operated in outer barrel mode, with a 1 master - 4 slaves scheme;

- clock and digital power will be distributed only to the portion of tracker traversed by the particle.

These solutions were devised at TIFPA in 2018, reducing the expected power consumption from 34 to 13 mW/cm².

The absence of information from signal amplitude can be partially recovered exploiting the size of the cluster of hit pixels. ALPIDE is designed to work with little bias tension (0 - 6 V) and for HEPD-02, the sensor will be operated with 0 bias, leaving charges to diffuse towards collection wells around the electrodes. It is worth stressing that the possibility of applying non-zero bias was foreseen just to reduce the cluster size and diminish the occupancy of the sensor when used at the ALICE experiment at LHC. The Limadou team at TIFPA is pursuing the opposite strategy: using cluster size as an observable to help the HEPD-02 to identify particles. To implement this solution, new to the community of users of ALPIDE, tests and simulation have been done for all 2018. Fig. 7(a) reports the average cluster size for 62 MeV/a.m.u. nuclei versus the incidence angle: the detector response is flat up to 60° and nuclei up to $Z = 6$ can be identified. Fig. 7(b) shows the cluster size versus proton kinetic energy. The trend is so clear to be exploitable in event reconstruction. The simulation chain pro-

vides "generated clusters" really similar to the measured ones, remarkable when considering that the prediction is only based on TCAD calculations and Geant4 simulations.

If the TIFPA effort for the HEPD-02 pixel tracker succeeds, the outcome will pave the way for a new generation of trackers for space. It must be recalled that from 2019 TIFPA will also coordinate the "Space application" work package of ARCADIA, the INFN program aimed at fabricating fully-depleted CMOS MAPSs with reduced power consumption and finer resolution. In two years, TIFPA has become one of the most active centers of development of trackers for future experiments of astro-particle Physics. This includes cosmic-ray observatories, but also gamma-ray telescopes, where major technological breakthroughs are needed for any credible successor for NASA's Fermi.

Silicon Photo-Multipliers HEPD-01 scintillators are all readout with 8 mm diameter Photo-Multiplier Tubes (PMTs) from HAMAMATSU. Because of limitations on the available power budget, no probe system was placed on board, making it impossible to flash scintillators and to scan PMT thresholds. The HEPD-01 is then prone to in-flight common systematic effects on the PMT readout system, impossible to correct for because no independent information is available.

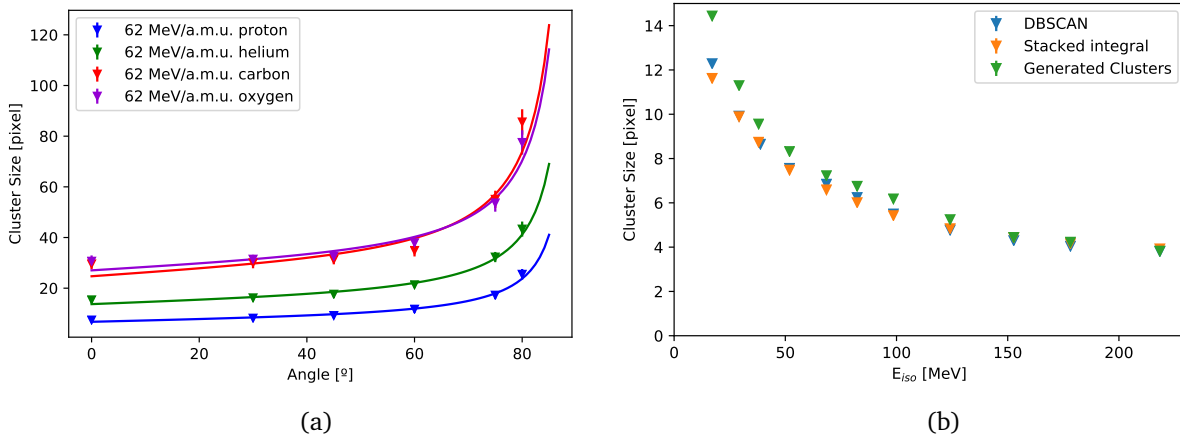


Figure 7: (a) Cluster size measured at INFN LNS (Catania) for nuclei of energy of 62 MeV/a.m.u. and for different incidence angles. (b) Cluster size for protons delivered by the APSS proton cyclotron at INFN TIFPA (Trento). Data are reconstructed with two different algorithms (DBSCAN and stacked integral, blue and orange respectively). "Generated cluster" (green) refers to TCAD calculation of the field in the pixel matrix and Geant4 simulation of the detector response.



Figure 8: FBK-AVANSID SiPMs before irradiation. All samples are $I - V$ characterised after irradiation. Several samples are mounted on PCB for studies of radiation damage at pixel level (blue box on the left).

For HEPD-02, TIFPA team proposed to superabound the readout of one or more plastic scintillators with Silicon Photo-Multipliers (SiPMs). SiPMs are matrices of avalanche photo diodes with a common cathode that are operated in Geiger mode. The main advantages of SiPMs over PMTs are:

- (i) substantially reduced operating voltage;
- (ii) low power consumption;
- (iii) unaffected by magnetic fields;
- (iv) mass producible with price fastly decreasing.

In recent years almost all companies producing low light-level sensors have launched SiPM devices for various applications. *So far, no successful application in space is reported.* For space usage, the major concern is their radiation hardness, a requirement not always met by products developed e.g. for gamma-ray cameras, PET scanners, X-Ray detection, calorimetry, neutrino detection, radiation monitoring.

TIFPA team started an intense activity of irradiation of SiPMs available on the market, produced by SENSL, HAMAMATSU, FBK-AVANSID and BROADCOMM. For each producer, SiPMs of different size and characteristics (pixel size/fill factor, spectral response, overall efficiency etc...) are under test. Fig. 8 shows as example SiPMs from FBK-AVANSID before the irra-

diation at the APSS proton line in Trento. Doses as high as 10^{10} , 10^{11} and 10^{12} n_{eq} were delivered on sensors, using 100 MeV protons, equivalent to expected doses for up to 10 years of mission lifetime.

While measuring standalone SiPM radiation hardness, a campaign of tests of irradiation of SiPMs optically coupled with HEPD-02 plastic scintillators was launched. This line of research and development aims at characterising the response of the scintillator-SiPM system as a whole, verifying whether the optical coupling may be damaged by radiation. Fig. 9 shows

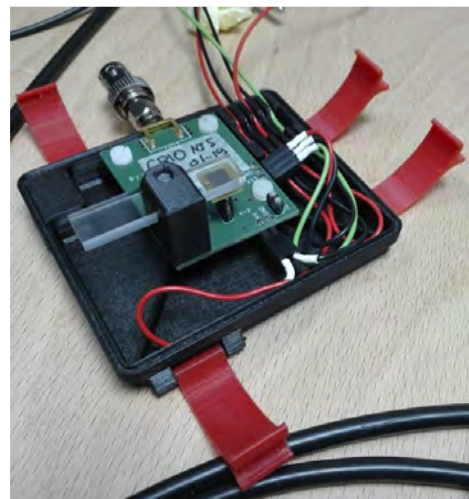


Figure 9: Test box for irradiation tests on SiPMs coupled with HEPD-02 plastic scintillators.

the test box designed to this purpose: a thin bar of plastic scintillator is clumped on a 3d-printed support and coupled with a SiPM, readout by the underlying PCB. The irradiation beam can be directed on the extreme of the scintillator readout by the SiPM or on the other, allowing to separate effects due to optical pads ageing from radiation damages of the SiPM itself.

The importance of making the SiPM technology ready for space cannot be sufficiently stressed. Independently of the science case, future experiments will be $\mathcal{O}(10)$ times bigger than current ones, making it too expensive to instrument large areas of fast trigger scintillators readout with PMTs. As for MAPSs, if HEPD-02 will successfully make use of SiPMs, it will greatly contribute to the advance of astroparticle Physics and high-energy astrophysics.

DEVELOPMENT OF HIGH TEMPERATURE SUPERCONDUCTING MAGNETS Since 2017, in the framework of a collaboration agreement between CERN and the Italian Space Agency (ASI), University of Trento and TIFPA contribute to develop a conceptual design of the superconducting magnet of a magnetic spectrometer for an astro-particle physics experiment in space. The High-temperature Demonstrator Magnet for Space (HDMS) project goes through three steps:

- preliminary design of a future antimatter experiment in space. The design of this “virtual” system is not optimised, but it serves as reference to scale up the technology developed in the project;
- design and fabrication of the demonstrator coil, such to guarantee the scalability of solutions and devices to the virtual system;
- test of the demonstrator in the temperature range 4–80 K in environment fields as high as up to 10 tesla.

If funds for a second coil will be available, tests at beam of new-generation particle trackers in high field will be performed (see page 8).

The selected magnetic configuration is a toroid with 8 superconducting coils wound with

High Temperature Superconducting (HTS) REBCO tape (about 50 km of 12 mm tape in total). The coil peak field is about 15 tesla and the operating temperature is 20 K. With the best available tape (from the H2020-ARIES program) engineering current densities as high as 1200A/mm² are attainable at 20 T, 4.2K, allowing to design a magnet providing a BL of 10 Tm, which allow to resolve the trace for proton of a rigidity up to 500 TeV/c, more than 100 times higher than the present spectrometric power of the AMS-02 space experiment.

All aspects for operating the toroid in space have been taken in consideration: power budget, mass budget, magnet protection, charge, quenching, coupling with the environment field, mechanical stability. For instance, Fig. 10 shows the deformation of the aluminum support structure after single coil failure at nominal engineering current: the color scale indicates pressure in units of MPa.

The conceptual design of the magnet for the experiment is currently used to derive a realistic, small scale (about 3:1 in size), coil to be manufactured and tested as demonstrator of the magnet technology. Fig. 11 shows the demonstrator coil under construction at CERN. With a maximum engineering current of 550 A/mm² (well below the maximum attainable on the market today), the coil features 8 tesla peak field and easily provides 5 tesla at just 50 mm off axis.

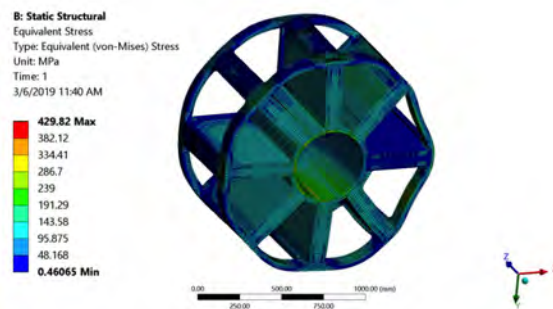


Figure 10: Aluminum support structure deformation after single coil failure for the reference experimental layout. Only the aluminum support is visible.

HDMS will be the first project validate most technical solutions recently envisaged to operate HTS magnets in space, allowing to measure working parameters that have been only com-

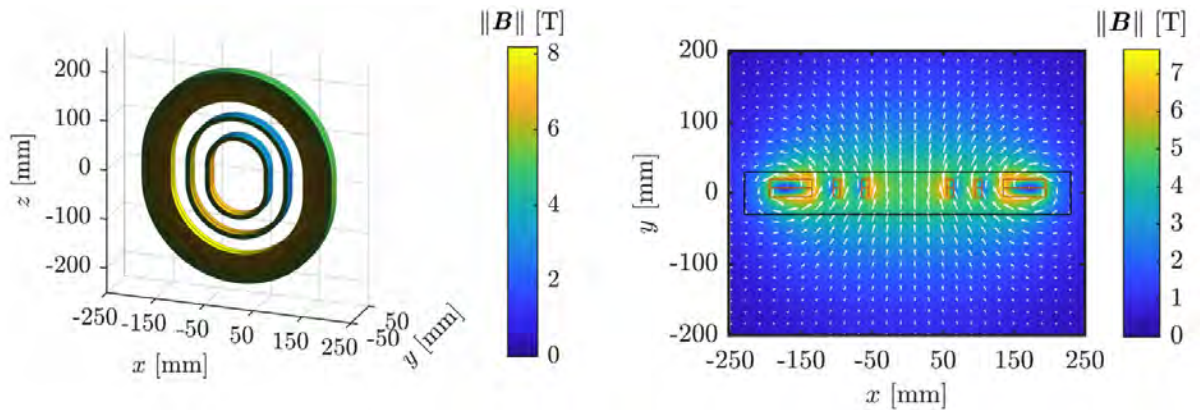


Figure 11: Design of the demonstrator coil under construction at CERN.

puted or simulated until now. The huge impact that HTS magnets would have on space activities is widely recognized. They are essential elements of plasma propulsion engines (see the VASIMR⁴ project by US Ad Astra Rocket Company)

and they have been shown to be at least as effective as passive shielding against cosmic radiation for long interplanetary manned missions (see the SR2S project, EU FP7 programme⁵).

LASER ABLATION The Pulsed Laser Deposition (PLD) facility of the Idea Laboratory is devoted to the study of laser interactions in matter. A research activity oriented toward the space applications of laser ablation began in the context of the CSN5 experiment New Reflections (2016-2018) (see p. 96), devoted to the development of laser technologies for space: geo-referencing, tracking, propulsion and debris mitigation.

Laser ablation refers to the ejection of matter from the surface of a material heated to high temperature by a laser beam. The thrust produced by the ejected mass may be used for launch, propulsion, or the deviation of the trajectory of an object in space.

Results from New Reflections The aluminium momentum-coupling coefficient C_m , which relates the impulse produced by the ablated mass to the energy density of the incident

laser beam, was measured with the 400 mJ, KrF excimer laser of the PLD. The experimental setup is shown in Fig. 12.

The target mass is mounted on a ballistic pendulum located in a vacuum chamber. The momentum coupling coefficient is obtained from the angular deflection of a second, pointing laser beam observed on a screen located 3.5 m above the chamber.

Aluminium is a common space construction material. The result was used to define the characteristics of space and ground laser systems for space debris removal. Their performance was evaluated with an orbital simulation program developed by the TIFPA group (Bazzanella et al. 2018).

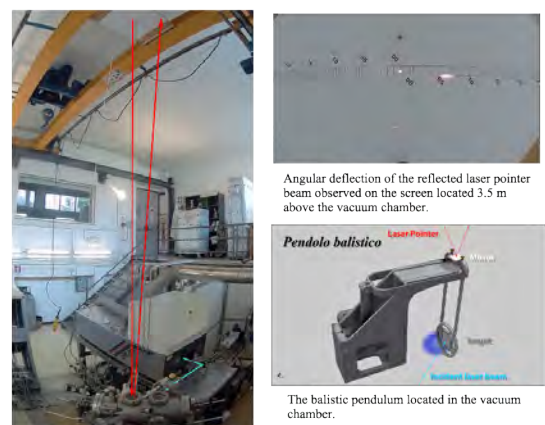


Figure 12: View of the experimental set-up in the PLD laboratory.

⁴Glover, T. W. et al. (2005), AIP Conference Proceedings **746**, pp. 976–982.

⁵Battiston, R. et al. (2013), IEEE Transactions on Applied Superconductivity **23**, p. 4101604.

Laser ablation is an attractive alternative to chemical propulsion for spacecraft propulsion. The measurements of the coupling coefficient, and corresponding mass loss, are used to define performance of the laser-propellant engine.⁶ The PLD results for aluminium, and two candidate propellant materials, Teflon (PTFE) and the graphite-enhanced polyimide Vespel sp21, are reported in Fig. 13.

The specific impulse $I_{sp} = v_E/g_o$, the thrust generated by a unit mass of propellant, indicates the efficiency of the propulsion system. The exhaust velocity v_E is related to C_m , the areal mass loss density μ , and the laser pulse energy density Φ by the expression

$$v_E = C_m \Phi / \mu. \quad (1)$$

The product $C_m I_{sp}$ is bounded by the expression

$$C_m I_{sp} = 2\eta_{ab}/(\psi g_o), \quad (2)$$

where η_{ab} is the conversion efficiency of the laser pulse energy Φ into exhaust kinetic energy,

$$\eta_{ab} = \mu \psi v_E^2 / (2\Phi), \quad (3)$$

and $\psi = \frac{\langle v_x^2 \rangle}{\langle v_x \rangle^2}$, which represents the correction required $\sim 15\%$,⁷ if a mono-energetic distribution is used instead of the real velocity distribution of the ablation plume. A mono-energetic distribution $\psi = 1$ is used to compute the ablation efficiency η_{ab} .⁷

An $I_{sp} > 600s$, with a value of $C_m \sim 400N/MW$, are optimal for a Low Earth Orbit (LEO) launch.⁸ The combustion temperatures of chemical propulsion systems limit their specific impulse to $\sim 500s$. Higher values of I_{sp} may be attained with laser propulsion as shown in Fig. 14.

⁶Phipps, C. et al. (2010), Journal of Propulsion and Power **26**, pp. 609–637.

⁷Phipps, C. et al. (2010), Journal of Propulsion and Power **26**, pp. 609–637.

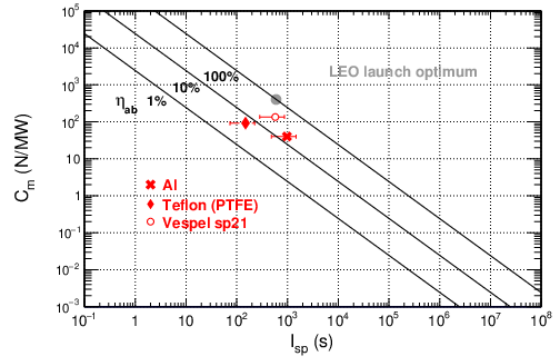


Figure 13: The peak value of the coupling coefficient and corresponding specific impulse of the PLD measurements are compared to the optimal combination for a LEO launch and the ablation efficiencies.⁸

The values of $\eta_{sp} > 1$ arise in the case the measurement is performed in air, and the air mass μ' interacting with the ablated mass μ is not taken into account. Similarly, η_{sp} may exceed unity if the material is exothermic, since the definition (Eq. 3) refers only to the optical, not the chemical energy input.

The PLD aluminium coupling coefficient (Fig. 13) is significantly higher than the result (Arad Al) reported in Fig. 14, while the inverse is observed for the specific impulse. A similar behavior is observed for the PLD Teflon (PTFE) measurements and the corresponding results (PTFE) reported in Fig. 14. However, the differences between the two measurements are smaller, in particular for the Teflon C_m .

The uncertainty of the PLD C_m values is $\sim 10\%$. The uncertainty of the mass loss measurements has not yet been evaluated. A 50% uncertainty is arbitrarily assigned to the pulse mass values used to calculate the I_{sp} presented in Fig. 13.

The value of the PLD aluminium coupling coefficient, measured with a 20 ns pulse width, is compared with values reported for smaller and higher pulse widths in Fig. 15. The PLD value is in good agreement with the previous results. The coefficient varies by a factor of ~ 4 over quoted pulse width.

⁸Phipps, C. et al. (2000), Laser and Particle Beams **18**, pp. 661–695.

The results for Vespel sp21 propellant (Fig. 13) were used for the design of a demonstrator model Laser Orbital Control System (LOCS) based on a 50 mJ, 2 kHz pulsed laser. The simulation results of the baseline design performance for a 1 km orbital altitude change of a 50 kg micro-satellite in a circular orbit at 600 km indicate a factor ~ 10 increase of C_m is required.

LASA program for 2019 The LASA activity continues in the new 3-y interdisciplinary CSN5 experiment (2019-2022) GLARE-X (Geo-referencing via LASer Ranging and LASer debris Redirection from spaceE-X), see p. . The activities programmed in 2019 include the acquisition of the LOCS laser, the installation of a second vacuum chamber dedicated to the LASA studies at the PLD, and the installation of mass flow meter for better vacuum control.

The second vacuum chamber is an essential upgrade which will allow a better exploitation of the PLD for studies specific to LASA. For example the precision of the pulse mass loss measurement, based on the average pulse mass loss obtained with N pulses, is limited by the statistics. An increase of the measurement time for the LASA activities is important to carry out the systematic studies required for the different applications, e.g. the optimization of the propellant material, and to explore new research topics.

The momentum-coupling coefficient of an asteroid simulant was measured in the context of asteroid deflection. Ablation also plays an important role in the breakup of meteorites in the atmosphere. The observation of the visible light emitted during the passage through the atmosphere is used to determine their chemical composition. Experimental simulations of the process on the ground are used to interpret the observations.⁹

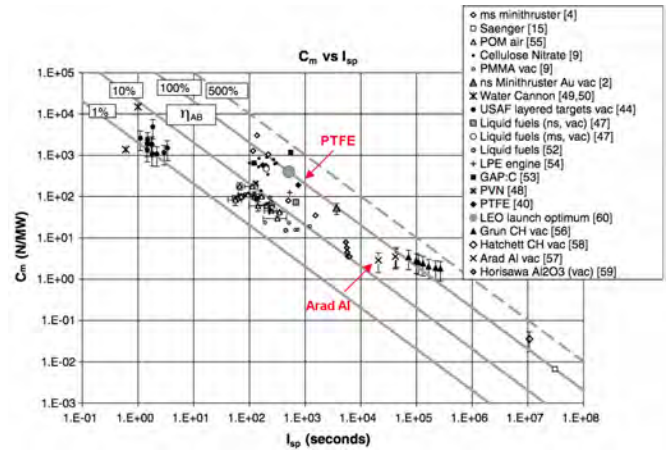


Figure 14: The original figure⁷ which shows the operating range of laser-ablation propulsion obtained with different propellant materials. The previously reported results for aluminium and PTFE (Teflon) are indicated.

An important part of the research performed at the PLD facility is based on the measurement of the composition of the ejected material. Laser ablation may provide an alternative, or complementary method for the interpretation of the meteorite observations.

The activity in the laboratory is accompanied by an important effort in the domain of computer simulation to model the fundamental physics of the laser interaction in matter, and to provide an estimate of the *in situ* performance of the laser systems.

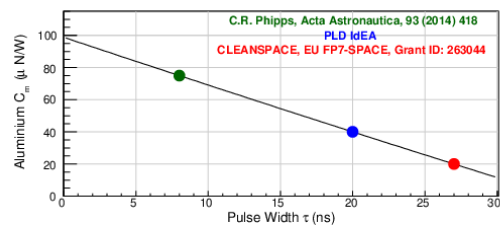


Figure 15: The values of the aluminium coupling coefficient reported with different pulse widths. The data are described by a line fit.

⁹Loehle, S. et al. (2017), The Astrophysical Journal 837, pp. 112–121.



Medical Technologies

Marco Schwarz^{1,3}

marco.schwarz@apss.tn.it

with contributions by Francesco Tommasino^{2,3}

During 2018 the medical physics activity at the proton therapy centre continued its development along similar lines as 2017, and did allow to combine an increased number of patients treated in the two gantry rooms (301 patients treated during the year 2018) with the technical design and clinical implementation of new treatment techniques and in developing new capabilities in the research area, in particular concerning the beamline devoted to radiobiological experiments.

In this report we will shortly describe a few of these developments, namely:

- Design and clinical implementation of new treatment planning approaches ("hybrid multifield optimization");
- Better managements of the preabsorber("range shifter splitting");
- Impact of dose calculation algorithm on breast proton therapy;
- Modeling the risk of toxicity in brain tumor patients treated with protons.

HYBRID MULTIFIELD OPTIMIZATION Proton therapy is getting gradually established for the treatment of specific tumour sites, as for instance brain and head and neck malignancies. Among the different beam delivery techniques, pencil beam scanning (PBS) is the most advanced. With PBS the target is covered by multiple beamlets delivered at different energies with their peak ending on spots that are located within the target or in a thin border around

it. In general, the proton fields can be optimized separately (i.e. single-field optimization, SFO), or simultaneously (i.e. multi-field optimization, MFO). MFO offers the highest modulation flexibility and thus the strongest potential of improving the plan quality both in terms of target coverage and organs at risk sparing. However, this might come at the price of high in-field dose gradients, eventually spoiling plan robustness. In radiation therapy, a treatment plan is considered robust if target prescription dose and healthy tissues tolerance limits are fulfilled even in presence of uncertainties. The current practice is to use safety margins, i.e. expanding the clinical target volume (CTV) to a planning target volume (PTV) large enough to account for treatment uncertainties. While it was found that the use of safety margins is a good way to improve SFO plans, the same does not hold for highly modulated MFO plans, for which only a marginal improvement in plan robustness could be detected through the definition of a PTV. For this reason, planning methods resulting into treatment plans that are less sensitive to such uncertainties were proposed and are commonly referred to as robust optimization techniques. Such approach implies the computation of several different scenarios during plan optimization, considering the effect of different setup and range uncertainty combinations on the final dose. An additional source of uncertainty is related to the dose calculation algorithm adopted. The application of analytical algorithms might be clinically unac-

¹Agenzia Provinciale per i Servizi Sanitari, Trento

²University of Trento, Italy

³INFN TIFPA, Trento, Italy

ceptable in PBS, while the accuracy is strongly improved when Monte Carlo (MC) algorithms are used, even though the increased computational time required by MC algorithms makes the application of MC-based robust optimization hardly practicable in clinical practice. Altogether, this scenario suggests that further investigations are necessary for a full exploitation of proton MFO. We introduced a novel hybrid methodology (hMFO) that allows combining MFO planning with a MC dose calculation algorithm in a clinical context. The proposed approach consists in planning dose coverage on an isotropic PTV accounting for setup errors, whereas range calibration uncertainties are directly incorporated in the robust optimization process. Such hybrid method drastically reduces the number of scenarios to be computed during robust optimization, making it practicable with the concurrent application of a MC algorithm. This approach has been implemented in clinical practice and it is now the norm whenever a patient's needs to be treated with MFO.

RANGE SHIFTER SPLITTING In pencil beam scanning proton therapy treatments it is possible to treat almost all tumors without using any passive object on the beamline. The only parameter that forces to use a passive beam modifier is the minimum energy. At our centre the minimum energy is 70 MeV, corresponding to 4.1 cm water equivalent thickness. This means that, tumors located at a water equivalent depth shallower than 4 cm cannot be treated if a pre-absorber is not used. This pre-absorber (also known as range shifter (RS)), is made of plastic material (e.g. acrylonitrile butadiene styrene, Lexan, Lucite, polyethylene, polystyrene, wax etc.) and placed between the end of the beamline and the patient. The range shifter behaves as a proton scatter source downstream of the latest beam collimating elements and far away from the patient. The increase in beam size translates into a shallower lateral penumbra and a more difficult beam tracing in the patient anatomy, i.e. worsened dose shaping capabilities and accuracy in dose calculation. There is

therefore an incentive in minimizing the use of the range shifter. We introduce a technique to use the RS only when strictly needed (i.e. only for the shallower part of the tumor) in contrast with the standard technique, which makes use of the RS to irradiate the entire volume. We demonstrated, via calculation and measurements, that such an approach brings dosimetric advantages that can be clinically relevant in specific treatment scenarios¹ (see e.g. Fig. 1.)

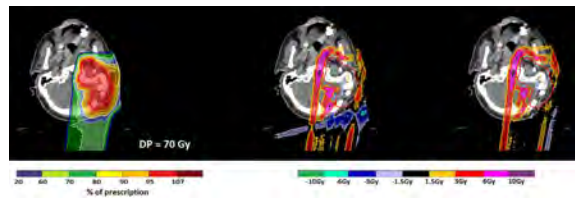


Figure 1: Improvements in dose distributions from the standard plan (left) associated with RS splitting (center) and RS splitting combined with a minimized air-gap. DP = prescribed dose.¹

IMPACT OF DOSE CALCULATION ALGORITHM ON BREAST PROTON THERAPY Proton therapy (PT) is an increasingly utilized radiation treatment in alternative to photon therapy for malignancies of the breast. The main motivation for the use of protons lies in the potential reduction of radiation-induced side effects such as cardiac toxicity (especially for left-side breast patients), pulmonary toxicity and induction of secondary cancers. PT could also be advantageous in the irradiation of breast gland plus internal mammary lymph nodes, due to the complex irradiation geometry. The standard method to calculate dose distributions in proton treatment planning is based on analytical pencil beam dose calculation algorithms, but the Monte Carlo (MC) simulation method is the gold standard to describe particle interactions and to calculate the resulting dose distribution. Improved pencil beam algorithms have been also proposed, which are mainly based on the improved description of proton nuclear interactions, but they have not yet found clinical application. Despite the recognised improved accuracy compared to pencil beam algorithms,

¹Fracchiolla, F. et al. (2019), *Physica Medica* 57, pp. 145–152.

the routine use of Monte Carlo in proton therapy has been hindered so far by the prohibitive computational times. The developments over the past few years made Monte Carlo algorithms a time consuming but realistic option for clinical practice, thus the interest of evaluating the improved accuracy of such an approach in proton therapy for breast. We therefore evaluated different treatment configuration for breast treatments, and compared both calculation with pencil beam vs Monte Carlo and calculations against measurements. The results unequivocally demonstrate that, when using proton pencil beam scanning for breast cancer treatment, Monte Carlo algorithms show (much) higher accuracy in all beam configurations tested and are therefore recommended.²

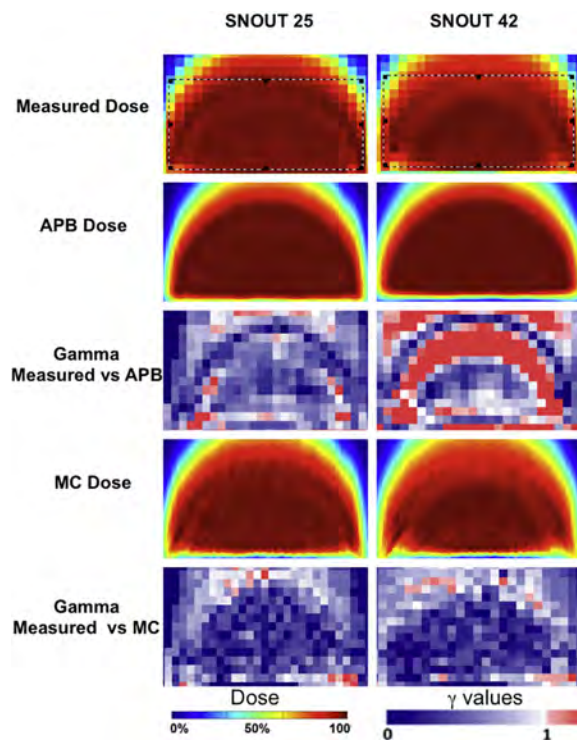


Figure 2: Comparison of Analytical Pencil Beam (APB) and Monte Carlo (MC) calculation vs measurements for two beam configurations (SN42 and SN25) used in breast cancer treatment with protons. The Gamma maps (3rd and 5th line from the top) quantify agreement between measurements of calculation with a metric combining dose difference and spatial difference.²

MODELING THE RISK OF TOXICITY IN BRAIN CANCER PATIENTS TREATED WITH PROTON THERAPY

Radiation induced toxicity on patients after radiotherapy treatment may be analyzed with a normal tissue complication probability model (NTCP). We developed such models for two exemplary toxicities as radiation-induced fatigue and alopecia, in patients treated with scanning beam proton therapy for brain tumors in Trento. Furthermore, we assessed the effect on these models when a model of variable relative biological effectiveness (RBE) is applied. We evaluated 85 patients undergoing proton therapy in a retrospective analysis assessing acute (< 90 days) and late (> 90 days) radiation-induced fatigue and radiation-induced alopecia. Brainstem and scalp were considered the most important organs impacting on fatigue and alopecia, respectively. Dose volume histograms of the brainstem and dose surface histograms of the scalp were extracted together with maximum(Dmaz) and average(Dmean) doses. Patient and treatment-related characteristics were analyzed with dose metrics extracted. Chi-square/Mann-Whitney tests were employed for univariate statistical analysis. NTCP models by multivariate logistic regression were developed and model performance was measured by AUC-ROC. A method for calculation the RBE based on the treatment planning system available in Trento was developed and validated with an independent Monte Carlo simulation code (Geant4), prior to apply it to a subset of the initial patient database. While fatigue analysis does not show a statistically significant association between the variables considered (either clinical or dosimetric) and the outcome, the analysis of radiation induced alopecia reveals strong statistical significance. Acute Grade 2 alopecia was found in 34 of 69 (49%) of the patients at a median time of 1.2 months from the end of proton therapy; late Grade 2 alopecia was found in 18 of 59 patients (31%) at a median time of 4.1 months. No patient was diagnosed with alopecia greater than Grade 2. Acute G2 events were significantly correlated

²Tommasino, F. et al. (2018), *Physica Medica* 50, pp. 7–12.

with late events ($p < 0.0001$). Younger age at irradiation was the only clinical risk factor for acute G2 events ($p < 0.006$). The relative scalp surface receiving at least 20 Gy (RS20) was significantly associated to late G2 RIA ($p = 0.033$). Median RS20 was 11% in patients developing G2 RIA and 2.9% in those who did not (Fig. 3). NTCP models derived for acute and late alopecia show very good prediction performances ($AUC > 0.8$) in determining the onset of toxicity. Moreover, the application of a variable RBE model on a patient subset shows statistically significant differences in the dose metrics between the original plans and the recalculated ones, and hence the need to consider this effect for more advanced NTCP models.³

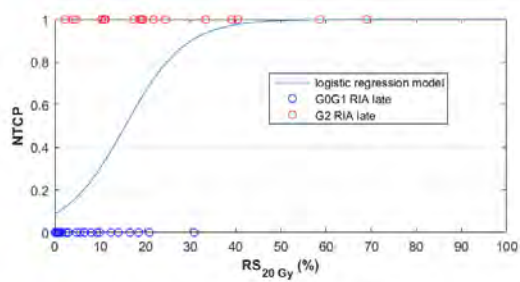


Figure 3: Representation of the NTCP model derived from multivariate logistic regression for late G2 RIA. Red points represent the portion of the skull receiving 20 Gy or more (S_{20Gy} [%]) for patients with outcome 1 (i.e. toxicity) for late G2 RIA. Blue points show S_{20Gy} [%] of patients with outcome 0 (i.e. no toxicity).

³Taffelli, A. et al. (2018), *Physica Medica: European Journal of Medical Physics* 56, pp. 92–93.



Sensors and Detectors

Maurizio Boscardin^{1,2}
boscardi@fbk.eu

The TIFPA Virtual Lab for Sensors and Detectors is a sum of skills and facilities focused on the realization of silicon radiation particles detectors that have their applications in different contexts such as high energy physics both in-ground facility and in space experiments than in biology and medicine.

In these contexts, the virtual laboratory of TIFPA aims to build a large technological platform that makes available to the Italian and international scientific community a set of skills and infrastructures that allow the development of silicon sensors. The presence in the same Institute of researchers that deal with detectors with the capability to realize silicon devices for various fields of application allows to be innovative and to be able to respond quickly to the technological challenges that the research activity requires.

The main contributions to the Virtual Lab for Sensors and Detectors are given by the Center for Materials and Microsystems (CMM) of FBK, the Department of Industrial Engineering of the University of Trento and TIFPA. These groups provide the Virtual Lab more than 20 years experience in the development of radiation sensors exploiting the microelectronics technology.

The key to the success of the laboratory is the presence inside FBK of a large technological facility that adds two main infrastructures:

- More than 500 mq of clean room fully equipped to process silicon devices
- a microanalysis capability based on the

availability of various physical/chemistry characterization technologies.

Whereby the Virtual Lab thanks to the presence of an internal silicon foundry combined with the use of external state-of-the-art CMOS foundries, has the capability to simulate, design, produce and test semiconductor sensors. The operating model, therefore, allows the access to a large number of competencies/technologies that allow both to develop new devices but also to realize a pre-production of custom devices. The technologies/skills available are described in the following sections.

Simulation and design In case of full-custom technology, we start from physics-based TCAD simulation of the device. It is possible to evaluate numerically both the electrical parameters inside the device and the measurable quantities at the electrodes. The device can also be stimulated with light or ionizing particles to model the induced electrical signal. Furthermore, to emulate as close as possible a real device, we simulate also the fabrication technology. The tools used are commercial ones (SILVACO or SENTAURUS). This software can be used both to predict the functioning of a device as well as to understand anomalous behavior or failures of existing ones. The output of the simulations is used to design the geometry of all the sensor components (layers) with the proper CAD software and to define the technology process flow. Geometry and process sequence are used

¹FBK, Trento, Italy

²INFN TIFPA, Trento, Italy

to build the device(s) on the silicon wafers in the internal foundry.

In case of the standard CMOS approach, usually, there is limited access to fabrication technology. So our competencies are mainly on circuit simulations and Integrated Circuit (IC) design. We have dedicated software tools to this purpose: CADENCE and MENTOR GRAPHICS. We design both analog and digital architectures. Quite important in this case is the capability of firmware design based on FPGA to control and read the ASIC.



Figure 1: In line inspection area.

FBK technological Facility The Microfabrication Area runs two separate cleanrooms that process 6-inch wafers: the Detector Cleanroom (500m² ISO 3-4 class) dedicated to the development of radiation sensors and the MEMS cleanroom (100m² ISO 4-5 class) where microdevices and sensors for different applications are developed. The Detectors cleanroom is a fully equipped CMOS like pilot line with lithographic capabilities down to a few hundred nanometers with a rather strict list of materials to be processed to avoid cross-contamination. The MEMS cleanroom a much more flexible laboratory devoted to the development of devices where the integration of different materials with silicon is needed. Strategic, in the sensor field, is the capability to perform low leakage and double-side processing.



Figure 2: Litho area.

Main equipment include:

- Ion implanter Varian Exitron 220, with energy range up to 200 KeV; Ions As75, B11, 49, P31, N, Ar40
- Deep reactive ion etching Alcatel AMS200 for silicon deep etching based on Bosch process
- Plasma etching of silicon oxide, silicon nitride, polysilicon dry and metal.
- Magnetron sputter (Eclipse MRC Mark II) for Al, AlSi1%, Ti/TiN deposition
- Stepper Nikon with a resolution of 350nm
- Mask aligner Karl Suess with backside alignment (2.5 μ m resolution)
- PECVD system (STS - MPS CVD) for deposition of Si Oxide, Si Nitride, SiON, Si-rich Oxide and Amorphous Si
- 5 Atmospheric Furnaces Centrotherm for dry and wet oxidation, N₂ annealing, doping from BBr₃ or POCl₃ and H₂ alloying/sintering
- 3 LPCV furnaces Centrotherm for TEOS doped and undoped, SiN standard and low stress - SiN, PolySi doped and undoped deposition.
- Isotropic silicon wet etching based on TMAH Bulk Si Wet
- Wet bench for wet etch process
- Wafer bonding AML for anodic and adhesive bonding
- Metrology in line: Interferometer, mechanical and optical profilometer, 4 point probe, Lifetime Sinton system, ellipsometer, SEM.

The packaging lab has been recently upgraded to a clean environment. It is dedicated to the development of prototype packages for mounting the silicon devices. It is equipped with ball and wedge wire bonders, die bonder, stencil screen printer, and tools necessary for encapsulation in resins and hermetic packaging.



Figure 3: Wet etching area.

Device Characterization Finally, there is a transversal know-how on device characterization. This includes competencies in parametric testing which is usually done at the wafer level contacting it with probes. It is mostly used to evaluate the functionality of the device measuring current and impedance. The testing labs are divided in wafer-level parametric testing and functional characterization. The first consists of 2 manual and 4 automatic probe-stations. The automatic ones allow a full wafer characterization to identify functional devices and to monitor the uniformity of electrical parameters. Two of that feature also a temperature-controlled chuck that allows setting the wafer temperature from -40 to 100 °C.

The functional testing laboratories are equipped with state-of-the-art instrumentation for a variety of characterizations. In particular: the electro-optical testing, that includes measurement of sensor efficiency/noise in the controlled environment and of time-of-flight with fast lasers and a test with radioactive sources. It includes coupling the photosensor with scintillators to measure energy and timing resolution in case of X-ray/Gamma radiation. Main

instruments are : multi-channel semiconductor analyzers; high-speed, four-channel digitizing oscilloscopes (600 MHz - 2.5 GHz; up to 40 GS/s); 3 PC-controlled thermostatic chambers; cooled CCD cameras for emission microscopy; fast lasers for time-of-flight measurements; integrating sphere and optical bench; pyroelectric detector; THz kit with drive synthesizer; radioactive sources of different energies; digital pattern generator; logic and network analyser and NI acquisition boards.

In addition, a range of skills and equipment are available within the FBK facility for the physical-chemical characterization of materials, techniques that allow an in-depth analysis on technological aspects of the devices created, such as the possibility of measuring doping profiles using SIMS techniques. The techniques available include Secondary Ion Mass spectrometry (SIMS), Proton Transfer Mass Spectrometry (PTRMS), X-Ray Fluorescence (XRF), X-ray Diffraction (XRD), X-Ray Photoelectron spectroscopy (XPS), Scanning Electron Microscopy (SEM) with Energy Dispersive Spectroscopy (EDS) and Electron Back Scatter Diffraction (EBSD), Scanning Probe Microscopy (SPM) with Atomic Force Microscopy (AFM), Scanning Spreading Resistance Microscopy (SSRM), Kelvin Probe Force Microscopy (KPFM), Scanning Capacitance Microscopy (SCM).



Figure 4: PE-CVD equipment.



Figure 5: Testing area

Within the virtual lab, a series of technological platforms have been developed that have allowed the realization of detectors for various applications/experiments. The main available technologies are described below.

Planar Detectors Planar devices for high-energy radiation detectors exploiting direct ionization of the particle in silicon are realized in FBK. These sensors are produced in the internal foundry on high-purity high-resistivity silicon material. According to the electrode geometry, they are classified in pixel (SPD), strip (SSD) or drift detectors (SDD).

As for pixels, p-on-n, n-su-p, and even n-on-n technologies are available; for the isolation, p-spray and/or p-stop are available. Regarding the microstrip, we have the capability to realize low leakage large area double side detector, AC or DC coupling and polarized by polysilicon resistor or punch through. These technologies are available on 6-inch substrates, such as Si-Fz, SOI and Si-Si with a wafer thickness of $275\ \mu\text{m}$

to 1 mm. FBK has also the capability to develop an optimize entrance window for the specific wavelength required by each specific application. FBK also has capabilities to realize medium quantity productions of detectors: as an example, in the past we have realized about 800 double sided microstrip detectors for AMS-O2 experiment and a similar quantity for ALICE - LHC (microstrip and pixel); more recently we have realized the microstrip double side, large area (about $7\times 10\ \text{cm}$) detectors for LIMADOU for the Chinese space agency.¹

A process module was developed on planar technologies to reduce the lateral dead area in order to obtain an "edgeless" detector. This process is based on the capability to define a deep and doped trench that surrounds the detector itself. The trenches can be both continuous and trimmed.²

Finally, it is possible to realize an "Active Edge" device based on the realization of a termination zone based on a "columns fence". This solution is based on the realization of a series of doped columns that surround the detector.

Silicon Drift Detectors The Silicon Drift Detectors (SDD)^{3,4} are currently mainly used for X-ray spectroscopy, thanks to the outstanding energy resolution that they can achieve. The most common application for SDD is in the field of analytical instrumentation, where they are employed in many different techniques such as X-ray fluorescence (XRF) analysis, energy dispersive x-ray spectroscopy (EDS) combined with electron microscopy, x-ray reflectivity (XRR), etc. Besides these applications, SDDs are also used for x-ray spectroscopy in astrophysics experiments and particle physics experiments and they are also considered as photosensors for scintillation detectors in gamma-ray spectroscopy, thanks to their high quantum efficiency for visible light. By starting this kind of detectors, FBK has developed the following internal technologies:

- realization of devices with a really low

¹Rashevskaya, I. et al. (2017), PoS proceedings *Vertex2016*, p. 064.

²Calderini, G. et al. (2016), *NIM A* **831**, pp. 133–136.

³Bellotti, G. et al. (2018), *IEEE Transactions on Nuclear Science* **65**(7), pp. 1355–1364.

⁴Bufon, J. et al. (2018), *Journal of Instrumentation* **13**(03), pp. C03032–C03032.

leakage current, in order to achieve the best energy resolutions and to reduce the requirements for the sensor cooling.

- process to obtain a thin entrance window, which makes possible to extend the SDD energy detection range to low energy x-rays (few hundreds of eV).
- adaptation of the SDD technology to many different applications, creating sensors with dedicated layouts and geometries;
- producing the largest SDD sensor ever made, with an active area of $\sim 11 \times 7 \text{ cm}^2$ for astrophysics applications;
- developing custom multi-pixel detectors, which are of the utmost importance to cover large areas in high-count-rate experiments at high luminosity facilities such as synchrotrons and x-ray free electron lasers (XFELs).⁵

The most recent developments include:

- the increase of the SDD thickness aimed at improving the detection efficiency of X-rays with energy above 15 keV;
- the realization of the low-leakage version of the large area SDD sensors.

Ultra-Fast Silicon Detectors Ultra-Fast Silicon Detector (UFSD) is an innovative silicon sensor optimized for timing measurements, based on the Low-Gain Avalanche Diode technology (LGAD). LGAD merges the best characteristics of traditional silicon sensor with the main features of Avalanche Photodiode (APD). LGAD is a silicon detector with output signal about a factor 10 larger than that of standard silicon detector and with noise comparable with that of traditional silicon sensor. UFSD recently obtained a time resolution of $\sim 30 \text{ ps}$ in beam tests and are now being considered in the upgrade of the CMS and ATLAS experiments as

⁵Evangelista, Y. et al. (2018), *Journal of Instrumentation* **13**(09), P09011–P09011.

⁶Paternoster, G. et al. (2017), *Journal of Instrumentation* **12**(02), p. C02077.

⁷Sola, V. et al. (2019), *Nuclear Instruments and Methods in Physics Research Section A: Accelerators, Spectrometers, Detectors and Associated Equipment* **924**, pp. 360–368.

timing detectors. Over the last few years, Fondazione Bruno Kessler, in collaboration with the universities of Trento and Turin, have been involved in developing of UFSD. The first production batch (completed in 2016) was fabricated on $275 \mu\text{m}$ thick Silicon substrates. It was aimed at testing both the functionality and the reliability of the new proposed fabrication technology, showing excellent results in terms of gain and timing resolution.^{6,7}

A second pilot batch (completed in late spring 2017) has been produced on Silicon-to-Silicon wafers with a thickness of $50 \mu\text{m}$, in order to improve the timing performance. In this production, we tested also new techniques to improve the radiation hardness of the devices. Two different dopant elements (Boron and Gallium) have been used to realize the multiplication junction, as well as carbon co-implant has been tested on some wafers. The first results obtained on irradiated samples show very promising results that allowing the use of such detectors for equivalent doses beyond the $10^{15} \text{ n}_{eq}/\text{cm}^2$.⁸ We plan to further investigate the property of carbonated gain layer by producing gain layers with several carbon doses, to optimize the radiation resistance of the LGAD design. We are confident that these findings, albeit obtained for LGAD sensors, can be successfully implemented in other silicon sensors with gain such as SiPM and APD.

Si-3D First introduced by Sherwood Parker in 1997, 3D silicon detectors consist of an array of columnar electrodes of both doping types, oriented perpendicularly to the wafer surface and penetrating entirely through the substrate. This unique structure enables to decouple the active sensor thickness from the electrode distance, offering important advantages in terms of low operation voltage, fast time response and high radiation tolerance. Additionally, 3D

⁸Ferrero, M. et al. (2019), *Nuclear Instruments and Methods in Physics Research Section A: Accelerators, Spectrometers, Detectors and Associated Equipment* **919**, pp. 16–26.

technology allows for “active edges”, i.e., deep trenches heavily doped to act as ohmic terminations of the sensors, able to reduce the insensitive edge region to a few micrometers. Obviously this is gained at the expense of a complex and expensive technology, due to the use of several non standard techniques, such as Wafer Bonding (WB) and Deep Reactive Ion Etching (DRIE).

The first Si-3D technology developed in FBK is a two-sided process, where the junction columns are engraved from the front side, the ohmic columns from the back side, without the presence of a wafer support. The columns are completely passing through the thickness of the wafer. We used this approach in the production of sensors for ATLAS IBL. In terms of functional characteristics, remarkable performance has been demonstrated for IBL 3D sensors: in particular, they have demonstrated a reconstruction efficiency of $>98\%$ for 15° slopes inclined to 160 V bias after $5 \times 10^{15} n_{eq}/cm^2$.⁹

As an alternative, a single-sided 3D technology with handle wafer has been proposed by FBK with modifications allowing for back-side sensor bias. The wafers is composed by two parts: a device layer of high quality and High resistivity silicon and a support wafers with low resistivity material.

The ohmic columns are etched deep enough to reach the highly doped handle wafer, so that a good ohmic contact is achieved on the sensor back-side and the junction column has a lower depth than the thickness of the device layer. FBK also demonstrated the feasibility of this technology with Silicon on Insulator (SOI) wafers: to this purpose, it was proved that the p+ columns can be etched by DRIE also through the bonding oxide, thus reaching the heavily doped handle wafer. Among the advantages offered by the single-sided solutions are the mechanical robustness provided by the thick handle wafer, which is also compatible with active edges; moreover, the active layer thickness can

be tailored to the desired value. With a thin active layer ($\sim 100 \mu m$), narrow columns can be etched even though the aspect ratio is not improved, and all the device dimensions can be more easily downscaled.^{10,11}

SPAD & SiPM SPAD and SiPMs are based on the Geiger-mode operation of photodiodes biased above the breakdown voltage. Single photo-diodes operated in this condition as photo-detectors are commonly known as SPADs (single-photon avalanche diodes). A densely packed array of SPADs is referred to as Silicon Photomultiplier (SiPM).

SiPMs are gradually replacing Photomultiplier Tubes (PMTs) in a number of applications, offering, among other features, higher sensitivity, ruggedness, lower operating voltage, lower cost and higher gain uniformity, insensitivity to magnetic fields, making them an excellent candidate for single and few-photon counting applications, with extremely good timing resolution. Typically, SiPMs are employed in the scintillation light readout in applications such as:

- (i) Medical Imaging: Time-of-Flight PET, MRI-compatible ToF-PET, Gamma Cameras, Prompt-Gamma Imaging, intra-operative probes;
- (ii) Big Physics Experiments: calorimetry and timing measurements in High-energy physics experiments, Cherenkov light detection, readout of liquid scintillators (LAr and LXe);
- (iii) Ionizing Radiation Spectroscopy: Low-energy to high-energy Gamma-ray spectroscopy and X-ray spectroscopy
- (iv) Security and Safety: homeland security, cargo inspection, radiation dosimetry and environmental monitoring.

Other applications of SiPMs include the measurement of fluorescence light intensity and lifetime and analytical instrumentation. Finally, thanks to recent extension of sensitivity

⁹Da Vià, C. et al. (2013), Nuclear Instruments and Methods in Physics Research Section A: Accelerators, Spectrometers, Detectors and Associated Equipment **699**, pp. 18–21.

¹⁰Sultan, D. et al. (2017), Journal of Instrumentation **12(01)**, p. C01022.

¹¹Oide, H. et al. (2018), Nuclear Instruments and Methods in Physics Research Section A: Accelerators, Spectrometers, Detectors and Associated Equipment.

to the NIR, SiPMs are currently one of the most promising photo-detectors for LiDAR, including automotive LiDAR.

We follow two approaches for this sensor development:

- (i) custom design and technology developed by FBK, sensors are usually fabricated in FBK;
- (ii) sensor design provided by FBK, fabrication in standard CMOS technology at an external silicon foundry.

In the first case, the detector is fully developed in house with optimized microelectronic processes, obtaining a custom SiPM technology. This allows to optimize the device performance such as efficiency and noise and to customize it to a specific application. In such solution, the technology does not allow the integration of the readout electronics on the same substrate as the SiPM and FBK fabricates what is called Analog SiPMs, which provides an analog signal that has to be processed by an external electronics. In the second case, the standard CMOS technology allows for the sensor and electronics to be integrated. This means that maximum compactness and integrated intelligence can be achieved. Clearly, the SPADs realized with this approach have sub-optimal performance since the technology is not accessible. Depending on the application, one or the other may be preferred. As an example, in the field of gamma-ray detection with scintillators (both in high-energy physics and medical equipment) the custom solution is preferred because of the better performance and the relatively relaxed requirements on the compactness.

Considering custom SiPM technologies, FBK started analog SiPM development more than one decade ago and now can offer different state-of-the-art technologies for different applications. Among them, Near Ultra Violet, High Density (NUV-HD) SiPM technology features a peak photon-detection efficiency (PDE) of 65% at 410 nm (including the fill factor), Dark Count Rate (DCR) in the order of

50 kHz/mm², correlated noise of 20% at 55% PDE, and microcell pitch ranging from 15 μ m to 40 μ m.¹² Sensitivity remains high in the near ultra violet, with a PDE of 48% at 320 nm. NUV-HD SiPMs provide state-of-the art 85 ps FWHM coincidence resolving time (CRT) in PET applications, reading out the light of a Ca co-doped LYSO crystal.¹³ Single Photon Timing Resolution (SPTR) of NUV-HD SiPMs was below 30 ps FWHM, when measured on single SPAD with covered edges, and increased to 75 and 180 ps FWHM for SiPMs with active areas of 1 \times 1 mm² and 3 \times 3 mm², respectively, because of the electronic noise.¹⁴ FBK also developed the capability of fabricating large-area NUV-HD devices, with a size up to 1 cm².

Recent interest in the SiPM readout of liquid scintillators (mainly LAr and LXe) triggered the development of a cryogenic-optimized variant of the NUV-HD technology (NUV-HD-Cryo), which is optimized for operation at cryogenic temperatures: at 77 K, it features a DCR of a few mHz/mm², low afterpulsing, below 10% and a recharge time constant of 270 ns. At this temperature, few-photon counting capability was demonstrated with very large sensitive areas, obtaining an S/N of 13.8 using a 24 cm² SiPM array coupled to a single analog readout channel (DarkSide collaboration). After this successful development, the NUV-HD-Cryo technology is being transferred to an external, CMOS foundry, for large-volume, low-cost production, to meet the needs of the science experiments.

Other ongoing optimizations of the NUV-HD technology include:

- (i) development of devices with extended deep-UV sensitivity: preliminary measurements show a PDE of approximately 20% at \sim 178 nm.
- (ii) Development of NUV-HD SiPM optimized for radiation hardness, to be used in the phase-II timing upgrade of CMS.
- (iii) Development of NUV-HD sensitive SiPMs with reduced optical crosstalk of 10% at 55% PDE, thanks to the addition of light-absorbing material between adjacent mi-

¹²Gola, A. et al. (2019), *Sensors* **19**(2).

¹³Nemallapudi, M. V. et al. (2015), *Physics in medicine and biology* **60** **12**, pp. 4635–49.

¹⁴Acerbi, F. et al. (2015), *NIM A* **787**, pp. 34–37.

crocells, for experiments such as CTA.

At FBK, we also developed the RGB-HD SiPMs with peak sensitivity of 45% at 550 nm and of $\sim 10\%$ at 900 nm. Based on the RGB-HD technology, we developed the Linearly-Graded SiPMs (LG-SiPMs), which provides XY position sensitivity over the active area down to the microcell level using only four analog read-out channels.¹⁵ Ongoing developments aim at increasing the sensitivity in the near-infrared (NIR-HD technology): preliminary results show a PDE higher than 20% at 850 nm.¹⁶

Ultra-High-Density SiPMs (RGB-UHD) are an evolution of RGB-HD SiPMs, characterized by an even smaller cell size to reduce the SiPM non-linearity. Cell pitch ranges from a $12.5 \mu\text{m}$ down to $5 \mu\text{m}$, corresponding to the remarkable cell density of 7400 and up to 46000 cells/ mm^2 . The $10 \mu\text{m}$ cell reaches a PDE of 35% at 515 nm, while the microcell recharge time constant is

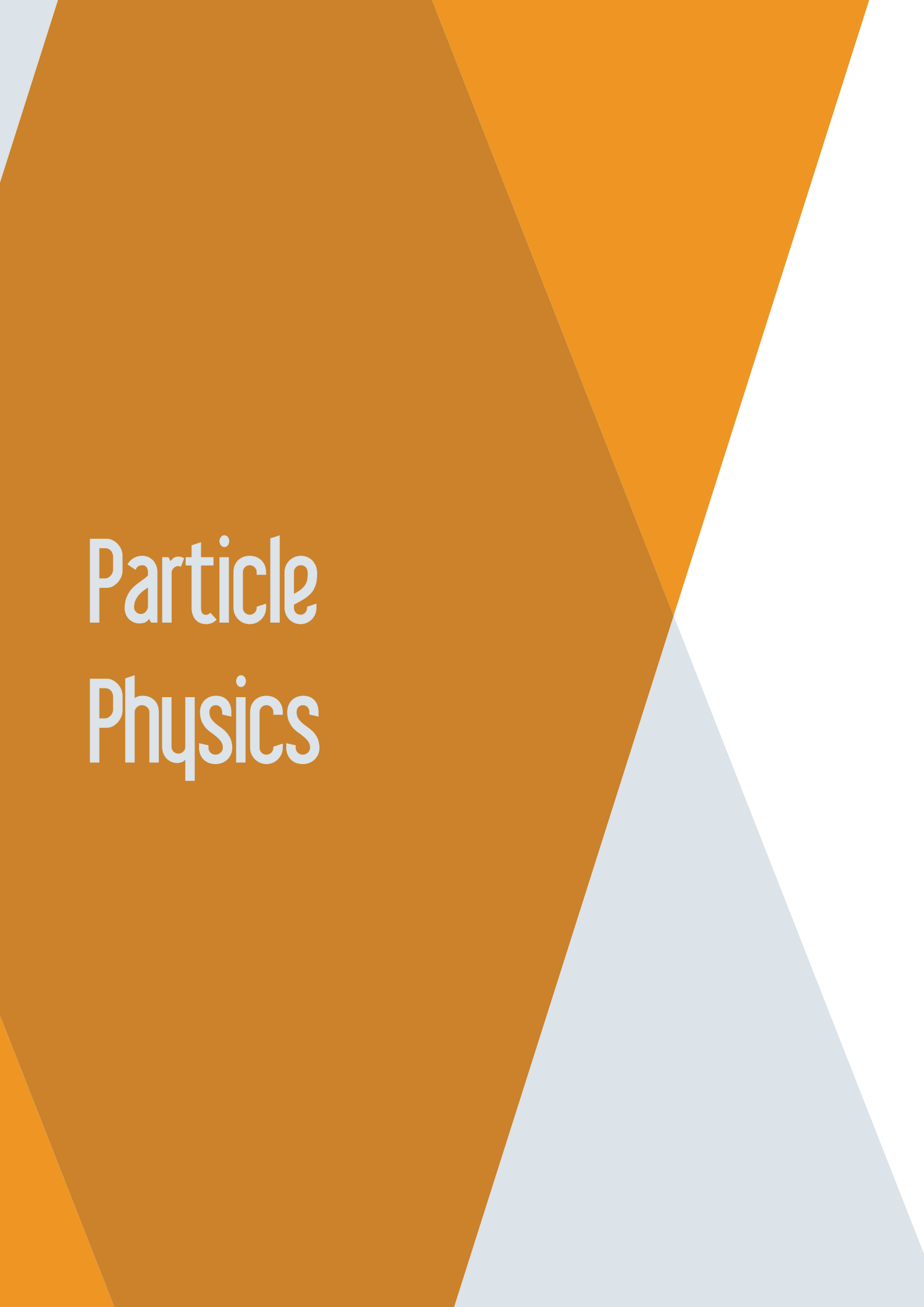
below 5 ns for the 7.5 microcells.

Considering CMOS-based SPADs and SiPMs, FBK skills are such that the entire flow can be managed, from the high-level simulation of the device into the physical system to the circuit-level design, simulation and layout, from the electrical and electro-optical characterization to the prototype implementation. On the other hand, fabrication is subcontracted to external foundries, exploiting existing cooperation and selecting the more appropriate technology for the specific task to be solved. Typical architectures of CMOS-based SPAD sensors include array arrangement with local (per-pixel) or global special processing features, such as time-stamping (time-to-digital converters, TDC, with tens of picoseconds timing resolution), energy evaluation through digital-SiPM topologies, high-speed readout and event-based operation for minimization of the data transfer load.

¹⁵Gola, A. et al. (2013), IEEE Nuclear Science Symposium Conference Record.

¹⁶Acerbi, F. et al. (2018), NIM A **912**, pp. 309–314.

INFN Experiments



Particle Physics

Gian-Franco Dalla Betta

gianfranco.dallabetta@unitn.it

Coordinator,
TIFPA Particle Physics Activities



The research activities of the INFN National Scientific Committee 1 (CSN1) deal with fundamental interactions of matter in experiments using particle accelerators, of which the Large Hadron Collider (LHC) is currently the largest and most powerful in the world. The LHC was built at CERN between 1998 and 2008 and its primary objectives are the discovery of the Higgs boson and other particles predicted by supersymmetric theories. The LHC is designed for proton-proton collisions delivering an unprecedented luminosity of $10^{34} \text{ cm}^{-2}\text{s}^{-1}$ and a maximum energy of energy 14 TeV in the center of mass. The particle beams are not continuous but in bunches with a repetition rate never shorter than 25 ns.

ATLAS (A Toroidal LHC ApparatuS) and CMS (Compact Muon Solenoid) are the two general-purpose particle detectors built at the LHC. ATLAS has many objectives, spacing between the discovery of new particles, the confirmation of current theories and the discovery of new physics models. The most famous of these objectives is, of course, the discovery of the Higgs Boson, which was announced, jointly with CMS, in July 2012. When looking for very rare events, like the Higgs boson, the luminosity must be very high in order to increase the probability of generating such events. Hence, the High Luminosity LHC (HL-LHC) is currently planned for 2022 and is referred to as Phase-2 upgrade. Many hardware upgrades will be required in order to go beyond the initially designed luminosity and reach $5 \times 10^{34} \text{ cm}^{-2}\text{s}^{-1}$ while maintaining the same energy in the center of mass. In particular, the ATLAS Inner Detector will be completely replaced with a new and more modern one.

The Trento group has collaborated with the ATLAS experiment since 2007, first within the CERN ATLAS 3D Collaboration and later, since 2011, also within INFN ATLAS Italy. The involvement with ATLAS has regarded the development of 3D pixel sensors for the Insertable B-Layer (IBL), the fourth layer of pixel sensors which was installed within the inner tracker in 2013: in particular, the group was responsible for the design of the 3D pixels fabricated at FBK. Following this successful contribution, since June 2015 the University of Trento / TIFPA Group has been officially an ATLAS institute.

The main commitment of the Trento group has been on the engineering side: in particular, within the INFN “RD-FASE2” project, TIFPA has led the Italian effort, in collaboration with FBK, towards a new generation of 3D pixel sensors for the Inner Tracker (ITk) of the ATLAS detector “Phase 2” upgrade. This activity is now continuing in the “FASE2-ATLAS” project.

More recently, since 2016, the group started to be involved also with the ATLAS physics program. In particular, in 2017 and 2018 it contributed to the analysis activities voted to searches for heavy resonances decaying to b-quark pairs, produced in association with a large p_T jet. A conference note was published, validating the strategy adopted for the analysis with 35 fb^{-1} of data. The analysis of the full dataset is ongoing, adopting very innovative machine learning-based techniques for the signal selection, developed by the Trento’s group in collaboration with FBK.

The most significant outcomes of the research activities in 2018 are summarised in the ATLAS and FASE2-ATLAS reports.

ATLAS

Marco Cristoforetti, Andrea Di Luca, Francesco Maria Follega, Gian-Franco Dalla Betta, Roberto Iuppa[†]

Boosted $H(b\bar{b}) + \text{jets}$. The largest decay mode of a 125 GeV SM Higgs boson is to b-quarks, with a branching ratio of 58%. As a consequence, studying $H \rightarrow b\bar{b}$ drives the measurement of the Higgs coupling and of the total boson decay width. The biggest experimental challenge deals with the large irreducible background that comes from QCD multi-jet production, that is about nine orders of magnitude above the cross section of the Higgs production modes. In 2017 it has been proposed to use events where the Higgs boson is produced in ATLAS recoiling against a high- p_T jet, achieving high sensitivity for highly boosted b-tagged jets from the Higgs decay. This analysis is the most sensitive channel to study $H \rightarrow b\bar{b}$ from gluon fusion and it is the most sensitive way to study the Higgs cross section at high p_T . During the last year our contribution was focused on devising a new strategy for the signal selection and modelling the uncertainty of the Z/W peaks in the large-R jets mass distribution.

Before our work, signal jet candidates were chosen to be the ones with the highest p_T in the event. This choice rejects a large fraction of background events, because QCD jets have usually low p_T , but it turned out to have efficiency as low as 60%. We introduced in the event selection a new calorimetric variable, called D_2 , defined as $D_2 = e_3 / (e_2)^3$, where the numerator and the denominator are respectively the three- and two-points correlation functions of energy depositions in calorimeters.¹ D_2 is designed to investigate the large-R jets substructure, revealing the presence of two sub-jets, as in our case $H \rightarrow b\bar{b}$. We proposed to select the signal candidate as the large-R jet with the smallest D_2 in the event. This approach improves the signal to noise ratio and increases the acceptance, so much to be the basis of the selection in the update of the analysis (ongoing).

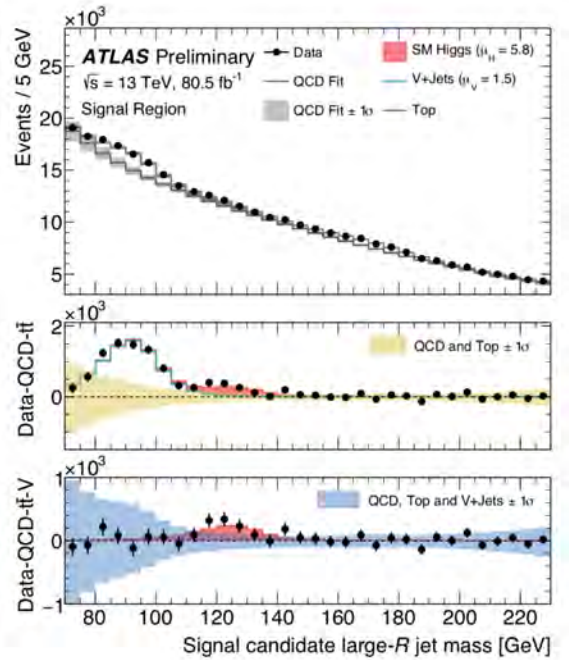


Figure 1: Postfit plot of the SM Higgs boson, V + jets, $t\bar{t}$ and QCD fit comparison to data. The middle panel shows the postfit and data distributions with the QCD and $t\bar{t}$ components subtracted. The lower panel shows the same distributions when also the V + jets component is subtracted.

We also contributed to estimate the systematic uncertainty on the Z/W modelling, both in scale and shape of the reconstructed invariant mass distribution. We did that by comparing two Monte Carlo samples generated with different generators (Sherpa and Herwig++). The results of this study gave the input for the estimation of systematic uncertainties associated to the V + jets modelisation, among the largest ones affecting the result. All these studies contributed to the result in Fig. 1 (ATLAS Collaboration 2018),² where the combined fit of Higgs + jets and V + jets signals to data is represented. The obtained signal strengths (defined as the ratio of the measured cross section to the ex-

[†]Contact Author: roberto.iuppa@unitn.it

¹Larkoski, A. J. et al. (2014), JHEP 12, p. 009.

²<https://cds.cern.ch/record/2649081>

pected Standard Model one) are:

$$\mu_V = 1.5 \pm 0.22(stat.)_{-0.25}^{+0.29}(syst.) \pm 0.18(th.)$$

$$\mu_H = 5.8 \pm 0.3(stat.) \pm 1.9(syst.) \pm 1.7(th.).$$

TrackML kaggle challenge. Our team participated in the TrackML Particle Tracking Challenge,³ focused on tracking particles in very dense environment using Deep- and Machine-Learning tools. Promoters provided participants with pseudo-data, simulated on a generic

next-generation High Energy Particle Physics experiment, to be operated at the High Luminosity LHC. Fig. 2 shows the points where tracking detectors are hit by particles generated *in a single pp collision*. Team participants were challenged to group all hits in different tracks, each one corresponding to a particle’s trajectory. The performance was evaluated in terms of efficiency and speed.

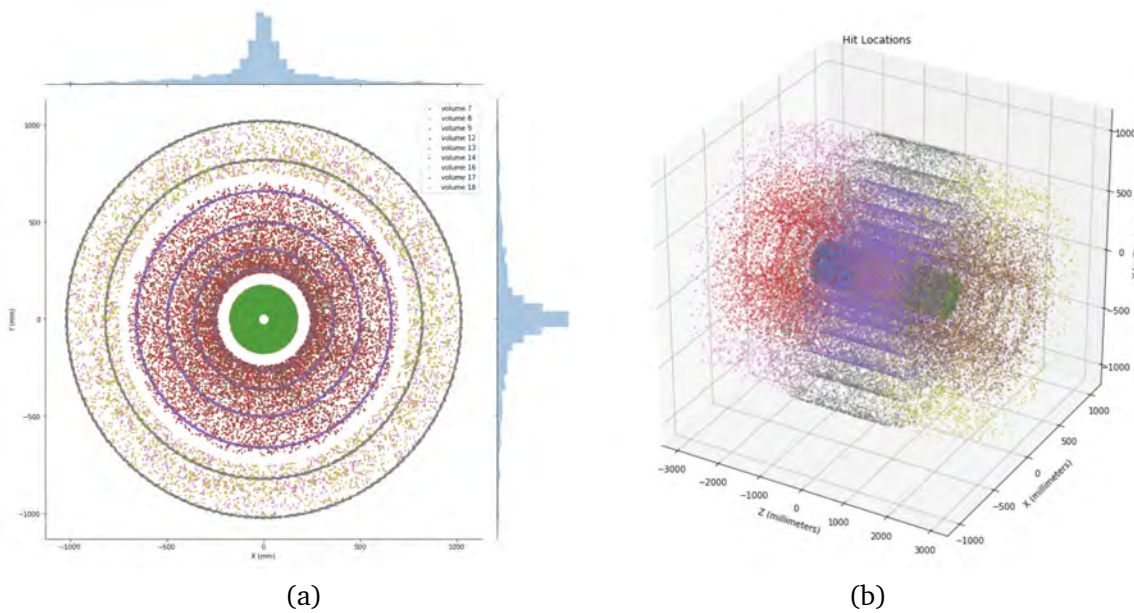


Figure 2: The hits collected by the pseudo-detector in a single event are shown in a 2D view (a) and in a 3D view (b). The color code represents the different volumes hit by the particle.

Our solution was based mostly on Machine Learning tools. We started tracking from mid detectors inwards, to profit from the low fake-hit rate of innermost detectors. The envisaged procedure was the following:

- (i) we used DBscan to find clusters of hits on each single detector layer;
- (ii) for each pair of consecutive detection layers, we trained a specific fully connected

- neural network to predict the hit position;
- (iii) we calibrated confidence interval to prepare the real hit association to the predicted position;
- (iv) we perform the real-hit/predicted-position matching if inside the calibrated interval;
- (v) each track is extended outwards using the KDTree library.

Selected Papers

ATLAS Collaboration (2018). *Search for boosted resonances decaying to two b-quarks and produced in association with a jet at $\sqrt{s} = 13$ TeV with the ATLAS detector.* (ATLAS-CONF-2018-052).

³Kaggle INC, TrackML Particle Tracking Challenge 2018. <https://www.kaggle.com/c/trackml-particle-identification>

FASE2-ATLAS

Gian-Franco Dalla Betta,[†] Giacomo Baldi, Maurizio Boscardin, Mostafa El Khatib, Roberto Iuppa, David Macii, Roberto Mendicino, Giulio Monaco, Neha Neha, Ester Ricci, Giovanni Verzellesi

The project is aimed at completing the R&D activities previously started in the “RD-FASE2” project, with a more focused approach aimed at solving some specific remaining issues in view of the construction of the new ATLAS detector for High-Luminosity LHC (Meschini et al. 2018; Dinardo et al. 2018).

Within the Inner Tracker sub-project (ITk), TIFPA is responsible for the development and optimisation of 3D pixel sensors for the innermost layer. This application requires very high hit-rate capabilities, increased pixel granularity (e.g., 50×50 or $25 \times 100 \mu\text{m}^2$ pixel size) and extreme radiation hardness (up to $2 \times 10^{16} \text{ n}_{eq} \text{ cm}^{-2}$ fluence). New 3D sensors are made at FBK with a single-sided process with thinner active regions ($\sim 100 \mu\text{m}$), narrower columnar electrodes ($\sim 5 \mu\text{m}$) with reduced inter-electrode spacing ($\sim 30 \mu\text{m}$), and very slim edges ($\sim 100 \mu\text{m}$).

In 2018, the main effort was devoted to the characterisation of samples from the second batch fabricated at FBK in 2017. Based on the electrical characterisation results, five wafers were sent for bump bonding to IZM and Leonardo. Several pixel modules were assembled with FEI4, PSI46dig, and the new RD53A read-out circuits (ROCs), and tested in laboratory and in beam tests at CERN and Fermilab. In spite of some failures with the RD53A ROCs, it was possible to demonstrate good performance with low noise figures ($\sim 100 \text{ e}^- \text{ rms}$, compatible with the pixel capacitance), and hit efficiency higher than 99% already at low voltage.

Proton irradiation of selected RD53A modules was carried out at CERN IRRAD up to a fluence of $2 \times 10^{16} \text{ n}_{eq} \text{ cm}^{-2}$, though with non uniform irradiation pattern. The data analysis is still under way. Preliminary results confirm that a hit efficiency higher than the specification value of 97% can be achieved.

[†]Contact Author: gianfranco.dallabetta@unitn.it

Very promising results were also obtained from the characterisation of 3D diodes of different geometries irradiated with neutrons up to very large fluences. To this purpose, a position resolved IR laser system was used. The signal efficiency (SE) was calculated normalising the signals acquired after irradiation to the maximum signals acquired before irradiation, taking into account the dependence of the light absorption coefficient on temperature and fluence. At the benchmark fluence of $2 \times 10^{16} \text{ n}_{eq} \text{ cm}^{-2}$, the signal efficiencies as a function of voltage for all geometries are compared in Fig. 1. Up to a voltage of 150 V, SE’s properly scale with the inter-electrode spacing: the maximum value is obtained in the $25 \times 100(2E)$ device, $\sim 85\%$ at 150 V, with a quasi-saturation trend observed already at 75 V. At 150 V, in the 50×50 device, the SE reaches a remarkable value of $\sim 67\%$, whereas it is smaller but still pretty good ($\sim 39\%$) in the $25 \times 100(1E)$ sample. In order to limit the power dissipation in the final application, operating at this voltage still seems to offer a sufficiently good trade-off with signal efficiency. At larger voltages, impact

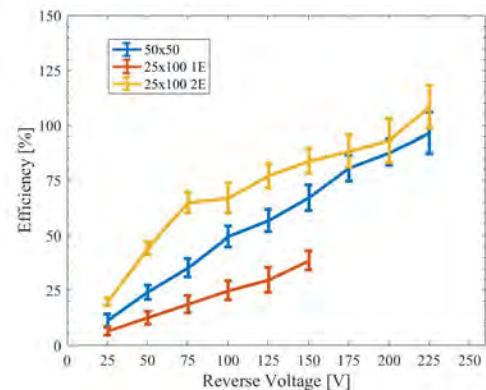


Figure 1: Signal efficiencies as a function of voltage in 3D diodes of different geometries irradiated with neutrons at $2 \times 10^{16} \text{ n}_{eq} \text{ cm}^{-2}$.

ionisation effects lead to charge multiplication, boosting the signal efficiency to 100% and beyond in both the $25 \times 100(2E)$ and 50×50 devices. This is not the case in the $25 \times 100(1E)$ sample where electrical breakdown prevents from reaching the much larger voltages that would likely be necessary for charge multiplication with its larger inter-electrode distance of $\sim 51 \mu\text{m}$.

In parallel, the fabrication process was revised and technological tests were performed at FBK in view of the fabrication of new sen-

sor batches using stepper lithography, in order to improve the process yield for future productions. Owing to the minimum feature size (350 nm) and alignment accuracy (80 nm) provided by the stepper, it was demonstrated that also the $25 \times 100(2E)$ pixel layout, that was critical with mask aligner, is feasible. A new reticle layout has been completed at UniTN, including all three pixel geometries: 50×50 (1E), 25×100 (1E), and 25×100 (2E). The fabrication of a batch on Si-Si DWB wafers with $150 \mu\text{m}$ active thickness is on going at FBK.

Selected Papers

Dinardo, M. et al. (2018). *The INFN R&D: New pixel detector for the High Luminosity upgrade of the LHC*. *Il Nuovo Cimento C* **41**, 75 pages.

Meschini, M. et al. (2018). "Pixel Detector Developments for Tracker Upgrades of the High Luminosity LHC". *Proceedings of International Conference on Technology and Instrumentation in Particle Physics (TIPP 2017)*. Springer, pp. 349–355.



Astroparticle Physics

Rita Dolesi

rita.dolesi@unitn.it

Coordinator,
TIFPA Astroparticle Physics Activities



Astroparticle physics is an interdisciplinary field at the intersection of particle physics, astrophysics, cosmology and fundamental physics. Within INFN, this field is competence of the Commissione Scientifica Nazionale II, that deals in fact with a wide spectrum of experimental investigations. They range from studies of the neutrino properties to experiments probing the dark Universe, from studies of radiation and gravitational waves from the Universe to experiments addressing the foundation of general and quantum physics. These activities differ for the topics, for the employed technologies and involve researchers working in various fields. Therefore they greatly benefit from the synergy between INFN and other research institutes, as happens at the TIFPA where INFN, Università di Trento, CNR, FBK and Trento Proton Therapy Center can work efficiently in joint projects. Lively and productive is obviously also the collaboration with ASI for the space based experiments. At TIFPA, the activities related to astroparticle physics currently involve about 40 researchers in 8 experiments briefly presented in this section, together with their recent highlights. It is noteworthy the high quality of the contribution of the TIFPA members in these projects: their remarkable ability to simulate, to design and then to fabricate cutting-edge devices and to realize challenging novel experimental apparatus allow for pushing the experimental performance to their limits and therefore to enhance the overall scientific return.

The astroparticle group celebrates the launch and the beginning of the measurement campaign of LIMADOU, an instrument with a TIFPA contribution on board the Italian-Chinese CSES mission, and aimed at studying temporal variations in energetic particle flows in correlation with variations in the Van Allen bands. TIFPA has a leading role in the LIMADOU data analysis activities, while on ground it will develop metrology for the study of astroparticles in future space missions. The participation to the investigation of the Universe and its origin by searching for antimatter and dark matter with AMS-02 is prosecuting, in particular with the analysis of electron and positron flows, and with the leadership position of the TIFPA group as regards the measurement of the isotopic components of light nuclei. A substantial contribution to the shifts at the AMS Control Center at CERN (POCC) which guarantees the operation of the experiment is also confirmed. VIRGO and LISA are the leading INFN experiments in the detection of gravitational waves field which is opening a new window for the exploration of the Universe. After the success of the LISA Pathfinder mission, ESA selected the LISA mission to realize the first gravitational wave space observatory in the sub-mHz band, and started Phase A of its development in spring 2018, for a launch around 2030. The TIFPA group is working on the definition of the measuring instrument and guides the ASI development of the Gravitational Reference Sensor (GRS) system to guarantee the free fall of the geodetic reference masses that are at the heart of the instrument. The LIGO-Virgo collaboration is completing the analysis of the 2017 joint observations; among the results stand out the opening of multi-messenger astronomy and the measurements of the properties of neutron stars. The Virgo detector is in the commissioning phase, and the 2019 program provides the first long joint observation run. At the same time, the Virgo detector upgrade project, Advanced Virgo+ project, begins. The Trento group contributes actively both in coordinating the LIGO-Virgo data analysis and in the instrumental science development. The detection of a possible dark matter candidate is the goal of DARKSIDE and QUAX while, in the domain of quantum simulations operates FISH, modelling interactions and mechanism at the basis of high energy system by means of quantum gases of ultra-cold atoms. HUMOR focuses on probing the granularity of space-time at the Planck scale expected by theory trying to unify General Relativity with Quantum Physics.

AMS

Laurent Basara, Roberto Battiston, William Jerome Burger, Francesco Dimiccoli, Konstantin Kanishev, Ignazio Lazzizzera, Francesco Nozzoli,[†] Paolo Zuccon

AMS-02 is a state-of-the-art particle physics detector (see Fig. 1) designed to operate as an external module on the International Space Station (ISS).

AMS-02 goal is to study the universe and its origin by searching for antimatter and dark matter, while performing precision measurements of cosmic ray composition and flux. The measurements high accuracy along with the large collected statistic allow to study cosmic ray component flux variations with rigidity and time. This is important to understand the origin, acceleration and propagation of cosmic rays in our galaxy.

Recently AMS published the measured flux of the light nuclei in cosmic rays, from He to Oxygen, in the rigidity range 1.9 GV to 3.3 TV (Aguilar et al. 2018d; Aguilar et al. 2018e).

Fig. 2 shows that the primary component fluxes (He, C, O) have identical rigidity dependence above 60 GV and they all deviate from a single power law above 200 GV in an identical way. An universal rigidity behavior with similar

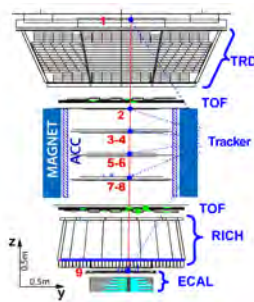


Figure 1: The AMS detector with an example of a measured 868 GeV positron event. Tracker planes 1-9 measure the particle charge, sign and momentum. The TRD identifies the particle as an electron/positron. The TOF measures the charge and ensures that the particle is downward-going. The RICH measures the charge and velocity. The ECAL independently identifies the particle as an electron/positron and measures its energy.

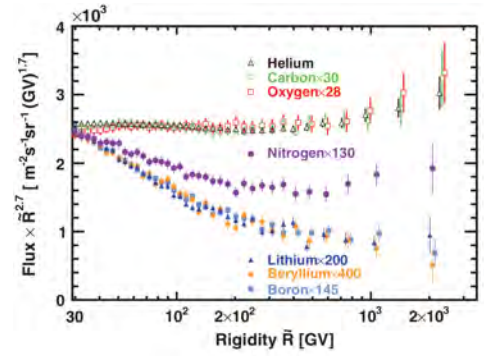


Figure 2: Comparison of the AMS measurements of the primary cosmic ray fluxes, secondary cosmic rays fluxes (Aguilar et al. 2018d) with the nitrogen flux (Aguilar et al. 2018e) multiplied by $R^{2.7}$. The three secondary fluxes have identical rigidity dependence above 30 GV as do the three primary fluxes above 60 GV, but they are different from each other. The R dependence of the N flux is distinctly different from the dependence of both the primary and secondary fluxes due to the mixed primary/secondary nature of N .

features has also been observed in the measurement of secondary cosmic rays (Li, Be, B) flux. However the rigidity dependencies of primary cosmic rays and of secondary cosmic rays are distinctly different. Finally, the nitrogen flux, N , can be fit over a wide rigidity range as the simple linear combination of primary and secondary fluxes. This is a new and important result, which permits the determination of the N/O abundance ratio at the source without the need to consider the Galactic propagation of cosmic rays (Aguilar et al. 2018d; Aguilar et al. 2018e).

The TIFPA group is currently analyzing the Deuteron flux as a first step for the study of the cosmic Anti-Deuteron flux, allowing the optimization of the detector performances and selection strategy. Moreover, the Deuteron flux measure is itself very important, because the flux ratio between exclusively secondary and primary produced CR particles gives important constraints to the propagation models of CR in

[†]Contact Author: francesco.nozzoli@unitn.it

the Galaxy.

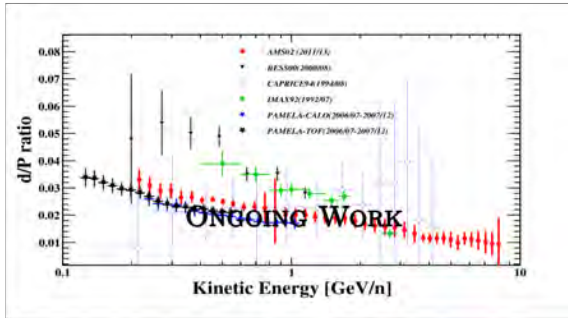


Figure 3: Preliminary Deuteron over Proton flux ratio measured with AMS-02 compared with previous measurements.

We developed both multivariate approach and a simple cut analysis for the distinction of Deuterons from the overwhelming proton background.

Fig. 3 shows a preliminary result of the measurement of the Deuteron to Proton flux ratio.

Moreover analysis tools developed for the Deuteron flux measurement may be applied also for other isotope mass separations, $^3\text{He}/^4\text{He}$ ratio and $^{10}\text{Be}/^9\text{Be}/^7\text{Be}$ abundances in cosmic rays, as well as for the search for strangelets.

Finally also the precision measurement of the proton, He, electron and positron fluxes as a function of the time from May 2011 to May 2017 (79 Bartels rotations) has been published (Aguilar et al. 2018c).

This data have been collected during the 24th solar cycle, with the solar maximum in April 2014. We observed that below 40 GV, the proton flux and the helium flux show nearly

identical fine structures in both time and relative amplitude, above 40 GV both fluxes are found to be time independent. Above ~ 3 GV the p/He flux ratio is time independent (Fig. 4) and we observed that below ~ 3 GV the ratio has a long-term decrease coinciding with the period during which the fluxes start to rise.

The TIFPA group continues its efforts at the forefront of the analysis of AMS-02 cosmic ray data. In the early 2019 a paper on $^3\text{He}/^4\text{He}$ isotopic ratio is expected to be published and Deuteron flux will be finalized. The work on light element isotopic composition is also moving forward and is expected to be presented at conferences along 2019.

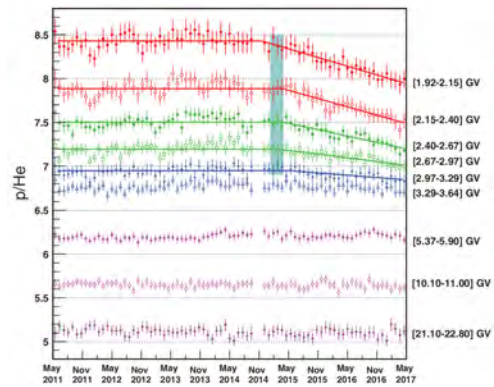


Figure 4: The AMS p/He flux ratio as function of time for 9 characteristic rigidity bins. The errors are the quadratic sum of the statistical and time dependent systematic errors. The solid lines are the best fit with a broken line for the first 5 rigidity bins from $[1.92-2.15]$ GV to $[2.97-3.29]$ GV. The vertical band (February 28, 2015 \pm 42 days) is the average of the best fit values of the transition time for these rigidity bins.

Selected Papers

- Aguilar, M. et al. (2018c). *Observation of Fine Time Structures in the Cosmic Proton and Helium Fluxes with the Alpha Magnetic Spectrometer on the International Space Station*. Phys. Rev. Lett. **121**(5), p. 051101.
- (2018d). *Observation of New Properties of Secondary Cosmic Rays Lithium, Beryllium, and Boron by the Alpha Magnetic Spectrometer on the International Space Station*. Phys. Rev. Lett. **120**(2), p. 021101.
- (2018e). *Precision measurement of cosmic-ray nitrogen and its primary and secondary components with the Alpha Magnetic Spectrometer on the International Space Station*. Phys. Rev. Lett. **121**(5), p. 051103.

DarkSide

Fabio Acerbi, Alberto Gola,[†] Marco Marcante, Alberto Mazzi, Stefano Merzi, Giovanni Paternoster, Veronica Regazzoni

The existence of dark matter in the Universe is commonly accepted as the explanation of many phenomena, ranging from internal motions of galaxies to the large-scale inhomogeneities in the cosmic microwave background radiation and the dynamics of colliding galaxy clusters.

A favored hypothesis that explains these observations is that dark matter is made of weakly interacting massive particles (WIMPs). However, no such particles exist in the Standard Model and none has been observed directly at particle accelerators or elsewhere. Hence, the nature of the dark matter remains unknown.

DarkSide-20k experiment (DS-20k) is a direct dark matter detection experiment based on a shielded underground detector, with 20 tons of liquid argon target mass (Aalseth, Acerbi, et al. 2018). It will be based on a two-phase time projection chamber (TPC) filled with low-background, depleted argon (DAR) and will be deployed in the underground Hall C at Gran Sasso National Laboratory (LNGS), inside a newly constructed, two-chamber veto, filled with atmospheric Argon, and a cryostat, as shown in Fig. 1. DS-20k constitutes an expanded version of the DS50 experiment, which finished taking data at LNGS in October 2017.

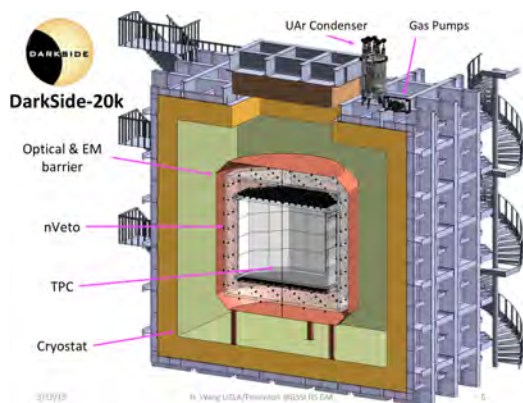


Figure 1: Cross sectional view of the DS20k experiment through its center plane, showing the inner TPC, the inner and outer active veto chambers, and the cryostat.

Silicon Photomultipliers The use of Silicon Photomultipliers (SiPMs) instead of Photo Multiplier Tubes as photodetectors in both TPC and Veto is one of the main technological challenges of the experiment, the other being the production of ultra-low-background depleted argon. There are several advantages in using these detectors in DS-20k, among them: low bias voltage (30 - 45 V), efficient integration into tiles to cover large areas, customizable size and performance, excellent photon counting capabilities and high Photon Detection Efficiency (PDE). The most important one, however, is that SiPMs are virtually radioactivity free (silicon is very radio pure material). SiPMs will be grouped in tiles and integrated in several photo-detection modules, to cover a total area of approximately 10 square meters.

DS-20k Activity at TIFPA The use of SiPMs at cryogenic temperatures is innovative and very few studies have been carried out on their characterization and optimization at cryogenic temperatures. Furthermore, the readout of such large active areas poses several challenges in the design and optimization of both SiPMs and front-end electronics, developed at LNGS, and in packaging techniques. In this context, TIFPA started the DS-20k activity in 2016, collaborating mainly with Fondazione Bruno Kessler (FBK), LNGS and Naples INFN section and Princeton University. The activity was focused on the cryogenic characterization of different SiPMs technologies developed by FBK to:

- (i) verify and characterize their functionality at cryogenic temperatures and, in particular, at 87 K;
- (ii) select the most suitable one for DS-20k;
- (iii) provide information to optimize the SiPM parameters and layout for the best possible performance in DS-20k.

[†]Contact Author: gola@fbk.eu

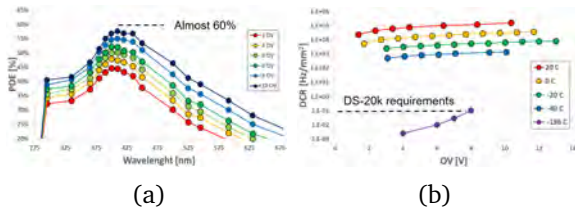


Figure 2: (a): PDE vs. wavelength measured at room temperature on NUV-HD-Cryo SiPMs, with 35 μm cell size. (b): DCR vs. over-voltage measured at different temperatures on NUV-HD-Cryo SiPMs, with 30 μm cell size.

To this aim, one of the most important results obtained in 2016 and confirmed in later SiPM productions is the exceptionally low Dark Count Rate (DCR) of NUV-HD-LF (low electric field variant) technology at 87 K, which is at the state of the art with a value of a few mHz/mm^2 . In 2017 and 2018, TIFPA commissioned different SiPM R&D runs to FBK, within the INFN-FBK agreement, to test new technology and layout splits aimed at further improving performance at cryogenic temperatures and at optimizing the detector characteristics for DS-20k. Experimental characterization of one of the splits showed that it is effective in suppressing the increase of the correlated noise previously observed at cryogenic temperatures, therefore increasing the maximum operating over-voltage of SiPMs at 87 K by a factor of 3. Another split was effective in increasing temperature stability of SiPM characteristics from room temperature to 87 K.

During 2018, SiPM technology and layout splits produced in 2017 were characterized in depth through functional measurements in a wide temperature range down to 77 K, in order to finally select the best option for the experiment. Among all the splits, SiPMs with a microcell size of 30 μm or 35 μm and built in FBK NUV-HD-Cryo technology, showed remarkable performance, in excess of the project specifications. SiPMs with 1 cm^2 active area operated at 6 V above breakdown showed a PDE of 50% at 420 nm (Fig. 2a), DCR of 10 mHz/mm^2

at 77 K (Fig. 2b), after-pulsing probability lower than 8%, direct crosstalk probability lower than 25%. Using cryogenic electronics further optimized at LNGS during 2018, remarkable few-photon counting capability was demonstrated at 77 K, with S/N in excess of 20, using a 24 cm^2 SiPM array coupled to a single analog readout channel (Fig. 3, left). The SiPMs produced at FBK were used by the DarkSide collaboration to mount the first batch of photo-detection modules (PDMs). The PDMs were assembled on the first test motherboard with a total photo-sensitive area of 600 cm^2 (Fig. 3, right).

An additional SiPM lot was produced at FBK in 2018 for the completion of the second and third test motherboards. In view of the SiPM mass production, necessary for DarkSide-20k, the NUV-HD-Cryo SiPM technology was selected to be transferred to an external CMOS foundry, capable of mass production, and FBK started the technology transfer activities. The first SiPM run was produced at the external foundry with customized process in 2018 and was tested at FBK. Electrical characterization of the SiPMs from the first technology transfer run showed SiPM parameters in line with FBK standards, with some process details to be adjusted in a second production lot, scheduled for 2019.

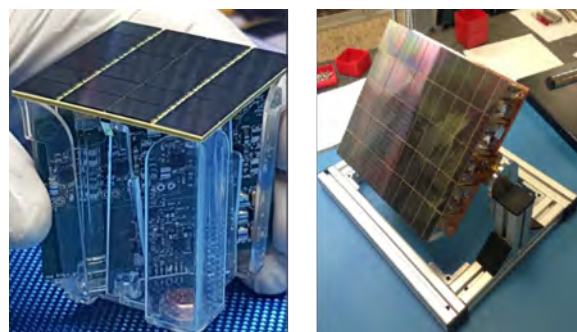


Figure 3: Left: 24 cm^2 PDM, composed of 24 NUV-HD-Cryo SiPMs connected to a single readout channel. Right: 600 cm^2 , fully functional motherboard, containing 25 PDMs.

Selected Papers

Aalseth, C. E., Acerbi, F., et al. (2018). *DarkSide-20k: A 20 tonne two-phase LAr TPC for direct dark matter detection at LNGS*. *Eur. Phys. J. Plus* **133**, p. 131.

FISH

Arturo Farolfi, Giacomo Colzi, Carmelo Mordini, Albert Gallemí, Iacopo Carusotto, Salvatore Butera, Alessio Recati, Sandro Stringari, Giacomo Lamporesi, Gabriele Ferrari [†]

FISH, Fundamental Interaction Simulations with quantum gases, focuses on the dynamics of quantum gases of ultracold atoms with the aim to model interactions and mechanisms at the basis of high energy physics. This research field belongs to the domain of quantum simulation, where physical systems difficult to address experimentally are studied through analogies with simpler systems. In particular we focus on the study of vortices in a system made of two Rabi-coupled atomic Bose-Einstein condensates to simulate quark confinement.¹

Spinor Bose-Einstein condensates, whose wavefunction has a spin term, play a crucial role within the community of ultracold/quantum gases. Since the early demonstration of Bose-Einstein condensation, these systems were studied mainly in the absence of stationary driving among the internal states, focusing on mean-field effects as, for instance, the stability of polarization, the miscibility, and the many-body dynamics of the superfluids under the action of external parameters such as the symmetry of the interactions, the confining potential, or the energy splitting of the internal states. The case of Hamiltonians containing a coupling term among the spin states has been fairly unexplored so far, at least experimentally, because of technical constraints imposed by the stability of the magnetic fields. On the other hand, binary condensates under the action of a resonant coupling among internal states have attracted a substantial theoretical interest since it was recognized that in such systems the additional degrees of freedom (i.e., the relative phase) give access to new kinds of topological excitations, such as domain walls and vortex molecules,¹ and magnetic solitons (Qu et al. 2017).

The early research activity of the FISH project was focused on the realization of a novel dedicated experimental apparatus, which cul-

minated with the successful implementation of a magnetic and optical hybrid trap which accounts for the saturation limits of a μ -metal magnetic shield enclosing the science cell. The activity of last year, following the full hybrid trap characterization (Colzi et al. 2018), was directed towards the technical upgrade of the experimental apparatus, and to the development of experimental techniques to produce and control resonantly coupled spinor BECs, as described below.

Magnetic shield characterization: the relative attenuation of external magnetic fields inside the shield volume was carried out experimentally for external magnetic field values of the order of 0.5 G. The results are reported in Fig. 1a. Relative attenuation values better than 10^{-5} and 10^{-4} are obtained for external fields directed along the axial and radial shield directions, respectively. Such values are satisfactory, and perfectly consistent with the results of simulations made at the shield design phase.

Development of coupling schemes: We compared experimentally different coherent coupling schemes (both single and two-photon), to produce and control spinor BECs composed of the the $|F = 1, m_F = -1\rangle$ and $|F = 1, m_F = +1\rangle$ states. The comparison allowed to identify the two-photon microwave coupling as the most promising strategy. Preliminary tests, in the absence of the magnetic shield, also showed that external field fluctuations induced by human activity in the vicinity of the laboratory are sufficient to shift the transition frequency in an uncontrolled manner, limiting the experimental reproducibility. This preliminary observation confirms the magnetic field stabilization requirements of the experiment.

[†]Contact Author: gabriele.ferrari@unitn.it

¹Son, D. T. and Stephanov, M. A. (2002), Phys. Rev. A **65**, p. 063621.

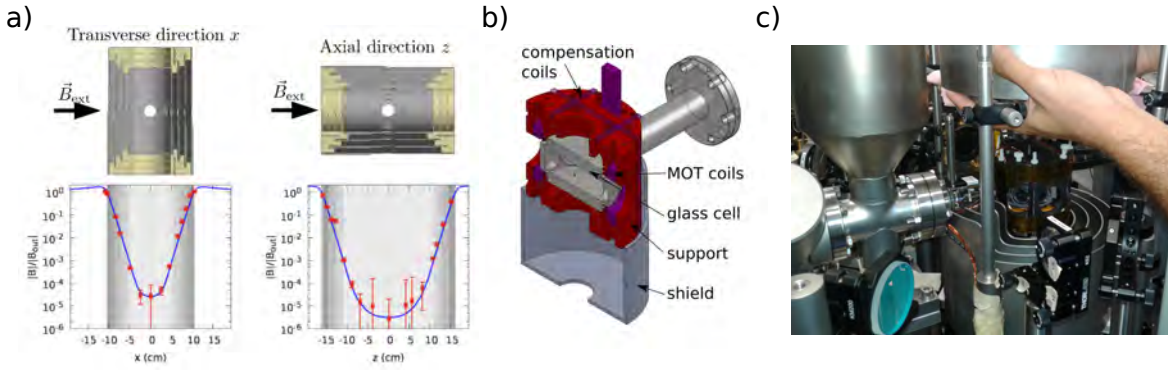


Figure 1: **a)** Experimental characterization of relative magnetic field attenuation, measured for an external uniform field $|\vec{B}_{\text{out}}| \simeq 0.6\text{G}$ directed along the radial (left panel) and axial (right panel) shield axis. Numerical simulation results are also reported (blue line). **b)** Sketch of the electromagnets and antenna system, and mechanical supports design. **c)** Actual enclosure of the science cell and magnetic coils inside the magnetic shield.

Experimental apparatus update: the experimental apparatus was upgraded. Such upgrade includes the design and construction of a new complete system of magnetic coils and mechanical supports (Fig. 1b), the magnetic shield assembly (Fig. 1c) and the realization of a new imaging system featuring a low readout noise CMOS camera.

System characterization: we characterized the system in the final experimental configuration. In the presence of the magnetic shield enclosing the science cell, we observed a significant improvement in the reproducibility and degree of control exerted on the spinor condensate. This result was further improved by including in the experimental sequence a demag-

netization cycle for the internal shield layer.

Additionally, we concluded the measurements and reported the first observation of spin superfluidity in a Bose-gas mixture, that we carried out in another experimental apparatus (Fava et al. 2018).

Current activity: we are further advancing the experimental apparatus by implementing optical phase imprinting, that will be used to produce topological excitations on the coupled spinor BEC system. Such excitations will be studied as a function of the accessible experimental parameters (e.g. the intensity of the coupling, or the confining external potential) within the FISH project framework.

Selected Papers

- Colzi, G., Fava, E., Barbiero, M., Mordini, C., Lamporesi, G., and Ferrari, G. (2018). *Production of large Bose-Einstein condensates in a magnetic-shield-compatible hybrid trap*. Phys. Rev. A **97** (5), p. 053625.
- Fava, E., Bienaimé, T., Mordini, C., Colzi, G., Qu, C., Stringari, S., Lamporesi, G., and Ferrari, G. (2018). *Observation of Spin Superfluidity in a Bose Gas Mixture*. Phys. Rev. Lett. **120** (17), p. 170401.
- Qu, C., Tylutki, M., Stringari, S., and Pitaevskii, L. P. (2017). *Magnetic solitons in Rabi-coupled Bose-Einstein condensates*. Phys. Rev. A **95** (3), p. 033614.

HUMOR

Michele Bonaldi, Antonio Borrielli, Enrico Serra,[†] Giovanni Andrea Prodi

One of the open questions in physics is to reconcile the two most successful theories of physics, Einstein's general relativity and quantum physics. Currently, there are many theories that aspire to achieve this unification, but none of them is convincing and it is not clear how they can be verified experimentally. A common feature of these theories is that the space-time changes nature, become "granular" at a very small length, called "Planck scale" ($L_p = \sqrt{\hbar G/c^3} = 10^{-35}$ m). The HUMOR (Heisenberg Uncertainty Measured with Optomechanical Resonators) experiment uses a new method for probing the space-time: the microscopic vibrations of oscillators of different sizes and masses, from a few nanogram up to a few milligrams, are measured with great accuracy, using lasers and/or electromagnetic sensors. The presence of a granularity of space-time at the Planck scale should be reflected in a nonlinear behavior of the oscillators, up to the dimensional scale currently measurable in the laboratory. In fact, in the framework of quantum mechanics, the measurement accuracy is at the heart of the Heisenberg relations, that, however, do not imply an absolute minimum uncertainty in the position. An arbitrarily precise measurement of the position of a particle is indeed possible at the cost of our knowledge about its momentum. This consideration motivated the introduction of generalized uncertainty principles (GUPs), such as

$$\Delta q \Delta p \geq \frac{\hbar}{2} \left(1 + \beta_0 \left(\frac{L_p \Delta p}{\hbar} \right)^2 \right), \quad (4)$$

that implies indeed a nonzero minimal uncertainty $\Delta q_{min} = \sqrt{\beta_0} L_p$. The dimensionless parameter β_0 is assumed to be around unity, in which case the corrections are negligible unless lengths are close to the Planck length. Any experimental upper limit for $\beta_0 > 1$ would constrain new physics below the length scale $\sqrt{\beta_0} L_p$. This GUP implies two relevant effects

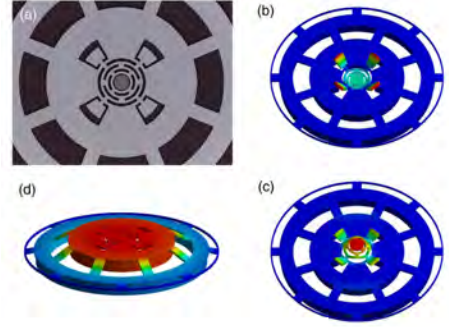


Figure 1: (a): Optical image of the full device, including the central oscillator and the external isolating wheel. The central dark disk is the 400 μm diameter highly-reflective coating. (b): FEM simulations of the displacement corresponding to the balanced oscillator mode exploited in this work; (c): the second, unbalanced mode; (d): the first wheel oscillator mode.

with respect to a harmonic oscillator: the appearance of the third harmonic and a dependence of the oscillation frequency on the amplitude. Therefore, to set a limit on the value of β_0 , we can measure the frequency of highly isolated oscillators at different oscillation amplitudes.

The micro-mechanical oscillators were built with micro-lithography on silicon wafers. In Fig. 1 we show for instance a device with a typical mass of 100 μg , with a shape designed to best isolate it from the external environment. The oscillators are then cooled down to a few degrees above absolute zero, to limit heat induced vibrations. The movement is measured with laser beams and low noise electrostatic sensors, with sensitivity to the displacement comparable to the size of the atomic nucleus. The setup can measure changes in the oscillation frequency of some part in a billion during the free decay of the oscillation after a resonant drive.

In Fig. 2 we report the results obtained with oscillators of different dimensions and shapes (as shown in the insets near the experimental points).¹ The resonators show their quan-

[†]Contact Author: enrico.serra@tifpa.infn.it

¹Bawaj, M. et al. (2015), Nature Comm. 6, p. 7503.

tum behaviours in a Quantum Non Demolition (QND) measurement scheme: exploiting the light field intensity as observable in the QND optical scheme we have demonstrated a reduced uncertainty on intensity fluctuations actually achieving a sub-shot noise level shown in Fig. 3 (reported in Pontin et al. 2018).

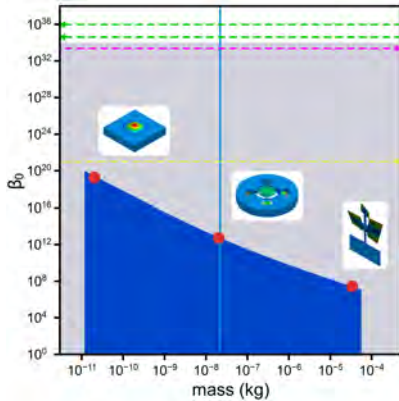


Figure 2: Red dots: upper limits to the parameter β_0 . Gray shows the area below the electroweak scale, dark blue the area that remains unexplored. Dashed lines reports some previously estimated upper limits, obtained in mass ranges outside this graph (as indicated by the arrows).¹ The vertical line corresponds to the Planck mass (22 μg).

These results improve the previous upper limits to quantum gravity effects by many orders of magnitude. The next challenge is to further cool an oscillator using laser light. At ultracryogenic temperature the behavior of the oscillator should be markedly quantum-like and it will thus be possible to highlight in the most direct manner any anomalies due to effects of quantum gravity.

For this experiment we have designed and produced a membrane resonator, equipped with a specific on-chip loss shield for a circular membrane (Fig. 4), that achieve a mechanical

quality factor of 10^7 (Serra et al. 2018).

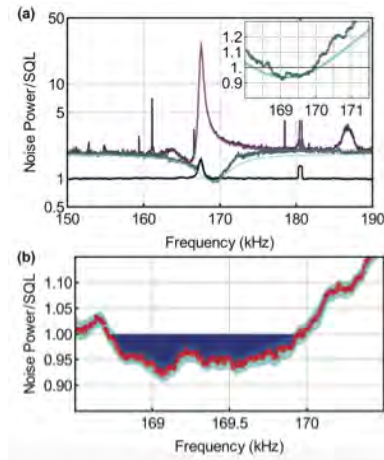


Figure 3: Signal and its residual uncertainty. Residual spectrum show that it falls below the standard quantum level in a proper frequency range.

Nanomembranes were successfully tested in advanced optical schemes (Rossi et al. 2018) for improving cooling efficiency and the optomechanical cooperativity. By the membrane’s surface functionalization with high-reflectivity metasurface, thickness reduction and increase in the intrinsic stress level we are able to improve the cooling efficiency of the resonator.

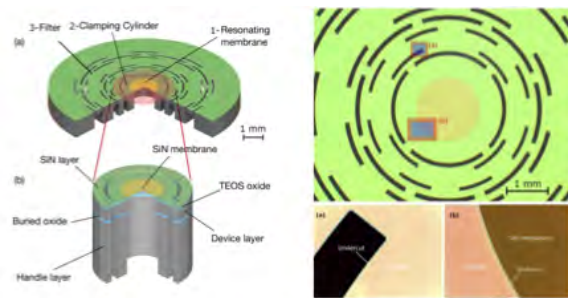


Figure 4: (Left): Design of the membrane’s resonator equipped with a “loss shield” structure. (Right): SEM image of the resonator.

Selected Papers

- Pontin, A., Bonaldi, M., Borrielli, A., Marconi, L., Marino, F., Pandraud, G., Prodi, G., Sarro, P., Serra, E., and Marin, F. (2018). *Quantum nondemolition measurement of optical field fluctuations by optomechanical interaction*. PHYSICAL REVIEW A **97**(033833).
- Rossi, M., Kralj, N., Zippilli, S., Natali, R., Borrielli, A., Pandraud, G., Serra, E., Di Giuseppe, G., and Vitali, D. (2018). *Normal-mode splitting in a weakly coupled optomechanical system*. PHYSICAL REVIEW LETTERS **120**(7).
- Serra, E., Morana, B., Borrielli, A., Marin, F., Pandraud, G., Pontin A. Prodi, G., Sarro, P., and Bonaldi, M. (2018). *Silicon Nitride MOMS Oscillator for Room Temperature Quantum Optomechanics*. IEEE JOURNAL OF MICROELECTROMECHANICAL SYSTEMS **27**(6).

LIMADOU

Laurent Basara, Roberto Battiston, William Jerome Burger, Francesco Dimiccoli, Benedetto Di Ruzza, Francesco Follega, Giuseppe Gebbia, Roberto Iuppa,[†] Ignazio Lazzizzera, Christian Manea, Francesco Nozzoli, Matteo Puel, Irina Rashevskaya, Ester Ricci, Enrico Serra and Paolo Zuccon

Limadou is the experiment made with the High Energy Particle Detector (HEPD) of the Chinese Seismo-Electromagnetic Satellite (CSES). The HEPD is designed to study the correlation between seismic activity and the trapped particle populations in the Van Allen radiation belts reported by instruments on different satellites.¹ The HEPD is designed to measure with good resolution the pitch angle and energy of the electrons and protons in the radiation belts. The detector includes a silicon micro-strip tracker, a segmented scintillator trigger plane, a scintillator-LYSO calorimeter, and 5 scintillator veto planes which surround the calorimeter volume (Ambrosi et al. 2018).

The CSES was launched on February 2, 2018. The satellite was placed in a circular, polar (inclination angle 97.4°), sun-synchronous orbit at an altitude of 506.9 km. The instruments on the satellite, which include an electric field detector, a high precision magnetometer, a Langmuir Probe and a low energy particle detector (HEPP-H), are all operational (Shen et al. 2018).

The HEPD commissioning phase was devoted to an optimization of threshold levels at the level of the individual sub-detectors, and a study of different trigger configurations to optimize the performance of the detector. The final HEPD configuration was uploaded on July 28, 2018. The HEPD is operational between the latitudes $\pm 65^\circ$. The detector power is switched off in the polar regions. The maximum trigger rate is 400 Hz limited by the onboard data processing hardware. Signal and pedestal levels are stable and in agreement with test beam mea-

surements and atmospheric muon data. The electron and proton rates, and preliminary proton fluxes, are consistent with expectations, as shown in Fig. 1. The saturation of the HEPD is visible on the South Atlantic Anomaly (SAA, over northern South America and South Atlantic) and the color scale shows the event rate increasing with the geomagnetic latitude.

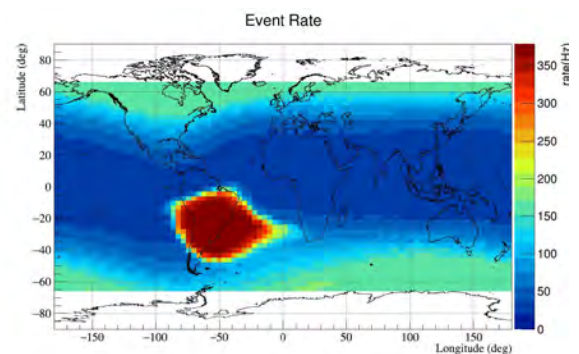


Figure 1: Average rate of events collected by the HEPD. Events mostly include triggers from protons and electrons. Period: August 2018.

The science of Limadou requires a good capability of identifying particles. Separating electrons from nuclei is of primary importance, because results from previous experiments report particle precipitations correlated with seismic phenomena in the electron channel, whereas space weather effects are often appreciable by looking at variations of flux of nuclei. Regarding nuclei, measuring their charge allows observations of low-energy cosmic rays, useful to constrain models of spallation and propagation in the nearby medium.² Particles can be preliminarily identified as reported in Fig. 2. After calibration and equalisation, the signal amplitude (ADC) from the first plane of plastic

[†]Contact Author: roberto.iuppa@unitn.it

¹Aleksandrin, S. et al. (2003), *Annales Geophysicae* 21, pp. 597–602.

²HEPD is sensitive to $Z \geq 2$ nuclei only over the highest latitude orbit's regions.

scintillator (P1) can be paired with the sum of the amplitudes from all planes. Flight data are distributed on two very distinct regions of the $calorimeter_{tot}/calorimeter_{P1}$ plane: for any given total signal, electrons release less energy on P1 than protons.

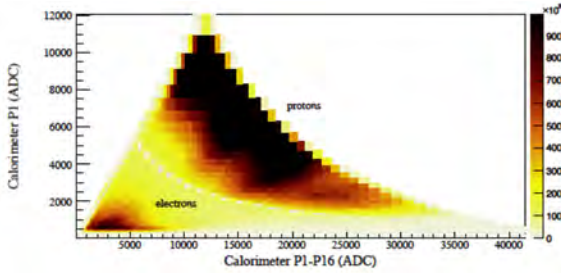


Figure 2: Particle identification on a selection of data collected in August 2018. See text for details.

The same approach is followed to identify nuclei with $Z > 1$, although low-gain readout is used to avoid the saturation of electronics. After calibration, the signal of the calorimeter is used to infer the energy of the particle with good accuracy.

Every position of the CSES along the orbit is associated to a certain L shell, namely the distance at the Equator of the local geomagnetic dipole field line. Low-energy particles are trapped in the geomagnetic field, gyrating around the field lines and bouncing back and forth among the geomagnetic hemispheres. To a very good approximation, they remain on the same L shell until shocking geomagnetic events occur.

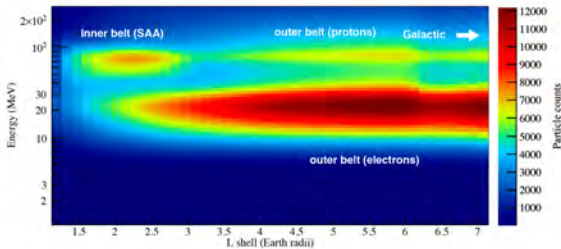


Figure 3: Populations of particles observable with HEPD. Based on a selection of data collected in August 2018. See text for details.

Fig. 3 reports the relative abundances of particles measured with the HEPD in August 2018.

³We recall that the shape of the outer Van Allen Belt is extremely varying, due to the influence of the solar activity.

Loose selection cuts are applied to ensure good data quality, but no particle identification is applied. The representation makes use of particle's energy and L shell at the detection, with the color scale depicting the number of events surviving the selection. Both Van Allen belts are visible: HEPD detects particles of 50–100 MeV up to $L \simeq 3$, corresponding to the SAA. The outer belt, from $L \simeq 2$,³ is visible with HEPD in the energy range 10–40 MeV (electrons) and 70–100 MeV (protons). The maximum intensity detected in the outer belt is at $L \simeq 5 \div 6$. Fig. 3 also shows that the HEPD is sensitive to low-energy galactic protons: the region $L \geq 6.5$ contains both trapped and un-trapped protons, which can be separated by back- and forth- tracing their trajectories.

The acquisition and reconstruction of data collected with HEPD were fine-tuned during commissioning, allowing to define optimal operating conditions. Fig. 4 remarkably shows the accuracy achievable with the HEPD, reporting the case of trapped protons over the SAA. The events are selected as follows:

- (i) the event must pass tight data-quality selections, strongly reducing the geometric acceptance;
- (ii) the signal in the calorimeter must identify a proton;
- (iii) the energy release in the HEPD detector must be greater than 40 MeV.

After selection, particle counts are normalised to the acquisition time, to be reported as event rate. The maximum detected rate is 200 Hz. This result must be compared with expectations from SPENVIS software,⁴ suitably configured for the HEPD case and reported on the left-hand side of Fig. 4. Both the shape and the gradient of flux are in agreement and a correct evaluation of the experiment's acceptance will readily translate the result into an absolute measurement of flux.

The HEPD on board the CSES has been successfully commissioned in February-August 2018 and it is currently taking high-quality data

⁴<https://www.spennis.oma.be>

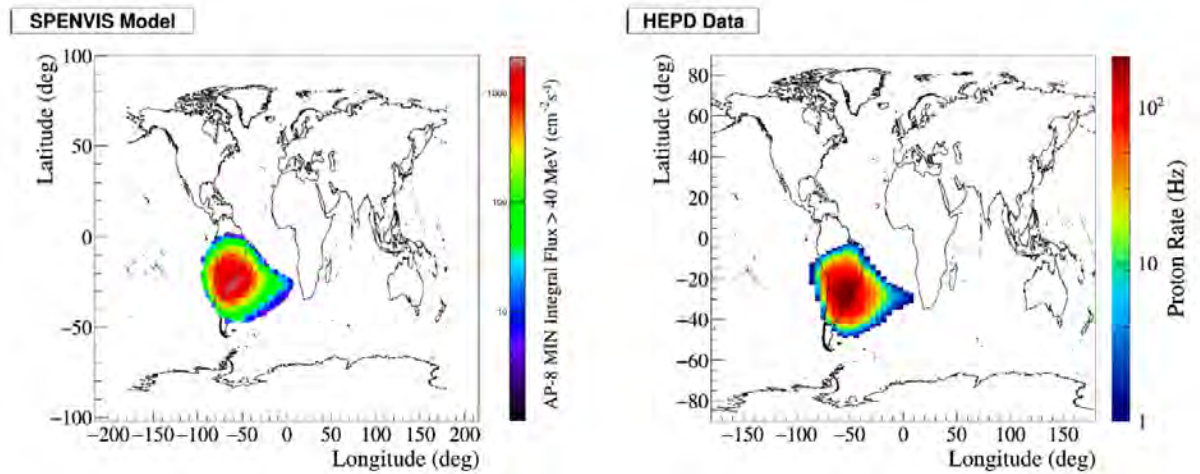


Figure 4: Comparison of data collected with the HEPD in August 2018 over the SAA (right) with the SPENVIS model (left). See text for details.

for seismic studies and measurements of space weather. The TIFPA members have contributed to the online monitoring and data analysis software, the Geant4 detector simulation, and the effort throughout 2018 in Italy, including test beams measurements with the HEPD qualification model.

A second satellite (CSES-02) is programmed for a launch in the later half of 2021,

with a ASI/INFN participation, namely an Electric Field Detector (EFD-02) and a HEPD-02. TIFPA members proposed innovative technologies for the HEPD-02, including Monolithic Active Pixel Sensors for the particle tracker and redundant readout of plastic scintillators with Silicon Photo-Multipliers (more details in the Space Virtual Lab report, p. 8).

Selected Papers

Ambrosi, G., Bartocci, S., Basara, L., Battiston, R., Burger, W. J., Carfora, L., Castellini, G., Cipollone, P., Conti, L., Contin, A., De Donato, C., De Santis, C., Follega, F. M., Guandalini, C., Ionica, M., Iuppa, R., Laurenti, G., Lazzizzera, I., Lolli, M., Manea, C., Marcelli, L., Masciantonio, G., Mergé, M., Osteria, G., Pacini, L., Palma, F., Palmonari, F., Panico, B., Patrizii, L., Perfetto, F., Picozza, P., Pozzato, M., Puel, M., Rashevskaya, I., Ricci, E., Ricci, M., Ricciarini, S. B., Scotti, V., Sotgiu, A., Sparvoli, R., Spataro, B., and Vitale, V. (2018). *The HEPD particle detector of the CSES satellite mission for investigating seismo-associated perturbations of the Van Allen belts*. *Science China Technological Sciences* **61**(5), pp. 643–652.

Shen, X., Zhang, X., Yuan, S., Wang, L., Cao, J., Huang, J., Zhu, X., Picozza, P., and Dai, J. (2018). *The state-of-the-art of the China Seismo-Electromagnetic Satellite mission*. *Science China Technological Sciences* **61**(5), pp. 634–642.

LISA Pathfinder and LISA

Daniele Bortoluzzi, Eleonora Castelli, Antonella Cavalleri, Rita Dolesi,[†] Valerio Ferroni, Ferran Gibert, Roberta Giusteri, Mauro Hueller, Martina Muratore, Giuliana Russano, Daniele Vetrugno, Davide Vignotto, Stefano Vitale, William Joseph Weber

Our current image of the Universe is essentially based on the observation of electromagnetic waves in a broad frequency spectrum. Much of the Universe, however, does not emit electromagnetic radiation, while everything interacts gravitationally. Despite being the weakest of the fundamental interactions, it is gravity that dominates the Universe on a large scale and regulates its expansion since the Big Bang. As predicted by Einstein’s General Relativity, gravity has its messenger: gravitational waves produced by massive accelerating bodies, such as coalescing black holes binaries or violent phe-

nomena like stellar core collapse. Gravitational waves propagate at the speed of light, essentially undisturbed, bringing often not otherwise accessible information about events across all cosmic ages, from Cosmic Dawn to the present. The observation of gravitational waves promises to open new extraordinary perspectives for investigation of crucial issues like the nature of gravity in weak and in strong field regime, the nature of black holes, the formation and evolution of stellar binary system, the formation and evolution of cosmic structures since the earliest stages of the Universe.

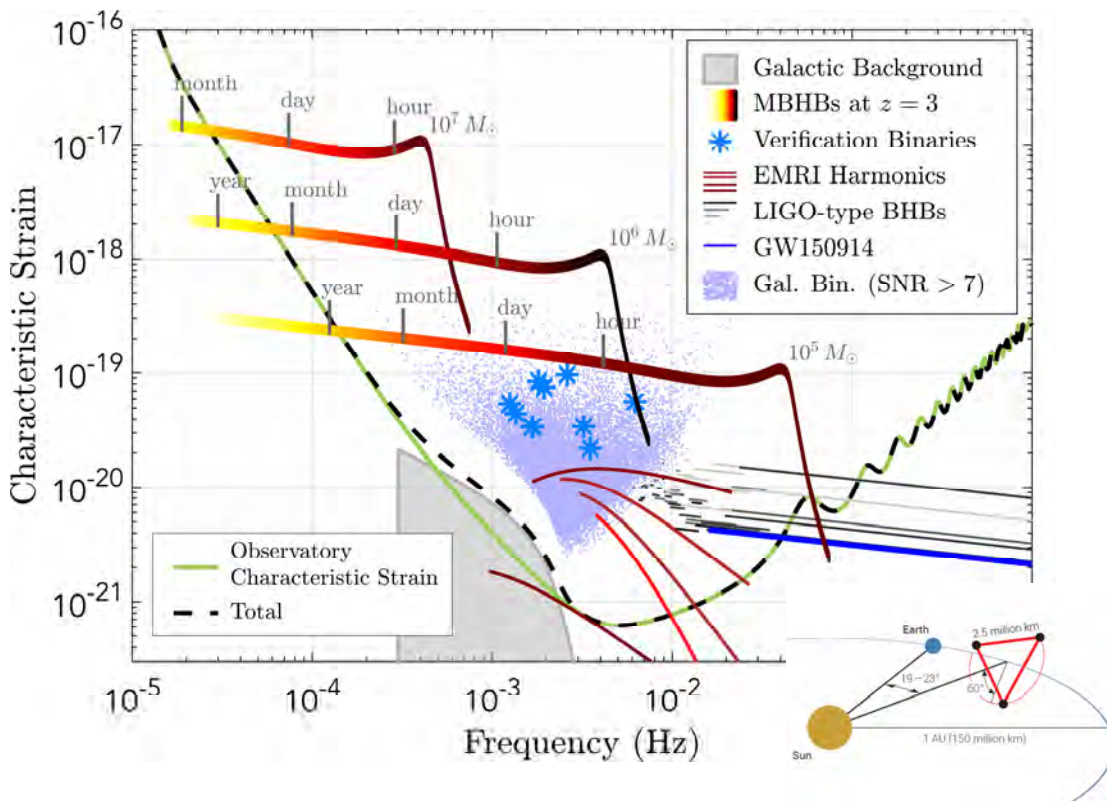


Figure 1: LISA’s sensitivity curve plotted with the signal levels for several GW sources. In the insert a schematic of the LISA-concept.

[†]Contact Author: rita.dolesi@unitn.it

While the ground-based observatories of the LIGO-VIRGO collaboration are going to start in 2019 the first long joint observation run, the project of LISA is rapidly progressing toward the implementation of the first space-based observatory devoted to the low-frequency sources that can not be detected from ground. Einstein's theory describes gravity in terms of the curvature of space-time that is deformed by the passing of gravitational waves. These effect can be detected in space by measuring with great precision the relative acceleration of masses in free fall, i.e. reference masses subject to gravity field but well-isolated from other types of disturbing forces. The precursor space mission LISA Pathfinder measured the relative acceleration of two 2 kg test masses in near-perfect geodesic motion, and its outstanding performance provided an experimental benchmark demonstrating the ability to realize the low-frequency science potential of the LISA mission. LISA consists of three identical satellite in a triangular constellation, with arms of several million km, orbiting around the Sun, shown in Fig. 1 with its strain sensitivity. It should allow for the observation of thousands of gravitational wave sources with high signal-to-noise, and in many cases very well characterized in terms of frequency, position in the sky, and luminosity distance. It targets massive sources emitting in the 0.1 mHz to 1 Hz band not accessible from ground due to the gravitationally noise terrestrial environment, ranging from stellar mass binaries in our own Galaxy to the merger of two galactic-core black holes, from 10^5 to 10^7 solar masses, from the recent Universe back to the epoch of the first galaxies.

The Trento Group, led by the Principal Investigator prof. Stefano Vitale, has contributed in a leadership role in all phases of the LISA PF mission, including hardware design and prototyping, laboratory torsion pendulum testing, scientific guidance of the industrial

aerospace contractors, and finally to the design and operation of the flight measurement campaign. A scientific event to conclude the LISA Pathfinder mission was organized in Trento in September 2018, the "LISA Pathfinder Mission Accomplished". The event gathered around 95 members of the collaboration from the scientific institutes, industries and space agencies, and was an opportunity to discuss the state of the scientific papers still in preparation and the heritage transfer to LISA.

LISA Pathfinder legacy consists in a LISA Gravitational Reference Sensor at TRL 9, a detailed physical model for parasitic forces close to quantitative demonstration at sub-femto-g level down to $20 \mu\text{Hz}$, a demonstration of local interferometry on free falling test-masses at tens of femto-m level down to mHz, the demonstration of drag-free satellite down to femto-g, the demonstration of gravitational balance, of test mass charge management system and of an in flight test mass releasing mechanism. Several papers documenting these performances has been published in 2018 (see p. 141) and others are still in preparation.

In spring 2018, ESA started Phase A of LISA mission development, an in-depth study of the implementation of the mission lasting about two years, with the adoption of the mission scheduled for 2020-2022 for a launch in 2030-2034. As internationally recognized leader in development and realization of systems of free-falling geodesic reference test masses for space based gravitational wave detector, the TIFPA group is currently working on the definition of the measuring instrument and guides the ASI development of the Gravitational Reference Sensor (GRS) system to guarantee the free fall of the geodetic reference masses that are at the heart of the instrument (for more information about LISA see <https://www.elisascience.org/>).

QUAX

Paolo Falferi,[†] Renato Mezzena

The signature of symmetry breaking at extremely high energies can be highlighted by the presence of long-range ultra-weak forces mediated by pseudo-Goldstone bosons. In particular, the pseudo-boson can be either the QCD axion or an axion-like-particle (ALP), which involves P and T violating forces with strength proportional to the product of the couplings at the pseudo-boson vertices. There are two options for coupling pseudo-scalar bosons with fundamental fermions. In a multipole expansion, these two fields are described by the *dipole* (pseudo-scalar coupling g_p) and *monopole* (scalar coupling g_s) moments, respectively. For instance, exchange of virtual axions - a possible solution of the strong CP problem - mediates a monopole-dipole force where g_s is proportional to the QCD vacuum angle $\theta \simeq 10^{-10} \sim 10^{-14}$.

The $g_p^e g_s^N$ interaction between an electron e and a nucleus N mediated by an axion or ALP can be represented by an effective magnetic field. Clearly, this field is not a genuine mag-

netic field, as the interaction potential is generated by pseudoscalar exchange rather than by photon exchange, and so it does not satisfy the Maxwell's equations. Once this effect is integrated over a macroscopic monopole source, the resulting total effective magnetic field can have a measurable amplitude or at least permit to improve current upper limits on $g_p^e g_s^N$.

In the past years we have performed a series of experiments by measuring the magnetization of a cubic sample of gadolinium oxyorthosilicate Gd_2SiO_5 crystal (GSO) with 1 cm edge length (*detector*), induced by 4 disk shaped lead masses (*sources*). GSO is a paramagnetic material with a magnetic susceptibility $\chi \simeq 0.7$ at cryogenic temperatures. The crystal was housed in the lower part of a liquid helium cryostat and cooled down to $\simeq 4$ K. The distance between the *source* of effective magnetic field and the GSO crystal was modulated in time by mounting the masses on a rotating wheel operating at room temperature. To detect the variation of magnetization of the crystal we used

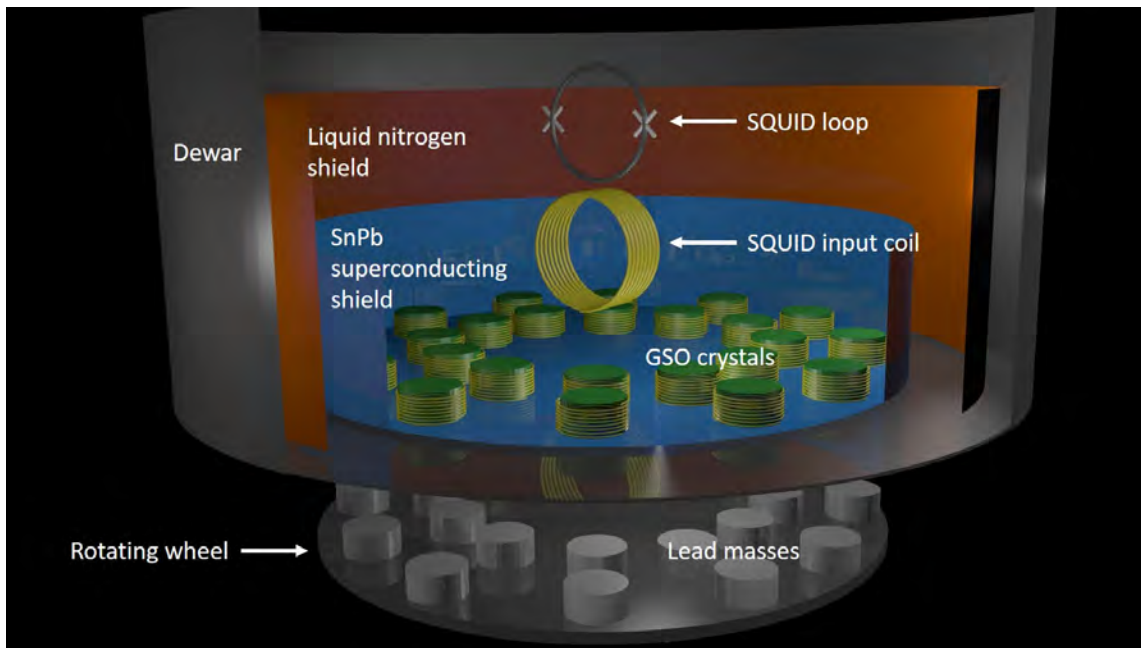


Figure 1: Schematic model of the apparatus. See text for a detailed description.

[†]Contact Author: paolo.falferi@unitn.it

a dc-SQUID operated at $\simeq 4$ K. The superconducting input coil of the SQUID was connected to a superconducting pick-up coil optimally wound around the GSO crystal in order to transfer the magnetic flux from the pick-up coil to the SQUID loop. From the measurements performed with this apparatus we were able to improve the upper limit of $g_p^e g_s^N / (\hbar c)$ to $\leq 4.3 \times 10^{-30}$ at 95% of confidence level in the range $1 \text{ cm} < \lambda_a < 20 \text{ cm}$ where λ_a is the Compton wavelength of the axion (interaction range).

In order to further improve this limit we have designed and realized a new experimental apparatus (see Fig. 1) in which 24 GSO crystals will be read at the same time. The volume of each cylindrical crystal is 6.77 cm^3 (diameter 2.8 cm, height 1.1 cm) so the total volume of the *detector* material is increased by a factor 163 with respect the previous apparatus. For an optimal coupling with the input coil of the readout SQUID, a 30 turns pick-up coil with $42 \mu\text{H}$ of inductance will be wound on each GSO crystal.

All the pick-up coils will be connected in parallel to form an inductance of $\simeq 1.8 \mu\text{H}$ in order to match the $1.8 \mu\text{H}$ input coil of the SQUID.

Crystals and SQUID are housed in a SnPb superconducting shield immersed in liquid helium. As shown in Fig. 1, the lead *sources*, 24 cylinders with the same dimensions of the GSO crystals, are placed, as near as possible to the bottom of the dewar, on a rotating wheel. The minimum distance between the surface of the lead *sources* and the surface of the GSO *detectors* is about 3 cm. The wheel can rotate up to a maximum frequency of 15 Hz thus producing an axion signal, if any, up to 12×15 Hz. This possibility permits us to tune the expected signal in a portion of the spectrum free from spurious noise (power-line interference, vibrational peaks and so on). When this new experimental apparatus will operate with all the 24 GSO crystals and with the SQUID additive flux noise as the dominant noise source, we should be able to improve the current upper limits on $g_p^e g_s^N$ by a factor of about 5000.

Virgo

Antonio Perreca,[†] Giovanni Prodi, Bruno Giacomazzo, Shubhanshu Tiwari, Giovanni Prodi, Matteo di Giovanni, Andrea Grimaldi, Andrea Miani, Michele Valentini, Anna Puecher

INSTRUMENT SCIENCE The activity of the Trento Virgo Hardware group follows two main research lines.

Optical losses in Gravitational Wave detectors. The first research line is the study of new methods to minimise optical losses in gravitational wave interferometers. This is a prominent research effort for both the current and the future (third generation) gravitational wave interferometers. Indeed, experimental tests have demonstrated how optical losses at the output path are the main limitation on the usage of squeezed light in gravitational wave interferometers, therefore reducing the achievable sensitivity of these detectors.

A source of loss comes from the non-ideal quantum efficiency of the photodetectors located at the output port of the gravitational wave detectors. For this purpose the Trento group developed the photon-recycling technique to optimise the photodetectors quantum efficiency.¹

Additionally the reduction of losses problem is addressed with the minimisation of mode-mismatch between the laser and the optical cavities in the interferometer. With this purpose, in close collaboration with the Padova section of Virgo (INFN), an optical setup was simulated and built at the Laboratori Nazionali di Legnaro (LNL) to test and develop adaptive mode matching systems.

Adaptive Mode matching systems actively detect and correct the mismatch between a laser beam and one or multiple optical cavities. Indeed, the high power circulating in the optical cavities of gravitational wave interferometers often leads to a change in the optical properties of the components over time, therefore requiring an active correction of the mismatch. The core components of an Adaptive Mode Matching system are therefore a detector that gener-

ates an error signal proportional to the mode-mismatch between a laser beam and an optical cavity, and actuators that correct the beam in order to minimise the detected mismatch.

One mode mismatch detection system, based on the usage of an Electro-Optic Lens (EOL), has already been built in Padova and it is currently under testing.

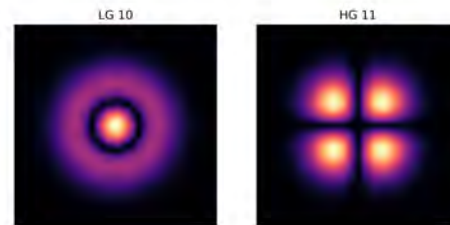


Figure 1: Simulated transverse intensity distribution of a Laguerre-Gauss (LG) 10 mode (on the left) and Hermite-Gauss (HG) 11 mode (on the right) beams.

Another mode-mismatch detector that is being prepared is instead based on a mode-converter device. This device uses cylindrical mirrors to convert the 10 Laguerre-Gauss mode (shown in Fig. 1) generated by the mismatch, into a Hermite-Gauss (HG) 11 mode. If the laser phase is modulated at Radio Frequency (RF), the beating between the HG 11 mode and the Gaussian (HG 00) side-bands can be then detected using RF quadrant photodiodes.

Additionally, several studies are ongoing to develop actuators that are able to provide high range of actuation and low noise.

Longitudinal control of the Signal Recycling Mirror: The second research line involves the design and simulation of the control strategy for the Signal Recycling Mirror (SRM) for the Advanced Virgo detector. The position of the SRM is shown in Fig. 2. The SRM will be commissioned after the O3 observation run that will

[†]Contact Author: antonio.perreca@unitn.it

¹Nagano, K. et al. (2018), Applied Optics 57(13), p. 3372.

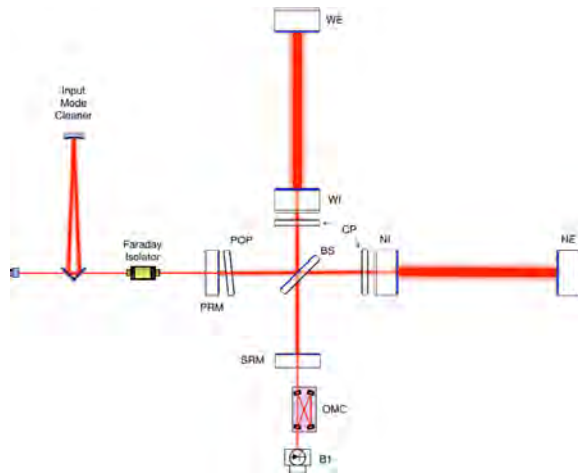


Figure 2: Simplified optical setup of the design Advanced Virgo interferometer. The Signal Recycling Mirror (SRM) is placed at the output (anti-symmetric) port of the interferometer and will be commissioned in year 2020.

last one year, starting in March 2019.

The simulations performed by the Trento Virgo group focus on finding good error signals to control the position of the SRM in a “variable finesse” locking technique and in studying the impact of the addition of the SRM to the other longitudinal control loops of the interferometer.

ANALYSIS AND INTERPRETATION OF THE OBSERVATIONS Our main contributions to the LIGO-Virgo joint activities in data analysis science and interpretation of the observations span from the general role of the Data Analysis Coordinator to more specific achievements related to the investigations of transient gravitational waves and the interpretation of the nature of the observed emission from Neutron Stars.

Preparation to the data analysis for the LIGO-Virgo observation run O3 (2019-2020).

The main new feature prepared for the O3 observation run is the Open Public Alert program (see <https://emfollow.docs.ligo.org/userguide/>). For the first time LIGO-Virgo will issue public alerts triggered by gravitational wave detections with a target latency of a few minutes, to enable the widest possible follow-up investigation with observatories across different messengers. The information released under this program include a broad

classification of the gravitational wave source, its significance in terms of false alarm rate, the reconstructed sky position and, for compact binary coalescences, the distance. The target average purity of the alerts related to compact binary coalescences is $\sim 90\%$. For all other transient sources, the astrophysical rate is yet unmeasured and the threshold is set to a false alarm rate of ~ 1 per year. The status and performances of the detectors can be monitored at www.gw-openscience.org/summary_pages/detector_status/.

Contribution to the study of compact binary coalescences. The most relevant LIGO-Virgo observational result in 2018 has been the publication of the first gravitational wave catalog of transients, GWTC-1² and its related data release (see www.gw-openscience.org/GWTC-1/). Our group contribution to the catalog consisted in the detection with better confidence of the more massive source, GW170729, and on the reconstruction of all the signal waveforms without using morphological assumptions by means of the coherent-WaveBurst pipeline. The comparison of such unmodeled reconstructions to the reconstructions based on an accurate theoretical models of the emission provide crucial evidence for the absence of unexpected signal features. Another main contribution from our group to LIGO-Virgo science has been the search for eccentric binary black hole coalescences. This is as well based on our unmodeled analysis methods, able to detect with the same efficiency low and high eccentricity coalescences, while template based searches are yet limited to low eccentricity ones. The LIGO-Virgo publication will be delivered in 2019.

Contribution to the study of Neutron Stars. Our group is developing data analysis methods to better catch details of detectable signals, aiming to improve the interpretation of general properties of the source, in particular in the case of neutron star emissions from the late inspiral, merger and post-merger phases. In addition the signal models developed within the Numerical Relativity studies are used to inspire and test the data analysis methods.

²Abbott, B. P et al. (2018), arXiv:1811.12907.

Activities starting in 2019

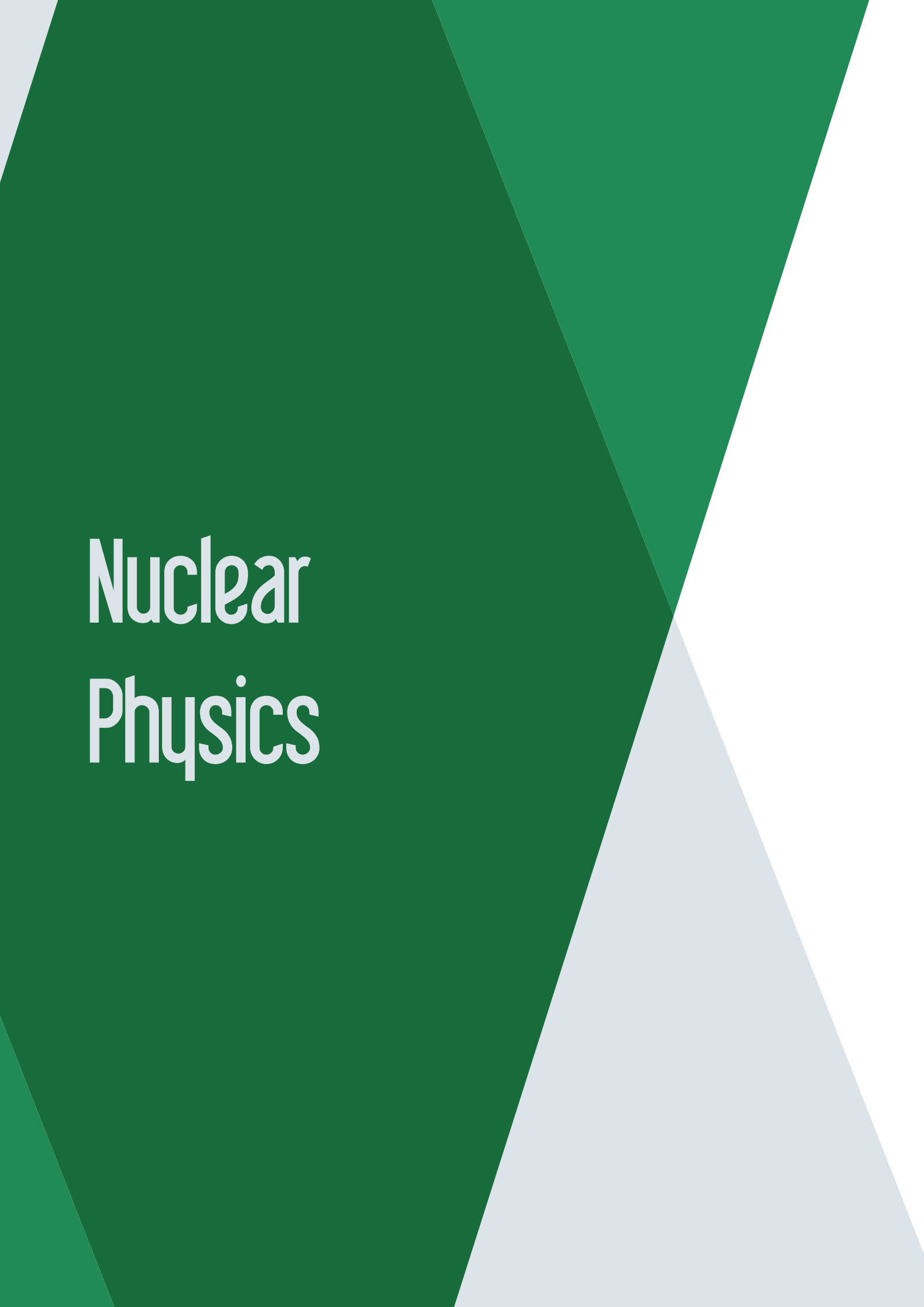
ADHD

Research outline The theoretically predicted antideuteron flux resulting from secondary interactions of primary cosmic rays with the Inter-Stellar medium is expected to be very low and in particular is kinematically suppressed at low energy (sub-GeV). Well motivated theories beyond the Standard Model contain viable dark matter candidates, which could lead to a significant enhancement of the antideuteron flux due to annihilation or decay of dark matter particles. This flux contribution is believed to be relatively large at low energies, where the secondary background is suppressed, which leads to a high interest in the development of new detection signatures for low energy antideuteron. Goal of the Anti Deuteron Helium Detector (ADHD) project is to study the signatures offered by an high pressure He target for the identification of antideuterons in space. In particular exotic atoms are produced by stopping antiprotons/antideuterons in helium gas. The antiparticle spontaneously removes one of the two electrons contained in a normal helium atom, then begins to orbit the helium nucleus in the electron's place. This is expected to happens in the case of few percent of the captures. The antideuteron's orbit, which has a large principal and angular momentum quantum numbers, lies far away from the surface of the helium nucleus inhibiting the annihilation. For the He target, the single existing electron cannot provide (fast) Auger deexcitation channels, moreover it prevents the Stark deexcitation and the (slow) radiative process is the main deexcitation channel. This meta-stability is an unique (and well measured) feature for the He target that is not expected/observed for other target nuclei. The captured antideuteron can thus orbit the He nucleus for tens of microseconds, before finally falling to its surface and annihilating providing a few charged pion tracks. This characteristic delayed annihilation signal in He is a distinctive signature to identify the antimatter nature of the stopping particle. Existing antiproton background can be separated from the antideuteron signal thanks to the half pion multiplicity and velocity vs kinetic energy measurement. Beam test of an high pressure scintillating He detector prototype and Montecarlo simulations are foreseen.

INFN groups TIFPA

Principal Investigator Francesco Nozzoli, TIFPA

TIFPA team Francesco Dimiccoli, Ignazio Lazzizzera, Francesco Nozzoli, Paolo Zuccon



Nuclear Physics

Roberto Sennen Brusa

robertosennen.brusa@unitn.it

Coordinator,
TIFPA Nuclear Physics Activities



At TIFPA, two experimental research groups have activities related to fields concerning INFN National Scientific Committee 3 (CNS3). One group works in the field of antimatter physics carrying out fundamental and applied studies with antihydrogen, positron and positronium at low energy. The second one deals with nuclear fragmentation experiments in an energy range that is of interest for particle therapy. CNS3 funds AEGIS (Antimatter Experiment: gravity, Interferometry, Spectroscopy) and FOOT (FragmentatiON Of Target) experiments.

AEGIS experiment is running at CERN's Antiproton Decelerator (AD). The experiment was designed to perform a direct measurement of Earth's gravitational acceleration on falling antihydrogen to investigate if antimatter falls with the same acceleration as the ordinary matter. If some asymmetry would be found it could help in answering the fundamental question of why only matter, in our universe, survived after the Big Bang. In fact, if a particle collides with its anti-particle they annihilate giving rise to energy and, at the origin of the Universe, it is expected by symmetry that the same amount of matter and antimatter would have been produced. The Trento-TIFPA group was among the main actor for the positron and positronium (Ps) manipulation. In 2018 AEGIS has achieved important milestone towards the production of a pulsed beam of antihydrogen. Antiprotons were captured and manipulated to prepare a cold plasma of antiprotons. Cold positronium was produced in vacuum and excited in Rydberg states. Measurements were run to form antihydrogen by charge exchange between antiprotons and excited positronium (Ps). Moreover, manipulation of Ps yielded as byproduct the development of a long-lived source of metastable Ps atoms that will open the possibility of first interferometry experiments with a pure matter-antimatter leptonic system. Finally, experiment on Ps production at cryogenic temperature were carried out with the slow positron beam set up at the Trento Department of Physics.

The **FOOT experiment** is dedicated to the investigation of target fragmentation processes in a proton therapy scenario. Specifically, the experiment will measure differential cross sections in the typical energy range of interest for proton therapy (i.e. $E < 230$ MeV), thus filling the current gaps in the nuclear fragmentation cross section databases. To reach this goal, FOOT consists in two different setups, one exploiting an emulsion cloud chamber for fragment detection, the other based on the combination of electronic detectors with a magnetic spectrometer. The measurements will be performed with the inverse-kinematic approach, i.e. by investigating the fragmentation of heavier ion beams (e.g. He, C, O) hitting hydrogen-enriched targets. As a consequence, the data collected by FOOT will also be of interest for heavy ion therapy applications, where projectile fragmentation processes deserve accurate description, as well as for space radioprotection. During 2018 extensive detector development and testing has been performed by the collaboration. In this context, the Trento-TIFPA group is responsible for running the Start Counter (250 μ m thickness scintillator) and the Beam Monitor (i.e. a drift chamber) detectors, which are part of both the measurement setups. The activity of 2018 has therefore being dedicated to the study of detector performances, which has been performed at the Trento proton therapy facility. This was an important step toward the shift scheduled for Spring 2019 at GSI (Darmstadt, Germany), where the first data taking based on the emulsion setup will take place.

AEGIS

Francesco Guatieri, Sebastiano Mariuzzi, Andrea Vespertini, Luca Penasa and Roberto S. Brusa[†]

AEGIS (Antimatter Experiment: Gravity, Interferometry, Spectroscopy) is an experiment set up at the antiproton factory at CERN with the aim to investigate experimentally if antimatter obeys to the weak equivalence principle (WEP), or universality of free fall, that states that in vacuum all bodies in gravitational field fall with the same acceleration. The existence of an asymmetry, in the free fall of matter and antimatter, could help to explain why after the Big Bang only matter survives and gives rise to the existing world.

The AEGIS experiment is designed to produce an antihydrogen (\bar{H}) pulsed beam and measure the free fall of \bar{H} in the Earth's gravitational field. The measurement of the gravitational acceleration g on \bar{H} will be performed by measuring the time of flight and the vertical displacement of each \bar{H} after its passage through a moire deflectometer. The AEGIS method is illustrated in Fig. 1. Antiprotons (\bar{p}) delivered by

AD (antiproton decelerator) are slowed down to a few keV passing through a degrader, caught in a Penning-Malmberg trap in the 5 T magnet and then transferred into a second Penning-Malmberg trap in the 1 T magnet where \bar{H}^* is to be formed. Positrons (e^+) are cooled in a two-stage Surko buffer trap and stored in a Penning-Malmberg accumulator delivering e^+ bunches that are transferred to the 1 T magnet where they are injected in a e^+ /Ps (positronium) porous silica converter. The fraction of formed Ps that is cooled by collisions in silica and emitted into vacuum is laser excited to long-lived Rydberg states. Rydberg Ps fly into the antiproton trap, where \bar{H} can be formed in an excited state by the charge exchange reaction: $\text{Ps}^* + \bar{p} \rightarrow \bar{H}^* + e^-$. Excited \bar{H}^* must be Stark accelerated and decays to ground state along its path towards the moire deflectometer. An extra chamber to perform R&D experiments on Ps is connected to the e^+ accumulator.

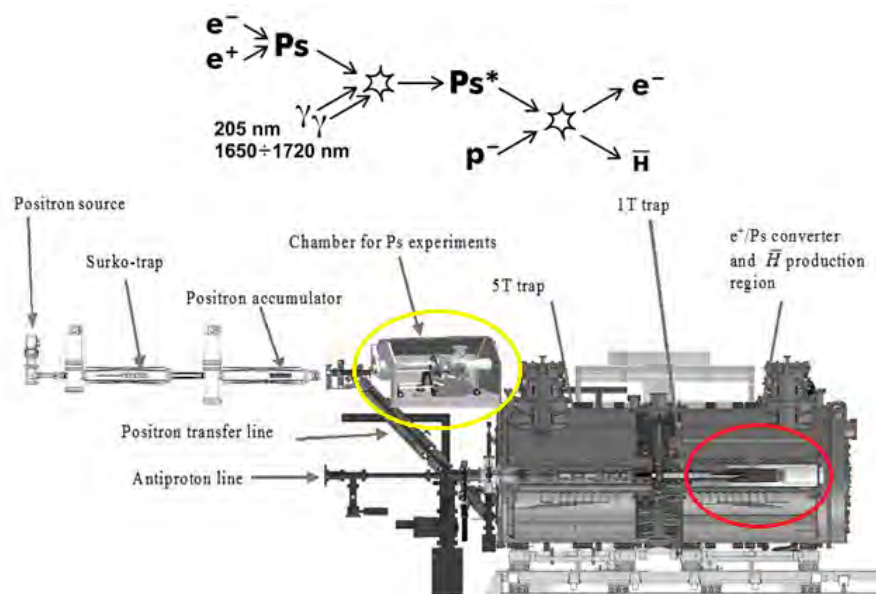


Figure 1: the AEGIS method and the AEGIS experimental set-up for the production of a pulsed cold \bar{H} beam. The chamber for Ps experiments and the \bar{H} production region are indicated by yellow and red circles, respectively.

[†]Contact Author: robertosennen.brusa@unitn.it

Status of the experiment In 2017 procedures for \bar{p} trapping and storage at few hundreds of kelvin were developed and the ability to produce Ps from the converted held at 15 K in the 1 T magnetic field and to laser excite them in Rydberg states via a two-step Ps excitation $1^3S \rightarrow 3^3P, 3^3P \rightarrow \text{Rydberg}$ was demonstrated. The excited Ps was detected with plastic scintillators employing the SSPALS (Single Shot Positron Annihilation Lifetime Spectroscopy) that allows to appreciate the extended lifetime of the Rydberg states.

In 2018 we improved the procedure for trapping \bar{p} in the \bar{H} production trap. Moreover, we re-designed the Ps converter geometry (see Fig. 2) increasing significantly our capability in observing, characterizing and manipulating the Ps cloud in vacuum. The new design also allows to precisely control the lasers alignment using a mesh grid on a MACOR screen.

A new and fast detection technique of excited Ps was developed: excited Ps in front of the target is laser, or field, ionized in flight when reach the gap between the target and the trap (see Fig. 2). Released positrons follow the magnetic field lines with a gyro-radius of about $0.5 \mu\text{m}$ and are imaged onto the MCP (multichannel plate, with intrinsic resolution of $80 \mu\text{m}$) .

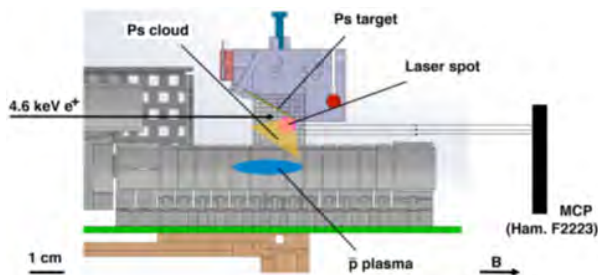


Figure 2: Sketch of the improved experimental layout to produce \bar{H} by charge exchange.

The MCP front face is negatively biased and

images are recorded with a CMOS camera outside the vacuum. The new diagnostic technique permitted to measure the Ps velocity distribution along the laser direction by scanning the wavelength of the laser exciting the $n=3$ level (Fig. 3), and the velocity distribution normal to the target by scanning the time delay between the e^+ implantation in the target and the laser shot.

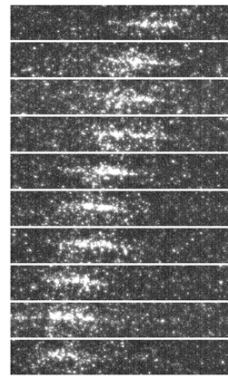


Figure 3: images of spatial distribution in the plane transverse to the 1.0 T field of e^+ freed by Ps photoionization. Each image corresponds to different wavelengths of the UV laser pulse i.e. different component of Ps velocity along the laser direction.

The characterization of the Ps cloud was fundamental for choosing the best parameters to guarantee that Ps fly towards the \bar{p} in the production trap and to select the best velocity to increase the cross section for \bar{H} production.

\bar{H} formation by charge exchange Measurements, running the protocol for searching \bar{H} formation by charge exchange, were done in the last month of 2018. An excess of signal with statistical significance above background, possibly consistent with production of \bar{H} in the first $15 \mu\text{s}$ after the positron injection was measured with plastic scintillators. Data are under analysis.

FOOT

Sofia Colombi, Yunsheng Dong, Marta Rovituso, Chiara La Tessa, Giuseppe Battistoni, Francesco Tommasino[†]

The main goal of the FOOT (FragmentatiOn Of Target) experiment is to measure target and projectile fragmentation differential cross section in the energy range of therapeutic application. These measurements will fill the existing gaps at the energies of interest in the nuclear fragmentation cross section databases, thus allowing the improvement of the accuracy of proton therapy cancer treatments. FOOT will allow a comprehensive characterization of target fragments in terms of double-differential cross sections. So far, this type of measurements were not performed with a systematic approach. In fact, target fragment spectra are peaked at very low energies and therefore they cannot travel distance larger than few microns, thus making their experimental detection extremely difficult. This issue will be handled by FOOT with the use of the inverse kinematic approach, i.e. studying the fragmentation of different ions beams (e.g. He, C, O) onto hydrogen enriched target, such as C₂H₄ (as already adopted in Bertazzoni et al. 2019; Silvestre et al. 2018). Final cross sections are then calculated by subtracting the data obtained from taking into account the interactions between the beam and the target. Secondary fragments in the inverse kinematics reference frame will have boosted energy and longer range, being therefore easier to detect. Considering the accuracy needed in clinics, cross section data must have maximum uncertainty below 5%, together with an energy resolution of the order of 1-2 MeV/u. At the same time, quite strict requirements also hold for the charge and isotopic identification (uncertainty below 3% and 5% respectively).

The FOOT experiment will be based on two alternative setups: a setup exploiting the emulsion chamber capabilities to measure the production in target fragmentation of light charged fragments ($Z \leq 3$); a setup based on electronic detectors and a magnetic spectrometer to iden-

tificate and measure fragments heavier than helium. The TIFPA unit of the FOOT experiment is dedicated to the study and the optimization of the performances of the detectors in the upstream region of both setups, namely the Start Counter (SC) and the Beam Monitor (BM). The initial design of the SC is a 250 μm thick scintillator disk with a radius of 26 mm. The light produced in the scintillator is collected radially by 160 optical fibers grouped in four bundles and readout with 40% quantum efficiency. The thickness of the scintillator was minimized to reduce the pre-target particle interaction probability. The SC, placed 20-30 cm upstream of the target, provides the trigger signal to the whole experiment and the measurement of incoming ion flux to be used for the cross section measurement. It provides the reference time for all the other detectors and allows the TOF measurement in combination with the ΔE scintillator detector. Between the SC and the target, a Drift Chamber acts as a beam monitor, tracking the direction and impinging point of the ion beam on the target. The BM consists of twelve layers of wires, with three drift cells (each cell is 16 mm \times 10 mm) per layer. Planes with wires oriented along the x and y axes are alternated in such a way to reconstruct the beam profile.



Figure 1: Drift Chamber and plastic scintillators used at the Trento Proton Therapy center for the experiment.

[†]Contact Author: francesco.tommasino@unitn.it

Experimental tests at the Experimental Room of the Trento Proton Therapy center were performed for the characterization and the performance assessment of the BM according to the FOOT requirements. The detector was filled with a mixture of Ar/CO₂ at 80/20% and the internal pressure of the gas mixture was 0.9 Bar, controlled by a fluxing system placed inside the irradiation room. Two thin plastic scintillators placed downstream the BM provided the trigger signal and the 36 channel signals of the BM were acquired with a Caen TDC v1190B. The isocenter was placed at the BM entrance window (e.g. 125 cm from the beam exit window), see Fig. 1.

The BM was irradiated with a proton beam of different energies from 70 MeV up to 228 MeV. We also placed a 2.5 mm layer of tantalum in front of detector entrance window in order to reach a lower beam energy and irradiate the whole surface of the BM. The detector efficiency as a function of the high voltage was investigated. The results were in good agreement with the data obtained in a previous experiment¹ (Fig. 2).

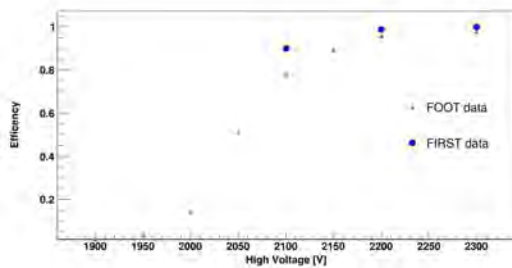


Figure 2: Efficiency as a function of the high voltage for the FOOT experiment and for the FIRST experiment data.

Selected Papers

Bertazzoni, M. et al. (2019). *Development and characterization of a δE -TOF detector prototype for the FOOT experiment*. Nuclear Instruments and Methods in Physics Research Section A **916**, pp. 116–124.

Silvestre, G. et al. (2018). *Evaluation of double-sided silicon microstrip sensor for the FOOT experiment*. Nuclear Instruments and Methods in Physics Research Section A.

The beam spot at different energies was correctly reconstructed by the BM and the reconstructed beam sigma was consistent with a previous beam characterization² (Fig. 3).

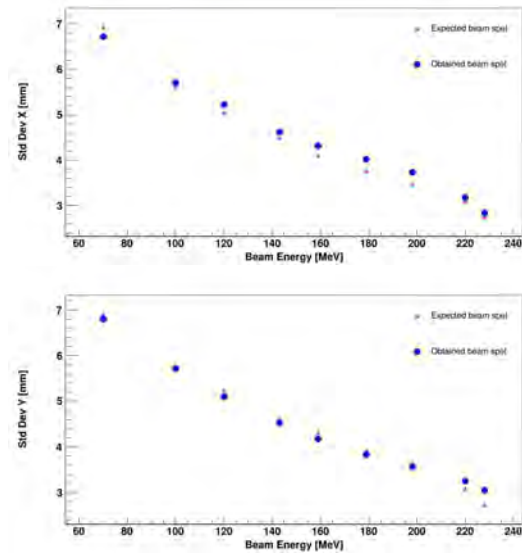
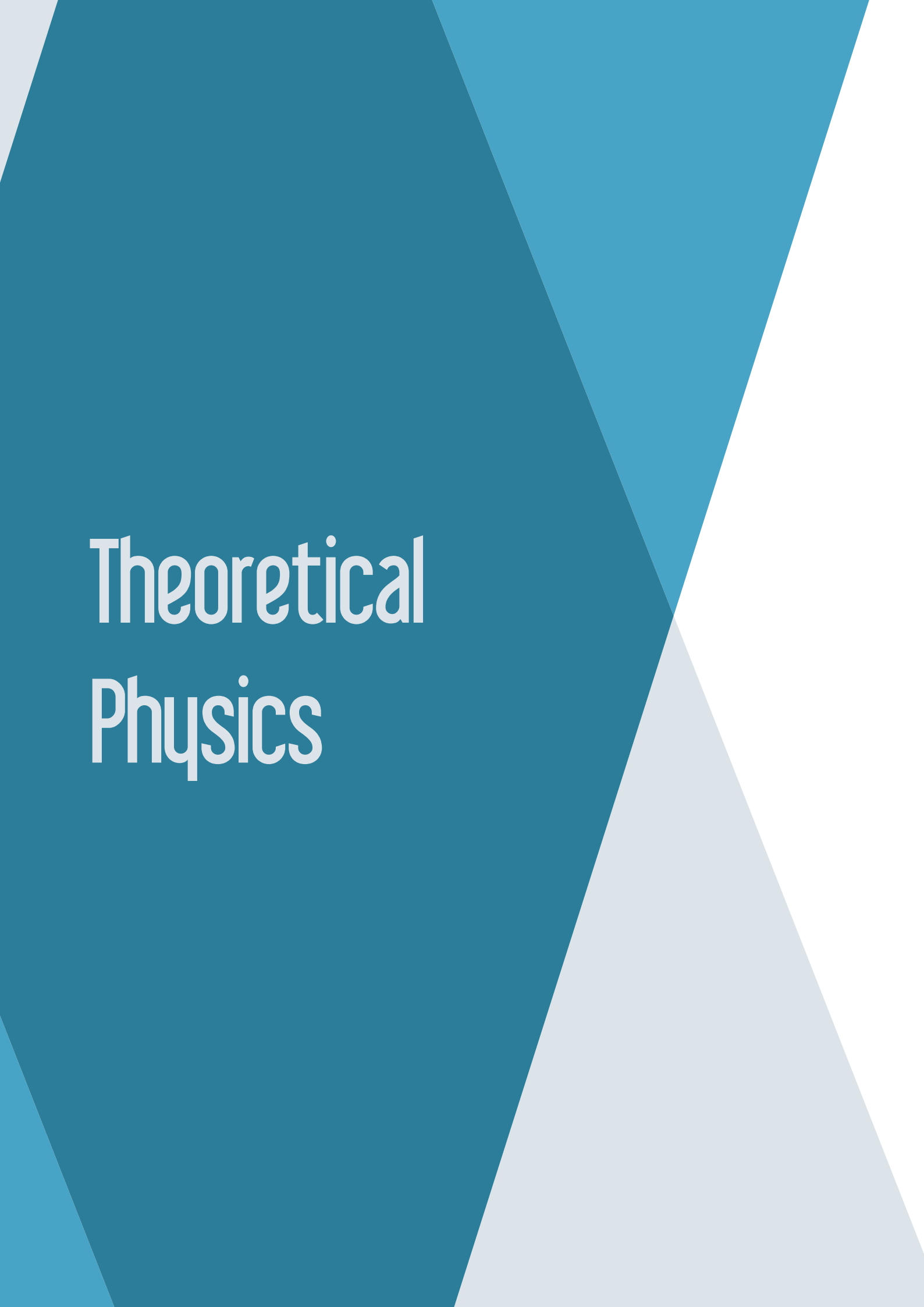


Figure 3: Sigma of the beam at the Proton Therapy center expected from the previous measurements and obtained with the Beam Monitor detector.

Further work will be dedicated to an improved calibration of the space-time relations at the level of single cells. An external tracker will be used to this purpose, providing information about the entrance and exit point of the particles inside the BM and then make the track reconstruction more precise. Experimental tests on the BM will be performed on the coming months in the same Experimental Room. In 2019 the first data taking of the FOOT experiment will take place at GSI (Germany), based on the emulsion chamber setup.

¹Paoloni, A. et al. (2012), SciVerse ScienceDirect **37**, pp. 1466–1472.

²Tommasino, F. et al. (2017), NIM **869**, pp. 15–20.

The background features abstract geometric shapes in various shades of teal and light blue, set against a white background. The shapes are angular and layered, creating a modern, minimalist aesthetic.

Theoretical Physics

Francesco Pederiva

francesco.pederiva@unitn.it

Coordinator,
TIFPA Theoretical Physics Activities



The theory group at TIFPA in 2019 saw a further expansion in its composition. We had the pleasure to welcome Dr. Raffaello Potestio, an expert of computer simulation of biomolecules. This new entry reinforces this research line that has demonstrated very successful, and that has been recognised by CSN4 as strategic, together with the studies related to Quantum Science and Information and Quantum Computing, as an opening towards more interdisciplinary subjects. Two post-docs joined the theoretical group, Lorenzo Sebastiani in the gravitation and cosmology group (FLAG), who joined within the INFN foreign post-docs program, and Federico Cipolletta in the gravitational simulations group TEONGRAV, funded by an initiative relative to high performance computing.

New proposals in theoretical physics are discussed within INFN every three years. Since the last call was in 2017, there has been no major change in the composition of the scientific research of our group.

TIFPA has a strong group of people working on the theory of fundamental interactions. In particular there is a unit carrying on modern views and perspectives in gravitation and cosmology (FLAG), and one working on the numerical solution of General Relativity equations related to the investigation of gravitational waves emission (TEONGRAV).

Nuclear physics has always played an important role in Trento. The structure and dynamics of nuclei, and the connections of nuclear theory to stellar physics and the more fundamental quantum chromodynamics theory are investigated with modern few-body (FBS) and many-body (MANY-BODY) numerical techniques.

An interesting development occurred after the establishment of TIFPA was the creation of a research team within the Mathematics Department working on fundamental aspects of quantum theory and extensions of quantum field theory in curved spaces (BELL).

Partly connected to the research in QSI is the activity of the ECT*-LISC group, which has a branch interested in various aspects of modern condensed matter physics, within the NEMESYS group.

The TIFPA theory group has always been connected to the INFN experimental activity in Italy and abroad, and is open to the new developments and new challenges brought by the center. Presently it counts 40 researchers. About half of them are University of Trento, FBK, INFN and other institutions staff members, and rest are M.Sc. and Ph.D. students, and post-docs.

BELL

Valter Moretti,[†] Romeo Brunetti, Riccardo Ghiloni, Sonia Mazzucchi, Alessandro Perotti, Davide Pastorello, Nicolò Canginiotti, Alberto Melati, Marco Oppio

BELL research group at TIFPA studies various foundational, axiomatic and mathematical topics of Quantum Theories, also in relation with quantum field theory and quantum gravity. Mathematical advanced technologies are exploited to solve difficult problems of theoretical physics or to construct physically significant, non-trivial, mathematical models, completely solvable which can be used as starting points for physical applications. During 2017-2018 we published several research papers on international research journals, a monograph is in print. Just to have a (not exhaustive) look of our intensive production we focus attention on three relevant papers about three corresponding topics of mathematical methods for physics.

Foundational Aspects of Quantum Theories

The paper (Moretti and Oppio 2019) concerns a longstanding issue about the formulation of quantum theories in complex Hilbert spaces continuing the research line of the last years. As is known from a famous 1995 theorem by Solér and an earlier conjecture by von Neumann himself, quantum theories can be formulated into real, complex or quaternionic Hilbert spaces. However up to now no quantum systems with real or quaternionic formulations are known. What is the physical reason for the absence of these systems though permitted by the general mathematical theory? In 2017, Moretti and Oppio discussed the real Hilbert space case, this paper concludes the discussion establishing that also the quaternionic formulation is ruled out by Poincaré symmetry. This is done also correcting the quaternionic formulation of the celebrated Gleason's theorem stated by Varadarajan in 1968, finding in particular that only the

real part of the trace is relevant in the three formulations of quantum mechanics when computing probability transitions and expectation values.

Quantum Field Theory in Curved Spacetime

Renormalization affects QFT in flat and curved spacetime. The problem is particularly relevant in curved spacetime where the finite renormalisation counterterms may have an important role, e.g., as source of the semiclassical gravitational field. In (Khavkine et al. 2019), Khavkine, Melati and Moretti tackled the problem of classification of the counterterms of Wick products of a generic bosonic (vectorial) quantum field theory, proving that these objects obey a classification theorem as soon as a list of physically meaningful axiomatic requirements are assumed, in particular a smoothness requirement which makes weaker a previous assumption by Hollands and Wald. This paper is the completion of a research programme started by Khavkine and Moretti some years ago.

Functional Integration Methods for Physical Theories

One of the most challenging mathematical-physics problems of ever is finding rigorous formulations of the various pervasive and powerful methods in physics based on functional integration technologies. The paper (Albeverio et al. 2018) deals with some advances in this field of research. This joint work by S. Albeverio, N. Canginiotti and S. Mazzucchi discusses some new applications of the said technology to the construction of a functional integral representation for solutions of a general class of higher-order heat-type equations with physical relevance.

[†]Contact Author: valter.moretti@unitn.it

Selected Papers

- Albeverio, S., Mazzucchi, S., and Cangiotti, N. (2018). *Generalized Feynman path integrals and applications to higher-order heat-type equations*. *Expositiones Mathematicae* **36**(3), pp. 406–429.
- Khavkine, I., Melati, A., and Moretti, V. (2019). *On Wick polynomials of boson fields in locally covariant algebraic QFT*. *Ann. Henri Poincaré* **20**, pp. 1000–1030.
- Moretti, V. and Oppio, M. (2019). *Quantum theory in quaternionic Hilbert space: How Poincaré symmetry reduces the theory to the standard complex one*. *Reviews in Mathematical Physics* **31**, p. 1950013.

BIOPHYS

Pietro Faccioli,[†] Giovanni Garberoglio, Gianluca Lattanzi, Raffaello Potestio, Gianfranco Abrusci, Simone Orioli, Michele Turelli

The research activity of the BIOPHYS unit concerns in general the development, testing and application of a wide range of theoretical methods to investigate the dynamics of complex systems both in and out of thermal equilibrium.

In addition to investigating the dynamics of biomolecules, our unit is also active in modeling, simulating and optimizing organic-based or bio-mimetic polymer-based systems which can be tuned and designed to achieve the desired opto-electronic properties. For example, we study charge mobility of organic based semiconductors or energy transfer efficiency in bio-mimetic materials to be employed solar cell technology.

Coarse-Grained and Multi-Scale Hamiltonians We continued developing coarse-grained and multi-scaled representations of proteins whose resolution is different in different regions, in order to provide the highest detail only where necessary (Heidari et al. 2018c). This is also the overarching objective of Potestio's ERC project VARIAMOLS - variable resolution algorithms for macromolecular modelling (see Fig. 1).

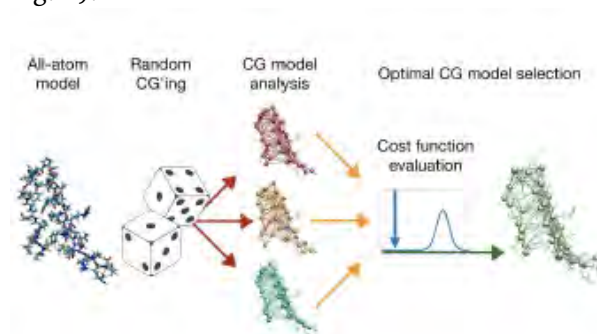


Figure 1: Illustration of a multi-scale approach developed by Potestio and co-workers

Non-Equilibrium Statistical Mechanics and Enhanced Transition Path Sampling Techniques Reactive processes, such as conformational transitions of biomolecules are intrin-

sically non-equilibrium processes. The need for a rigorous theoretical description recently led to the establishment of a framework called Transition Path Theory (TPT). In 2018, our unit showed how the relevant statistical distributions of TPT can be very efficiently computed through specific type of biased Molecular Dynamics (MD) simulations, with a computational cost which is exponentially smaller than of plain MD (Bartolucci et al. 2018). The reduction of the huge amount of data emerging from computer simulations of biomolecular dynamics provide a prototypical example of big data problem. Our unit, in collaboration with the team led by Prof. A. Laio at SISSA, has worked towards developing an unsupervised scheme to perform reliable data reduction of molecular simulation data in order to identify the kinetically relevant meta-stable states (Markov Macro-States). This is an intrinsically multi-disciplinary project which involves combining concepts and tools of differential geometry, renormalization group (RG) techniques, non-equilibrium statistical mechanics and machine learning algorithm.

Applications to Biophysics The theoretical methods and models developed in our unit have been extensively tested and applied in a number of studies focused on specific biophysical systems. These research lines have been carried out within close collaboration with our experimental colleagues, and included: the study of ion transport in aqua-poring membrane proteins; the predictions of time-resolved (linear and non-linear) spectroscopy observables to investigate exciton energy transfer in photosynthetic complexes; and protein folding, specifically the study of the misfolding pathway of prion proteins, which are involved in the formation of pathogenic fibrils, and the folding of topologically complex (knotted) proteins.

[†]Contact Author: pietro.faccioli@unitn.it

Applications to Material and Molecular Science

We have developed and published a statistical mechanical model which enables to predict the charge mobility of organic semiconductors with complex morphology (Segatta et al. 2018b) (see Fig. 2). We also reported on a new method to compute *ab-initio* virial coefficients of molecules with no uncontrolled approximation. The method has been validated on water and used to calculate virial coefficients of heavy water.

We published works concerning the characterization of a family of graphene-based microporous materials as well as their performance in common adsorption task. We also studied numerically a novel form of carbon nanofoam and ore-shell SiC-SiO_x nanowires.

Technological Transfer and Translational Research

Some of the original theoretical approaches and computational algorithms for molecular simulations developed within the BIOPHYS SI have been applied to translational research in collaboration with scientists at the Physics Department and at the Centre for Integrative Biology of Trento University and of the Department of Pharmaceutical Chemistry of Perugia University. This research led to a patent

of an innovative protocol for computer aided rational drug discovery. 50% of the corresponding Intellectual Property (IP) is currently own by INFN. The filing of additional patent covering a pharmaceutically relevant small molecule discovered with such an innovative method is presently under filing. INFN will own 30% of the corresponding IP. INFN-TT participates to this translational research also through a R4I 2019 grant, awarded to Pietro Faccioli.

Sibylla Biotech SRL is a research startup founded to exploit and further develop this technology. This company has acquired the status of INFN-TT spinoff and research startup of Trento University.

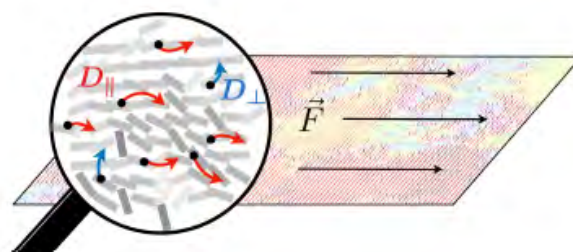


Figure 2: Illustration of the statistical mechanical model used to compute charge mobility in organic semiconductors with complex morphology.

Selected Papers

- Bartolucci, G., Orioli, S., and Faccioli, P. (2018). *Transition Path Theory from Biased Simulations*. J. Chem. Phys. **149**.
- Heidari, M., Kremer, K., Cortes-Huerto, R., and Potestio, R. (2018c). *Spatially Resolved Thermodynamic Integration: An Efficient Method To Compute Chemical Potentials of Dense Fluids*. J. Chem. Theor. Comput. (in press).
- Segatta, F., Lattanzi, G., and Faccioli, P. (2018b). *Predicting Charge Mobility of Organic Semiconductors with Complex Morphology*. Macromolecules **51**(21), pp. 9060–9068.

FBS

Giuseppina Orlandini,[†] Winfried Leidemann, Paolo Andreatta

The research activity in the year 2018 has evolved in two different directions. On the one hand we have turned our attention to the prospects of the present and future generation of neutrino oscillations experiments. In fact our expertise in *ab initio* calculations of perturbative induced reactions in the few-body continuum (see Rocco et al. 2018a, and references therein), can give a valuable contribution to the data analysis. In a work of few years ago we had also shown that, when the few-body calculations are carried out in a proper reference frame, the results obtained from the full solution of the Schroedinger equation can be stretched to higher energy and momentum transfer, in the kinematical regions of neutrino-experiments. Proof of the reliability of our approach has been obtained by the successful comparison between theoretical and experimental results on electron scattering cross sections of ${}^4\text{He}$ in the quasi elastic peak region (see Fig. 1) (Leidemann 2018). The non relativistic *ab initio* results have been obtained within the integral transform method, benchmarking different kernels and methods. Such results offer a promising prospect for the data analysis of neutrino-oscillation experiments that requires an accurate description of nuclear dynamics in which relativistic effects are fully accounted for.

Another direction of our research has been the development of the Non Symmetrized Hyperspherical Harmonics (NSHH) code, created in the last two-three years, which has been extended to perform full diagonalization of the Hamiltonian on the HH basis, for systems composed of a mixture of distinguishable and undis-

tinguishable particles. In particular we have devoted it to the treatment of ${}^9\text{Be}$ as an $\alpha - \alpha - n$ system. The interest in ${}^9\text{Be}$ lays on the fact that it could play a non negligible role in the ${}^{12}\text{C}$ nucleosynthesis, alternative to the most famous three-alpha process. Results have been obtained for an effective field theory (EFT) potential, developed for that scope, taking advantage of the clear separation of scales between α and ${}^9\text{Be}$ excitations. Such results will be part of the Ph.D. thesis of Paolo Andreatta.

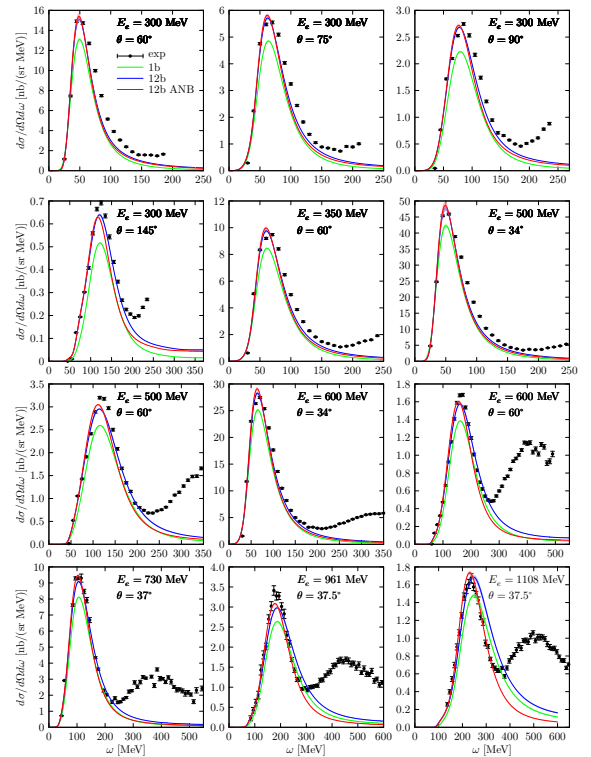


Figure 1: (e,e') cross sections on ${}^4\text{He}$. Complete calculation: red line.

Selected Papers

- Leidemann, W. (2018). *Ab initio calculations for non-strange and strange few-baryon systems*. J. Phys.: Conf. Ser. **981**, pp. 1–12.
- Rocco, N., Leidemann, W., Lovato, A., and Orlandini, G. (2018a). *Relativistic effects in ab-initio electron-nucleus scattering*. Phys. Rev. C **97**, p. 055501.

[†]Contact Author: giuseppina.orlandini@unitn.it

FLAG

Luciano Vanzo,[†] Sergio Zerbini, Massimiliano Rinaldi, Lorenzo Sebastiani, Aimeric Colleaux, Stefano Chinaglia, Alessandro Casalino, Silvia Vicentini

Scientific Activity Most of the research activity 2018 focussed on the following research areas:

- (i) quantum corrections to scale invariant models of inflation,
- (ii) the information complexity of Black holes,
- (iii) Horndeski theories, mimetic gravity and applications,
- (iv) the nature of dark energy (and possibly of dark matter),

(i) This is still work in progress, with a draft for a paper already prepared. In summary, a scale invariant model of inflation proposed in the late 2016 has been considered as the background for a one-loop quantum corrected solutions. A master thesis was assigned and completed on this topic during 2018, on the supervision of M. Rinaldi and L. Vanzo. Renormalization group analysis has been performed. Thesis by S. Vicentini, (U. of Trento) - *Quantum corrections to a scale invariant classical model of inflation with spontaneous symmetry breaking*.

(ii) The rate of action growth is a measure of the information complexity of black holes. The general form of the action growth for a large class of static black hole solutions in modified gravity which includes $F(R)$ -gravity models was computed (Sebastiani et al. 2018). The cases of black hole solutions with non constant Ricci scalar was also considered, generalizing the results previously found and valid only for black holes with constant Ricci scalar. An argument was put forward to provide a physical interpretation of the results, which seem tightly connected with the generalized second law of black hole thermodynamics.

(iii) In 2018 some of us mainly worked in Mimetic gravity and its viability in light of the constraints on the speed of lights discovered with the neutron stars merger event GW170817

(Casalino et al. 2018; Casalino et al. 2019). Dr. Rinaldi also studied a particular aspect of the Jordan frame - Einstein frame equivalence and the viability of a sector of Horndeski gravity in cosmology (Rinaldi 2018). Special solutions of this theory with spherical symmetry has been obtained (Sebastiani 2018), with the aim of studying corrections to black holes and neutron stars.

(iv) The fundamental and difficult problem of tracing out the origin of the dark energy component responsible for the current accelerated expansion of the world, is always at the center of the interest of members of the FLAG initiative, here in TIFPA as well elsewhere. And apart from modified classical gravity models, a line of research is been pursued on the role of quantum effects due to conformal scalars, which is still work in progress. The Euclid group is the experimental counterpart, to which one of us, M. Rinaldi, belongs as a founder member (see Amendola et al. 2018). Non polynomial extension of the Einstein-Hilbert action with the same purpose are to be found in joint work with A. Colleaux (Colléaux et al. 2018).

MSc thesis - On these research fields few master thesis have been assigned during 2018:

- *Quantum corrections to a scale invariant classical model of inflation with spontaneous symmetry breaking*, by S. Vicentini, (U. of Trento).
- *Numerical study of quantum correlations in a Lorentzian spinfoam geometry*, by F. Gozzini, (U. of Trento, in collaboration with Dr. F. Vidotto, U. of Basque Country).
- *Spectral indices in a scale invariant $f(R, \phi)$ -theory*, by L. Zoldan, (U. of Trento).
- *A special class of vacuum solutions in $f(R)$ -gravity*, by Marco Calzà, (U. of Trento,

[†]Contact Author: luciano.vanzo@unitn.it

in collaboration with Dr. L. Sebastiani, TIFPA-INFN).

We add also some outreach activity in secondary schools, due to Rinaldi:

- 5 Mar 2018 public talks “Un secolo di relatività”, Liceo Prati, Trento, Italy.

- 9 Feb 2018 High-school level seminar “Un secolo di relatività”, Istituto Fermi, Mantova, Italy.

Seminar and Events A number of talks have been delivered at conferences, the complete list is available at p. 156.

Selected Papers

Casalino, A., Rinaldi, M., Sebastiani, L., and Vagnozzi, S. (2018). *Mimicking dark matter and dark energy in a mimetic model compatible with GW170817*. Phys. Dark Univ. **22**, p. 108.

Sebastiani, L., Vanzo, L., and Zerbini, S. (2018). *Action growth for black holes in modified gravity*. Phys. Rev. **D97**(4), p. 044009.

MANYBODY

Francesco Pederiva,[†] Alessandro Lovato, Maurizio Dapor, Simone Taioli, Lorenzo Andreoli, Luca Riz

The TIFPA unit of the MANYBODY collaboration pursues development and applications of quantum many-body techniques to both systems of interest for nuclear physics and nuclear astrophysics (Lovato, Riz, Andreoli, Pederiva), and applications to condensed matter physics (Dapor, Taioli, Pederiva). The methods toolbox is quite diverse, ranging from Quantum Monte Carlo and transport Monte Carlo to density functional theory and direct diagonalization of the Hamiltonian.

Quasi-elastic neutrino scattering is an important aspect of the experimental program to study fundamental neutrino properties including neutrino masses, mixing angles, mass hierarchy, and charge-conjugation parity (CP)-violating phase. Proper interpretation of the experiments requires reliable theoretical calculations of neutrino-nucleus scattering. We recently published an article reporting on our GFMC calculations of response functions and cross sections by neutral-current scattering of neutrinos off ^{12}C (Lovato et al. 2018). These calculations are based on realistic treatments of nuclear interactions and currents, the latter including the axial, vector, and vector-axial interference terms crucial for determining the difference between neutrino and antineutrino scattering and the CP-violating phase. Consistently with our electromagnetic responses calculations, we find that the strength and energy dependence of two-nucleon processes induced by correlation effects and interaction currents are fundamental to provide the most accurate description of neutrino-nucleus scattering in the quasi-elastic regime. This year, we have implemented and optimized the charged-current subroutines in the GFMC code. Our results have been successfully checked by making a thorough comparison with a fully independent code, based on the hyperspherical-harmonics formalism. We have computed the

charged-current Euclidean responses ^{12}C for five values of the momentum transfer, namely $q = 100, 200, 300, 500, 700$ MeV. We will now employ the maximum entropy algorithm to retrieve the energy-dependence of these responses, allowing us to compute the cross section for both neutrino- and antineutrino- ^{12}C scattering.

The study of neutrino propagation in infinite nucleonic matter is a key ingredient to determine the cooling of neutron stars and to shed light on the supernovae explosion mechanism. These processes, characterized by a lower energy scale than those typically involved in neutrino-oscillation experiments, requires an accurate modeling of nuclear dynamics, which also encompasses the excitation of collective modes. We computed the longitudinal and transverse density- and spin-density response functions in pure neutron matter (PNM) over a wide range of densities within the Time Dependent Local Spin Density Approximation (Riz et al. 2018). The underlying density functional was derived from an auxiliary field Diffusion Monte Carlo computation of the equation of state of unpolarized and fully spin polarized pure neutron matter. In order to assess the dependence of the results on the specific underlying nucleon-nucleon Hamiltonian, we used both the phenomenological, and local chiral forces up to next-to-next to leading order. The resulting response function has then been applied to the study of the neutrino mean free path.

In most simulations of non-relativistic nuclear systems, the wave functions found solving the many-body Schrödinger equations describe the quantum-mechanical amplitudes of the nucleonic degrees of freedom. In those simulations, pionic contributions are encoded in nuclear potentials and electroweak currents, and they determine the low-momentum behavior.

[†]Contact Author: francesco.pederiva@unitn.it

In our recent work (Madeira et al. 2018) we presented a novel quantum Monte Carlo formalism in which both relativistic pions and non-relativistic nucleons are explicitly included in the quantum-mechanical states of the system. We computed the renormalization of the nucleon mass as a function of the momentum cut-off, an Euclidean-time density correlation function that deals with the short-time nucleon diffusion, and the pion cloud density and momentum distributions. In the two-nucleon sector, we have shown that the interaction of two static nucleons at large distances reduces to the one-pion exchange potential (see Fig. 1) and we fit the low-energy constants of the contact interactions to reproduce the binding energy of the deuteron and two neutrons in finite volumes. We are currently studying $A = 3, 4$ nuclei and we do not envision conceptual difficulties in extending the method up to nuclei as large as ^{12}C .

As previously mentioned, the activity of the MANYBODY group, also encompasses applications to other fields. Particularly important is the research in condensed matter theory. A substantial part of this work is developed within the ECT*-LISC unit, whose activity are described elsewhere. However, the group also deals with the development of novel Quantum Monte Carlo techniques, such as the recently introduced Configuration Interaction Monte Carlo (CIMC), or general algorithms to deal with spin-dependent Hamiltonians. In this context, the first natural applications are on Coulombic systems, and therefore part of our scientific production did and will concern ap-

plications to many-electron systems such as the electron gas or atoms and molecules.

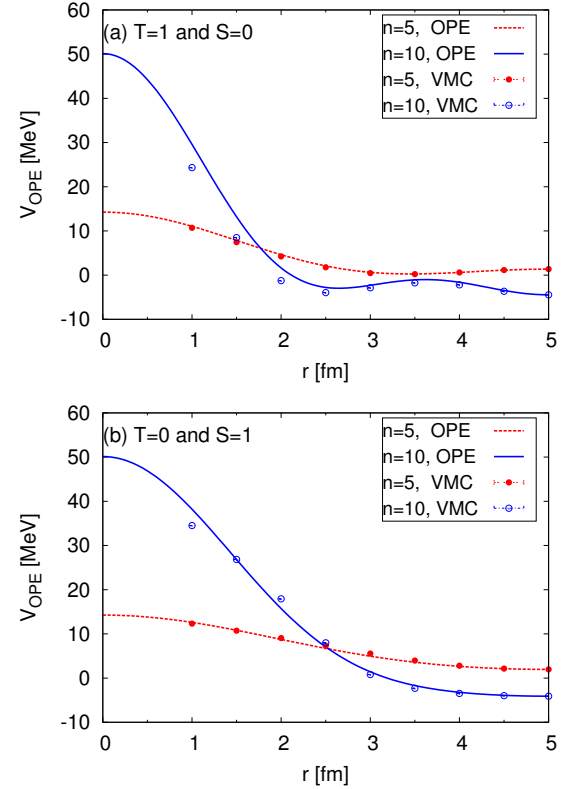


Figure 1: One-pion exchange potential for two nucleons a distance r apart along in the $T = 1, S = 0$ channel (upper panel) and $T = 0, S = 1$ channel (lower panel). The points (VMC) correspond to our variational results obtained explicitly including the pionic fields for two values of the regulator; the softer corresponding to the full red circles and the stiffer to the open blue circles. For comparison the analytic curves describing the one-pion exchange potential in a box for the same values of the regulator as the VMC are also shown.

Selected Papers

- Lovato, A., Gandolfi, S., Carlson, J., Lusk, E., Pieper, S. C., and Schiavilla, R. (2018). *Quantum Monte Carlo calculation of neutral-current ν - ^{12}C inclusive quasielastic scattering*. Phys. Rev. **C97**(2), p. 022502.
- Madeira, L., Lovato, A., Pederiva, F., and Schmidt, K. E. (2018). *Quantum Monte Carlo formalism for dynamical pions and nucleons*. Phys. Rev. **C98**(3), p. 034005.
- Riz, L., Pederiva, F., and Gandolfi, S. (2018). *Spin response and neutrino mean free path in neutron matter*.

NEMESYS

Simone Taioli,[†] Maurizio Dapor

A novel theoretical and computational method for computing electroweak β -decay spectra of medium and heavy-mass nuclei, as well as the electronic structure of atomic and molecular systems was developed (Morresi et al. 2018b). Starting from the phenomenological electroweak interaction of the Standard Model, a general expression of the β -decay rate was derived. Relativistic effects are taken into account by solving the many-electron Dirac–Hartree–Fock (DHF) equation from first-principles. Furthermore, an extension of this approach to include the nucleon–nucleon interaction at the same level of theory of the electronic correlations has been devised. It was shown that post-collisional effects, and to a lesser extent the electronic exchange and correlation, can modify significantly the cross-section only at low energies (< 10 keV), while nuclear correlations considerably affect the lineshape of both the absorption and emission spectra particularly in odd-odd nuclear transitions, where the independent particle approximation, on which the nuclear shell model is framed, is more likely to fail. These findings demonstrate the importance of moving beyond the independent particle picture to obtain an accurate description of the experimental data by adding the many-body correlations between the spectator and participant hadrons and leptons involved in the decay. The application of our approach to a number of test cases, such as the modeling of β -decay of ^{36}Cl , ^{63}Ni , ^{129}I , ^{210}Bi , ^{241}Pu and of the electron capture of $^{138}\text{La}^{3+}$, leads to an extremely good agreement with the relevant experimental data.

Furthermore, the extension of this method to atomic and molecular systems by calculating the electronic structures of $^{138}\text{La}^{3+}$ and several isomers (MgCN, MgNC) and molecules (HMgCN, MgCNO, and BrCF_3) relevant to astrophysical scenarios is presented. This method, which is capable to deal with both

nucleonic and electronic degrees of freedom, has far-reaching implications also in neutrino physics and nuclear astrophysics. This work gained the journal cover of *Advanced: Theory & Simulations* (see Fig. 1)

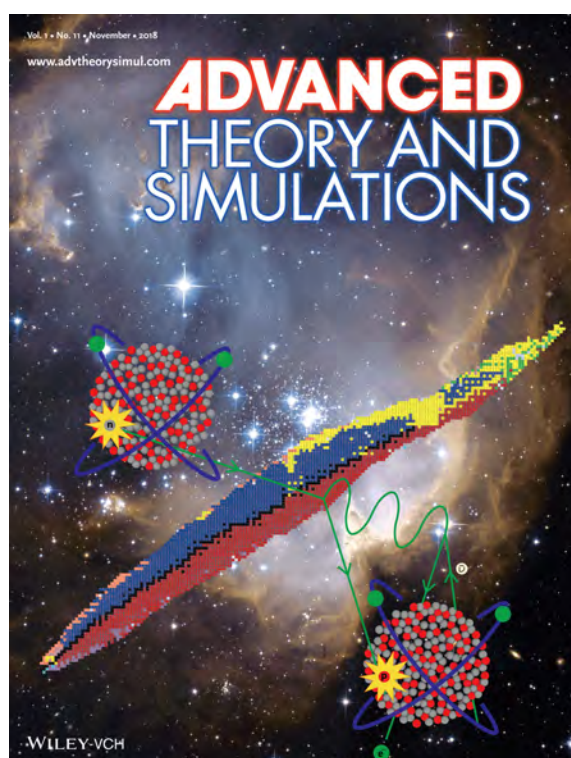


Figure 1: The journal cover of *Advanced Theory & Simulations* presenting our work on the relativistic theory of nuclear β -decay in heavy-nuclei

Second, we studied Pillared Graphene Frameworks (PGF), which are a novel class of microporous materials made by graphene sheets separated by organic spacers. One of their main features is that the pillar type and density can be chosen to tune the material properties. In this work, in particular we presented a computer simulation study of adsorption and dynamics of H_2 , CH_4 , CO_2 , N_2 and O_2 and binary mixtures thereof, in PGFs with nitrogen-containing organic spacers. In general, we find

[†]Contact Author: taioli@ectstar.eu

that the amount of gas adsorbed is an increasing function of pillar density in the low pressure (< 10 bar) regime while at higher pressure the opposite trend is observed. Good performance for the gas separation in CH_4/H_2 , CO_2/H_2 and CO_2/N_2 mixtures was found, with values comparable to those of MOF and ZIF.

Third, we presented a computational method, based on the Monte Carlo approach, for calculating electron energy emission and yield spectra of metals (Azzolini et al. 2018a). The calculation of these observables proceeds via the Mott theory with a DHF spherical potential to deal with the elastic scattering processes, and by using the Ritchie dielectric approach to model the electron inelastic scattering events. The dielectric function, which is needed to evaluate the electron energy loss, is obtained from experimental REEL spectra. The generation of secondary electrons upon ionization of the samples is also implemented in the calculation. A remarkable agreement is obtained between both theoretical and experimental electron emission spectra and yield curves.

Fourth, we combined sub-20 fs transient absorption spectroscopy with state-of-the-art computations to study the ultrafast photoinduced dynamics of trans-azobenzene (AB). We are able to resolve the lifetime of the $\pi\pi^*$ state, whose decay within ca. 50 fs is correlated to the buildup of the $n\pi^*$ population and to the emergence of coherences in the dynamics, to date unobserved. Nonlinear spectroscopy simulations call for the CNN in-plane bendings as the active modes in the subps photoinduced coherent dynamics out of the $\pi\pi^*$ state. Radiative to kinetic energy transfer into these modes drives the system to a high-energy planar $n\pi^*/$ ground state conical intersection, inaccessible upon direct excitation of the $n\pi^*$ state, that triggers an ultrafast (0.45 ps) nonproductive decay of the $\pi\pi^*$ state and is thus responsible for the observed Kasha rule violation in UV excited trans-AB. On the other hand, cis-AB is built only after intramolecular vibrational energy redistribution and population of the NN torsional mode.

Fifth, we proposed a realistic model of nanometer-thick SiC/SiO_x core/shell

nanowires (NWs) using a combined first-principles and experimental approach (Morresi et al. 2018d). SiC/SiO_x core/shell NWs were first synthesised by a low-cost carbothermal method and their chemical-physical experimental analysis was accomplished by recording X-ray absorption near-edge spectra (XAS). In particular, the K-edge absorption lineshapes of C, O, and Si are used to validate our computational model of the SiC/SiO_x core/shell NW architectures, obtained by a multiscale approach, including molecular dynamics, tight-binding and density functional simulations.

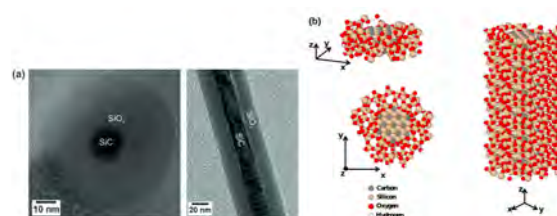


Figure 2: (a) TEM images of a SiC/SiO_x core/shell NW in axial view (left panel) and cross-sectional view (right panel). (b) Computational model of a single SiC/SiO_x core/shell NW; left panel shows the NW unit cell side view (upper part) and top view (lower panel); right panel shows a side view of the NW supercell obtained by periodically repeating the unit cell along the rotational symmetry axis direction.

Moreover, we presented ab initio calculations of the electronic structure and the theoretical interpretation of XAS SiC/SiO_x core/shell NWs, studying the modification induced by several different substitutional defects and impurities into both the surface and the interfacial region between the SiC core and the SiO_x shell. This computational investigation shows that our model of SiC/SiO_x core/shell NW, reported in Fig. 2, proves to be a valuable tool towards the optimal design and application of these nanosystems in actual devices.

Finally, we developed a systematic approach to the search for all- sp^2 bonded carbon allotropes with low density. In particular, we obtained a number of novel energetically stable crystal structures, whose arrangement is closely related to the topology of graphene, by modifying the packing of congruent discs under the condition of local stability. Our procedure starts from an initial parent topology and

proceeds to generate daughter architectures derived by lowering the packing factors. Furthermore, we assessed both the electronic properties, such as the band structure and the density of states, and the mechanical properties, such as the elastic constants and the stress–strain characteristics, of parent’s and daughter’s geometries from first-principle simulations. We

find, using geometrical packing arguments, that some arrangements lead to a density as low as half that of graphene, obtaining some of the least dense structures of all-bonded carbon allotropes that could ever be synthesized, showing specific mechanical characteristics almost unchanged while having lower weight.

Selected Papers

- Azzolini, M., Angelucci, M., Cimino, R., Larciprete, R., Pugno, N. M., Taioli, S., and Dapor, M. (2018a). *Secondary electron emission and yield spectra of metals from Monte Carlo simulations and experiments*. *Journal of Physics: Condensed Matter* **31**(5), p. 055901.
- Morresi, T., Taioli, S., and Simonucci, S. (2018b). *Nuclear Beta Decay: Relativistic Theory and Ab Initio Simulations of Electroweak Decay Spectra in Medium-Heavy Nuclei and of Atomic and Molecular Electronic Structure*. *Advanced Theory and Simulations* **1**(11), p. 1870030.
- Morresi, T., Timpel, M., Pedrielli, A., Garberoglio, G., Tatti, R., Verucchi, R., Pasquali, L., Pugno, N., Nardi, M. V., and Taioli, S. (2018d). *A novel combined experimental and multiscale theoretical approach to unravel the structure of SiC/SiO_x core/shell nanowires for their optimal design*. *Nanoscale* **10**, pp. 13449–13461.

NINPHA

Marco Claudio Traini [†]

Diffractive J/Ψ photoproduction: the role of gluon fluctuations In collaboration with Jean-Paul Blaizot (Paris-Saclay, University) I proposed a new framework for the interpretation of diffractive vector meson production and the role of gluon fluctuations (in Traini and Blaizot 2019).

It was in particular recently suggested, based on the Impact-Parameter dependent Saturation model (IPSat), that geometrical fluctuations triggered by the motion of the constituent quarks within the protons could explain incoherent diffractive processes observed at HERA. We propose a variant of the IPSat model which includes spatial and symmetry correlations between constituent quarks, thereby reducing the number of parameters needed to describe diffractive vector meson production to a single one, the size of the gluon cloud around each valence quark. The application to J/Ψ , ρ , and ϕ diffractive electron and photon production cross sections reveal the important role of geometrical fluctuations in incoherent channels, while other sources of fluctuations are needed

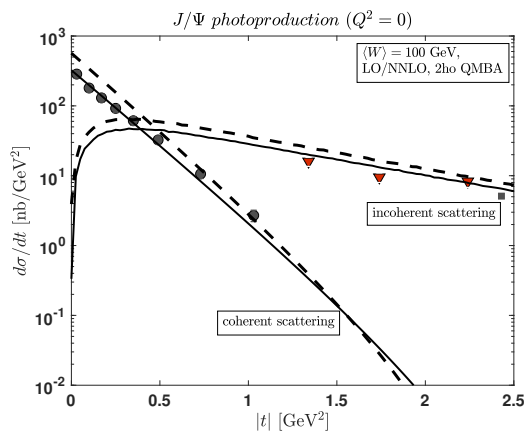


Figure 1: Coherent and Incoherent photoproduction ($Q^2 = 0$) cross sections within the kinematical conditions of the HERA experiments. The incoherent scattering cross section vanishes if the fluctuations of the geometrical gluon profile are neglected. (Data from HERA experiments).

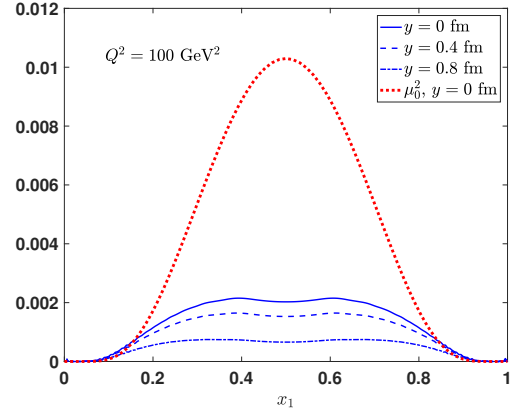


Figure 2: The quantity $x_1(1-x_1)F_{u\bar{d}}(x_1, 1-x_1, y, Q^2 = 100 \text{ GeV}^2)$ is plotted as a function of x_1 at different y -values. The input distribution at μ_0^2 and $y = 0 \text{ fm}$ is also shown.

to fully account for electroproduction of light mesons, as well as photo production of J/Ψ mesons at small momentum transfer. An example is shown in Fig. 1 where the coherent and incoherent J/Ψ photoproduction cross sections are shown.

Double Parton Distributions of the pion

In (Rinaldi et al. 2018) parton correlations in the pion have been investigated in terms of double parton distribution functions. A Poincaré covariant light-front framework has been adopted. As non perturbative input, the pion wave function obtained within the so-called soft-wall AdS/QCD model has been used. Results show how novel dynamical information on the structure of the pion, not accessible through one-body quantities, are encoded in double parton distribution functions. At the hadronic scale since only two valence particles are present, the support condition, preserved within the lightfront approach, forces the dPDF to exist only when $x_1 + x_2 = 1$. At higher scale a first important effect of the evolution procedure can be seen in Fig. 2 where the double distribution $x_1 x_2 F_{u\bar{d}}(x_1, x_2, y, Q^2 = 100 \text{ GeV}^2)$ is

[†]Contact Author: marcoclaudio.traini@unitn.it

shown in the domain $(x_1, x_2 = 1-x_1)$ as a function of x_1 and for different values of the parton distance y . The comparison with the same distribution at the hadronic scale μ_0^2 and $y = 0$ clearly emphasizes the effects of the evolution. The evolution from μ_0^2 to $Q^2 = 100 \text{ GeV}^2$ pro-

duces a reduction of the distribution, a behavior physically interpretable as the creation of new partonic species carrying momentum, in particular gluon distributions. Recall that the latter are zero at the hadronic scale for the models considered.

Selected Papers

- Rinaldi, M., Scopetta, S., Traini, M., and Vento, V. (2018). *A model calculation of double parton distribution functions of the pion*. European Physics Journal C **78**, pp. 781–789.
- Traini, M. and Blaizot, J.-P. (2019). *Diffraction incoherent vector meson production off protons: a quark model approach to gluon fluctuation effects*. European Physics Journal C **in print**, 15 pages.

TEONGRAV

Bruno Giacomazzo,[†] Riccardo Ciolfi, Federico Cipolletta, Andrea Endrizzi

The main research activity of the TEONGRAV group in Trento concerns fully general relativistic simulations of compact binaries, either neutron stars (NSs) or black holes (BHs). We here very briefly summarize the main results from two representative papers published by our group in 2018. The first one concerns the study of the effects of a new equation of state (EOS) on the dynamics and on the gravitational wave (GW) emission of a binary neutron star (BNS) merger. The second one is instead a study of the electromagnetic counterpart of the first GW detection from a binary NS merger (GW170817). Our group is also continuously working on code development and in particular on a new fully general relativistic magneto-hydrodynamic code.

Effects of a new EOS on BNS mergers Neutron stars are the remnants of supernova explosions (the spectacular deaths of massive stars) and the densest objects in the universe besides black holes. A typical neutron star concentrates more than the mass of the Sun within a radius of only around 10 km. Because of their extreme gravity a proper description of neutron stars requires Einstein’s theory of General Relativity. Investigating neutron star properties can shed light on the behavior of matter at very high densities, which is not yet understood well by nuclear physics. Two neutron stars can also bind together in a binary system, and orbit around each other for millions of years with a smaller and smaller separation. Eventually, the two merge together in an instant (just a few milliseconds) resulting either in a black hole or in a rapidly rotating neutron star, which can still collapse to a black hole later on.

Binary neutron star systems are powerful sources of gravitational and electromagnetic signals. The first GW detection from such a system happened on August 17 2017 (GW170817). GW170817 provided, among

other spectacular results, the first constraints on the NS EOS via GW observations. Since the NS EOS is still largely unknown, it is important to study different models and estimate the effects they may have on the GW emission. The EOS can indeed impact both the last phase of the inspiral and the post-merger emission.

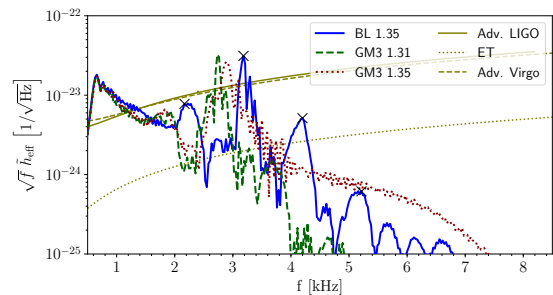


Figure 1: Power spectrum of the GW strain for our simulations plotted together with the sensitivity curves for advanced LIGO and Virgo and the planned Einstein Telescope. The source is assumed at a distance 100 Mpc from the detector, oriented with orbital angular momentum along the line of sight. Caption and figure published in (Endrizzi et al. 2018).

In (Endrizzi et al. 2018) we performed fully general relativistic simulations of three BNS systems. Two of them were evolved with an “old” EOS model (GM3) while the third one instead used a new and more accurate calculation performed by nuclear physicists Bombaci and Logoteta from the University of Pisa (the BL EOS). Both equations of state are computed at zero temperature and thermal effects were added via a simple ideal fluid EOS.

In Fig. 1 we plot the GW spectrum of the different models and one can clearly observe the different post-merger frequency peaks. By detecting the frequency at which the post-merger GW signal is emitted one may be able to distinguish between different EOS models and further constrain the properties of NS matter. Moreover, the BL EOS produces more compact NSs than the GM3 one and this leads to a larger

[†]Contact Author: bruno.giacomazzo@unitn.it

amount of ejecta that could therefore produce a brighter kilonova signal.

Future simulations will use a new version of the BL EOS that includes also finite temperature effects. We will also consider the effects of magnetic fields and of neutrino emission.

Modeling the Late Time Afterglow of GW170817 The first detection of GWs from a BNS merger (GW170817) was followed by detections of electromagnetic counterparts across the whole spectrum. In particular, the simultaneous detection of a short gamma-ray burst (SGRB) provided evidence that (at least some type of) SGRBs are produced by BNS mergers. The SGRB afterglow was quite peculiar instead, since the X-ray afterglow emission was detected quite late with respect to standard SGRB observations.

In (Lazzati et al. 2018) we demonstrated that the delay and the lightcurve of the afterglow emission detected after GW170817 are consistent with a structured jet emitted after the merger.

In Fig. 2 we show the results of our numerical simulation and the corresponding lightcurves. As discussed in our paper, the propagation of the jet through non-relativistic ejecta in the vicinity of the merger site causes the emergence of a structured jet, with a light, fast core (the low-density, blue region) and less energetic, slower wings (the orange and green material surrounding the jet). Our results agree very well with observations (small dots in the right top panel) demonstrating the validity of our model and showing that the jet emitted by

GW170817 was observed off-axis (our best fit gives $\sim 30^\circ$), contrary to all previous SGRBs observed along the direction of the collimated jet.

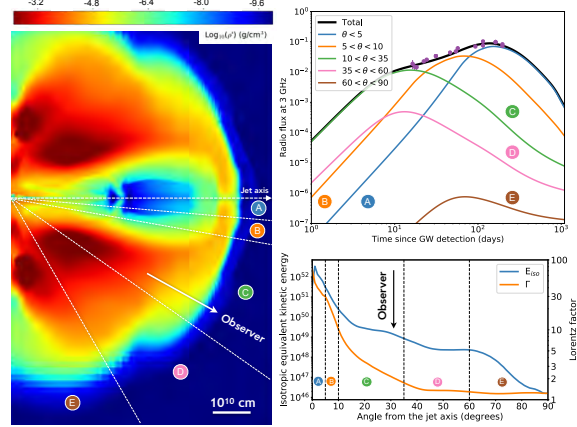


Figure 2: Left panel: pseudocolor density image of the simulation of an SGRB jet from a BNS merger used to compute the afterglow light curves. The line of sight to the observer (lying at 33 degrees from the jet axis) is shown with a white arrow. The polar distribution of energy and velocity of the ejecta is shown in the bottom right panel. The top right panel shows the best-fit afterglow model decomposed into radiation coming from the core of the jet (blue), the fast wings of the jet (orange), the material moving along the line of sight (green), and material at large angles (pink and brown). The solid black line is the sum of the colored lines. Figure and caption published in (Lazzati et al. 2018).

Future studies will be based on the use of different general relativistic BNS simulations in order to be able to compute the afterglow emission from different BNS mergers. Future simultaneous detections of GW and SGRBs may be used together with our theoretical models to infer the properties of the detected BNS systems.

Selected Papers

- Endrizzi, A., Logoteta, D., Giacomazzo, B., Bombaci, I., Kastaun, W., and Ciolfi, R. (2018). *Effects of Chiral Effective Field Theory Equation of State on Binary Neutron Star Mergers*. Phys. Rev. **D98**(4), p. 043015.
- Lazzati, D., Perna, R., Morsony, B. J., Lopez-Camara, D., Cantiello, M., Ciolfi, R., Giacomazzo, B., and Workman, J. C. (2018). *Late time afterglow observations reveal a collimated relativistic jet in the ejecta of the binary neutron star merger GW170817*. Phys. Rev. Lett. **120**(24), p. 241103.



Technological Research

Alberto Quaranta

alberto.quaranta@unitn.it

Coordinator,
TIFPA Technological Research Activities

At the end of 2018 the CSN5 group at TIFPA is involved in 7 standard projects, 6 calls, 1 INFN_E project and 1 Young Researcher Grant, involving 75 researchers and 8 technicians from three Departments, that are Physics (DF), Industrial Engineering (DII), Civil, Mechanics and Environment (DICAM), and from Bruno Kessler Foundation (FBK). These institutions, together with INFN persons in charge at TIFPA, contribute to all the projects with a total amount of 43.7 Researcher Equivalent Time (FTE).

This year is remarkable the high number of CSN5 calls involving TIFPA unit. SICILIA is a call on the production of SiC detectors which achieved a one year extension in 2019; MOVE_IT is a call on hadrontherapy at its last year of activity; TIMESPOT is a call on fast detectors at the second year of activity. Finally ARCADIA, FIRE and NEPTUNE are three new calls starting on 2019. ARCADIA is an experiment on detectors with advanced readout CMOS architectures based on fully depleted monolithic technology. NEPTUNE aims to study innovative nuclear reactions for the enhancement of the therapeutic effectiveness of proton beam therapies. FIRE is focused on the development of organic flexible radiation detectors for dosimetry in different radiation fields. For 2019 the approved new standard experiments are 3D-SIAM, GLARE-X and THEEOM-RD. 3D-SIAM will work on the development of 3D structured detectors based on amorphous silicon. GLARE-X will extend the activity developed with NEWREFLECTIONS by developing experimental studies on the reliability of laser systems for the deflections of satellite orbits. THEEOM-RD will be devoted to the development of nano-membranes for the realization of optical resonators for high sensitivity single-photon detectors. Finally, for the first time TIFPA is involved in an INFN_E experiment, named DRAGON, for the development of neutron detectors on drones. As far as old experiments are concerned, ASAP, ISOLPHARM-Ag and the young researcher grant DEEP-3D will go on for 2019.

Again it is worth noting that the TIFPA activity in CSN5 is characterized by highly multidisciplinary, involving competences and researchers from a wide range of disciplines and laboratories.

ARDESIA

Nicola Zorzi,[†] Giacomo Borghi, Francesco Ficorella, Antonino Picciotto

ARDESIA project aims at the realization of a versatile and high-performance X-ray Spectroscopy detection system for synchrotron experiments in the energy range between 0.2 keV and 25 keV. The basic detection module is built around a 2×2 monolithic array of Silicon Drift Detectors (SDDs) realized using the technology available at FBK (Trento). The readout chain is based on a monolithic version with four channels of the CMOS preamplifier CUBE developed by Politecnico di Milano. Both the analog and the digital processing systems are developed to be compatible with several filtering and data acquisition interfaces available in different synchrotron facilities.

The role of INFN-TIFPA in the project concerns simulation, design, development of the fabrication technology, production and preliminary characterization of the SDD array detectors in close collaboration with the FBK micro-fabrication laboratory. The other INFN units involved in the project and their corresponding roles and tasks are as follows: INFN-Milan (overall project coordination, supervision of detector design, detection module development, integrated electronics and DAQ, spectroscopic measurements, support to experimentation in final applications) and INFN-LNF Frascati (detector module development, DAQ, installation of the detection modules in the synchrotron facilities, X-ray characterization measurements). The activity in 2018 was aimed at two different goals:

- (i) accurate characterization of the spectrometer realized with the devices fabricated in the previous years;
- (ii) design and fabrication of new SDD devices with improved detection efficiency for X-rays in the energy range above 15 keV.

A thorough experimental characterization of the detection module has been carried out

at -27°C with a laboratory test set-up, a X-ray calibration ⁵⁵Fe source and both analog and digital signal processing systems (Bellotti et al. 2018a). The module provides state-of-the-art spectroscopic performances. At moderate count rates (2-kcps per channel) optimum energy resolution is 126 eV at 2.4-μs peaking time, with both analog and digital readout. Reducing the peaking time to 96 ns, the measured resolution is 159 eV. From the comparison of measurements of circular and square detector geometries, it was found that the ballistic deficit is not more pronounced in the square one; therefore, the latter is preferable providing a larger active area (and correspondingly less dead area). The detector can be successfully operated at high count rates (measured total output count rate 3.4 Mcps) with an energy resolution of 180 eV, thus paving the way of its use in high-throughput applications of fluorescence analytical techniques based on synchrotron light. A study of the charge sharing contribution among the adjacent channels demonstrated that it is of no concern for the ARDESIA detector, thanks to the planned adoption of a proper collimator.

Based on this detection module, a complete spectrometer has been designed and constructed. It is engineered in a cold finger-like structure that can be placed inside the scattering chamber of a synchrotron facility. Characterization tests were performed at two different beamlines to assess the performance of the instrument (Hafizh et al. 2019b), (Hafizh et al. 2019a). At the LNF DAΦNE-Light DRX1 soft X-ray beamline the good energy resolution of the instrument was demonstrated by the acquisition of a fluorescence spectrum from a graphite sheet containing trace elements. The instrument is able to resolve the peaks in the spectrum from the fluorescence emission of the low-atomic number elements, as low as $Z = 6$ for carbon (277 eV). In addition, it allowed acquisition of the first XAFS spectrum of silicon K-

[†]Contact Author: zorzi@fbk.eu

edge in a glass sample. At the high-intensity ESRF LISA BM-08 beamline, XAFS measurements on different samples were performed, demonstrating the high count rate capability and the stability of the instrument over time. The achieved results represent an improvement with respect to state-of-the-art commercial instruments sharing the same detector technology and applications and currently the ARDESIA instrument installed at the LISA beamline is routinely used.

The specific TIFPA activity in 2018 was mainly focused to the development of SDD detectors with increased thickness, in order to improve the X-ray detection efficiency in the energy range above 15 keV. In collaboration with FBK, extensive device simulations of thick SDD devices up to 1mm were carried out to properly size the drift rings and the border regions. Then a set of detectors were designed, including a number of layout variations in order to experimentally study the impact of the different solutions on the device performances. The wafer layout includes 2×2 SDD arrays with an optimized layout, and 4×4 arrays with both reduced pitch (2 mm) and standard pitch (5 mm). These last are targeted at improving the total throughput of the spectrometer. The production adopting this layout was affected by a

substantial delay caused by equipment breakage in the FBK laboratory and the fabrication batch has only recently been completed (January 2019). Now devices realized on 0.8mm- and 1 mm-thick wafers (see Fig. 1) are available for measurements. After a preliminary automatic characterization at wafer level, selected devices will be diced and delivered to the partners for the packaging and the spectroscopic tests at higher energies.

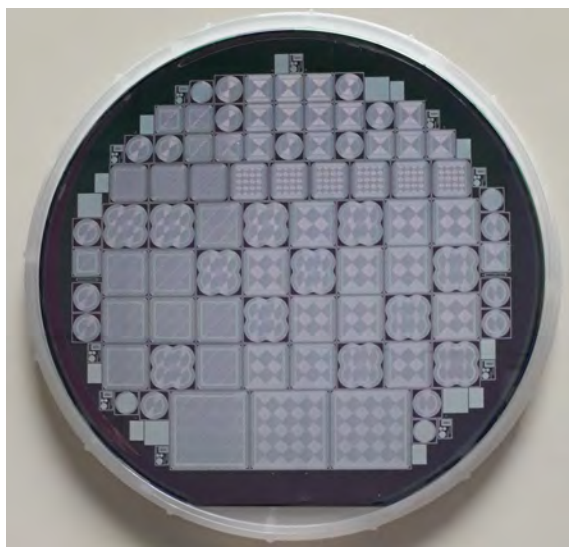


Figure 1: Picture of a wafer containing the thick ARDESIA SDD detectors.

Selected Papers

- Bellotti, G., Butt, A., Carminati, M., Fiorini, C., Bombelli, L., Borghi, G., Piemonte, C., Zorzi, N., and Balerna, A. (2018a). *ARDESIA Detection Module: A Four-Channel Array of SDDs for Mcps X-Ray Spectroscopy in Synchrotron Radiation Applications*. *IEEE Transactions on Nuclear Science* **65**(7), pp. 1355–1364.
- Hafizh, I., Bellotti, G., Carminati, M., Utica, G., Gugiatti, M., Balerna, A., Tullio, V., Borghi, G., Ficarella, F., Picciotto, A., Zorzi, N., Capsoni, A., Coelli, S., Bombelli, L., and Fiorini, C. (2019a). *ARDESIA - a Fast SDD X-ray Spectrometer for Synchrotron Applications*. *Journal of Synchrotron Radiation* **submitted**.
- Hafizh, I., Bellotti, G., Carminati, M., Utica, G., Gugiatti, M., Balerna, A., Tullio, V., Borghi, G., Picciotto, A., Ficarella, F., Zorzi, N., Capsoni, A., Coelli, S., Bombelli, L., and Fiorini, C. (2019b). *ARDESIA: a Fast SDD X-ray Spectrometer for Synchrotron Applications*. *X-Ray Spectrometry* **in press**.

ASAP

Lucio Pancheri,[†] Andrea Ficorella, David Macii, Marco Zanoli, Mahid Zarghami

The ASAP project aims at improving the technology demonstrated in the APiX2 project with the goal of building a buttable module of suitable area, of improving the efficiency and reducing the noise characteristics and the thickness of the sensor. As for the APiX2 demonstrator, the ASAP sensor is based on the concept of vertically-integrated avalanche pixels made of two layers, using coincidence to reject thermally-generated spurious signals (Fig. 1). This approach offers several advantages in applications requiring low material budget and fine detector segmentation as, for instance, for tracking and vertex reconstruction in particle physics experiments and charged particle imaging in medicine and biology. A sensor based on this concept can have low noise, low power consumption and a good tolerance to electromagnetic interference. In addition, a timing resolution in the order of tens of picoseconds can be achieved thanks to the fast onset of avalanche multiplication in Geiger-mode regime.

The ASAP project will explore the feasibility of hybrid bonding to obtain the vertical interconnection of the two layers. In contrast with the technique of bump-bonding, that requires a separate post-processing stage whereby the upper and lower chips are aligned and paired together (a technique employed successfully for the prototypes developed in APiX2 project), the possibility to perform the bonding at wafer level allows the thinning of the upper silicon layer

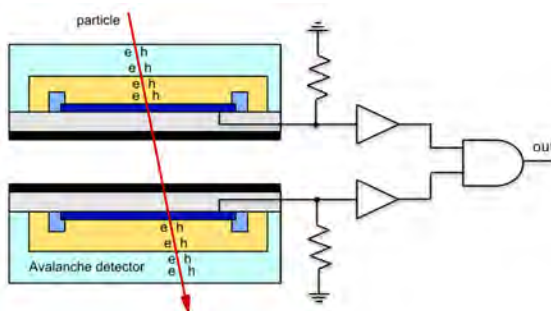


Figure 1: Concept view of a two-tier avalanche pixel.

[†]Contact Author: lucio.pancheri@unitn.it

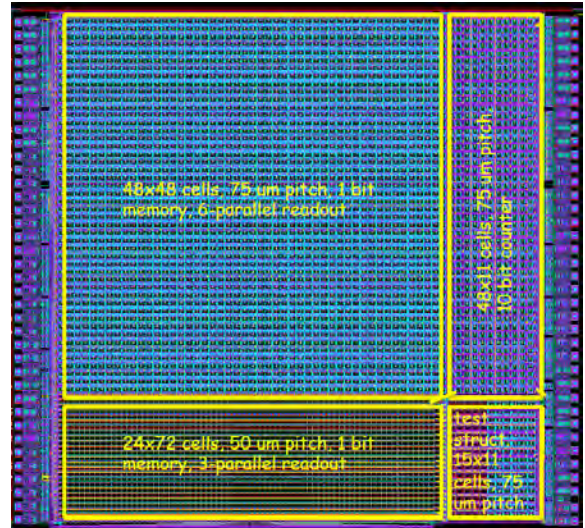


Figure 2: Floorplan of the new prototype chip designed in $0.15 \mu\text{m}$ CMOS.

down to $10 \mu\text{m}$ or less. This possibility is particularly appealing for the ASAP detector because it allows the detection of ionizing radiation down to very low energies (hundreds of keV), a crucial feature for the imaging of beta-emitters. In addition, a more scaled technology will be adopted, offering the opportunity of minimizing the area of the readout circuitry, and thus improving the pixel area efficiency. The chosen technology will be also optimized for imaging applications, thus intrinsically offering a reduced thermal generation rate and therefore a lower noise. The ASAP project will further explore the application of the technology in particle tracking for HEP and space applications, as well as in the imaging of beta-tracers for radio-guided surgery.

To optimize the efficiency of the two-tier detectors, that is basically determined by the sensor fill factor, a second design was submitted at the end of 2017 and fabricated in 2018 in a commercial $0.15 \mu\text{m}$ CMOS process, the same used in the design of APiX2 prototype. The design contains several subarrays with pixel size of $50 \mu\text{m} \times 50 \mu\text{m}$ and $75 \mu\text{m} \times 75 \mu\text{m}$ (Fig. 2).

The operation of the two separate tiers has been validated and the chips are now ready for vertical integration.

In parallel, the design of a first test chip in 110 nm project, aimed at implementing new avalanche detector structures in this process, has started and will be completed and submitted for fabrication during 2019.

Further characterization and system activities have been conducted on the first APiX2 prototypes (Ficorella et al. 2018; Musacci et al. 2018). Irradiation campaigns with both X-rays and neutrons have been carried out in 2017 and 2018 to investigate the effect of ionizing and non-ionizing radiation damage. Measurements with a proton microbeam, performed in LNL in the first months of 2018, have showed the localized degradation of the sensors when low-energy protons are incident. Radiation damage results have been analyzed and a predictive model is being implemented.

An application case for the use of ASAP approach in radio-guided surgery has been studied using GEANT4 simulation (Fig. 3), and

a hand-held probe for the detection of beta-tracers has been designed and fabricated (Marrocchesi et al. 2018). The probe will be validated in 2019 using radioactive laboratory sources.

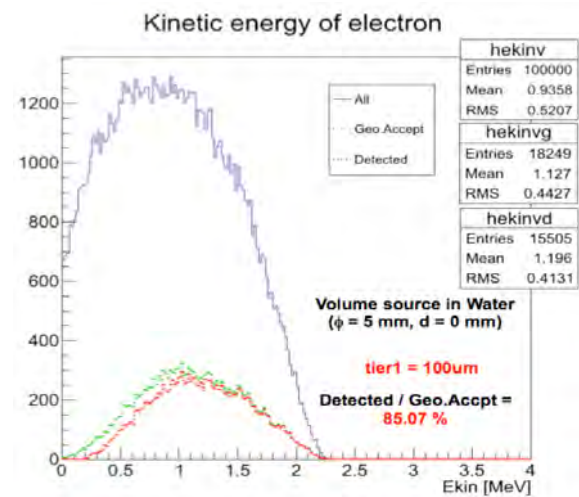


Figure 3: Example of simulation with a β - volume source positioned directly on the entrance surface of a 5 mm \times 5 mm 2-tiers detector with a first thinned layer (thickness = 100 μ m).

Selected Papers

- Ficorella, A., Pancheri, L., Brogi, P., Collazuol, G., Betta, G.-F., Marrocchesi, P., Morsani, F., Ratti, L., and Savoy-Navarro, A. (2018). *Crosstalk Characterization of a Two-Tier Pixelated Avalanche Sensor for Charged Particle Detection*. IEEE Journal of Selected Topics in Quantum Electronics 24(2).
- Marrocchesi, P. S., Brogi, P., Bigongiari, G., Checchia, C., Collazuol, G., Betta, G. F. D., Ficorella, A., Lodola, L., Morsani, F., Musacci, M., Noli, S., Pancheri, L., Savoy-Navarro, A., Silvestrin, L., Stolzi, F., Sulaj, A., Suh, J. E., Ratti, L., Vacchi, C., Zanolini, M., and Zarghami, M. (2018). "APiX: a Geiger-mode Avalanche Digital Sensor for Particle Detection". *2017 IEEE NSS-MIC Conference Record*. Piscataway, U.S.A.: IEEE.
- Musacci, M., Bigongiari, G., Brogi, P., Checchia, C., Collazuol, G., Betta, G.-F. D., Ficorella, A., Marrocchesi, P., Mattiazzo, S., Morsani, F., Noli, S., Pancheri, L., Ratti, L., Navarro, A. S., Silvestrin, L., Stolzi, F., Suh, J., Sulaj, A., Vacchi, C., and Zarghami, M. (2018). *Radiation tolerance characterization of Geiger-mode CMOS avalanche diodes for a dual-layer particle detector*. Nuclear Instruments and Methods in Physics Research Section A: Accelerators, Spectrometers, Detectors and Associated Equipment.

DEEP_3D

Roberto Mendicino,[†] Gian-Franco Dalla Betta, Alberto Quaranta, Matteo Perenzoni, Giacomo Borghi

Solid-state sensors for thermal neutron detection have been developed in different fabrication technologies with encouraging results. Most imaging systems are based on scintillator materials coupled with a CCD camera and their detection efficiency can be up to 10%. By using lens systems it is possible to achieve a spatial resolution of $10\ \mu\text{m}$. In order to achieve good contrast in the images it is necessary to have exposition times of 1 s and the CCD must be cooled in order to maintain low values of dark current. As a result, the performance are good enough for imaging, but neutron tomography would be very slow and difficult with this technology. Semiconductor detectors theoretically can offer good spatial (comparable with CCD camera and scintillator) and temporal resolution, and very high gamma rejection ratio making them very appealing for many applications (Mendicino and Dalla Betta 2018). In this framework, the DEEP_3D project addresses the most promising solutions for neutron imaging, with two main objectives:

- (i) to build a 2D neutron imager for artwork tomography, based on the interconnection of a Medipix-2 chip to a silicon 3D neutron detector,
- (ii) to develop a high performance neutron detector with a monolithic approach.

Since silicon is not sensitive to neutrons, a converter material is required, so that a silicon detector can easily detect the reaction products. In order to increase the detection probability, 3D geometries have been studied and developed.

In the first part of the project a custom 3D silicon detector with trenches filled with enriched LiF will be coupled with a Medipix-2 chip, that will be characterized under neutron fluxes. The technological approach is sketched in Fig. 1 where a cross section of the device is

shown in detail. The p^+ Ohmic contact region is on the top of the sensor (cavity side) and it is made before the DRIE step; as a result, the cavity walls are not highly doped in order to reduce the thickness of the dead region. A thin alumina (Al_2O_3) layer with negative fixed charge of $\sim -10^{12}\ \text{cm}^{-2}$ is used as a passivation of the walls.

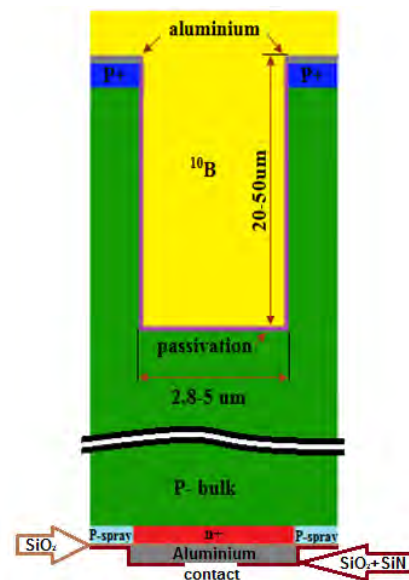


Figure 1: Schematic cross-section of the 3D sensor with detail of a single cavity (not to scale).

This technology may substantially increase the neutron detection efficiency and reduce the gamma sensitivity. The silicon sensors with trenches for the hybrid approach were produced at FBK (Fondazione Bruno Kessler) in Trento, which is part of the collaboration, with good results in terms of electrical characteristics.

Filling 3D sensors with a neutron converter material represents a big challenge due the very small dimensions of the cavities. In the DEEP_3D project, different solutions are under development in collaboration with partner laboratories within the network of scientific collab-

[†]Contact Author: roberto.mendicino@unitn.it

orations.

The relatively large dimensions of the cavities in case of lithium fluoride converter allows for a mechanical filling, performed by pressing the LiF powder with an average grain size smaller than $1\ \mu\text{m}$ into the cavities. This step will be made at the Czech Technical University in Prague. On the other hand, filling with boron is more complex and requires using LPCVD. The main issues of this technique are related to the relatively high temperature of deposition and the difficulty to adequately mask the pixel side of the detector. The material science group of the Industrial Engineering Department of the University of Trento (DII) is developing processes useful for this purpose.

The second goal is the development of a monolithic 3D detector for neutron imaging, that is highly innovative and can represent a turning point for this field. The demonstrator will have smaller area and a less sophisticated electronics as compared to the hybrid detector, in order to maximize the flexibility in the testing, but it will have globally a better performance.

Sensors are fabricated on high resistivity wafer that allows a full depletion of the volume, isolated from the electronics by a buried oxide layer (SOI). This technology has been developed by KEK (The High Energy Accelerator Research Organization) and Lapis technology in Japan. The advantages of this approach are multiple: there is no mechanical bump bonding, resulting in a reduction of material budget and smaller pixel sizes, there is a lower parasitic capacitance, allowing higher speed and lower noise. Moreover, the sensor can work in a very wide temperature range (200 - 500 K) and the full CMOS circuitry can be implemented in the pixel, with technology based on industry standards.

The first demonstrator has been designed in SOI technology with 200 nm CMOS process.

Selected Papers

Mendicino, R. and Dalla Betta, G.-F. (2018). *Three-Dimensional detectors for neutron imaging*. Nucl. Instrum. Methods A **878**, pp. 129–140.

The prototype chip will be composed of a matrix 25×25 pixel array. Each pixel, having a $40 \times 35\ \mu\text{m}^2$ area, includes detectors and electronics. The front end is analog: it maintains information of collected charge and allows for cluster size study. It consists of a charge preamplifier with a constant current feedback and an analog time over threshold. The reading architecture is very similar to CCD camera with a 3T architecture.

The data can be acquired by programmable acquisition setup based on FPGA (or microcontroller). The system can work up to 1 kHz acquisition frequency.

In order to reach a high neutron detection efficiency, also in this case the back side of the detector is processed. Fig. 2 shows a cross section of the SOIPIX technology after the post processing.

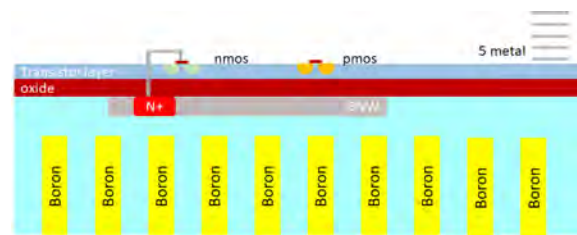


Figure 2: Schematic cross-section of 3D monolithic sensors of neutrons with SOIPIX technology (not to scale).

It is then planned to perform the etching of the cavities at the Leibniz Institute of Photonics Technology. The etching will be performed by using DRIE etching (Bosch and Cryo process) on single device ($2.9 \times 2.9\ \text{mm}^2$). The following step is the passivation of the cavities by the deposition of Alumina with an ALD technique. Similarly to what has been done for hybrid detectors, a geometrical process split should be considered for the size of the cavities in order to make them suitable for both boron and lithium fluoride.

ELOFLEX

Alberto Quaranta,[†] Viviana Mulloni, Andrea Ficorella, Enrico Zanazzi, Matteo Favaro

The aim of the experiment ELOFLEX (ELECTRO-Optical FLEXible detectors for mixed radiation fields) is to study the feasibility for the realization of flexible detectors for real-time dose measurements in mixed radiation fields. Such detectors should be obtained by combining organic semiconductor detectors (OSD) with quantum dots based scintillators (QDS).

In the first year, concerning the scintillator fabrication and testing two issues are of crucial interest:

- (i) studying the irradiation effects on the QD optical properties and
- (ii) studying the possible influence of the polymer matrix on the QD optical properties in irradiated samples.

For this purpose, colloidal QDs have been first embedded in two different polymer matrices: polydimethylsiloxane (PDMS) and polyvinyl alcohol (PVOH). PDMS samples were prepared by dispersing InGaP/ZnS QDs at concentrations of 10^{15} QD/cm³. The samples were irradiated with 2 MeV H⁺ ions at three different fluences, namely 10^{14} , 5×10^{14} , and 10^{15} H⁺ cm⁻². PL spectra and time resolved measurements showed a lowering of the intensity

and of the average lifetime with the increasing irradiation fluence, due to the formation of quenching centres. The analyses evidenced that radiation defects are easier to be formed at the QD surface, through the shell damage or by bond cleavage of both ligands and network. Samples based on PVOH were obtained by dispersing colloidal CdSe/ZnS into the polymer up to a concentration of about 10^{16} QD/cm³.

In irradiated samples the rising of a new band located around 440 nm and having its excitation maximum around 395 nm was observed, related with the formation of unsaturated C=C carbon bonds and carbon clusters in the PVOH. By increasing the fluence, the luminescence yield of QDs optical properties are partially recovered (5×10^{13} H⁺ cm⁻²) and enhanced (10^{14} H⁺ cm⁻²) due to a mechanism of energy transfer from the polymer defects to the nanocrystals.

The Research Unit Bologna¹ optimized the deposition process of the new organic small molecule TIPGe-pentacene (TIPGe) with the dropcast method. Moreover, they fabricated 3-terminals low-voltage OTFT on PET flexible substrate, employing TIPGe molecules.

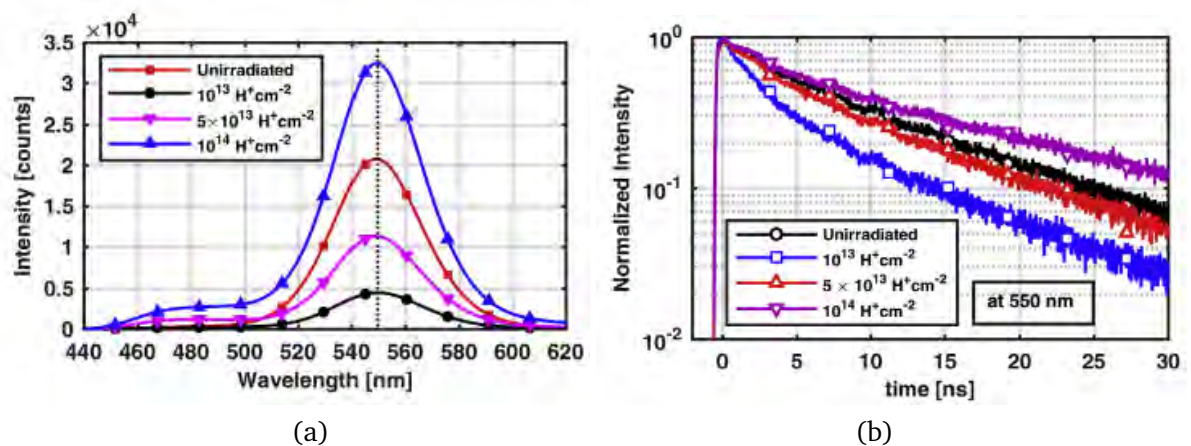


Figure 1: (a): PL emission spectra of irradiated and unirradiated PVOH-based samples embedding CdSe/ZnS QDs, (b): PL decays of unirradiated and irradiated samples acquired at the QDs emission wavelength (550 nm).

[†]Contact Author: alberto.quaranta@unitn.it

¹composed by Beatrice Fraboni (LI), Laura Basiricò and Laura Fabbri

The characterization of TIPGe devices as direct X-ray detectors showed an average sensitivity of 4460 ± 50 nC/Gy. The value is more than four times higher than what has been reported for other molecules. The improvement of the performance of TIPGe devices is due to a combination of higher X-ray absorption and of more efficient transport and collection of generated charges. The X-ray responses of the samples are very reliable and the minimum detectable dose rate has been measured at $6.4 \mu\text{Gy/s}$. This value is in the range of a single irradiation of most medical applications.

The detectors closed in the boxes have been characterized under collimated proton beam at TIFPA. At 70 MeV, TIPGe detectors show large current increase, up to 300 pA at about 5×10^7 p/s and sensitivity of $(9.2 \pm 0.3) \times 10^{-18}$ C/p. The photocurrent increases linearly with the proton flux, without the satu-

ration effects observed instead in the previous tests. The proton beam does not affect mobility, on/off ratio and subthreshold slope, suggesting that the protons do not damage the material forming the thin film. The threshold voltage instead shift from -0.4 V to -1.1 V, meaning that there is an accumulation of negative charges between the organic film and the dielectric layers. This effect could be exploited to make an organic RADFET, working on intensity ranges much lower than 10^7 protons/s where the effect quickly reach a saturation.

ELOFLEX closed this year due to the opening of the call FIRE (Flexible organic Ionizing Radiation dEtectors), see p. 107, where the ELOFLEX collaboration joined with Roma 3, Napoli and LNL units for a larger experiment for the realization of flexible organic detectors for applications in dosimetry.

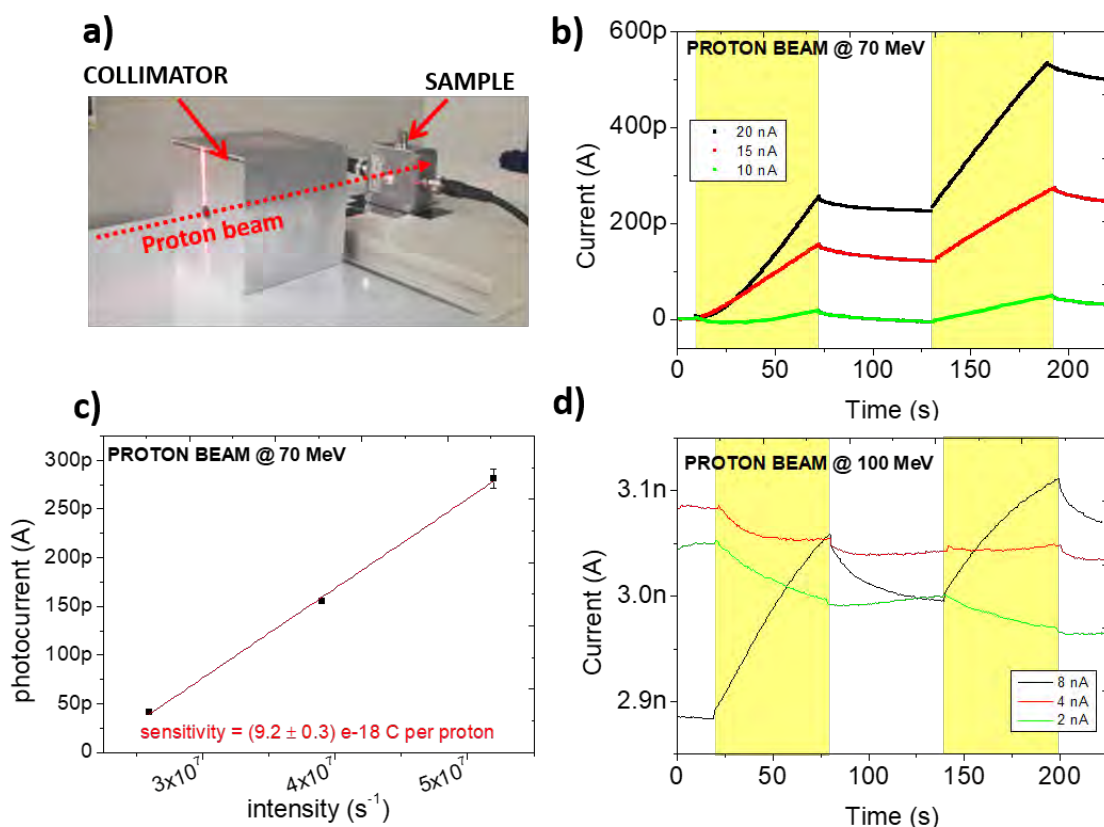


Figure 2: a): Detail of the collimator and sample at TIFPA. b) and c): Direct response of TIPGe detectors under proton irradiation at 70 MeV and d): at 100 MeV.

IsolpharmAg

Antonella Motta,[†] Devid Maniglio, Alessandra Bisio, Walter Tinganelli, Alberto Quaranta

In targeted radiation therapy, a fundamental part of the radiopharmaceutical moiety is the targeting agent, i.e. the vector molecule. This portion is used for the molecular recognition between the drug and a biological entity, like a receptor, usually over-expressed on cancer cells. This moiety can be decorated with different chelators, opportunely spaced with a linker, depending on the radiometal to incorporate.

In this project two different biological targets are considered: calreticulin and cholecystokinin receptor. While for the second one the targeting strategies are quite well established, the focus in the first year of the project was mainly on finding a suitable targeting agent for calreticulin.

Calreticulin (CRT) is an endoplasmic chaperon molecule that can translocate from the cytosol to the cell surface, particularly during ER stress induced by e.g., drugs, UV irradiation and microbial stimuli. CRT is also exposed on the surface of many cancer cells and plays a role in recruiting macrophages thus promoting engulfment. Currently, CRT is recognized as a very promising molecular target for many anticancer immunotherapy protocols.

CRT can be considered then as a good and innovative target for the development of receptor targeting radiopharmaceuticals. The design and synthesis of a vector molecule with high affinity for CRT is crucial to deliver the radioactive payload selectively to tumor cells. As proof of concept, we aim at designing and synthesizing new molecules endowed with affinity towards CRT. For the development of a molecule with affinity for calreticulin, we set up several experiments to assess the targeting capability of different commercial CRT specific antibodies. Their performances have been compared with sugar-based molecules (oligosaccharides), among which, mannose resulted to have significant affinity for CRT.

To verify targeting efficiency, we set up

several *in vitro* cell experiments using B16-F10 and A375M cell lines and testing CRT translocation with fluorescence tagged antibodies through confocal microscopy. Translocation was obtained exposing cells to different agents: H₂O₂, Doxorubicin, and Camptothecin (CPT) (see Fig. 1). To ensure a better *in vitro* simulating system, we have started developing a gelatin based material suitable for cell incorporation. The commercial pig skin-derived gelatine underwent to chemical functionalization, to allow methacrilation of the polymer chains. This allow, with the use of a suitable photoinitiator, the complete conversion of the liquid solution into a homogeneous crosslinked hydrogel. Since the process is quite soft and can be made in physiological conditions, cells can be incorporated in the liquid suspension to realize living constructs. Their use in culture conditions will permit to realize experiments on radiopharmaceutical targeting more significant than those obtained on standard 2D conditions.

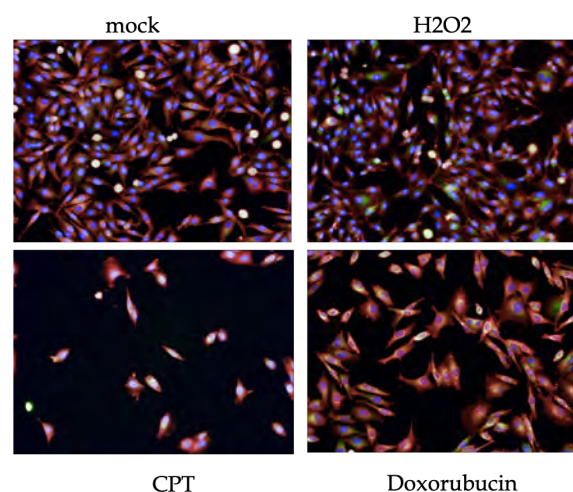


Figure 1: Confocal images of A375M cells after exposure to H₂O₂, Doxorubicin and CPT to induce CRT translocation, versus non treated cells (mock). CRT-specific antibodies (orange), nuclei (blue), cytoskeleton (red).

[†]Contact Author: antonella.motta@unitn.it

KIDS_RD

Renato Mezzena,[†] Benno Margesin

The development of Microwave Kinetic Inductance Detectors (MKIDs), within the framework of the project KIDS_RD, reached the third year. KIDS_RD aims at realizing MKIDs for broad band high energy resolution X-ray spectroscopy, as well as MKIDs able to resolve photon number at infra-red wavelengths. These sensors, proposed for the first time in 2003, are thin film, superconducting microwave microresonators operating at a temperature $T \leq T_c/10$, where T_c is the critical temperature of the constituting material. They are called pair breaking detectors because incident photons with an energy $h\nu > 2\Delta$ can be absorbed by breaking up Cooper pairs and creating a number of quasi-particle excitations $N_{qp} = \eta h\nu/\Delta$ where $\eta \simeq 0.59$ is the efficiency of creating quasi-particles and Δ is the energy gap of the superconductor. The quasiparticles population above the thermal equilibrium changes the complex surface impedance of the superconductor $Z_s = R_s + j\omega L_s$ where R_s is a resistive component associated with the quasiparticles, and L_s is the kinetic inductance due to the Cooper pairs. This impedance change causes a change of the quality factor and the resonant frequency of the superconducting microresonator which is coupled to a superconducting feed line. The feed line transmits a microwave probe signal at a frequency (typically 1 - 10 GHz) very close to the microresonator resonant frequency. Radiation absorbed results in a change of the transmitted signal magnitude and phase. An homodyne detection scheme is typically employed wherein an IQ-mixer produces as an output value the real part of the transmission signal in the I channel and the imaginary part in the Q channel. This readout scheme is very advantageous, because frequency domain multiplexing can be exploited in order to read hundreds of resonators. Only two coaxial lines are required to send a multi-tone probe signal to the low temperature device and to receive, amplified by

a cryogenic amplifier, the output signal.

The research activity of the INFN-TIFPA-FBK group in 2018 focused on two main targets. The first concerned the development of photon number resolving MKIDs operating at infra-red wavelengths. More specifically we intended to prove that irradiating our detectors with a pulsed laser operating at a wavelength of 1550 nm, the energy sensitivity was suitable to detect a single photon which has 0.8 eV of energy. In order to achieve this result, the proper film material must be identified and the resonator layout has to be carefully designed. The ideal film should have high kinetic inductance, low superconducting energy gap, high resistivity in the normal state, low electrical dissipation at microwaves frequencies and small volume. These properties can be suitably tuned employing the Ti/TiN multilayer technology because they depend on the total and relative layer thickness. The many tests carried out on the films fabricated by FBK foundation eventually lead to select the film composed of a bilayer of Ti/TiN repeated 2 times as the best solution. The Ti and TiN single layer thickness are respectively 10 nm and 12 nm and the film superconducting transition temperature is 1.21 K. As regards the resonator design, we have simulated and experimentally studied several layouts, the one with lumped (L, C) elements reported in Fig. 1 has made possible the best performances.

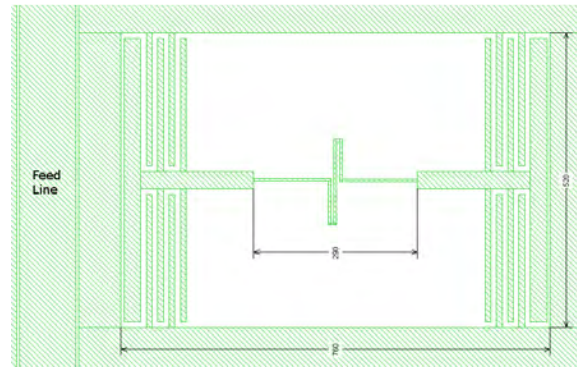


Figure 1: KID layout

[†]Contact Author: renato.mezzena@unitn.it

It consists of two blocks of interdigitated capacitors connected by an inductive element. The resonator and the feed line are separated by a ground area which determines the coupling between the two. The resonator was simulated with Sonnet in order to foresee the resonance frequency, coupling with the feed line and the current density. Since the most sensitive detector part is that with the highest current, we believe that the effective detector volume is limited to the inductor central part which corresponds to $128 \mu^3$. The detector volume V is important because the sensitivity is proportional to $\alpha Q/V$, where α is the ratio between the kinetic inductance and the total resonator inductance, and Q is the resonator quality factor. The sensitivity is investigated irradiating the MKID with light pulses produced by a laser diode. Typically 50000 pulses at the detector output are sampled by a 16 bit A/D converter and after filtering a histogram is built. A fitting procedure with n gaussian functions convolved with a Poisson distribution returns the mean photon number and the standard deviation of the n th gaussian peaks. In Fig. 2 is reported an histogram with 4 photons resolved. We obtained a FWHM Energy Resolution = 0.44 eV, which is only a factor of two worse than the best resolution value published for this kind of detectors. Further improvements are still possible and work is in progress in order to define a new detector layout with a smaller volume.

The second task carried on in 2018 concerns the investigation of the unwanted dissipation effects revealed on the detectors made for high energy resolution X-ray spectroscopy. This devices were fabricated at the end of 2017 (*TIFPA Activity Report 2017*).¹ After some preliminary measurements carried on the film resistivity

and the transition temperature, the detectors resonance frequency have been searched for. Unexpectedly the signal transmitted through the feed line was found attenuated by about 30 dB and no resonances have been detected. In order to get rid of this behaviour specific tests have been performed on expressly fabricated devices. Eventually it was discovered that the silicon nitride layer, deposited by PECVD process to obtain a suspended membrane in the resonator area, was responsible for the dissipation effect. In order to address the issue the silicon nitride deposition process was changed and LPCVD was adopted. In the devices fabricated with this process the signal transmitted trough the feed line showed the correct intensity and the resonances have been detected approximately in the expected frequency band. In spite of these improvements, we have to face another drawback because the resonances showed a quality factor about a factor 10 lower than what we expected. Some further investigations are in progress in order to identify the cause of this remaining dissipation.

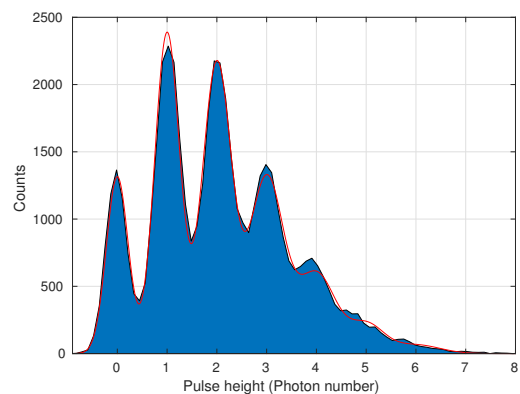


Figure 2: Histogram of 50000 pulse heights

¹http://www.tifpa.infn.it/wp-content/uploads/2018/05/TIFPA_actRep2017web.pdf

MoVe IT

Elettra Bellinzona and Emanuele Scifoni[†] on behalf of the MoVe IT collaboration¹

WP1 - Radiobiological Modeling for Treatment Planning The goal of the task 1 is the analysis of RBE impact of nuclear fragmentation of the target by considering each secondary particle contribution separately and combining them with a mixed field approach for biological effect.

The first description has been based on Monte Carlo simulations performed with SHIELD-HIT12A v.7.0.3 with the support of the Polish partner (L. Grzanka, PL-Grid infrastructure and Krakow University), reported in Fig. 1.

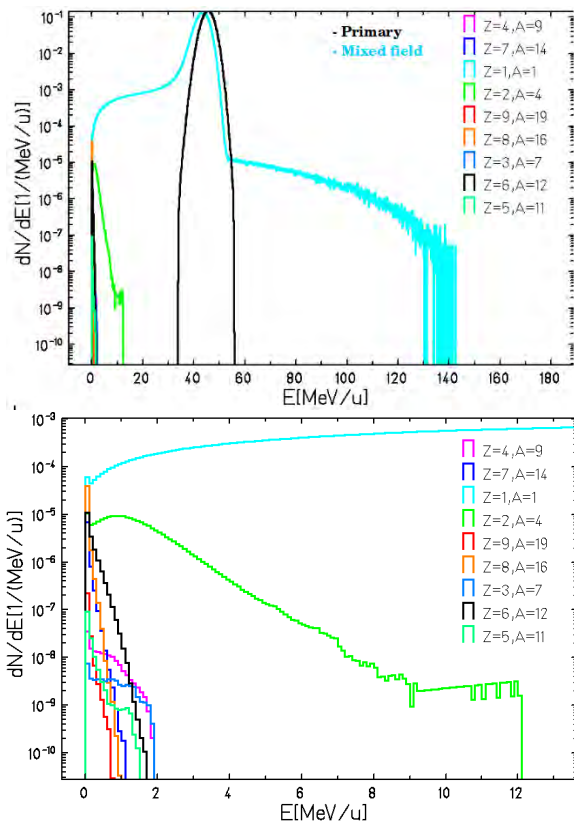


Figure 1: Fluence spectra of 150 MeV proton in water simulated with SHIELD-HIT12A; on top panel, the black curve represents the default spectra, on bottom panel a zoom on the new implemented fragments.

[†]Contact Author: emanuele.scifoni@tifpa.infn.it

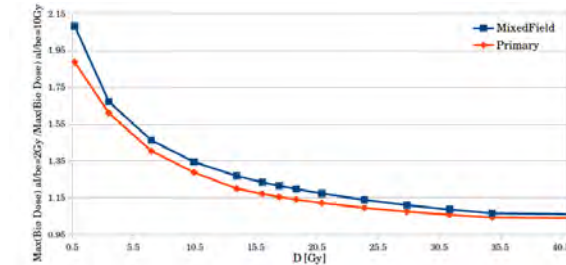


Figure 2: Dose dependence study of the ratio between the maximum biological dose for two sample tissues with respectively an α/β value of 2 Gy and 10 Gy.

A conversion tool has been also developed to create input files for TRiP98 TPS, and an initial RBE description has been given for various geometries, where the non negligible contribution of secondaries (in particular secondary protons) is underlined (see Fig. 2).

A micro-dosimetric study has been started in collaboration with LNS laboratory and INFN-Milano group and will be validated with experimental data. Beside this, a sensitivity analysis has been conducted to correlate the uncertainty of the cross sections experimental measurements with the final biological dose error. The data will be provided by the FOOT (FragmentatiON Of Target) experiment and used to validate the Monte Carlo simulations results. In Task 2 at the same time, the first worldwide treatment planning implementation for multiple ion beams has been realized (Sokol et al. 2019) (see Fig. 3).

WP2 - NTCP/TCP Modeling Important advances were reached in this WP during the last year, namely the first assessment of skin toxicities from proton beams on a large cohort of Trento Proton Therapy patients (submitted to IJROBP) and a voxel based analysis comparing photon and proton plans from an american clinical trial, in collaboration with MD Anderson (USA), solving the long-standing unexplained low dose paradox (accepted in IJROBP). See

¹for full list of contributors see www.tifpa.infn.it/projects/move-it/

Virtual Lab Medical Technologies, p. 19 for details.

WP3 - Biological Dosimetry The major part of the work performed at TIFPA in this section is related to the development of biophantom for RBE measurements. Several different alginate based cell containing phantoms have been developed in collaboration with CIBIO and BioTech and tested with 150 MeV proton beam, in the newly developed bio-line of TIFPA, in conjunction with a parallel irradiation of TLD dosimeters, in order to compare physical and biological dose profiles (see corresponding report in the proton beam lab section). Moreover, new prototypes for the hypoxia chamber have been developed and are now under preparation for a Patent application to the TT office.

WP4 - Facilities and beamline simulations

Main advances in this context, from the local team, were dedicated to the set up of the radiobiology line (0°) at the TIFPA proton beam lab, both on the simulation side and on the hard-

ware implementation, summarized in a couple of publications (Tommasino et al. 2018b; Tommasino et al. 2019). The double ring passive scattering system, with 2 different setups and thus beamsizes, allows a dose uniformity above 92.9% and is now regularly used for the biological sample irradiations.

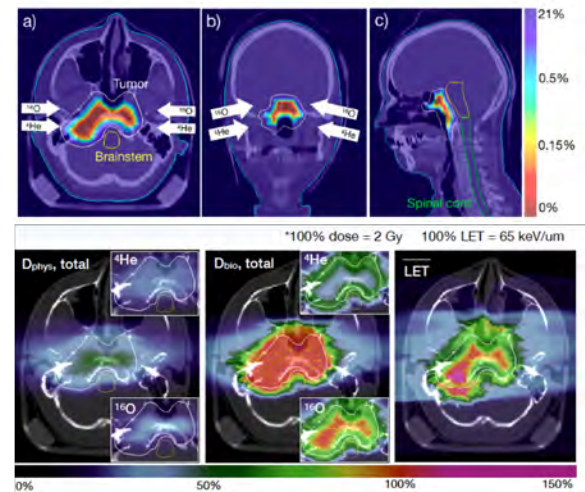


Figure 3: Scheme and results from simultaneous optimization of helium and ion beams on an hypoxic tumor (Sokol et al. 2019).

Selected Papers

- Sokol, O., Kraemer, M., Hild, S., Durante, M., and Scifoni, E. (2019). Kill painting of hypoxic tumors with multiple ion beams. *Physics in medicine and biology* **64**.
- Tommasino, F., Rovituso, M., Lorentini, S., La Tessa, C., Petringa, G., Cirrone, P., Romano, F., Scifoni, E., Schwarz, M., and Durante, M. (2018b). *Study For A Passive Scattering Line Dedicated To Radiobiology Experiments At The Trento Proton Therapy Center*. Radiation protection dosimetry.
- Tommasino, F., Rovituso, M., Bortoli, E., Tessa, C. L., Petringa, G., Lorentini, S., Verroi, E., Simeonov, Y., Weber, U., Cirrone, P., Schwarz, M., Durante, M., and Scifoni, E. (2019). *A new facility for proton radiobiology at the Trento proton therapy centre: Design and implementation*. *Physica Medica* **58**, pp. 99–106.

New Reflections

William Jerome Burger,[†] Alvise Bagolini, Roberto Battiston, Nicola Bazzanella, Massimo Cazzanelli, Claudio Cestari, Riccardo Checchetto, Roberto Iuppa, Christian Manea, Antonio Miotello, Francesco Nozzoli, Michele Orlandi, Jacopo Terragni

In the last year, a series of measurements of the coupling coefficient C_m (Ns/J) of materials relevant for the space applications of laser technology specific to New Reflections, spacecraft propulsion and debris mitigation, as well as possible applications for Near-Earth Asteroids (NEA), were made by the Laboratory IdeA. The coupling coefficient is a fundamental parameter relating the impulse generated by the ablated material to the incident laser pulse energy.

Propulsion The coupling coefficient measurements of several candidate propellant materials are compared in Fig. 1. The larger C_m obtained with a lower fluence and density (1.5 g/cm^3), make the Vespel sp21 polyimide resin an attractive candidate with respect to aluminium (2.7 g/cm^3) and Teflon (2.2 g/cm^3).

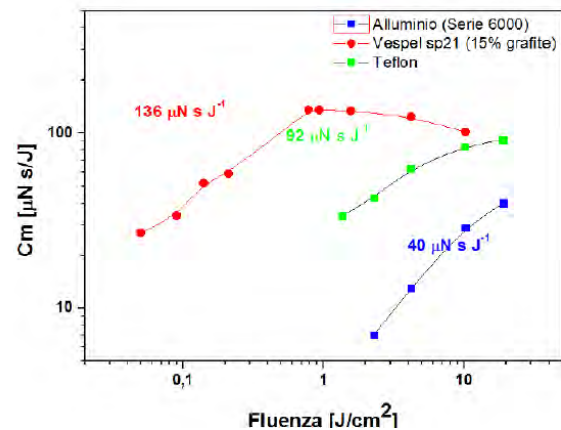


Figure 1: The coupling coefficients of candidate propellant materials.

[†]Contact Author: william.burger@tifpa.infn.it
¹OHB Italia S.P.A., via Gallarate 150, 20151 Milan (MI)

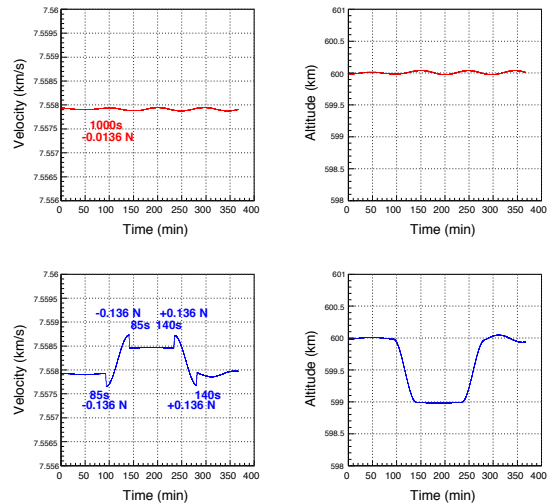


Figure 2: Simulated orbital transfers of a 50 kg satellite for the baseline LOCS design (red) and a factor 10 larger force (blue).

The experimental results were used in the proposal, submitted to the Italian Space Agency, in collaboration with OHB Italia,¹ to develop a demonstrator model Laser Orbital Control System (LOCS). The LOCS design is based on a 50 mJ, 2 kHz pulsed laser and the Vespel sp21 propellant. The laser-propellant combination provides a force of 0.0136 N/s. The simulation results of the baseline design performance, and a laser-propellant combination with a factor ten larger force, for a 1 km orbital altitude change of a 50 kg micro-satellite in a circular orbit at 600 km are shown in Fig. 2.

The performance of the baseline design is not sufficient. The factor of ten increase in force required for the manoeuvre may be obtained by a further optimization of the propellant material. A C_m of $1170\text{ }\mu\text{N/W}$ has been reported for volume ablation with an exothermic material.² OHB Italia is responsible for the overall satellite design. The TIFPA group is responsible for the

²Phipps, C. et al. (2004), Journal of Propulsion and Power 20, pp. 1000–1011.

laser and propellant material, which should satisfy all the requirements of the propulsion system, including the manoeuvres required by the planned end-of-life scenario.

Debris Mitigation The peak value of the aluminium coupling coefficient, a material commonly used in satellite construction, measured with a 20 ns pulse width in the IdEA laboratory is compared to values reported for smaller and larger pulse widths in Fig. 3. The open circle refers to value cited in (Ebisuzaki et al. 2015)³ for pulse widths below 1 ns. In the pulse width range between 1 and 30 ns, C_m varies by a factor of five.

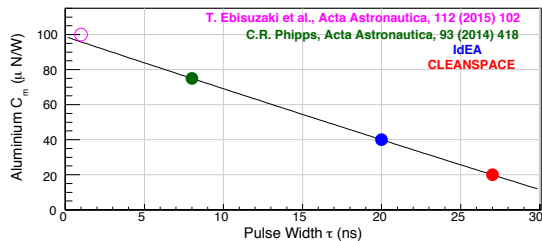


Figure 3: The measurements of the aluminium coupling coefficient with different pulse widths. The data (filled) circles are described by a line fit.

The generated mechanical impulse and required laser pulse energy is proportional to the coupling coefficient. The data indicate the advantage of low pulse width, high frequency lasers for debris mitigation, particularly for systems deployed in space where the available power is a critical constraint. The laboratory measurements, coupled with an effort to reproduce the data with models of the underlying physics, are fundamental for the optimization of the laser (debris mitigation) and laser-propellant combination (propulsion).

NEA Laser ablation is among the technologies, kinetic deflectors and spacecraft armed with a nuclear explosive, considered for an asteroid avoidance strategy. The measured cou-



Figure 4: The asteroid simulant material, the darker horizontal line denotes the ablated region.

pling coefficient of asteroid simulant material,⁴ which mimic the mineralogy of type C1 carbonaceous chondrite meteorites, $60\mu\text{Ns}/\text{J}$, is 50% larger than the value for aluminium (Fig. 1). Fig. 4 shows the surface of the simulant material sample after the measurement. The chemical composition of the simulant material obtained with a Scanning Electron Microscope (SEM) is shown in Fig. 5.

Ablation also plays an important role in the breakup of meteorites in the atmosphere. Experimental simulations of the process are used to interpret meteorite observations used to determine their chemical composition by the visible light emitted in the atmosphere.⁵ An important part of the research performed at Laboratory IdEA is based on the measurement of the composition of the ejected material. The possibility to use laser ablation to simulate meteorite breakup in the atmosphere is under study.

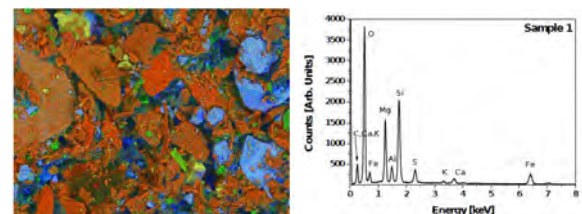


Figure 5: SEM view of the asteroid simulant material (left); chemical composition obtained from energy-dispersive X-ray (EDX) analysis (right).

³Ebisuzaki, T. et al. (2015), Acta Astronautica 112, pp. 102–113.

⁴courtesy Dr. Daniel Britt, Center for Lunar and Asteroid Surface Science, Dept. of Physics, University of Central Florida, Orlando FL, USA

⁵Loehle, S. et al. (2017), The Astrophysical Journal 837, pp. 112–121.

Redsox2

Irina Rashevskaya,[†] Pierluigi Bellutti, Giacomo Borghi, Francesco Ficorella, Giancarlo Pep-
poni, Antonino Picciotto, Nicola Zorzi

In 2018 the TIFPA group in the REDSOX2 col-
laboration continued the activities for the char-
acterisation of a large number of silicon drift
detectors of batch Redsox3. This batch, pro-
duced by FBK in 2016, includes different sen-
sors for various experiments and applications.
The sensors selected and catalogued were then
mounted in the TwinMic, XAFS, HERMES, and
other experiments within the project (Bufon et
al. 2018b).

The measurements of the electrical char-
acteristics and stability of PixDD 4×4 struc-
tures were performed and the PixDD 4×4 sen-
sor were tested after the first bump bonding
(Evangelista et al. 2018b). The first bump de-
position tests on the PixDD structures were car-
ried out in March 2018 at Institute for Data Pro-
cessing and Electronics (IPE) of Karlsruhe Insti-
tute of Technology (KIT). The results of mea-
surements and tests demonstrated the possibil-
ity of vertical integration of the PixDD struc-
tures with the readout chips.

Electrical test of all anods of PixDD 32×32
sensor showed the variation of the doping con-
centration of the wafers used for the production
of the sensors. The problem has been carefully
studied on different structures and presented at
the Collaboration Meeting in Bologna 6-8 June
2018.

In 2018 the Redsox group worked on design
of new Silicon Drift Sensors. For the optimisa-
tion of charge collection new structures were
implemented in the design of the sensors. New
detectors and test structures were implemented
in batch Sesame. The wafer contains 40 sensors
for Sesame project, some prototype for Hermes
experiment, various SDD as well as new PixDD
16×8 sensors. The 17 wafer of batch Sesame
were produced by FBK at the end of June. The
first automatic test of test structures and some
SDD were performed by FBK on the wafer. Then
a test of a large number of Sesame sensors were

performed with a probe card that optimises the
test process and applies a bias on all eight cells
of the structures at the same time. Sensor test-
ing has revealed great variation of doping con-
centration from the center to the edge of the
wafer.

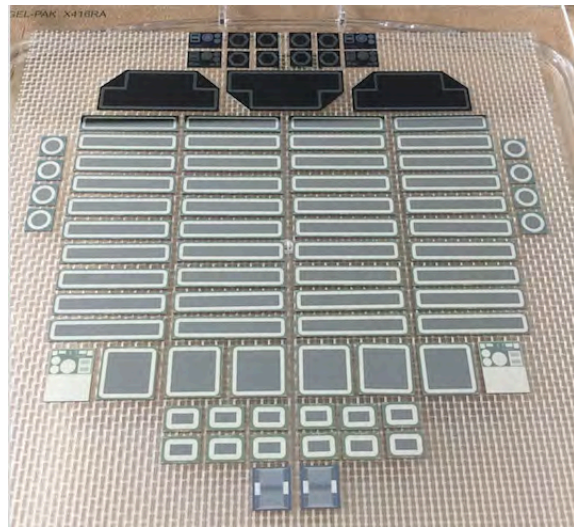


Figure 1: Batch Sesame.

This fact introduced a further parameter of
uniformity in the choice of the sensors and re-
quired some changes in the power supply of
whole system. This work for the realisation of
the SESAME detectors with 64 readout chan-
nels that INFN will realise for the Jordanian
synchrotron facility is still in progress.

The close collaboration between the RED-
SOX project and FBK that jointly develop the
SDD sensors has produced remarkable achieve-
ments in the design of very-large area, low leak-
age current, spectroscopy detectors for low X-
ray measurements (Hernanz et al. 2018). The
batch LOFT2018 produced in FBK in Septem-
ber of 2018 showed very promising results at a
preliminary test. The new probe card will be de-
signed and produced for the complete double-
sided test of LOFT detectors with active area of
76 cm².

[†]Contact Author: irina.rashevskaya@tifpa.infn.it

Selected Papers

- Bufon, J., Schillani, S., Altissimo, M., Bellutti, P., Bertuccio, G., Billè, F., Borghes, R., Borghi, G., Cautero, G., Cirrincione, D., Fabiani, S., Ficorella, F., Gandola, M., Gianoncelli, A., Giuressi, D., Kourousias, G., Mele, F., Menk, R., Picciotto, A., Rachevski, A., Rashevskaya, I., Sammartini, M., Stofa, A., Zampa, G., Zampa, N., Zorzi, N., and Vacchi, A. (2018b). *A new large solid angle multi-element silicon drift detector system for low energy X-ray fluorescence spectroscopy*. *Journal of Instrumentation* **13**(03), p. C03032.
- Evangelista, Y., Ambrosino, F., Feroci, M., Bellutti, P., Bertuccio, G., Borghi, G., Campana, R., Caselle, M., Cirrincione, D., Ficorella, F., Fiorini, M., Fuschino, F., Gandola, M., Grassi, M., Labanti, C., Malcovati, P., Mele, F., Morbidini, A., Picciotto, A., Rachevski, A., Rashevskaya, I., Sammartini, M., Zampa, G., Zampa, N., Zorzi, N., and Vacchi, A. (2018b). *Characterization of a novel pixelated Silicon Drift Detector (PixDD) for high-throughput X-ray astrophysics*. *Journal of Instrumentation* **13**(09), P09011.
- Hernanz, M., Brandt, S., Feroci, M., Orleanski, P., Santangelo, A., Schanne, S., Wu, X., Zand, J., Zhang, S., Xu, Y., Bozzo, E., Evangelista, Y., Galvez, J. L., Tenzer, C., Zwart, F., Lu, F. J., Zhang, S., Chen, T. X., Ambrosino, F., Argan, A., Monte, E. D., Budtz-Jorgensen, C., Lund, N., Olsen, P., Mansanet, C., Campana, R., Fuschino, F., Labanti, C., Rachevski, A., Vacchi, A., Zampa, G., Zampa, N., Rashevskaya, I., Bellutti, P., Borghi, G., Ficorella, F., Picciotto, A., Zorzi, N., and Limousin, O. (2018). "The wide field monitor onboard the eXTP mission". *PROCS. SPIE - 2018*, p. 149.

SEED

Lucio Pancheri,[†] Fabio Acerbi, Damiano Martorelli, Giancarlo Pepponi, Matteo Perenzoni, Antonino Picciotto

SEED project was born with a two-fold objective: to develop an innovative technology for monolithic sensors in CMOS technology and, at the same time, to demonstrate the possibility of a technology transfer between INFN and industry in the field of microelectronics. From the technology point of view, the goal of the project is the development of a monolithic fully-depleted sensor suitable for a wide range of energies, embedding different dedicated IP blocks. This achievement will demonstrate how monolithic CMOS can meet different requirements in radiation detection applications with a performance that goes beyond the current state of the art. At the same time, the active participation of an industrial partner (LFoundry) providing support on process technology, offers the unique opportunity to create a synergy between microelectronic designers and a silicon foundry, which has been sought for a long time by the national scientific community.

The first phase of the project has been devoted to the tailoring of the CMOS fabrication technology to include the particle sensors. The optimal substrate doping and process parameters have been identified by means of an extensive TCAD device simulation campaign, which was carried out at TIFPA, in tight collaboration with the foundry process engineers.

In parallel, a first test chip including pixels with different geometry parameters has been designed at INFN Torino. This chip was conceived as a first test bench for the proposed technology, suitable for an experimental char-

acterization with particles, X-rays and optical sources. A micrograph of the implemented pixel array, featuring $50\ \mu\text{m} \times 50\ \mu\text{m}$ pixels, is shown in Fig. 1.

A first MPW run has been produced in 2017 on wafers with a thickness of $300\ \mu\text{m}$. The first tests demonstrated the possibility of fully depleting the sensors and the complete functionality of electronics (Panati et al. 2018). A first test campaign showed a depletion voltage lower than 200 V and a pixel electronic noise of 40 electrons rms. The first spectra were acquired with an X-ray source of ^{55}Fe and with a pulsed laser source. A second production run was finished at the end of 2018, and demonstrated the possibility of realizing monolithic sensors with a thickness of 100 and $400\ \mu\text{m}$. A complete characterization campaign of the produced sensors is currently under way.

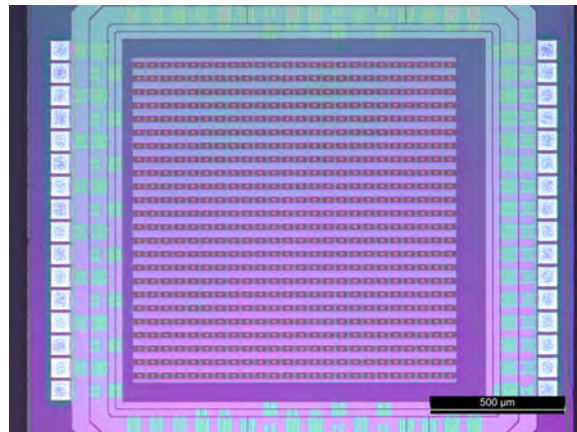


Figure 1: Micrograph of SEED pixel array

Selected Papers

Panati, S., Olave, J., Rivetti, A., Pancheri, L., Cossio, F., Giubilato, P., Pantano, D., Mattiazzo, S., Rolo, M. D. D. R., and Demaria, N. (2018). “MATISSE: A Versatile Readout Electronics for Monolithic Active Pixel Sensors Characterization”. *2017 IEEE NSS-MIC Conference Record*. Piscataway, U.S.A.: IEEE.

[†]Contact Author: lucio.pancheri@unitn.it

SICILIA

Maurizio Boscardin,[†] Pierluigi Bellutti, Giacomo Borghi, Sabina Ronchin

Silicon carbide (SiC) is one of the compound semiconductor which has been considered as a potential alternative to Silicon (Si) for the realization of charge particles detectors. The chemical and physical material properties are promising for high temperature and high radiation operation conditions (Tudisco et al. 2018). SiC diodes are predicted to be radiation harder than Si due to the high displacement threshold energy and potentially used as radiation detectors in high radiation conditions. The recent progresses in the material growth and device technology, allowed to realize high performances SiC detectors. The potentialities of SiC as detectors are many, they have been used to detect neutrons, X-rays, protons, alpha particles and heavy-ions.

The radiation-hardness of the material makes it particularly interesting for all those activities where high flux must be detected. One of these activities is the NUMEN project. The Schottky junctions represent today the state of art for SiC devices. The thin surface layer of the junction reduces the straggling of the particles with respect to the p/n junctions and produces higher resolution detectors. The first step for the development of new devices is the realization of some 4H-SiC prototype detectors with performances suitable to monitor heavy ions at high energy and at high dose. SiC is considered to be radiation harder than Si, however a direct comparison between the two types of detectors is not reported in the literature.

We performed a comparison of different Schottky diodes realized with different metals (Ni₂Si, Au) both from the electrical characteristics point of view and from the energy resolution analysis using alpha particles to evaluate the detectors performances. Also the performances of these detectors as X-Ray detectors have been analysed in details.

The SiC Schottky diodes have been realized in the Fondazione Bruno Kessler Microfab-

rication Facility on 4H-SiC wafers supplied by LPE, the epilayer is 10 μm thick and doped in $5 \times 10^{13} \text{ cm}^{-3}$.

A Schottky diode is made of a thin metal layer to form the Schottky contact on the semiconductor surface, for this process we have used two different metals: Au and Nickel. In particular, the nickel (deposited at the IMM-CNR Catania) has been annealed by the RTA in order to obtain the nickel silicide. On the top of this metallization, we add 1.2 μm of Al1%Si in order to realize the bonding pads. A silicon oxide deposited at 720 °C (TEOS) but annealed at high temperature was used as a passivation. For the final back-side metallization, we used a Ti metallization layer.

Devices have been made with different geometry and area:

- (i) circular diode 300 and 500 μm in diameter;
- (ii) square diodes with an area of about $2.5 \times 2.5 \text{ mm}^2$ and $5 \times 5 \text{ mm}^2$.

Also different types of terminations have been explored in particular:

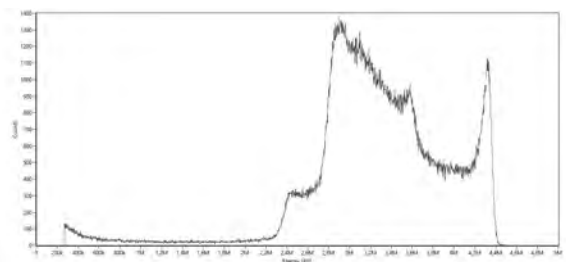


Figure 1: The figure shows the preliminary energy spectrum taken illuminating a SiC detector with a ²⁴¹Am alpha source in air. The detector is a Schottky diode obtained with a Au deposition on a 10 μm SiC epitaxial layer. The device, W1-2.5_JTE1_GR_JTE1_6,1, was produced in the first run in 2018. The active area of the device is 2.5 mm². The spectrum, presently under study, has a complex structure due to the junction termination extensions and the floating guard ring.

[†]Contact Author: boscardi@fbk.eu

- (i) The first is based on an annular Schottky contact surrounding the main diode that acts as guard electrode for collecting the surface currents, both singular and multiple ring structures have been realized;
- (ii) The second is based on junction termination extension (JTE) technique.

The JTE is implemented through a boron implantation done at RT, followed by annealing step at 1050 °C. Furthermore, combinations of the two previous structures have been designed. All the diodes detectors have been characterized by an automatic probe station with an I-V scan from -200 V to 5 V and with a C-V char-

acterization up to 40 V.

The device characterization with Alpha sources, was carried on at INFN Milano lab. A vacuum system has been assembled with the camera sitting on the pump through a valve. The hybrid CSP (Cremat CR110) is connected to the feedthrough flange on one side and to the Amplifier (Cremat CR220-2us) and digital pulse analyzer on the other. The flexibility of the solution allows the CSP to stay both inside and outside the vacuum chamber. A preliminary Alpha spectrum of ^{241}Am source, collected with a silicon reference PiN diode, on a SiC detectors is shown in Fig. 1.

Selected Papers

Tudisco, S. et al. (2018). *Silicon Carbide Detectors for Intense Luminosity Investigations and Applications*. *Sensors* **18**(7), p. 2289.

TIMESPOT

Gian-Franco Dalla Betta,[†] Maurizio Boscardin, Giulio Tiziano Forcolin, Mostafa El Khatib, David Macii, Roberto Mendicino, Sabina Ronchin, Giovanni Verzellesi

The project is aimed at the development and implementation of a complete integrated system for tracking having very high precision both in space ($100\ \mu$ or less) and in time (100 ps or less) per pixel. The main use and scope is in HEP experiments at high luminosity (e.g., upgrade of LHCb VELO), where the high density tracking, both in space and time, is an issue. The approach is based on 3D geometry Silicon and Diamond pixelated sensors, dedicated integrated front-end and pre-processing chip (time measurement electronics) in 28 nm CMOS, and real-time processors for data elaboration both at front-end and back-end level (fast tracking algorithms). TIFPA is responsible for WP1: 3D Si sensors development and characterisation, and is also involved in WP6: System integration and tests.

In 2018, the main effort was devoted to the development of 3D pixel sensors optimised for timing, while retaining their usual advantages of low depletion voltage (hence low power dissipation), extreme radiation hardness, owing to the very short inter-electrode distance, and active edges.

The work leverages on the experience within the INFN-FBK collaboration for 3D pixel sensors oriented to ATLAS and CMS upgrades at the HL-LHC, and the fabrication process is based on the FBK single-sided approach using Si-Si Direct Wafer Bonded substrates.

Nevertheless, in order to achieve good timing performance, 3D sensors with columnar electrodes are not the best solution: the signal response to particles is not spatially uniform because of very low-field regions within the active volume. The pixel geometries should therefore be optimised in terms of size, electrode configuration and shape. In particular, trenches should be used instead of columns, in order to achieve more uniform electric field and weighting field profiles.

The pixel design has been carried out with the aid of TCAD simulations, while keeping into account some relevant constraints for manufacturability, that have been investigated by dedicated technological tests at FBK. The pixel layout has been optimised aiming at the best trade-off between the intrinsic speed and the capacitance, the latter affecting the bandwidth of the read-out channel and its noise, thus degrading the timing performance. We have targeted an active thickness of $150\ \mu\text{m}$ and a pixel size of $55\times 55\ \mu\text{m}^2$ (in order to be compatible also with the readout chips of the TIMEPIX family). An example of pixel layout and the corresponding 3-dimensional simulation domain, including all details of FBK technology, are shown in Fig. 1. Exploiting the existing symmetry, half of the pixel was simulated to estimate the capacitance.

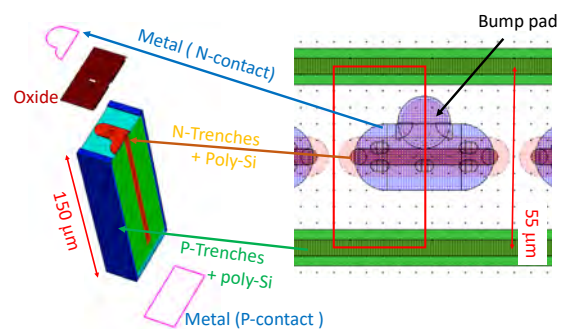


Figure 1: Example of pixel layout of a 3D trenched-electrode pixel of $55\times 55\ \mu\text{m}^2$ size, and 3D cut of the structure used as a domain for capacitance simulations.

Fig. 2 shows the simulated capacitance-voltage (C-V) curves for different values of the gap in between trenches. It can be seen that the backplane contribution is not sensitive to the gap dimension. On the contrary, the inter-pixel capacitance saturates at very low voltage

[†]Contact Author: gianfranco.dallabetta@unitn.it

and is strongly dependent on the gap dimension, as expected. In order to obtain the total pixel capacitance, the two contributions should be multiplied by two (only one half of a pixel is simulated) and then summed. The values at 100 V bias vary from ~ 110 fF at a gap of $14 \mu\text{m}$ to ~ 160 fF at a gap of $6 \mu\text{m}$.

Since the sensor capacitance has a strong impact on the timing performance of the full system, a gap of $15 \mu\text{m}$ has been chosen for the first sensor implementation, for which the intrinsic signals are still fast enough, with rise times of just a few tens of ps. Incorporating the sensor current transients and capacitance in circuit simulations of the pixel read-out yields a jitter of about 50 ps, good enough for the intended application.

Preliminary simulations of radiation hardness are also encouraging, with very high charge collection efficiency up to an irradiation fluence of $2 \times 10^{16} \text{ n}_{eq} \text{ cm}^{-2}$.

At FBK, the entire process sequence was tested, and the recipes for the most critical steps

were tuned. The reticle layout was designed at UniTN. It includes a main pixel sensor compatible with Timepix readout chip, and a number of different test devices (pads, strips, pixels). The fabrication of the first batch of sensors is under way.

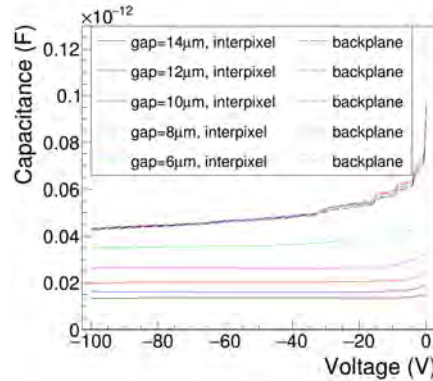


Figure 2: Simulated capacitance-voltage curves of a 3D trrenched-electrode half-pixel of $55 \times 55 \mu\text{m}^2$ size for different values of the gap in between trenches (backplane and interpixel contributions).

XDET

Lucio Pancheri,[†] Maurizio Boscardin, Sabina Ronchin, Giovanni Verzellesi, Majid Zarghami, Giacomo Baldi, Giulio Monaco

The use of large accelerator-driven X-ray sources, such as synchrotron light and free-electron lasers (FEL) facilities, continues to grow and expand to many scientific disciplines worldwide. A large number of synchrotron radiation sources is available around the world. Each of them features a large number of beam-lines, providing photons with wavelengths spanning from the atomic level to biological cells, which can be used as probes for advanced research in material science, physical and chemical science and in the medical and pharmaceutical fields. On the other hand, newly proposed X-ray FELs, with their outstanding properties in terms of brilliance and pulse duration, can offer unprecedented capabilities in penetrating the microscopic structure of organic and inorganic systems, new materials and matter under extreme conditions and in recording and understanding the time evolution of fast biochemical phenomena at the nanoscale.

The XDET project aims to develop advanced instrumentation for X-ray imaging applications compliant with the very challenging specifications set by the FEL environment in terms of input dynamic range, processing speed, amplitude resolution and radiation hardness. The collaboration also plans to extend the use of the developed instrument to synchrotron light source experiments.

The research has considered two different approaches, one based on hybrid, the other based on monolithic sensor technology (Fig. 1). While the currently existing solutions in imag-

ing at FELs is based on the first one, the second one is appealing for its lower cost and for its easier integration process. The feasibility of monolithic sensors optimized for the high photon fluxes found in XFELs has been explored with the help of TCAD simulation, and the necessary process modifications for the optimization of charge collection have been identified. Meanwhile, a preliminary study to port the circuit blocks designed in PixFEL project (Ratti et al. 2018) to a suitable process has been performed.

In parallel, the 3D integration of the ROIC and the sensors developed in PixFEL project has been pursued, and the integrated assemblies have been delivered.

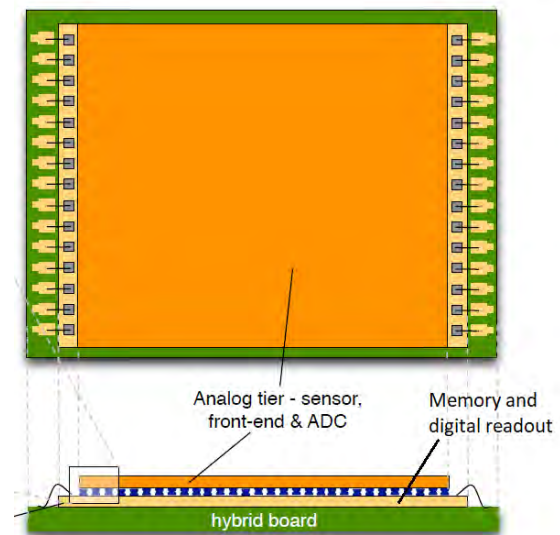


Figure 1: Concept view of XDET sensor

Selected Papers

Ratti, L., Comotti, D., Fabris, L., Grassi, M., Lodola, L., Malcovati, P., Manghisoni, M., Re, V., Traversi, G., Vacchi, C., Batignani, G., Bettarini, S., F., C. F., Morsani, F., Paladino, A., Paoloni, E., Rizzo, G., Benkechache, M., Dalla Betta, G.-F., Mendicino, R., Pancheri, L., Verzellesi, G., and Xu, H. (2018). "The PixFEL front-end for X-ray imaging in the radiation environment of next generation FELs". *2017 IEEE NSS-MIC Conference Record*. Piscataway, U.S.A.: IEEE.

[†]Contact Author: lucio.pancheri@unitn.it

Activities starting in 2019

ARCADIA

Research outline The purpose of the project is to develop a novel CMOS platform tailored for the realization of pixel sensors with the following characteristics:

- Active sensor thickness in the range 50 μm to 500 μm or more;
- Operation in full depletion with fast charge collection only by drift;
- Small charge collecting electrode for optimal signal-to-noise ratio;
- Scalable readout architecture with ultra-low power capability;
- Compatibility with standard CMOS fabrication processes.

Fully depleted CMOS sensors have gained the attention of the scientific community. Novel designs exploiting commercial bulk technologies have been recently proposed, while the more traditional SOI-based process has been improved. Nevertheless, a technology incorporating all the characteristics listed above does not yet exist. Such a technology will allow to replace the more expensive standard hybrid pixel and silicon sensors in most applications. It is hence relevant for all those experiments that plan to use silicon detectors, including experiments at future colliders and space-born experiments. The project relies on the positive results achieved in the explorative research SEED, which led to the development of a patent-pending approach, validated on small scale sensors with an elementary readout.

A strict cooperation with the silicon foundry will allow to further improve the sensor performance in terms of signal-to-noise ratio and power consumption. By using the latest design integration and verification methodologies, large area sensors, indispensable for a thorough validation of the concept will be deployed. A common readout framework makes it possible to characterise different sensor flavours by changing only the substrate material. The federation of a large number of INFN units provides the critical mass and allows to foster the expertise of the national community in the field of CMOS radiation imagers, improving the competitiveness of INFN in this critical field.

INFN groups Bologna, Milan, Padua, Pavia, Perugia, Turin, TIFPA

Principal Investigator Manuel Rolo, INFN Turin

TIFPA team Lucio Pancheri (coordinator), Gian-Franco Dalla Betta, Andrea Ficorella, Majid Zarghami, Matteo Favaro, Roberto Iuppa, Paolo Zuccon, Francesco Nozzoli, Benedetto Di Ruzza, Ester Ricci

DRAGON

Research outline Nuclear materials may compose a threat to public health and homeland security in the form of terrorism threats, lost orphan sources, nuclear accidents or radioactive contamination, special nuclear material (SNM). The goal of the Dragon project is to design, develop and characterize a mobile system composed of an Unmanned Aerial Vehicle (UAV). The UAV will be equipped with a detection system able to identify radioactive contamination spread over an area of a few to tens of square meters. Moreover, it can be easily brought to the site rather than bringing

the suspicious vector to the screening device. Being mounted on a UAV, the detection system and electronics shall be defined by size, weight and power constraints. The proposed technology incorporates thermal and fast neutron detectors along with gamma ray detectors. These measurements are complementary: their combined power is expected to improve the system performances. In particular SNM (Highly Enriched Uranium and Plutonium) are difficult to detect, especially when masked or shielded: gamma rays and neutrons emitted by SNM have to be detected in order to increase the sensitivity against natural background.

INFN groups Padova, TIFPA

Principal Investigator Sandra Moretto (INFN Padova)

TIFPA team Davide Brunelli (coordinator), Alberto Quaranta

ERFNet

Research outline The development of a ground network, using irradiation facilities, habitat simulators, and a smart managing system would be a key achievement to optimize radiation physical countermeasures, providing also the first smart support for this endeavor: this is the key motivation driving the development of ERFNet. This project aim is to support studies relevant for radiation risk mitigation in exploration class space missions. In the first stage, ERFNet goal will be to help studies on radiation shielding, including works targeted at optimizing the design and development of space habitats. Future upgrades will likely include also radiobiology studies. The infrastructure is based on three main pillars: irradiation facilities, habitation facilities and smart knowledgebase and managing system. ERFNet will provide a single access point (Web-interface) to the system, developed for an easy and complete access to most of the relevant information in the field, to operate on this information (i.e. perform new simulations to characterize and use new materials for shielding purposes), to provide suggestions for design optimization, to facilitate use of the linked facilities.

involved external institutions Thales Alenia Space (TAS), Italy; Helmholtzzentrum für Schwerionenforschung — GSI, Germany

INFN groups Rome Tor Vergata, TIFPA

Principal Investigator Livio Narici, Rome Tor Vergata

TIFPA team Chiara La Tessa (coordinator), Francesco Tommasino

FIRE

Research outline The project FIRE (Flexible Organic Ionizing Radiation Detectors) will develop innovative radiation detectors based on Organic Thin Film Transistors (OTFTs) in both direct and indirect configurations. We aim at detecting different radiation fields (X and gamma-rays, charged particles and neutrons) by tuning the optical and electrical properties of organic materials through their molecular structure. As a final result, FIRE will develop, implement and validate in relevant environment flexible, low-power 2D pixel detector matrices (up to 3x3 pixels) equipped with read out electronics. In particular we will develop:

1) indirect detectors based on Organic Photo Transistors (OPTs) coupled with plastic scintillators. Organic semiconductors are very efficient for near UV-IR light detection. We will fabricate OPTs with a photoresponse optimized for the light emission from organic scintillators synthesized in our laboratories. Polymeric scintillators (e.g. Polysiloxanes) will be developed where the higher average Z of the monomeric unit based on silicon can be exploited for applications in High Energy Physics. Suitable compounds of Li and B will be used to enhance thermal neutron detection. OTFTs will be fabricated with lithographic processes, with Au electrodes on flexible PEN substrates. 2) direct X-ray detectors based on semiconducting organic thin films OTFTs. The proof of concept of such detectors was recently demonstrated. We will develop novel X- and gamma-ray OTFT detectors by appropriately selecting novel and more efficient organic molecules (e.g. TIPGe) and by adding high Z molecules/compounds in the blend of the sensing organic thin film.

involved external institutions CNR

INFN groups Bologna, LNL, Napoli, Roma III, TIFPA

Principal Investigator Beatrice Fraboni (University of Bologna and INFN Bologna)

TIFPA team Alberto Quaranta (coordinator), Davide Brunelli, Matteo Favaro, Lorenza Ferrario, Viviana Mulloni, Enrico Zanazzi

GLARE-X

Research outline GLARE-X (Georeferencing via LAser Ranging and LAser debris Redirection from spaceE-X), a new 3-y interdisciplinary CSN5 experiment, is devoted to the development of innovative applications of lasers systems in space for georeferencing, debris removal and asteroid deflection. The georeferencing applications include precise position measurements in space, and on Earth from space, using arrays of cube corner retroreflectors. The objective is to integrate the functionalities of the laser beam for positioning and communication by employing semi-active modulated retroreflectors. The research effort is important for global navigation satellite systems, and applications related to fundamental science, namely the study of the orbital trajectories of moons and asteroids and their composition. The LNF and LNGS are responsible for these activities, with a participation of the TIFPA (FBK) for the design and production of the micro electro-mechanical systems of the modulated retroreflectors.

The TIFPA is responsible for the applications of laser ablation related to propulsion, space debris and asteroids. The Pulsed Laser Deposition (LPD) of the IdEA Laboratory is devoted to the study of the physics of the laser interaction in materials. The measurement of the mass of the ablated material, and the corresponding thrust generated by the ablated mass, are the key parameters for the space applications. Aluminium (space debris), candidate propellant materials and an asteroid simulating material were studied in the context of the New Reflections interdisciplinary CSN5 experiment. An understanding of the underlying physics is fundamental to technological innovation. The competences of the IdEA Laboratory are particularly suited for propulsion, where the propellant material has a primordial role. The objectives in GLARE-X are a further optimization of the measurements, which represent a new activity at the LPD, and an extension of the study, in terms of material and laser operational parameters, to define the laser-material combination adapted to each application. The *in situ* performance of the candidate combinations is evaluated with an orbit simulation program.

involved external institutions ASI for georeferencing; US industry SpaceX for the design of the space mission (launch, satellite platform and orbit); University of Central Florida for the asteroid simulating material.

INFN groups LNF, TIFPA, LNGS

Principal Investigator Giovanni Delle Monache (LNF)

TIFPA team William Jerome Burger (coordinator), Alvise Bogolini, Nicola Bazzanella, Massimo Cazzanelli, Claudio Cestari, Riccardo Checchetto, Christian Manea, Michele Orlando, Antonio Miotello and Jacopo Terragni

NEPTUNE

Research outline Protontherapy is an important radiation modality that has been used to treat cancer for over 60 years. In the last 10 years, clinical proton therapy has been rapidly growing with more than 80 facilities worldwide. The interest in proton therapy stems from the physical properties of protons allowing for a much improved dose shaping around the target and greater healthy tissue sparing. One shortcoming of protontherapy is its inability to treat radioresistant cancers, being protons radiobiologically almost as effective as photons. Heavier particles, such as ^{12}C ions, can overcome radioresistance but they present radiobiological and economic issues that hamper their widespread adoption. Therefore, many strategies have been designed to increase the biological effectiveness of proton beams. Examples are chemical radiosensitizing agents or, more recently, metallic nanoparticles. The goal of this project is to investigate the use of nuclear reactions triggered by protons generating short-range high-LET alpha particles inside the tumours, thereby allowing a highly localized DNA-damaging action. Specifically, we intend to consolidate and explain the promising results recently obtained, where a significant enhancement of biological effectiveness was achieved by the $p\text{-}^{11}\text{B}$ reaction. Clinically relevant binary approaches were first proposed with Boron Neutron Capture Therapy (BNCT), which exploits thermal neutron capture in ^{10}B , suitably accumulated into tumour before irradiation. The radiosensitising effects due to the presence of ^{10}B will be compared to those elicited by $p\text{-}^{11}\text{B}$, using the same carrier and relating the observed effects with intracellular ^{11}B and ^{10}B distribution as well as modelled particle action and measured dose deposition at the micro/nanometer scale. Moreover, the $p\text{-}^{19}\text{F}$ reaction, which also generates secondary particles potentially leading to local enhancement of proton effectiveness, will be investigated. The in-vivo imaging of ^{11}B and ^{19}F carriers will be studied, in particular by optimizing ^{19}F -based magnetic resonance.

involved external institutions Institute of Molecular Bioimaging and Physiology (IBFM) — CNR, Italy; Institute for Microelectronics and Microsystems (IMM) — CNR, Italy; Institute for Complex System (ISC) — CNR, Italy; University of Wollongong (UoW), Australia; University of Naples (UNINA), Italy; University of Campania (UNICAMPANIA), Italy; Istituto Superiore di Sanità (ISS), Italy; Treatment Planning and Computational Dosimetry group of GNEA, Argentina; Bruno Kessler Foundation (FBK), Italy.

INFN groups LNS, Milan, Naples, Rome 3, Pavia, TIFPA

Principal Investigator Giacomo Cuttone, INFN-LNS

TIFPA team Chiara La Tessa (coordinator), Sofia Colombi

tHEEOM-RD

Research outline The tHEEOM-RD project aims at development of technologies for High Efficiency Electro-Optical Modulators (EOM) based on RF/Optical conversion to realize Quantum Sensing in the context of emerging Quantum Technologies. Reversible transduction between optical and RF/Optical signals is nowadays particularly relevant, both in classical and quantum communication systems. The RF/Optical conversion is based on two resonating subsystems (optical & RF) strongly interacting with a metalized nanomechanical vibrating membrane. The mechanical resonator bridges the RF to the Optical domain and viceversa. On one side the vibrating membrane interface with the radiation pressure of a high finesse cavity while on the other the capacitive coupling is realized with the metalization of the membrane.

The EOM three-oscillator system can be readout with a shot-noise limited homodyne detection scheme able to detect RF/Optical weak signals. This feature opens to applications that ranges from medical imaging nuclear magnetic resonance, RF non-reciprocal insulators and, classical/quantum communications links. For instance, a EOM device may links superconducting qubits to high-speed optical fibers or realize a state transfer between two nodes. Nano-Micro Electro-Mechanical Systems (N/MEMS) technologies will be used to fabricate a device with a high mechanical susceptibility that is need for coupling with the radiation pressure. N/MEMS technologies are also exploited to scale-down the devices for possible system-on-a-chip integration of the EOM in a RF/Optical apparatus.

The major outcome of the project will be the study the interaction phenomena between the three-resonators, develop and fabricate state-of-the-art high efficiency EOM modulator and RF and Optical measurement protocols. Notably, to reach the transduction and conversion performances of the EOM device we will focus on:

- minimizing the mechanical losses due to the presence of the metallized electrode. Reducing losses, increase the readout sensitivity and at the same time to reduce the decoherence rate produced by the surrounding thermal bath;
- increasing the optical and electromagnetic coupling with a proper electrode design of the variable capacitance.

This is achieved maximizing the overlap between the fixed electrode and the membrane's modes that works as variable capacitance electrode. N/MEMS silicon bonding technologies will be exploited for enhancing the capacitive and optical coupling while the bulk-micromachining techniques will be used to pattern the acoustic insulating stage for the seismic vibrations.

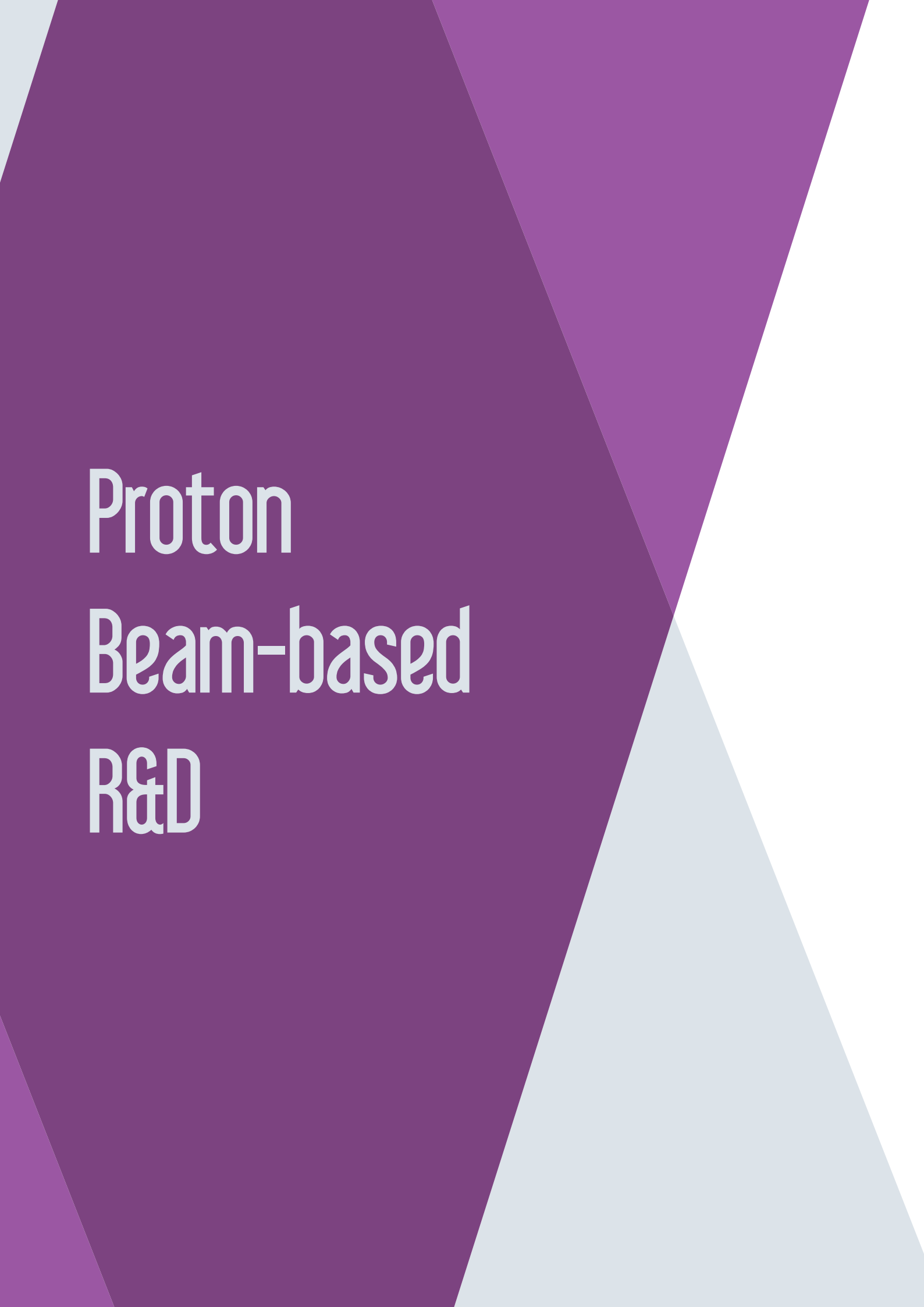
Operationally, we will start from a promising opto-mechanical resonator developed in the framework of HUMOR experiment (INFN CSN-II) that recently has shown a thermal occupation number lower than 4 in a moderate cryogenic regime. We first fabricate an EOM prototype for the RF-to-Optical conversion of weak signals at room temperature and the project will further explore the compatibility of the system with cryogenics for possible quantum state transfer.

involved external institutions Technical University of Delft - Else Kooi Laboratory (TU-Delft-EKL), The Netherlands

INFN groups TIFPA, Perugia

Principal Investigator Enrico Serra, TIFPA

TIFPA team Enrico Serra (coordinator), Michele Bonaldi, Antonio Borrielli, Giovanni Andrea Prodi



Proton Beam-based R&D

Francesco Tommasino

francesco.tommasino@unitn.it

Coordinator,

TIFPA Protontherapy Experimental Room Activities



The last year has been dense of activities for what concerns the Experimental Room at the Trento Proton Therapy Centre (PTC). Specifically, extensive work has been performed in order to setup a passive scattering line to be installed at the 0° beam line. This was necessary to pave the way to all the experiments that need irradiation over a large field. Two dual-ring setups have been optimized by means of Monte Carlo simulations and then experimentally characterized. The results of the characterization (summarized in Tommasino et al. 2019, see p.149) show that the setup allows obtaining dose uniformity above 94% over a 6 or 16 cm diameter region (depending on the setup adopted), which makes feasible performing a large spectrum of radiobiology experiments. Moreover, two monitor chambers have been installed during 2018 (one for each beam line), thus offering the possibility of an on-line feedback of the beam delivery that was previously missing.

In parallel to that, the activities performed by external users continued over 2018, and the overall number of proposals received since the PAC was established is now above 40. As usual, a large spectrum of activities was performed, as demonstrated by the reports collected in this section ranging from detector testing (MoVe-IT TLD and Beam Profiling devices, PRIMA-RDH) to radiation hardness (ALICE-TOF), including also the first radiobiological experiments (BIRD, pFDG). We were also glad to host an experiment performed by high-school students, named PROMETHEUS, which was dedicated to the test of a SiPM-based sampling calorimeter for beam characterization.

As now usual, users interested in performing experiments with proton beam at the Experimental Room can submit a proposal to the PAC, which meets three times per year. The documentation needed for proposal preparation can be found online (<http://www.tifpa.infn.it/sc-init/med-tech/p-beam-research/>).

Irradiation campaign for electronic components to be used in ALICE TOF

Pietro Antonioli,^{1†} Casimiro Baldanza,¹ Davide Falchieri,¹ Marco Giacalone,² Roberto Preghenella¹

As part of the upgrade programme foreseen for the ALICE experiment at the LHC, the readout system of the Time Of Flight (TOF) detector will be renewed: in the existing custom VME crates housing TDC cards, the DRM (Data Read-out Module) VME master card will be replaced by a new version DRM2, housing new data links to DAQ and trigger systems.

The DRM2 is going to work in a moderately hostile environment, with a total dose of 0.13 krad in 10 years and a flux of 0.26 kHz/cm² of hadrons with energy above 20 MeV. Given the radioactivity foreseen the damages for TID are here less relevant: we wanted to estimate SEU (Single Event Upset) rates and potential SEL (Single Event Latchups). We used previously TIFPA facility at Trento *Centro di Protonterapia* (proton therapy centre) during two irradiation campaigns in 2016 to test several COTS components candidates to be used on DRM2. At that time a prototype card (the GBTx test board) was used.

In 2018 we had an additional test, using the final card (showed in Fig. 1) with the purpose of validating two remaining key components. This was due to non satisfactory results emerged during 2016 campaigns. These are the Microsemi Igloo2 FPGA M2GL090T-1FG676I and the optical transceiver (a commercial SFP+) to be used to implement the slow control optical link. This link implements a CONET link protocol, paired with a commercial PCIe card distributed by CAEN. The Microsemi Igloo2, being Flash memory based, is inherently immune to SEUs in the configuration memory, but the first silicon revision tested in 2016 revealed the occurrence of SEL. This also prevented the possibility to take a proper measurement of the SEU cross section in the internal FPGA RAM

(BRAM). The SEL problem was then corrected by Microsemi. Presence of SEL was also observed in SFP+ from Finisar (FLTL8524P28BNL and FLTL8524P28BNV). Much better performance were observed on SFP+ from Avago (AFBR-57R5APZ and AFBR-57R5AEZ) but with insufficient statistics. The campaign in 2018 was therefore aimed to verify the absence of SEL in the new silicon revision of the FPGA and to collect enough statistics on the Avago SFP+.

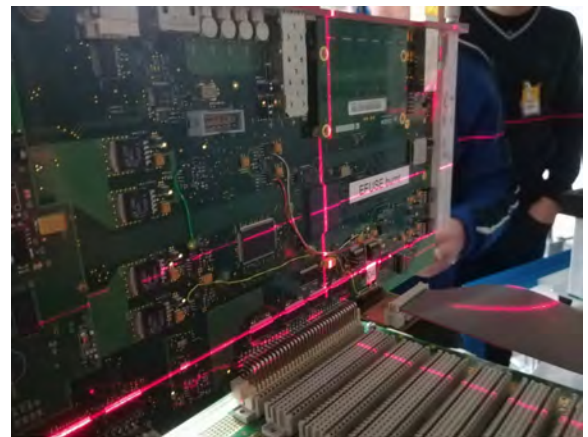


Figure 1: The DRM2 card

To monitor SEL and protect against them a LabView interface to DC power supplies was implemented. To monitor SEU we used both data transmission via the SFP+ commercial link and via TCP/IP exploiting the ARM CPU hosted by the DRM2 card: fixed memory patterns were written in BRAM memory cells and continuously tested.

The beam intensity delivered in the TIFPA experimental cave was measured with a detector consisting of a stack of coupled strip and integral IC. The dimension of the beam spot, fitted with a Gaussian approximation, was estimated at $\sigma = 5.8$ mm (used for SFP+ and

[†]Contact Author: pietro.antonioli@bo.infn.it

¹INFN Bologna, Italy

²INFN Bologna and Bologna University, Italy

one FPGA). We decided then to move the DUT downstream in the beam direction to obtain a more uniform irradiation of the actual silicon device die ($1.0 \times 1.0 \text{ cm}^2$) and we measured a $\sigma = 11.2 \text{ mm}$. We used the proton beam at 100 MeV energy.

Table 1 summarizes the number of devices tested, the maximum radiation dose and the flux intensity used. The results obtained during 2018 campaign are:

- (i) no SEL observed on the FPGA with silicon revision 3.
- (ii) no TID damages on the FPGA. In particular it was always possible to reprogram the irradiated FPGA. For the one irradiated at the larger doserate - 2.12 rad/s - it was needed, though, some annealing period (reprogramming failed immediately after irradiation, succeeded after 12 hours).
- (iii) a SEU cross section was estimated for the BRAM $\sigma_{SEU} \approx (2.0 \pm 0.3) \cdot 10^{-14} \text{ cm}^2/\text{bit}$ based on collected statistics of $\mathcal{O}(100)$ errors. This is consistent with results reported by other groups on this device;
- (iv) no SEL and TID damages on the AVAGO SFP+. The SFP+ registers were also monitored (via I²C interface): no upset and/or transients were observed during irradiations.
- (v) no transmission errors (link loss) or data transmission data corruption (SEU) when

SFP+ was under irradiation.

The results on the PZ and EZ transceivers are slightly different with respect to those obtained in October 2016 (a configuration lost and 2 SEU). We believe some instabilities observed at that time might be due to a problem - now fixed - in the CONET driver of the receiving Linux machine at the other end of the link. For the final card, at the end, we opted for the EZ version that has better EM shielding (as stated by the manufacturer).

Together with the measurements done in 2016, these results allowed us to qualify (or to exclude) several electronic components to be used in the DRM2 ALICE TOF card and not yet tested elsewhere. The 2018 campaign confirmed results obtained by other groups about the immunity to SEL of the chosen FPGA and it allowed us to select the commercial SFP+ after a robust test. The DRM2 card is now under production and will be installed in 2019 at the ALICE pit. Remarkably, with respect to irradiation campaigns operated preparing DRM1 in the early 2000s, this time we were able to qualify all relevant components in an Italian facility.

Acknowledgements we gratefully acknowledge the continuous support received by TIFPA personnel during the irradiation campaign, in particular for monitoring beam conditions, for providing beam characterization and an efficient interface with the IBA personnel.

DUT	Type	# chip	I (p/cm ² s)	TID (krad)
M2GL090T-1FG676I	FPGA	3	$1.9 \cdot 10^8$	3.82
AFBR-57R5APZ	SFP+	4	$1.0 \cdot 10^8$	5.87
AFBR-57R5AEZ	SFP+	4	$1.0 \cdot 10^8$	5.87

Table 1: Devices under test (DUT) during the 2018 irradiation campaigns. The reported proton beam intensities (I) and total doses (TID) refer to the highest used irradiating a given device.

BIRD (Biological Ionizing Radiation Damages)

Simonetta Croci,^{1†} Massimo Manghi,¹ Luca Bruni,¹ Francesco Tommasino^{2,3}

Since radiobiology was born its role in medical and oncological fields became more and more crucial, in several cases being at the core of breakthroughs of new therapeutical and diagnostic techniques. The study of biological effects of radiation is at the centre of this investigation for the implications this has in the refinement of radiotherapy optimization. The aim of the project is the development of a quantitative index capable of accounting for the effects born to living matter by ionizing radiation. In literature the bulk of experiments aim at the evaluation of DNA damages and their effects on the cellular life. Still, beyond DNA cytoskeleton is another element of a cell. The cytoskeleton is made of three main structures: microtubules, microfilaments and intermediated filaments. Cytoskeleton makes up not only cell scaffold, but it is also a central player in the process of cell migrations and tissue invasion. These features are shared by immune system cells and cancer cells as well. The cytoskeleton forms a sort of protein network embedded into the cytoplasm, which stretches from the nucleus to the cell edge and vice versa. Because of the physical and biological role played by the cytoskeleton it's worth investigating it as a biological target of protons and X-rays, in order to correlate the biological effects of two diverse ionizing radiations.

Sample preparation In detail, the goal of our study is the evaluation effects of ionizing radiations (X-rays and protons) on cytoskeleton of two different cell lines. A non-cancer, non-immortalized human breast epithelial cell line and a mammary infiltrating ductal carcinoma Hs 578T, coming from the same patient whom Hs 578Bst line origins from; both of them are

purchased by ATCC. In the 2018 we performed experiments only on the non-cancer Hs 578Bst cell line. The sample cultures were handled at the TIFPA cell laboratory. Cells processing phases were:

- cell line defrosting followed by stabilization;
- cell medium refreshing in the following days, as soon as the demanded cell concentration was reached;
- cells seeding into suitable dishes for the irradiations experiments.

The samples irradiation took place the day after the cells were sowed. From thawing to seeding the procedure took 5 days on the average. Proton irradiation occurred at the Protontherapy Centre, while the X-ray irradiation took place at TIFPA. The sample preparation was the same for both types of the irradiation techniques.

X-ray irradiation - TIFPA Hs 578Bst cell lines were irradiated with XSTRAHL CABINET IRRADIATOR. The doses delivered were: 2, 8 and 25 Gy (not fractionated); the beam energy was 195 KV. The cell dishes were placed on the irradiator cabinet dish and then radiation was administered as long as the required dose was reached. Immediately after irradiation cells were placed back into the incubator for the time needed to complete the irradiation of all samples. Soon after, the plasmatic membranes of the cells were denatured as to expose the bare cytoskeleton. Then the cells were fixed by mean of the biological cape airflow. Cell fixation took about 40 minutes. Finally the samples kept in their dishes were stored in the darkness. Fig. 1a shows the cell cytoskeleton of a cell, after delivering 25 Gy of X-ray. The whole fibres are recognizable despite the dose magnitude.

[†]Contact Author: simonetta.croci@unipr.it

¹University of Parma, Italy

²University of Trento, Italy

³INFN TIFPA, Trento, Italy

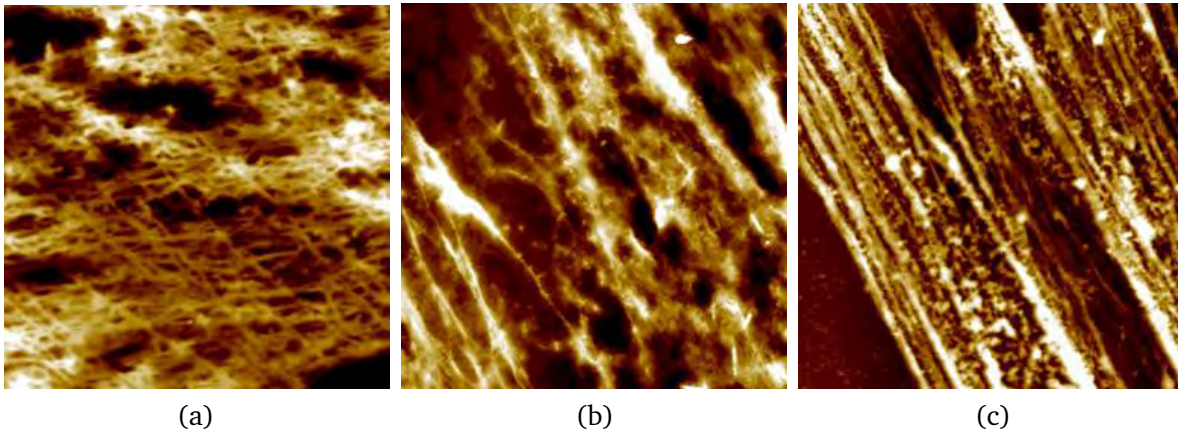


Figure 1: (a): Portion of Hs 578Bst control cell cytoskeleton; (b): Part of Hs 578Bst cell cytoskeleton irradiated with 8 Gy proton; (c): Part of Hs 578Bst cell cytoskeleton irradiated with 25 Gy of X-ray

Proton irradiation - protontherapy centre

Hs 578Bst cell lines were irradiated with protons at the protontherapy centre. The beam characteristics were: energy of 150 MeV, dose rate 1.2 Gy/min. Furthermore the combination of a scattering foil (tantalium) and a collimation system (PVC) allows to deliver to the sample a homogeneous dose. The squared irradiation field is 6 cm edge length. In Fig. 2 is depicted the experimental room within all the components previously described. The doses delivered were 2 and 8 Gy. In Fig. 1c is pictured the cell cytoskeleton after delivering 8 Gy of protons. It is clear how the cell cytoskeleton structure is damaged after irradiating, compared to the control sample (Fig. 1a) in which the cytoskeleton structure is visibly undamaged. The samples were managed in the same way as it had been done for X-ray irradiations, except for the amount of medium. Since the irradiation set up requested the cell dishes be positioned upright, they had been filled of cell medium in order to keep the sample covered by medium. To prevent medium leaking dishes were wrapped with parafilm®[®], before bringing them to the protontherapy centre. The samples were carried into polystyrene box to keep the samples at 37 °C and in the darkness. For each sample we allowed adequate time waiting

for the induced radioactivity to decay. Later on samples were brought back to the TIFPA laboratory for the cell membrane denaturation and fixation and storage procedure. All of the post irradiation steps were managed as planned for the X-ray irradiation protocol. In order to analyse the cell cytoskeleton structure by atomic force microscopy (AFM) it's necessary to have the cytoskeletal structures exposed and therefore as much as possible cellular membrane has to be removed.

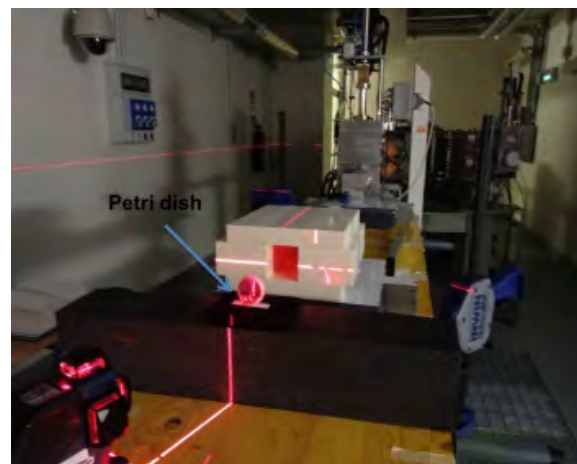


Figure 2: Experimental room at the proton therapy center. The cell dish stands upright in front of the PVC collimator (with structure). Behind it there is the tantalium foil to scatter the beam.

Scintillator-based beam profiling system

R. Catalano,^{1†} G. Petringa,¹ S.M.R. Puglia,¹ G. Cuttone,¹ E. Scifoni,² F. Tommasino,^{3,2} G.A.P. Cirrone^{1,4}

We report the results of the initial tests carried out to study the performances of a scintillator-based beam profiling system developed at the INFN-LNS for transversal relative dose profiles reconstruction. A comparison with other common quality control devices, routinely adopted in QA tests (i.e. EBT3 films and Lynx detector), has been also carried out both at the CATANA and TIFPA facilities. A comparison against the Timepix, a commercial silicon pixelated detector, has been performed as well.

Material and Methods A previous version of the beam profiling system was already designed and tested at INFN-LNS in 2002.^{1,2} This updated version consists of a (50×50) mm² EJ-204 plastic scintillator screen, characterized by high scintillation efficiency, high speed and good attenuation length, mounted perpendicularly to the beam axis. The light emitted when the scintillator is hit by the proton/ion beam is detected by a highly sensitive Peltier cooled, low-noise 14-bit monochromatic CCD camera with a resolution of 1928×1452 pixels (4.54 μ m wide square). A 45° mirror, positioned behind the plastic scintillator sheet reflects the light coming from the scintillator itself in the direction perpendicular to the beam axis, thus avoiding the direct irradiation of the CCD-chip. All the components of the system are assembled in Teflon light-tight box that can be easily transported (Fig. 1).

A dedicated software developed on the LabView 2016 platform (National Instruments, Austin, TX) for real-time data acquisition and processing, allows for the determination of the beam profile quality parameters (FWHM, field ratio, lateral penumbras, flatness, symmetry)

along both horizontal and vertical directions.

Results All measurements were performed setting the acquisition time of a single frame at 20 ms, while the beam images were obtained averaging over 1000 CCD frames in order to reduce the noise and ensure an uncertainty on the released dose of less than 3%. A 150×150 pixels region of interest (ROI) is then extracted from the averaged image and used for the analysis.

The short-term stability was evaluated performing consecutive irradiations under the same conditions. The relevant clinical parameters, extracted from the X-Y lateral dose distributions, have been derived and their average and variance evaluated, showing a system stability within 2.5% for each of the studied parameter.

A remarkable linear behavior of the detector over a wide range of exposure to clinical radiation dose values was observed, the signal increasing linearly as a function of the dose rate, in the studied range between 10.5 and 30.0 Gy/min, with a correlation fitting factor $R^2 > 0.99$. No saturation effects were observed,



Figure 1: External case of the prototype

[†]Contact Author: catalano@lns.infn.it>

¹INFN LNS, Catania, Italy

²INFN TIFPA, Trento, Italy

³University of Trento, Italy

⁴Institute of Physics ASCR, Prague, Czech Republic

¹Cirrone, G. A. P et al. (2004), IEEE Transactions on Nuclear Science 51, pp. 860–865.

²Cirrone, G. A. P et al. (2004), IEEE Transactions on Nuclear Science 51, pp. 1584–1587.

being the light output at the maximum delivered dose rate well below the saturation limit of the system. The image width from the scintillator does not increase with particle intensity, indicating an excellent stability of the screen.

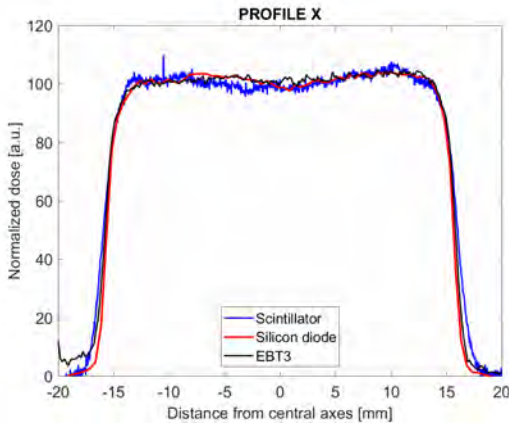


Figure 2: Comparison between horizontal dose profiles measured with different devices for 62 MeV protons. Similar results were obtained for the vertical profiles.

In order to investigate its potential capability for daily QA measurements, the system response was compared at the CATANA facility with a silicon diode, routinely used for QA tests, and the EBT3 radiochromic film, used as a reference. The normalized lateral profiles of the 62 MeV proton beam were extracted both in X and Y directions (Fig. 2).

The profile size shows a quite good agreement, with differences in terms of FWHM within 1%. The performances of the system result in good agreement with EBT3 films also in terms of field ratio (90%-50%), flatness and symmetry with relative differences up to 5%. At the same time, lateral penumbras (80%-20%) measured with the scintillator are systematically larger than those obtained with EBT3, probably due to scattering phenomena inside the scintillator itself.

The lateral relative dose profiles were extracted also for a 100 MeV proton beam at TIFPA and compared with those obtained with the Lynx detector, the Timepix and EBT3 (Fig. 3).

All the FWHM values obtained with the different detectors are comparable within the experimental errors, being, in particular, the dis-

crepancies below 1% for the beam profiling system. The lower spatial resolution of the Lynx detector appears evident from the comparison of its lateral penumbra as respect to the corresponding EBT3 film, being the relative differences significantly higher (more than 70%), while a discrepancy of less than 6% and 3.5% is recorded for the beam profiling system and the Timepix respectively.

In general, the Timepix detector shows a better accuracy in the lateral dose profile detection but a lower radiation hardness as compared to the beam profiling system. Overall, the cross-check with the other devices demonstrated the suitability of beam profiling system for the online lateral dose distribution characterization.

Conclusions The device appears to be a promising quality control system for 2-D relative dosimetry thanks to its linear response in a wide dose rate range useful for proton-therapy treatments, its high spatial resolution and its short acquisition and processing time. A validation with respect to EBT3 radiochromic films and a comparison with other devices have also been performed.

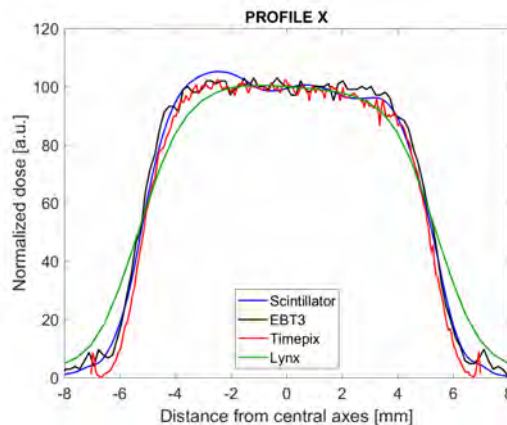


Figure 3: Comparison between horizontal dose profiles measured with different devices for 100 MeV protons. Similar results were obtained for the vertical profiles.

Acknowledgements The present work was partially supported by the INFN CSN5 call MOVE_IT and ASIF INFN activity.

Microdosimetry

Marta Missiaggia,^{1,2} Marta Rovituro,² Emanuele Scifoni,² Francesco Tommasino,^{1,2} Maurizio Boscardin,^{2,3} Chiara La Tessa^{1,2†}

The traditional approach to dosimetry makes use of the standard methods which are based on macroscopic concepts, and it depends on the validity of calculations based on average values. Ionizing radiation deposits energy in discrete packages which are the result of their interactions with the atoms of the medium. These packages are distributed non uniformly throughout the irradiated volume. Not only the average energy deposited per unit mass, but the number of events, their magnitude and their spatial distribution is expected to influence the effect of the radiation on biological structures.

In fact, it is well known that features of radiation track structure at nanometer level (namely at DNA scale) have important implications in terms of radiation effects in biological targets. So, it is necessary to develop concepts which take into account the stochastic nature of ionizing radiation in microscopic volumes. This is the objective of *Microdosimetry*.

Microdosimetry provides information about the radiation quality and the biological effectiveness, making use of the lineal energy transfer y (the microdosimetric equivalent of the Linear Energy Transfer (LET)) and its probability distribution. Moreover, the quality of the radiation field can be assessed from the spectra and used to indirectly estimate the Relative Biological Effectiveness (RBE) values for any radiation type (Kase et al. 2012).

In order to produce those microdosimetric spectra and values for radiotherapy applications, two main experiments have been performed.

The experiments The goal of the experiments is to characterize the radiation delivered during a treatment both inside and outside the target tumor. In order to do that, the radiation field was evaluated both along the beam

direction (in beam) and at lateral distances (off beam). The experiments consisted on microdosimetry measurements of three different beams:

- ^1H beam of 154 MeV (taken at the TIFPA Protontherapy Center in Trento).
- ^4He beam of 160 MeV (taken at the NASA Space Radiation Laboratory in Brookhaven).
- ^{16}O beam of 360 MeV/u (taken at the NASA Space Radiation Laboratory in Brookhaven).

The rationale for the particle selection is that protons are the most widely used ions in radiotherapy while helium and oxygen are considered the most promising alternative candidates to protons and carbon ions. In addition, carbons and lithium ions have already been studied (Martino et al. 2010).

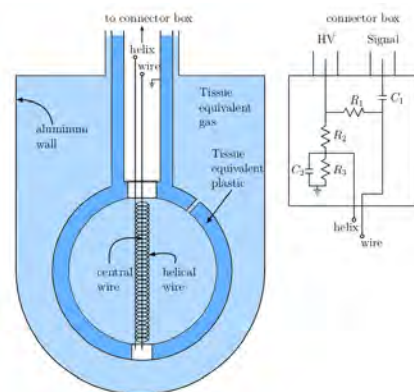


Figure 1: Tissue-equivalent proportional counter. The inner wire is encircled by a helix wire which generates the cylindrically symmetric electric field in the sphere.

TEPC A Tissue Equivalent Proportional Counter (TEPC) microdosimeter was used for all measurements. It consists of a spherical chamber with tissue equivalent walls and a

†Contact Author: chiara.latessa@unitn.it

¹University of Trento, Italy

²INFN TIFPA, Trento, Italy

³FBK, Trento, Italy

tissue equivalent filling gas. Its purpose is to measure the dose in small volumes of biological tissue. To achieve a uniform electric field, especially at the ends of the inner wire which are close to the wall, a wire helix around the internal wire confines the high electric field region close to the wire (Fig. 1). This is where the actual proportional region is located.

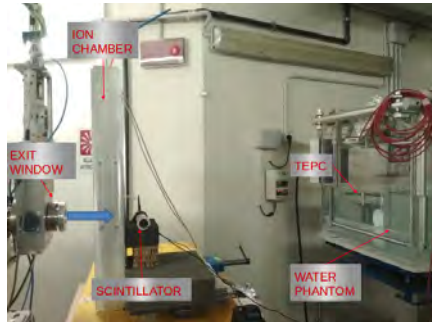


Figure 2: Experimental setup used at the protontherapy Center in Trento. The primary beam emerging from the exit window goes through an ionization chamber and a plastic scintillator before reaching the water phantom with the TEPC placed inside.

In order to relate the energy deposition to microscopic volume of biological tissue, it is replaced by a much larger cavity filled with tissue-equivalent gas of much lower density. The inner diameter of the TEPC gas filled sphere is 12.7 mm and the wall thickness is 1.27 mm. A pressure of 90 Torr simulates a sphere of biological tissue, with a diameter of $2.7 \mu\text{m}$.

The same setup was used for all experiments. A Model LET-1/2 (Far West Technology) TEPC was placed inside a standard water phantom (model Blue Phantom, IBA) and moved at different depths both inside and outside the primary ion field. An ionization chamber and a plastic scintillator were placed in front of the

water phantom to monitor the number of incoming primary ions.

A picture of the experimental setup used at the TIFPA protontherapy center is shown in Fig. 2. All elements were aligned with a laser system.

An example of a microdosimetric spectrum of obtained with protons (the so-called $y_d(y)$ spectrum) is shown in Fig. 3.

Silicon microdosimeter In parallel, the creation and production of a new silicon microdosimeter is under study in a collaboration with FBK.

The most attractive feature of a silicon microdosimeter is the possibility to construct devices of micrometric sensitive volume. This characteristic allows to measure physical events in a real micrometric site, differently from TEPCs whose real volume is on the order of the mm or higher. Further advantages of such a detector are its compactness, low cost, transportability, low bias voltage and a low sensitivity to vibrations.

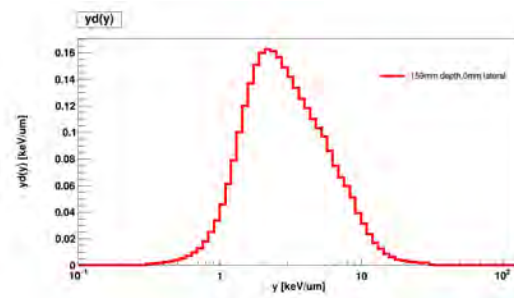


Figure 3: $y_d(y)$ spectrum of ^1H (154 MeV) along the beam direction (in beam), at a 159 mm of depth in water (the Bragg peak position).

References

- Kase, Y., Yamashita, W., Matsufuji, N., Takada, K., Sakae, T., Furusawa, Y., Yamashita, H., and Murayama, S. (2012). *Microdosimetric calculation of relative biological effectiveness for design of therapeutic proton beams*. Journal of radiation research **54**(3), pp. 485–493.
- Martino, G., Durante, M., and Schardt, D. (2010). *Microdosimetry measurements characterizing the radiation fields of 300 MeV/u ^{12}C and 185 MeV/u ^7Li pencil beams stopping in water*. Physics in Medicine & Biology **55**(12), p. 3441.

MoVe IT-TLD: TLD dosimetry for proton beam biophantoms

Consiglia Piccolo,¹ Giuseppe La Verde,¹ Walter Bonani,² Walter Tinganelli,³ Francesco Tommasino,² Palma Simoniello,⁴ Alessandra Bisio,² Emanuele Scifoni,³ Mariagabriella Pugliese^{1†}

Materials and Methods Thermoluminescent dosimeters, TLDs 100 (LiF: Mg, Ti) were used to obtain the dose profile when irradiated by a monoenergetic proton beam at TIFPA facility, in order to obtain the RBE value for the simultaneously irradiated CHO-K1 cells (a subclone of Chinese Hamster Ovary cells), inserted in a biophantom. The biophantom was developed by the biological dosimetry team (head Dr. W. Bonani) and designed to contain both the cells and the TLD, as shown in Fig. 1a. The experiment took place twice, once in July 2018 and once in October 2018. In July only one biophantom (containing two arrays of TLDs and CHO-K1 cells, as shown in Figs. 1b, 1c) was irradiated by a monoenergetic proton beam of initial energy of 150 MeV (about 80 MeV on the phantom entrance) with a dose in the Bragg peak of 1.5 Gy. In October two different biophantoms were used and irradiated at the same experimental conditions of the first time. In this case, only one array of TLDs was allocated to each biophantom together with the CHO-K1 cells (see Fig. 1d).

Prior to each irradiation, TLDs were annealed in air at 400 °C for 1 hour, followed by a 2 hours annealing at 100 °C and by rapid cool-

ing to room temperature. The readout of TLDs was performed by a Harshaw model 3500 manual TLD reader. TLDs have been read at 300 °C using a heating rate of 10 °C/s. From the two groups of TLDs used in the two experiments, ten dosimeters were previously subtracted to carry out the calibration using a monoenergetic proton beam of energy 100 MeV, to calculate the calibration factor ($CF=nC/mGy$).

The dosimeters were calibrated at 2 Gy dose value. We used the CF to obtain absorbed dose values by exposed TLDs. The calibration factor can obviously be used only for the dose range in which the response is linear. So, it is interesting in the future to make a dose calibration with the proton beam at TIFPA facility, because we have already found that while in the dose range of 0-10 Gy the calibration curve was confirmed to be linear for the conventional photon beam, in the same dose region, the quadratic model performs better than the linear model when high dose-per-pulse electron beams were used.¹

The calibration factors were found to be 4.4 for the first group of dosimeters and 4.8 for the second ones. The experimental setup provided that the beam entered orthogonally to the biophantom.

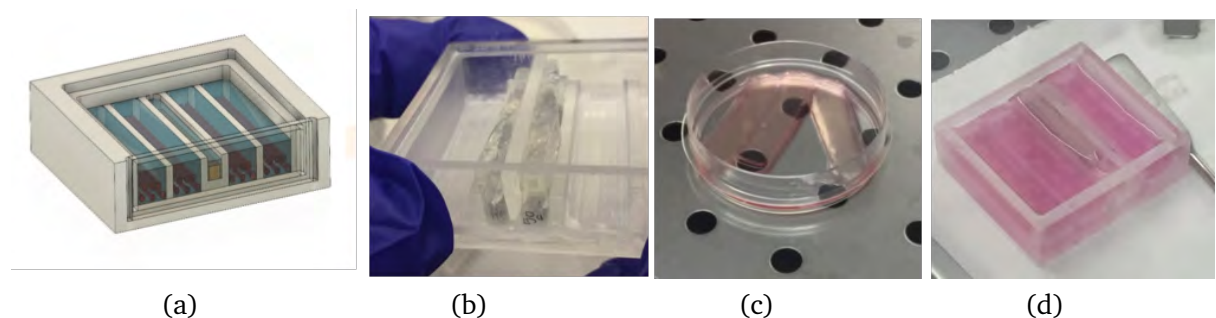


Figure 1: (a): Design of biophantom ; (b): placement of two TLDs arrays; (c): CHO-K1 cells; (d): biophantom with an array of TLDs and cells ready for irradiation.

[†]Contact Author: pugliese@na.infn.it

¹INFN and University of Naples Federico II, Italy

²University of Trento and INFN TIFPA, Trento, Italy

³INFN TIFPA, Trento, Italy

⁴University of Naples Parthenope, Italy

¹Liuzzi, R. et al. (2015), PloS one 10(10), e0139287.

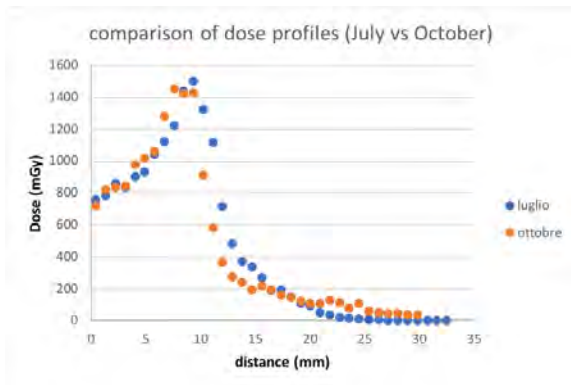


Figure 2: Comparison between the two depth dose profiles obtained by TLD readings, along the biophantom path, in the 2 irradiations (July and October 2018).

Results July 2018: the dose profiles of the two arrays allocated in the same biophantom were found to be perfectly overlapping. This confirms both the reliability of the calibration performed and the uniformity of the proton beam.

October 2018: the results are related to the

two TLD arrays, each positioned in a biophantom. The experimental setup of the first biophantom was the same adopted in the July experiment, while in the second biophantom the energy of the entrance proton beam was deliberately increased and this produced a shifted dose profile. The shift was planned to be sure to observe the Bragg peak in TLDs and therefore a greatest damage into CHO-K1 cells. In Fig. 2 the comparison of dose profiles between the two experiments is reported. The results confirm the reliability of the measurement technique used.

Conclusions The results show that the physical dosimetry performed with TLD is reliable, so it is necessary to characterize the dosimeters by performing a calibration curve in dose, for values up to 10 Gy at TIFPA. Subsequently, the TLDs will be calibrated at the LNS facility, irradiated to a 60 MeV proton beam, in a 0-30 Gy dose range, as higher doses are required for in vivo experiments planned in MoVe IT project.

pFDG: testing ^{19}F FDG as a nuclear reaction-driven sensitizer of proton beams

Emanuele Scifoni,^{1†} Alexander Helm,^{1,2} Francesco Tommasino,^{3,2} Walter Tinganelli,^{1,2} Dante Rotili,⁴ Chiara La Tessa,^{3,2} Marco Durante,^{1,2} Vincenzo Patera^{4,5}

Introduction, Materials and Methods The scope of the present exploratory experimental campaign, was to investigate a new way for exploiting a nuclear resonant process ($p+^{19}\text{F}$ reaction) for differentially enhance cell killing in the target region of a proton beam irradiation, through the use of ^{19}F -FDG (2 (or 3) fluoro-2-deoxy-D-glucose) molecule as added compound, thus demonstrating a possibility to improve protontherapy through a specific nuclear reaction occurring at low energy and generating a boost of biological effectiveness, i.e., acting as a radiosensitizer.

The idea was based on a similar research carried out and published in recent times,¹ showing a relevant and measurable radiosensitization effect occurring with the use of a Boron compound (BSH), exploiting the $p + ^{11}\text{B} \rightarrow 3\alpha$ nuclear fusion reaction at low energy, i.e. a resonant process having the possibility to produce 3 alpha particles of relatively low energy, delivering thus a highly localized DNA damage and then enhanced cell killing.

The suggested alternative, based on a similarity in the cross sections entity in the energy range of interest (Fig. 1a), aims at testing some peculiar advantages of the use of FDG as nuclear reaction-driven sensitizer, mostly based on the possibility to enhance the concentration.

Considering the different features of the 2 approaches, a similar estimate of produced alphas arises from preliminary Monte Carlo (Geant4) calculations (Fig. 1b), indicating the need to observe a similar radiosensitization.

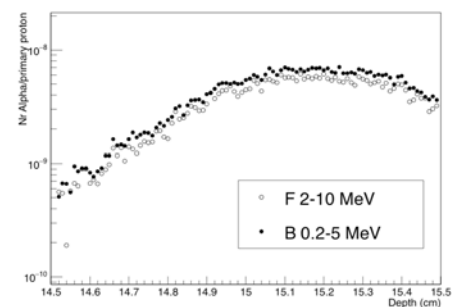
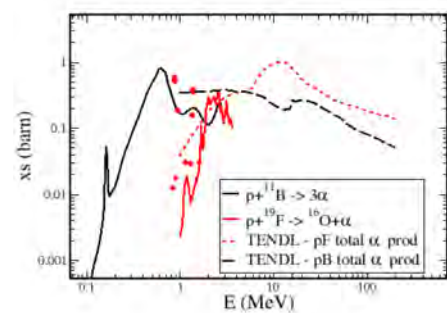


Figure 1: cross sections for the relevant ^{19}F and ^{11}B induced nuclear processes and corresponding computed number of α particles in a proton beam

Thus, 2 and 3 FDG isomers, prepared by the CTF Department of the University of Rome, were used to prepare 2 stock solutions, from which the concentration of 5mg/g of molecule to medium was obtained, and CHO-K1 cells were harvested 5 hours before irradiation according to the normal protocol used for FDG delivery to patients for imaging. Irradiation at different positions of a proton spread out Bragg peak (SOBP) with initial energy 148 MeV, was realised at the TIFPA bio-beam line. Control data and 4 different doses were collected in any condition, and clonogenic assay was per-

[†]Contact Author: emanuele.scifoni@tifpa.infn.it

¹INFN TIFPA, Trento, Italy

²GSI, Darmstadt, Germany

³University of Trento, Italy

⁴University of Rome "La Sapienza", Italy

⁵INFN Roma1, Rome, Italy

¹Cirrone, G. et al. (2018), Scientific Reports 8(1), p. 1141.

formed to obtain standard survival curves with no dopant, 2FDG, 3FDG, both at 5 mg/g concentration, and in the last 2 cases, also double concentration of 3FDG (10 mg/g) in order to test a possible concentration effect.

The results were analysed in terms of dose enhancement factor (DEF), i.e. the ratio of doses delivering the same survival effect with and without the given amount of sensitiser. Such a quantity, as the RBE, depends obviously on the survival level (S) observed, and it was considered at $S = 10\%$ (DEF_{10}), which is normally assumed as a good average effect estimation.

Results In the first experiment, performed in May 2018 a slight sensitization ($DEF_{10} = 1.41$) was observed (Fig.2a) for the distal position when using 3FDG, while 2FDG was returning an unexpected radioprotective effect, which was attributed to an impact on the cell cycle dynamics. In the mid-SOBP irradiation, instead, the effect was on the threshold to be negligible ($DEF_{10} = 1.05$, Fig.2b).

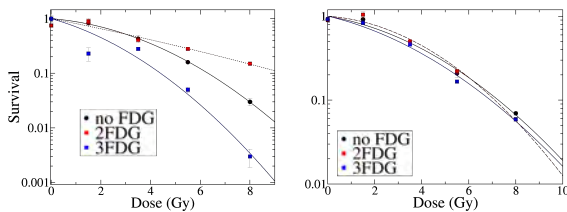


Figure 2: Survival level plots at different conditions in the first experiment.

In the second experiment performed at July, while the beam line has been finalised with the double ring set up (see MoVe IT report at p. 94), a different position on the SOBPs was chosen, which we called “predistal”, i.e. 5 mm before the “distal” one, in order to avoid possible oscillations due to small range uncertainties at the

very end of the peak and get more robust data. Another modification in this case has been the addition of a second concentration, but while the normal concentration reported still a sensitive effect $DEF_{10} = 1.19$, the double concentration (FDG+ in Fig. 3) lead to disappearing of the effect. The latter could have been due to increased toxicity with this larger amount of dopant.

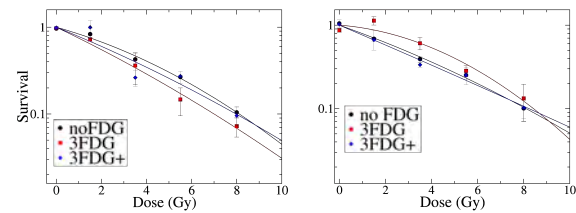


Figure 3: Survival level plots at different conditions in the second and third experiment.

Finally the July experiment was repeated identical in September, with a slightly different protocol for cell seeding, returning no evident sensitization effect.

Conclusions The present preliminary results, because of large oscillations in the colonies counted at different conditions, probably due to complexity in the biological effect of the FDG with the cell samples used needing to optimise the protocol, provide no clear indication for the presence or not of a definite radiosensitization effect in the studied combination. A slight indication of no effect seems to appear from the overall collection of the data. For this reason, the experiment is going to be repeated in April 2019 at LNS, where the exact procedure performed with B compounds will be repeated, in particular, irradiation with full flasks, to improve the contact of the dopant with the cells, and same tissue samples.

Prima-RDH-IRPT

Mara Bruzzi,^{1,2} Carlo Civinini,¹ Matteo Intravaia,^{1,3†} Nunzio Randazzo,⁴ Marta Rovituso,⁵ Monica Scaringella,¹ Valeria Sipala,^{6,7} Francesco Tommasino^{8,5}

In hadron therapy the setup of a treatment plan, which efficiently covers the tumor volume with the required dose sparing as much as possible adjacent healthy tissues, requires the patients' Stopping Power (SP) maps, normalized to liquid water SP (Relative Stopping Power - RSP). These maps are presently extracted from X-rays tomographies converting photon Hounsfield units into SP, with the unavoidable introduction of uncertainties that reduce the potential benefits of hadron therapy. A direct measurement of SP maps, using proton themselves for tomographies (proton Computed Tomography - pCT), may mitigate this source of errors. To be effective in reducing the uncertainties in dose distribution, this method should keep the SP map position error below one millimeter and the error in evaluating material density below one percent. Furthermore, pCT images can be of paramount importance when a metal prosthesis is installed in the proximity of the region to be irradiated. In this case the direct measurement of the SP of the prosthesis may overcome the problems due to poor X-CT imaging of metal structures.

A pCT apparatus should be able to reconstruct the trajectories of each proton (Most Likely Path - MLP) inside the target (phantom) and to measure the energy associated to each track. Data is acquired with the phantom rotated at different angles in order to reconstruct a 3D SP image. The reconstruction is carried out through algebraic reconstruction algorithms.

The pCT system (Fig. 1), built by the Prima-RDH-IRPT collaboration,¹ is composed of a four planes silicon microstrip tracker followed by a YAG:Ce scintillating calorimeter. The apparatus

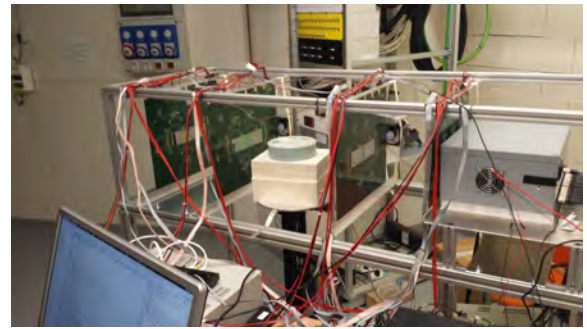


Figure 1: The Prima-RDH-IRPT pCT system mounted on the Trento Proton Therapy center experimental beam line. The four tracker planes (green boards), the electron density phantom and the calorimeter (inside the grey box) are visible. The proton beam enters the apparatus from left.

field of view is about $20 \times 5 \text{ cm}^2$. The phantom is placed between the second and the third plane while the calorimeter just after the fourth plane. A remotely controlled rotating platform and a vertical stage are used to move the phantom during data taking without the need to enter the beam area.

During June 2018 a new test of the complete pCT apparatus has been performed at the Trento Proton Therapy center experimental beam line; data for three tomographies has been acquired using a 9 cm radius cylindrical electron density phantom, an anthropomorphic head phantom and a 10 cm radius cylindrical phantom for spatial resolution estimates (Catphan 528). The calorimeter energy response has been calibrated using runs at six different beam energies in the range 83-211 MeV; the highest energy run has been also used for the alignment of tracker planes. The proton beam has been widened to cover the entire system field of view by placing a 2.5 mm Tantalum

[†]Contact Author: matteo.intravaia@phd.unipi.it

¹INFN Florence, Italy

²University of Florence, Italy

³University of Siena, Italy

⁴INFN Catania, Italy

⁵INFN TIFPA, Trento, Italy

⁶University of Sassari, Italy

⁷INFN LNS, Catania, Italy

⁸University of Trento, Italy

¹Civinini, C. et al. (2013), Nucl. Inst. and Meth. A **732**, pp. 573–576.

scattering foil just after the beam pipe exit.

Compared to the previous experiment, the most relevant upgrades in the system consisted of a tenfold number of different phantom angles (400 instead of 40) at which data has been taken (about 5×10^4 protons per projection) and a new front-end electronic board for the calorimeter. Data has been analyzed using an iterative Algebraic Reconstruction Technique (ART) algorithm running on a GPU.²

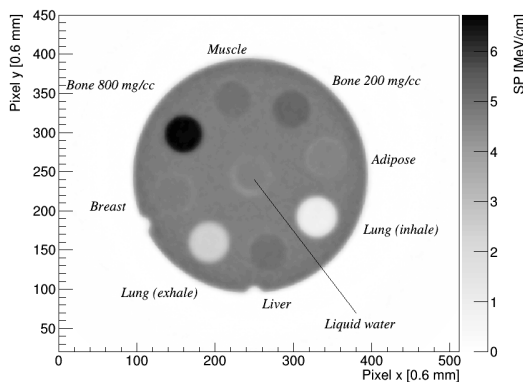


Figure 2: Tomographic reconstruction of the axial view of the electron density phantom. The grey scale corresponds to the proton SP [MeV/cm]. The x-y axes units are number of pixels ($600 \times 600 \mu\text{m}^2$ each).

An image of the electron density phantom after 50 iterations of ART algorithm is shown in Fig. 2. In this phantom eight different radial inserts are plugged into a water equivalent bulk plastic material. A central insert containing liquid distilled water, to measure the Relative Stopping Power (RSP) of other materials, is also present. All the inserts are visible, even those with a density difference of 1% only.

In Fig. 3 a fit to the measured RSP using a straight line is also reported. The two parameters of the line are compatible with 1 and 0 within the errors. A 0.8 mm thick axial slice of the anthropomorphous head at the level of the lower jaw is shown in Fig. 4. The jaw's bone, a vertebral section and a section of a titanium prosthesis located near the vertebral bone are clearly visible.

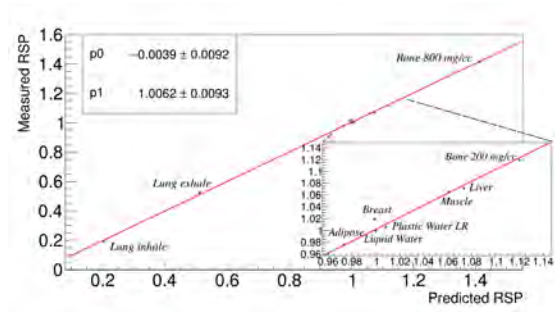


Figure 3: Correlation between predicted RSP (on x axis) and measured RSP (on y axis).

In both Fig. 2 and Fig. 4 the radial artifacts which affected images previously reconstructed have now disappeared, thank to the incremented angular resolution.

Acknowledgements The authors wish to thank Dr. Marco Schwarz of Trento Proton Therapy Center, for useful discussions and for having made available to us the phantoms. In addition, we gratefully acknowledge the help of the IBA and TIFPA personnel at the Trento Proton Therapy Center for quickly setting up the cyclotron to produce a reliable proton beam with the required intensity and quality. This work has been supported by INFN CSN5 PrimaRDH and MIUR IRPT experiments.

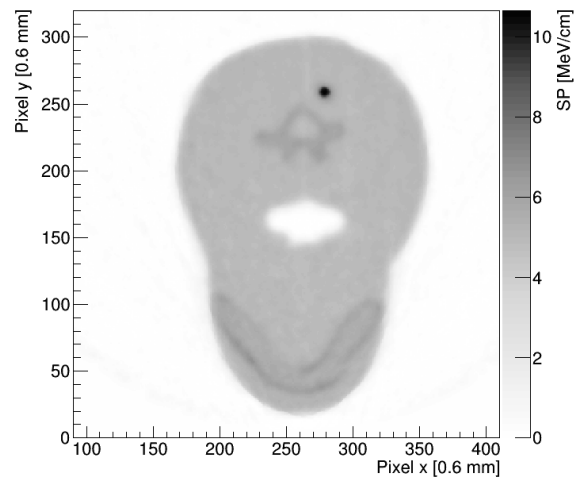


Figure 4: Tomographic reconstruction of a 0.8 mm thick axial slice of the anthropomorphous phantom. Axes units are the same of Fig. 2.

²Civinini, C. et al. (2016), 2016 IEEE Nuclear Science Symposium, Medical Imaging Conference and Room-Temperature Semiconductor Detector Workshop (NSS/MIC/RTSD), pp. 1–6.

PROMETHEUS SiPM-based detector

Valerio Pagliarino,^{1†} Francesco Serra,¹ Aurora Robino,¹ Federico Filippa,¹ Riccardo Ponte,¹ Giulio Branda,¹ Alessia Massolino,¹ Alessandra Lovisolo,¹ Fabio Boido¹

PR.O.ME.THE.U.S. is a SiPM-based sampling calorimeter for beam characterization that aims to measure the energy loss curve of various kinds of light ions, with a particular focus on the Bragg Peak, employing a cheaper and easier to use setup with respect to commonly available ionization chamber phantoms. It has been designed to run water-equivalent measurements in the energy range between 85 – 205 MeV with a proton beam, to be suitable for proton therapy beam characterization. This detector has been designed and built by a student team of the “I.I.S. Nicola Pellati” High School (Nizza Monferrato, Italy) for the CERN Beamline for School 2017 competition and thanks to the collaboration with INFN it has been tested on the research beamline managed by TIFPA at the Trento Proton Therapy center (the PROMETHEUS detector is visible in Fig. 1).

The structure of PRO.ME.THE.U.S. consists of a PMMA tank filled with an absorber liquid in which is immersed a waterproof and light-proof 3D-printed box hosting a calcium fluoride scintillator coupled with a silicon photomultiplier, the temperature sensors and the bias injector circuit. The detector box is fixed on a motorized head that can move along 3 axes using servo and stepping motors. Thanks to inductive, optical and resistive sensors, the absolute position is known with an uncertainty on the beam axis of about 2×10^{-4} m. The signal from the SiPM is analyzed by a PSAU (Power Supply and Amplification Unit, a CAEN model) that provides the trigger signal, sets and traces the electronic parameters and produces the temperature-compensated biasing voltage; finally, a 250 MSa/s 12 bit digitizer acquires the signal providing a single-event integration value which is proportional to the energy deposited in the scintillator by one particle.

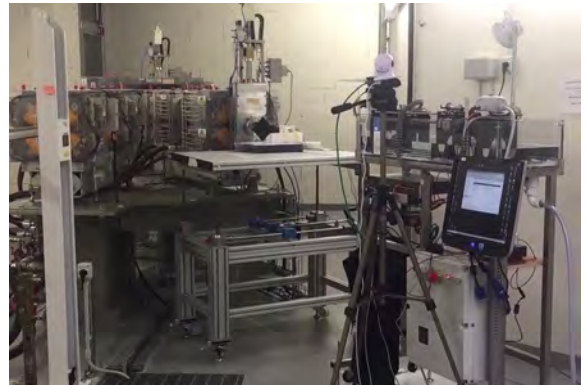


Figure 1: The PR.O.ME.THE.U.S. detector on the research beamline of the Trento Proton Therapy centre

The PR.O.ME.THE.U.S. detector is totally remote controlled and can be operated via Ethernet network not limited to the LAN, but also from the WAN using VPN; this feature, added to the provision of visible and IR cameras that allow supervising the machine mechanics and alignment, makes PR.O.ME.THE.U.S. adapt for collaborative and educational projects, that can be carried on also in "remote workbench" mode. Moreover the sensor box is installed on a standard din rail which allows replacing or modifying the particle detector, keeping the structure unchanged; this makes the apparatus more versatile for different experiments: for example, a SiPM matrix instead of the single-pixel SiPM can be used for 3D beam imaging. Another relevant field of study that can involve PR.O.ME.THE.U.S. is related to the characterization of SiPM for purposes that now are satisfied by more expensive detectors, for example radiotherapy and particle therapy QA, where ionization chambers are the most widespread technology.

Thanks to the support from INFN and TIFPA in particular, in February 2018 PR.O.ME.THE.U.S. has been tested on the research beamline of the Trento Proton Therapy

[†]Contact Author: pagliarinovalerio@gmail.com

¹I.I.S. “Nicola Pellati” Nizza Monferrato, Italy

facility where we carried out a Bragg peak measurement with a 150 MeV, 10^4 Hz proton beam. The energy loss curve (see Fig. 2) has been reconstructed distributing the values of each single-energy and single-position run on a Gaussian fitted histogram and then plotting for each measurement step the Gaussian mean value and the relative error in correspondence of the scintillator position. The Bragg curve has been fitted employing a convoluted Moyal formula and has then been compared with the water-equivalent profile measured at the same facility with a state-of-the-art IBA Giraffe detector. (Tommasino et al. 2017b)

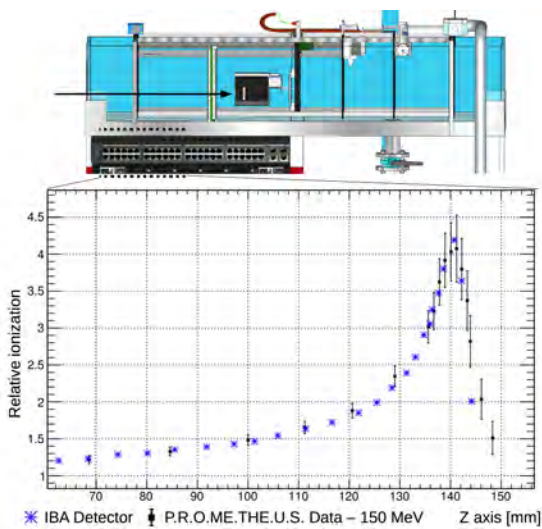


Figure 2: Measured Bragg curve at 150 MeV

This comparison has shown some limita-

tions on the linearity of P.R.O.ME.THE.U.S. charge response due to the scintillator quenching effect, (L. L. W. Wang et al. 2012) this has been corrected with the Birks' formula, resulting to fully match the IBA detector curve, except for the last measurement points in the peak falling edge, where the poor statistic due to the lack of an external trigger introduces a small discrepancy. Experimental data has finally been compared with a Geant4 Monte Carlo simulation.

In conclusion, the SiPM-based approach of P.R.O.ME.THE.U.S. has shown different advantages, like a very good signal-noise ratio in a large spectrum of beam rates, the possibility to track single particles, a good energy resolution and the possibility to employ water-equivalent materials as a detector. Furthermore, this setup does not require expensive electrometers for signal readout with respect to ionizing chambers. Finally, the P.R.O.ME.THE.U.S. detector was not meant to be used for very high precision characterizations, but considering its relatively low cost (about € 7000) and its unexpectedly good performances, it opens up new scenarios in educational projects and for case studies of scintillator and SiPM behaviors in Bragg Peak QA applications. We are grateful with INFN-MIB, INFN-TO, INFN-TIFPA, CAEN, Università degli Studi di Trento and Università degli Studi dell'Insubria researchers¹ who supported us in this project and CERN BL4S initiative.

References

- Tommasino, F. et al. (2017b). *Proton beam characterization in the experimental room of the Trento Proton Therapy facility*. Nuclear Inst. and Methods in Physics Research A **869**, pp. 15–20.
- Wang, L. L. W. et al. (2012). *Determination of the quenching correction factors for plastic scintillation detectors in therapeutic high-energy proton beams*. Phys. Med. Biol IOP **57**, p. 7767.

¹In particular Dr. D. Menasce (INFN-MIB), Dr. N. Pastrone (INFN-TO), Dr. M. Caccia, Dr. S. Lomazzi, Dr. R. Santoro (Università degli Studi dell'Insubria), Dr. M. Durante, Dr. M. Rovituso, Dr. C. Manea (INFN-TIFPA), Dr. F. Tommasino (Università degli Studi di Trento and INFN-TIFPA), Dr. C. Mattone (CAEN)

SEE-GOLD: Secondary electron emission measurements from gold target after 160 MeV proton irradiation

F. Hespeels,^{1†} E. Scifoni,² T. Tabarrant,¹ M. Krämer,³ F. Tommasino,^{4,1} S. Lucas¹

The 3 days experiment at the TIFPA proton beam facility, situated at the Trento Proton Therapy center, aimed at measuring the 160 MeV proton induced secondary electron energy spectra from nanometer thin films and gold nanoparticles (GNP). This project is part of an investigation of the potential use of Gold Nanoparticles as radiosensitizers, through increased electron emission and, after measuring this at low energy (Hespeels et al. 2017), scope of the present test was to quantify the effect in an entrance channel of therapeutic energies. Backscattered electron energy spectra were measured within an energy range from 0 to 1500 eV using a Retarding Field Analyser (RFA). The detection chamber was mounted in the experimental physics beam line.

The incident proton beam was generated with the IBA cyclotron (Proteus 235), and delivered in the experimental cave, as described in details in (Tommasino et al. 2017c). At the end of the 30° derivation of the experimental line referred as the “Physics” beam line, a Ti film (70 μm thick) allows the beam to pass from vacuum to air. Then, another 70 μm Ti film allows the beam to enter into the “irradiation chamber” (base pressure: 10^{-5} mbar). The beam size is shaped with two 4 cm long inox steel collimator (3 mm inner diameter). Then, the collimated beam passes through the RFA and through the sample. Backscattered secondary electron emitted from the sample are collected within an acceptance angle of 102° by the RFA detector. The proton beam intensity is measured continuously with a two Aluminum Faraday cup (5 cm long) connected to a current digitizer. To ensure charge collection, two mag-

nets are placed on the faraday tube. Magnets are used instead of negative potential (-100 V) in order to avoid additional noise coming from power supply. A schematic representation of the irradiation and detection chamber is presented in Fig. 1.

Results The sample was placed at 0.7 m from the Ti exit window to maximize the proton current. In order to appraise the chamber alignment, we used gafchromic films to measure the size of the beam at several positions. Resulting spots are presented in Fig. 1.

First, we observed that the beam was collimated down to ≈ 3 mm by both Al collimators. Experimental spots are slightly larger than the collimators diameter due to the proton beam divergence. Then, after passing through the RFA, a ≈ 3 mm beam spot is measured at the center of the sample holder. Finally, the beam spot was detected between both Al Faraday cup. These results proved the good alignment of the chamber. It also showed that the detection chamber can be easily moved from one irradiation center to another.

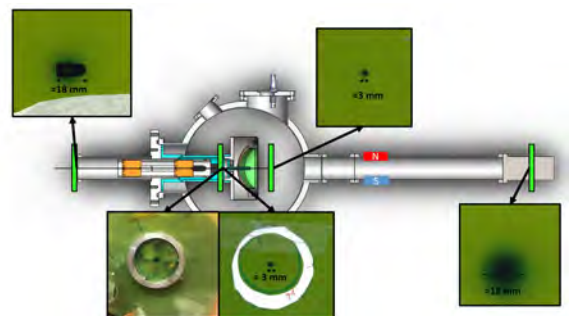


Figure 1: Setup testing with Gafchromic film irradiation. The beam spots in the irradiated films are clearly visible.

[†]Contact Author: felicien.hespeels@unamur.be

¹University of Namur, Belgium

²INFN TIFPA, Trento, Italy

³GSI, Darmstadt, Germany

⁴University of Trento, Italy

At 160 MeV proton and 300 nA cyclotron extraction current, an average proton beam current on target of ≈ 410 pA was measured. Considering the data reported in (Tommasino et al. 2017c), the proton beam current is estimated to be around 2.6 nA before collimation for the same beam parameters. This indicated a collimation/reduction factor of 7 using both inox collimators. Since the beam spot profiles are energy dependent, the collimation factor is function of the beam energy.

Secondary electron current was collected after irradiation of a 200 nm thick gold film. A correlation between the proton beam current and the secondary electron current was measured and highlighted the good sensitivity of the detection device (Fig. 2).

For extraction current of 50 nA, 100 nA and 150 nA, we did not observe any effect of the retarding grids. This is surprising since the secondary electron current is expected to decrease for an increasing retarding potential. For those extraction currents, the proton beam current on the target is too low as compared to electron noise to detect a significant signal from the irradiated sample. Nevertheless, for 300 nA extraction current, the electron current was affected by the retarding grids voltage. Using TRAX simulation, for a 410 pA proton current on target, the calculated secondary electron current is 6 pA which is extremely low and near the level observed experimentally. For 160 MeV, the mass stopping power is equal to $2.6 \text{ MeVcm}^2/\text{g}$ for gold target which is 18 times lower than for 2 MeV protons ($46.5 \text{ MeVcm}^2/\text{g}$) where previous measurements have been performed (Hespeels et al. 2017). Thus, for 160 MeV proton, the beam current has to be high enough to lead

to a significant secondary electron current.

In addition, we did not notice any effect of activation of the chamber in the secondary electron current but we don't have sufficient amount of data to quantify this noise effect. Thus additional measurements will be necessary to assess this quantity, also contemplating the option to record the forward scattered spectrum, by turning the analyzer, where a larger total yield of electron is expected to appear.

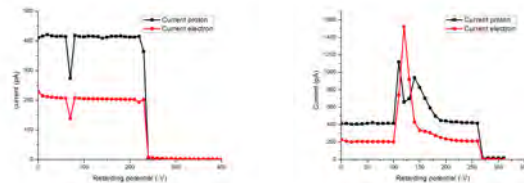


Figure 2: Proton and secondary electron current measurements recorded during the experiment, for different runs of 10 minutes with 160 MeV protons and 300 nA, showing correlation at current spikes and beam losses

In conclusion, the experimental chamber dedicated to secondary electron measurement was successfully installed in the Trento Proton Therapy facility. As expected, for an increasing retarding potential, a decrease in the secondary electron current was measured. However, the low proton current on target (≈ 410 pA) did not allow to measure with good accuracy the secondary electron energy spectra from the gold targets. Indeed, from 0 to 200 V retarding voltage, the secondary electron current dropped down from ≈ 230 pA to ≈ 200 pA which means that most of the measured current is part of the noise. Since the irradiation time was limited, the number of measurements was too low to enable the extraction of the secondary electron signal from the noise.

References

- Hespeels, F., Heuskin, A., Scifoni, E., Kraemer, M., and Lucas, S. (2017). *Backscattered electron emission after proton impact on carbon and gold films: Experiments and simulations*. Nucl. Instruments Methods Phys. Res. Sect. B **401**, pp. 8–17.
- Tommasino, F., Rovituro, M., Fabiano, S., Piffer, S., Manea, C., Lorentini, S., Lanzone, S., Wang, Z., Pasini, M., Burger, W., Tessa, C. L., Scifoni, E., Schwarz, M., and Durante, M. (2017c). *Proton beam characterization in the experimental room of the Trento Proton Therapy facility*. Nucl. Instruments Methods Phys. Res. Sect. A Accel. Spectrometers **869**, pp. 15–20.

Testing of novel solid-state radiation detectors for space applications

Marco Povoli,^{1†} Angela Kok,¹ Ozhan Koybasi,¹ Chiara La Tessa,^{2,3} Enrico Verroi³

The goal of the experiment carried out at the TIFPA Proton Therapy Centre in Trento, Italy, was to verify the correct operation of the latest generation of 3D silicon detectors fabricated at SINTEF MiNaLab, Oslo, Norway. The devices were produced in a project funded by the European Space Agency (ESA), called “Three-dimensional low voltage silicon detectors”, in the framework of the Technology Research Programme (TRP), and are intended for low-power radiation measurements for future ESA missions.

Devices under test The devices under test in this experiment were 3D silicon detectors. The concept of 3D silicon detectors was first introduced in the mid 90’s (Parker et al. 1997), intended for creating a type of silicon detector that could operate at very low voltage with an increased tolerance for radiation damage. The main feature of 3D detectors is the geometry and the placement of the electrodes. The electrodes are columns etched vertically into the silicon bulk to allow reduced inter-electrode spacing. This delivers very low power consumption both before and after irradiation, as well as mitigation of charge trapping effect in irradiated and damaged silicon bulk. The sensors in this study were completed at the end of 2017 using the latest 3D fabrication process available at SINTEF MiNaLab (Povoli et al. 2018). The detectors feature short inter-electrode spacing (25, 50 and 100 μm) and a total active bulk thickness of 100 μm .

Proton beam radiation tests A total of 10 hours of beam time were granted at the TIFPA Proton Therapy Centre, through the public beam time application. The experiment was

carried out using three proton energies, 70, 119 and 202 MeV for all sensors. SRIM simulations were performed to estimate the amount of charge released for each proton energy, with the lowest charge generation for 202 MeV proton corresponding to roughly 2.5 Minimum Ionising Particles (MIPs). Each sensor was irradiated with all the chosen proton energies using different bias voltages, starting from 0V, to demonstrate that 3D detectors can operate efficiently with minimal power consumption

Experimental setup Initial electrical characterisation and sensor selection were carried out at wafer level. The wafers were then diced, and the sensors were mounted on the desired printed circuit boards (PCB). The chosen readout system is composed by off-the-shelf electronics. The full readout chain consists of an Amptek A250 charge amplifier, a Cremat CR200 shaping amplifier with 1 μs shaping time, and an Amptek MCA8000D Multi Channel Analyzer. The raw spectrum data acquired by the MCA are sent to a PC in the control room over an ethernet connection. The sensor and the readout electronics are mounted into dedicated metal enclosure to ensure shielding from external noise and are then placed on a table that allows the system to be aligned with the beam.

Experimental results The detectors worked as expected both in terms of charge collection and in term of noise performance. For the sensors with larger inter-electrode spacing (50 and 100 μm), excellent performance was achieved, while, for the sensor with the shortest inter-electrode spacing (25 μm), the increased sensor capacitance made it more difficult to detect 202 MeV protons. All sensors demonstrated the

[†]Contact Author: marco.povoli@sintef.no

¹SINTEF MiNaLab, Oslo, Norway

²University of Trento, Italy

³INFN TIFPA, Trento, Italy

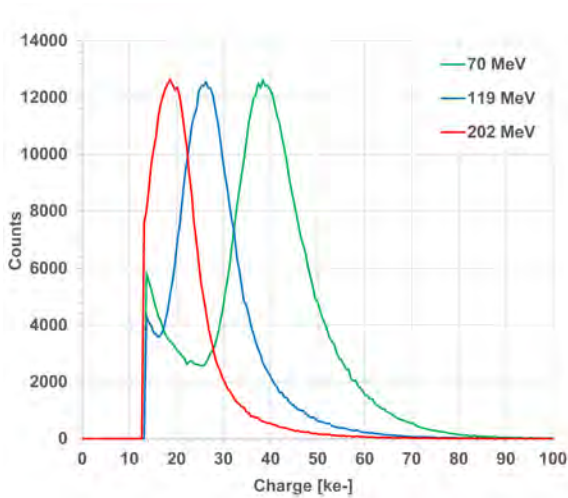


Figure 1: Spectra acquired at 5 V of bias.

ability of clearly separating protons of different energies and the amount of collected charge agreed with numerical simulations. Furthermore, all sensors were demonstrated to have reached saturation of the collected charge when the applied voltage was lower than 10 V, as expected for this unique sensor technology. A selection of results obtained with a sensor with 100 μm inter-electrode spacing, are reported here. In Fig. 1, the spectra acquired at all three proton energies demonstrates how the sensors generate signals that are clearly distinguished for the different proton energies. The Most Probable Value (MPV) of the Landau distribu-

References

- Parker, S., Kenney, C., and Segal, J. (1997). *3D-A proposed new architecture for solid-state radiation detectors*. Nuclear Instruments and Methods A **395**, pp. 328–343.
- Povoli, M., Koybasi, O., Kok, A., Summanwar, A., Breivik, L., Hansen, T., Lietaer, N., Rohne, O., and Sandaker, H. (2018). *Status of 3D detector development at SINTEF for the ITk Upgrade*. URL: <https://indico.cern.ch/event/666427/contributions/2882585/> (visited on 12/28/2018).

tions is plotted against the applied bias voltage in Fig. 2, showing how charge saturation is achieved at less than 10V.

Conclusions The results obtained during the performed tests were essential to demonstrate the functionality of thin 3D detectors, which was the primary objective of this project. These results are vital in allowing further collaboration with ESA using our novel technologies and to demonstrate the suitability and potential of this newly emerging technology for space applications.

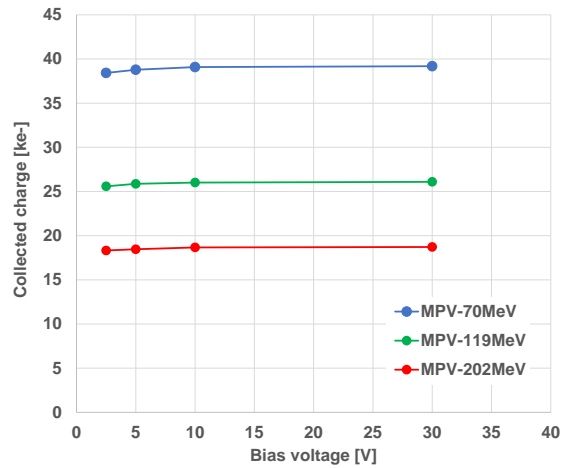


Figure 2: Charge collection efficiency.

TIFPA Publications

Virtual Labs

Medical Technologies

- Fracchiolla, F. et al. (2019). *A pre-absorber optimization technique for pencil beam scanning proton therapy treatments*. *Physica Medica* **57**, pp. 145–152.
- Taffelli, A., Amelio, D., Fellin, F., D'Avino, V., Palma, G., Tommasino, F., Scifoni, E., Durante, M., Schwarz, M., Amichetti, M., et al. (2018a). *48. Dosimetric predictors of radiation induced alopecia in brain tumours proton therapy*. *Physica Medica: European Journal of Medical Physics* **56**, pp. 92–93.
- Tommasino, F., Fellin, F., Lorentini, S., and Farace, P. (2018a). *Impact of dose engine algorithm in pencil beam scanning proton therapy for breast cancer*. *Physica Medica* **50**, pp. 7–12.

Sensors and detectors

- Bufon, J., Schillani, S., Altissimo, M., Bellutti, P., Bertuccio, G., Billè, F., Borghes, R., Borghi, G., Cautero, G., Cirrincione, D., Fabiani, S., Ficorella, F., Gandola, M., Gianoncelli, A., Giuressi, D., Kourousias, G., Mele, F., Menk, R., Picciotto, A., Rachevski, A., Rashevskaya, I., Sammartini, M., Stolfi, A., Zampa, G., Zampa, N., Zorzi, N., and Vacchi, A. (2018a). *A new large solid angle multi-element silicon drift detector system for low energy X-ray fluorescence spectroscopy*. *Journal of Instrumentation* **13**(03), pp. C03032–C03032.
- Da Vià, C., Boscardin, M., Betta, G.-F. D., Darbo, G., Fleta, C., Gemme, C., Giacomini, G., Grenier, P., Grinstein, S., Hansen, T.-E., Hasi, J., Kenney, C., Kok, A., Rosa, A. L., Micelli, A., Parker, S., Pellegrini, G., Pohl, D.-L., Povoli, M., Vianello, E., Zorzi, N., and Watts, S. (2013). *3D active edge silicon sensors: Device processing, yield and QA for the ATLAS-IBL production*. *Nuclear Instruments and Methods in Physics Research Section A: Accelerators, Spectrometers, Detectors and Associated Equipment* **699**. Proceedings of the 8th International “Hiroshima” Symposium on the Development and Application of Semiconductor Tracking Detectors, pp. 18–21.
- Evangelista, Y., Ambrosino, F., Feroci, M., Bellutti, P., Bertuccio, G., Borghi, G., Campana, R., Caselle, M., Cirrincione, D., Ficorella, F., Fiorini, M., Fuschino, F., Gandola, M., Grassi, M., Labanti, C., Malcovati, P., Mele, F., Morbidini, A., Picciotto, A., Rachevski, A., Rashevskaya, I., Sammartini, M., Zampa, G., Zampa, N., Zorzi, N., and Vacchi, A. (2018a). *Characterization of a novel pixelated Silicon Drift Detector (PixDD) for high-throughput X-ray astrophysics*. *Journal of Instrumentation* **13**(09), P09011–P09011.
- Ferrero, M., Arcidiacono, R., Barozzi, M., Boscardin, M., Cartiglia, N., Betta, G. D., Galloway, Z., Mandurrino, M., Mazza, S., Paternoster, G., Ficorella, F., Pancheri, L., Sadrozinski, H.-F. W., Siviero, F., Sola, V., Staiano, A., Seiden, A., Tornago, M., and Zhao, Y. (2019). *Radiation resistant LGAD design*. *Nuclear Instruments and Methods in Physics Research Section A: Accelerators, Spectrometers, Detectors and Associated Equipment* **919**, pp. 16–26.
- Gola, A., Acerbi, F., Capasso, M., Marcante, M., Mazzi, A., Paternoster, G., Piemonte, C., Regazzoni, V., and Zorzi, N. (2019). *NUV-Sensitive Silicon Photomultiplier Technologies Developed at Fondazione Bruno Kessler*. *Sensors* **19**(2).
- Oide, H., Alimonti, G., Boscardin, M., Betta, G.-F. D., Darbo, G., Ficorella, F., Fumagalli, E., Gariano, G., Gaudiello, A., Gemme, C., Meschini, M., Messineo, A., Mendicino, R., Ronchin, S., Rovani, A., Ruscino, E., Sultan, D., Zorzi, N., and Furelos, D. V. (2018). *INFN-FBK developments of 3D*

sensors for High-Luminosity LHC. Nuclear Instruments and Methods in Physics Research Section A: Accelerators, Spectrometers, Detectors and Associated Equipment.

Sola, V., Arcidiacono, R., Boscardin, M., Cartiglia, N., Betta, G.-F. D., Ficorella, F., Ferrero, M., Mandurrino, M., Pancheri, L., Paternoster, G., and Staiano, A. (2019). *First FBK production of 50 μm ultra-fast silicon detectors*. Nuclear Instruments and Methods in Physics Research Section A: Accelerators, Spectrometers, Detectors and Associated Equipment **924**. 11th International Hiroshima Symposium on Development and Application of Semiconductor Tracking Detectors, pp. 360–368.

Cartiglia, N. et al. (2018). “Tracking in 4 dimensions”. *Proceedings of Science - EPS HEP 2017*. Trieste, Italy: Sissa, p. 489.

Ferrero, M. et al. (2018). “Developments in the FBK Production of Ultra -Fast Silicon Detectors”. *2017 IEEE NSS-MIC Conference Record*. Piscataway, U.S.A.: IEEE.

Mandurrino, M., Cartiglia, N., Staiano, A., Arcidiacono, R., Obertino, M., Ferrero, M., Cenna, F., Sola, V., Boscardin, M., Patetnoster, G., Ficorella, F., Pancheri, L., and Dalla Betta, G.-F. (2018). “Numerical Simulation of Charge Multiplication in Ultra-Fast Silicon Detectors (UFSD) and Comparison with Experimental Data”. *2017 IEEE NSS-MIC Conference Record*. Piscataway, U.S.A.: IEEE.

Particle Physics

ATLAS

Aaboud, M. et al., ATLAS collaboration (2018a). *Combined measurement of differential and total cross sections in the $H \rightarrow \gamma\gamma$ and the $H \rightarrow ZZ^* \rightarrow 4\ell$ decay channels at $\sqrt{s} = 13$ TeV with the ATLAS detector*. Phys. Lett. **B786**, pp. 114–133.

— ATLAS collaboration (2018b). *Measurement of dijet azimuthal decorrelations in pp collisions at $\sqrt{s} = 8$ TeV with the ATLAS detector and determination of the strong coupling*. Phys. Rev. **D98**(9), p. 092004.

— ATLAS collaboration (2018c). *Observation of Higgs boson production in association with a top quark pair at the LHC with the ATLAS detector*. Phys. Lett. **B784**, pp. 173–191.

— ATLAS collaboration (2018d). *Search for a Structure in the $B_s^0 \pi^\pm$ Invariant Mass Spectrum with the ATLAS Experiment*. Phys. Rev. Lett. **120**(20), p. 202007.

— ATLAS collaboration (2018e). *Search for dark matter in events with a hadronically decaying vector boson and missing transverse momentum in pp collisions at $\sqrt{s} = 13$ TeV with the ATLAS detector*. JHEP **10**, p. 180.

— ATLAS collaboration (2018f). *Search for electroweak production of supersymmetric particles in final states with two or three leptons at $\sqrt{s} = 13$ TeV with the ATLAS detector*. Eur. Phys. J. **C78**(12), p. 995.

— ATLAS collaboration (2018g). *Search for flavour-changing neutral current top-quark decays $t \rightarrow qZ$ in proton-proton collisions at $\sqrt{s} = 13$ TeV with the ATLAS detector*. JHEP **07**, p. 176.

— ATLAS collaboration (2018h). *Search for Higgs boson pair production in the $\gamma\gamma b\bar{b}$ final state with 13 TeV pp collision data collected by the ATLAS experiment*. JHEP **11**, p. 040.

— ATLAS collaboration (2018i). *Search for low-mass dijet resonances using trigger-level jets with the ATLAS detector in pp collisions at $\sqrt{s} = 13$ TeV*. Phys. Rev. Lett. **121**(8), p. 081801.

— ATLAS collaboration (2018j). *Search for pair production of heavy vector-like quarks decaying into hadronic final states in pp collisions at $\sqrt{s} = 13$ TeV with the ATLAS detector*. Phys. Rev. **D98**(9), p. 092005.

— ATLAS collaboration (2018k). *Search for pair production of higgsinos in final states with at least three b-tagged jets in $\sqrt{s} = 13$ TeV pp collisions using the ATLAS detector*. Phys. Rev. **D98**(9), p. 092002.

- ATLAS collaboration (2018l). *Search for resonant WZ production in the fully leptonic final state in proton-proton collisions at $\sqrt{s} = 13$ TeV with the ATLAS detector.* Phys. Lett. **B787**, pp. 68–88.
- ATLAS collaboration (2018m). *Search for the Decay of the Higgs Boson to Charm Quarks with the ATLAS Experiment.* Phys. Rev. Lett. **120**(21), p. 211802.
- ATLAS collaboration (2018n). *Search for the Higgs boson produced in association with a vector boson and decaying into two spin-zero particles in the $H \rightarrow aa \rightarrow 4b$ channel in pp collisions at $\sqrt{s} = 13$ TeV with the ATLAS detector.* JHEP **10**, p. 031.
- Aaboud, M. et al., ATLAS collaboration (2018o). *A search for lepton-flavor-violating decays of the Z boson into a τ -lepton and a light lepton with the ATLAS detector.* Phys. Rev. **D98**, p. 092010.
- ATLAS collaboration (2019a). *A search for pairs of highly collimated photon-jets in pp collisions at $\sqrt{s} = 13$ TeV with the ATLAS detector.* Phys. Rev. **D99**(1), p. 012008.
- ATLAS collaboration (2019b). *A strategy for a general search for new phenomena using data-derived signal regions and its application within the ATLAS experiment.* Eur. Phys. J. **C79**(2), p. 120.
- ATLAS collaboration (2018p). *Angular analysis of $B_d^0 \rightarrow K^* \mu^+ \mu^-$ decays in pp collisions at $\sqrt{s} = 8$ TeV with the ATLAS detector.* JHEP **10**, p. 047.
- ATLAS collaboration (2018q). *Combination of searches for heavy resonances decaying into bosonic and leptonic final states using 36 fb^{-1} of proton-proton collision data at $\sqrt{s} = 13$ TeV with the ATLAS detector.* Phys. Rev. **D98**(5), p. 052008.
- ATLAS collaboration (2018r). *Combination of the searches for pair-produced vector-like partners of the third-generation quarks at $\sqrt{s} = 13$ TeV with the ATLAS detector.* Phys. Rev. Lett. **121**(21), p. 211801.
- ATLAS collaboration (2018s). *Comparison between simulated and observed LHC beam backgrounds in the ATLAS experiment at $E_{\text{beam}} = 4$ TeV.* JINST **13**(12), P12006.
- ATLAS collaboration (2018t). *Constraints on off-shell Higgs boson production and the Higgs boson total width in $ZZ \rightarrow 4\ell$ and $ZZ \rightarrow 2\ell 2\nu$ final states with the ATLAS detector.* Phys. Lett. **B786**, pp. 223–244.
- ATLAS collaboration (2019c). *Correlated long-range mixed-harmonic fluctuations measured in pp , p + Pb and low-multiplicity Pb + Pb collisions with the ATLAS detector.* Phys. Lett. **B789**, pp. 444–471.
- ATLAS collaboration (2018u). *Cross-section measurements of the Higgs boson decaying into a pair of τ -leptons in proton-proton collisions at $\sqrt{s} = 13$ TeV with the ATLAS detector.* Submitted to: Phys. Rev.
- ATLAS collaboration (2019d). *Electron and photon energy calibration with the ATLAS detector using 2015-2016 LHC proton-proton collision data.* JINST **14**, P03017.
- ATLAS collaboration (2019e). *In situ calibration of large-radius jet energy and mass in 13 TeV proton-proton collisions with the ATLAS detector.* Eur. Phys. J. **C79**(2), p. 135.
- ATLAS collaboration (2018v). *Measurement of colour flow using jet-pull observables in $t\bar{t}$ events with the ATLAS experiment at $\sqrt{s} = 13$ TeV.* Eur. Phys. J. **C78**(10), p. 847.
- ATLAS collaboration (2018w). *Measurement of jet fragmentation in Pb + Pb and pp collisions at $\sqrt{s_{NN}} = 5.02$ TeV with the ATLAS detector.* Phys. Rev. **C98**(2), p. 024908.
- ATLAS collaboration (2019f). *Measurement of photon-jet transverse momentum correlations in 5.02 TeV $Pb + Pb$ and pp collisions with ATLAS.* Phys. Lett. **B789**, pp. 167–190.
- ATLAS collaboration (2018x). *Measurement of the azimuthal anisotropy of charged particles produced in $\sqrt{s_{NN}} = 5.02$ TeV Pb + Pb collisions with the ATLAS detector.* Eur. Phys. J. **C78**(12), p. 997.
- ATLAS collaboration (2018y). *Measurement of the Higgs boson mass in the $H \rightarrow ZZ^* \rightarrow 4\ell$ and $H \rightarrow \gamma\gamma$ channels with $\sqrt{s} = 13$ TeV pp collisions using the ATLAS detector.* Phys. Lett. **B784**, pp. 345–366.

- Aaboud, M. et al., ATLAS collaboration (2019g). *Measurement of the nuclear modification factor for inclusive jets in Pb+Pb collisions at $\sqrt{s_{NN}} = 5.02$ TeV with the ATLAS detector*. Phys. Lett. **B790**, pp. 108–128.
- ATLAS collaboration (2019h). *Measurement of the photon identification efficiencies with the ATLAS detector using LHC Run 2 data collected in 2015 and 2016*. Eur. Phys. J. **C79**(3), p. 205.
 - ATLAS collaboration (2018z). *Measurement of the suppression and azimuthal anisotropy of muons from heavy-flavor decays in Pb+Pb collisions at $\sqrt{s_{NN}} = 2.76$ TeV with the ATLAS detector*. Phys. Rev. **C98**(4), p. 044905.
 - ATLAS collaboration (2018aa). *Measurement of the top quark mass in the $t\bar{t} \rightarrow$ lepton+jets channel from $\sqrt{s} = 8$ TeV ATLAS data and combination with previous results*. Submitted to: Eur. Phys. J.
 - ATLAS collaboration (2018ab). *Measurement of the $Z\gamma \rightarrow \nu\bar{\nu}\gamma$ production cross section in pp collisions at $\sqrt{s} = 13$ TeV with the ATLAS detector and limits on anomalous triple gauge-boson couplings*. JHEP **12**, p. 010.
 - ATLAS collaboration (2018ac). *Measurements of b-jet tagging efficiency with the ATLAS detector using $t\bar{t}$ events at $\sqrt{s} = 13$ TeV*. JHEP **08**, p. 089.
 - ATLAS collaboration (2018ad). *Measurements of differential cross sections of top quark pair production in association with jets in pp collisions at $\sqrt{s} = 13$ TeV using the ATLAS detector*. JHEP **10**, p. 159.
 - ATLAS collaboration (2018ae). *Measurements of fiducial and differential cross-sections of $t\bar{t}$ production with additional heavy-flavour jets in proton-proton collisions at $\sqrt{s} = 13$ TeV with the ATLAS detector*.
 - ATLAS collaboration (2019i). *Measurements of gluon-gluon fusion and vector-boson fusion Higgs boson production cross-sections in the $H \rightarrow WW^* \rightarrow e\nu\mu\nu$ decay channel in pp collisions at $\sqrt{s} = 13$ TeV with the ATLAS detector*. Phys. Lett. **B789**, pp. 508–529.
 - ATLAS collaboration (2018af). *Measurements of Higgs boson properties in the diphoton decay channel with 36 fb^{-1} of pp collision data at $\sqrt{s} = 13$ TeV with the ATLAS detector*. Phys. Rev. **D98**, p. 052005.
 - ATLAS collaboration (2018ag). *Measurements of inclusive and differential fiducial cross-sections of $t\bar{t}\gamma$ production in leptonic final states at $\sqrt{s} = 13$ TeV in ATLAS*. Submitted to: Eur. Phys. J.
 - ATLAS collaboration (2018ah). *Measurements of $t\bar{t}$ differential cross-sections of highly boosted top quarks decaying to all-hadronic final states in pp collisions at $\sqrt{s} = 13$ TeV using the ATLAS detector*. Phys. Rev. **D98**(1), p. 012003.
 - ATLAS collaboration (2019j). *Measurements of W and Z boson production in pp collisions at $\sqrt{s} = 5.02$ TeV with the ATLAS detector*. Eur. Phys. J. **C79**(2), p. 128.
 - ATLAS collaboration (2018ai). *Observation of centrality-dependent acoplanarity for muon pairs produced via two-photon scattering in Pb+Pb collisions at $\sqrt{s_{NN}} = 5.02$ TeV with the ATLAS detector*. Phys. Rev. Lett. **121**(21), p. 212301.
 - ATLAS collaboration (2018aj). *Observation of electroweak $W^\pm Z$ boson pair production in association with two jets in pp collisions at $\sqrt{s} = 13$ TeV with the ATLAS detector*. Submitted to: Phys. Lett.
 - ATLAS collaboration (2018ak). *Observation of $H \rightarrow b\bar{b}$ decays and VH production with the ATLAS detector*. Phys. Lett. **B786**, pp. 59–86.
 - ATLAS collaboration (2018al). *Operation and performance of the ATLAS Tile Calorimeter in Run 1*. Eur. Phys. J. **C78**(12), p. 987.
 - ATLAS collaboration (2018am). *Performance of missing transverse momentum reconstruction with the ATLAS detector using proton-proton collisions at $\sqrt{s} = 13$ TeV*. Eur. Phys. J. **C78**(11), p. 903.
 - ATLAS collaboration (2018an). *Performance of top-quark and W-boson tagging with ATLAS in Run 2 of the LHC*.

- ATLAS collaboration (2018ao). *Probing the quantum interference between singly and doubly resonant top-quark production in pp collisions at $\sqrt{s} = 13$ TeV with the ATLAS detector.* Phys. Rev. Lett. **121**(15), p. 152002.
- ATLAS collaboration (2018ap). *Prompt and non-prompt J/ψ and $\psi(2S)$ suppression at high transverse momentum in 5.02 TeV Pb+Pb collisions with the ATLAS experiment.* Eur. Phys. J. **C78**(9), p. 762.
- ATLAS collaboration (2018aq). *Prompt and non-prompt J/ψ elliptic flow in Pb+Pb collisions at $\sqrt{s_{NN}} = 5.02$ TeV with the ATLAS detector.* Eur. Phys. J. **C78**(9), p. 784.
- ATLAS collaboration (2019k). *Properties of $g \rightarrow b\bar{b}$ at small opening angles in pp collisions with the ATLAS detector at $\sqrt{s} = 13$ TeV.* Phys. Rev. **D99**(5), p. 052004.
- ATLAS collaboration (2018ar). *Search for a heavy Higgs boson decaying into a Z boson and another heavy Higgs boson in the $\ell\ell b\bar{b}$ final state in pp collisions at $\sqrt{s} = 13$ TeV with the ATLAS detector.* Phys. Lett. **B783**, pp. 392–414.
- ATLAS collaboration (2018as). *Search for charged Higgs bosons decaying into top and bottom quarks at $\sqrt{s} = 13$ TeV with the ATLAS detector.* JHEP **11**, p. 085.
- ATLAS collaboration (2018at). *Search for charged Higgs bosons decaying via $H^\pm \rightarrow \tau^\pm \nu_\tau$ in the τ +jets and τ +lepton final states with 36 fb^{-1} of pp collision data recorded at $\sqrt{s} = 13$ TeV with the ATLAS experiment.* JHEP **09**, p. 139.
- ATLAS collaboration (2018au). *Search for chargino and neutralino production in final states with a Higgs boson and missing transverse momentum at $\sqrt{s} = 13$ TeV with the ATLAS detector.* Submitted to: Phys. Rev.
- ATLAS collaboration (2018av). *Search for chargino-neutralino production using recursive jigsaw reconstruction in final states with two or three charged leptons in proton-proton collisions at $\sqrt{s} = 13$ TeV with the ATLAS detector.* Phys. Rev. **D98**(9), p. 092012.
- ATLAS collaboration (2019l). *Search for doubly charged scalar bosons decaying into same-sign W boson pairs with the ATLAS detector.* Eur. Phys. J. **C79**(1), p. 58.
- ATLAS collaboration (2018aw). *Search for flavor-changing neutral currents in top quark decays $t \rightarrow Hc$ and $t \rightarrow Hu$ in multilepton final states in proton-proton collisions at $\sqrt{s} = 13$ TeV with the ATLAS detector.* Phys. Rev. **D98**(3), p. 032002.
- ATLAS collaboration (2018ax). *Search for four-top-quark production in the single-lepton and opposite-sign dilepton final states in pp collisions at $\sqrt{s} = 13$ TeV with the ATLAS detector.* Submitted to: Phys. Rev.
- ATLAS collaboration (2019m). *Search for heavy charged long-lived particles in proton-proton collisions at $\sqrt{s} = 13$ TeV using an ionisation measurement with the ATLAS detector.* Phys. Lett. **B788**, pp. 96–116.
- ATLAS collaboration (2019n). *Search for heavy long-lived multi-charged particles in proton-proton collisions at $\sqrt{s} = 13$ TeV using the ATLAS detector.* Phys. Rev. **D99**(5), p. 052003.
- ATLAS collaboration (2019o). *Search for heavy Majorana or Dirac neutrinos and right-handed W gauge bosons in final states with two charged leptons and two jets at $\sqrt{s} = 13$ TeV with the ATLAS detector.* JHEP **01**, p. 016.
- ATLAS collaboration (2018ay). *Search for heavy particles decaying into top-quark pairs using lepton-plus-jets events in proton-proton collisions at $\sqrt{s} = 13$ TeV with the ATLAS detector.* Eur. Phys. J. **C78**(7), p. 565.
- ATLAS collaboration (2018az). *Search for heavy resonances decaying to a photon and a hadronically decaying Z/W/H boson in pp collisions at $\sqrt{s} = 13$ TeV with the ATLAS detector.* Phys. Rev. **D98**(3), p. 032015.
- ATLAS collaboration (2019p). *Search for Higgs boson decays into a pair of light bosons in the $b\bar{b}\mu\mu$ final state in pp collision at $\sqrt{s} = 13$ TeV with the ATLAS detector.* Phys. Lett. **B790**, pp. 1–21.

- Aaboud, M. et al., ATLAS collaboration (2018ba). *Search for Higgs boson decays into pairs of light (pseudo)scalar particles in the $\gamma\gamma jj$ final state in pp collisions at $\sqrt{s} = 13$ TeV with the ATLAS detector.* Phys. Lett. **B782**, pp. 750–767.
- ATLAS collaboration (2018bb). *Search for Higgs boson decays to beyond-the-Standard-Model light bosons in four-lepton events with the ATLAS detector at $\sqrt{s} = 13$ TeV.* JHEP **06**, p. 166.
 - ATLAS collaboration (2018bc). *Search for Higgs boson pair production in the $b\bar{b}WW^*$ decay mode at $\sqrt{s} = 13$ TeV with the ATLAS detector.*
 - ATLAS collaboration (2018bd). *Search for Higgs boson pair production in the $\gamma\gamma WW^*$ channel using pp collision data recorded at $\sqrt{s} = 13$ TeV with the ATLAS detector.* Eur. Phys. J. **C78**(12), p. 1007.
 - ATLAS collaboration (2018be). *Search for Higgs boson pair production in the $WW^{(*)}WW^{(*)}$ decay channel using ATLAS data recorded at $\sqrt{s} = 13$ TeV.* Submitted to: JHEP.
 - ATLAS collaboration (2018bf). *Search for Higgs bosons produced via vector-boson fusion and decaying into bottom quark pairs in $\sqrt{s} = 13$ TeV pp collisions with the ATLAS detector.* Phys. Rev. **D98**(5), p. 052003.
 - ATLAS collaboration (2018bg). *Search for High-Mass Resonances Decaying to $\tau\nu$ in pp Collisions at $\sqrt{s}=13$ TeV with the ATLAS Detector.* Phys. Rev. Lett. **120**(16), p. 161802.
 - ATLAS collaboration (2018bh). *Search for invisible Higgs boson decays in vector boson fusion at $\sqrt{s} = 13$ TeV with the ATLAS detector.* Submitted to: Phys. Lett.
 - ATLAS collaboration (2018bi). *Search for large missing transverse momentum in association with one top-quark in proton-proton collisions at $\sqrt{s} = 13$ TeV with the ATLAS detector.* Submitted to: JHEP.
 - ATLAS collaboration (2018bj). *Search for lepton-flavor violation in different-flavor, high-mass final states in pp collisions at $\sqrt{s} = 13$ TeV with the ATLAS detector.* Phys. Rev. **D98**(9), p. 092008.
 - ATLAS collaboration (2019q). *Search for light resonances decaying to boosted quark pairs and produced in association with a photon or a jet in proton-proton collisions at $\sqrt{s} = 13$ TeV with the ATLAS detector.* Phys. Lett. **B788**, pp. 316–335.
 - ATLAS collaboration (2019r). *Search for long-lived particles in final states with displaced dimuon vertices in pp collisions at $\sqrt{s} = 13$ TeV with the ATLAS detector.* Phys. Rev. **D99**(1), p. 012001.
 - ATLAS collaboration (2019s). *Search for long-lived particles produced in pp collisions at $\sqrt{s} = 13$ TeV that decay into displaced hadronic jets in the ATLAS muon spectrometer.* Phys. Rev. **D99**(5), p. 052005.
 - ATLAS collaboration (2018bk). *Search for new phenomena in events with same-charge leptons and b -jets in pp collisions at $\sqrt{s} = 13$ TeV with the ATLAS detector.* JHEP **12**, p. 039.
 - ATLAS collaboration (2018bl). *Search for new phenomena using the invariant mass distribution of same-flavour opposite-sign dilepton pairs in events with missing transverse momentum in $\sqrt{s} = 13$ TeV pp collisions with the ATLAS detector.* Eur. Phys. J. **C78**(8), p. 625.
 - ATLAS collaboration (2018bm). *Search for pair- and single-production of vector-like quarks in final states with at least one Z boson decaying into a pair of electrons or muons in pp collision data collected with the ATLAS detector at $\sqrt{s} = 13$ TeV.* Phys. Rev. **D98**(11), p. 112010.
 - ATLAS collaboration (2018bn). *Search for pair production of heavy vector-like quarks decaying into high- p_T W bosons and top quarks in the lepton-plus-jets final state in pp collisions at $\sqrt{s} = 13$ TeV with the ATLAS detector.* JHEP **08**, p. 048.
 - ATLAS collaboration (2019t). *Search for pair production of Higgs bosons in the $b\bar{b}b\bar{b}$ final state using proton-proton collisions at $\sqrt{s} = 13$ TeV with the ATLAS detector.* JHEP **01**, p. 030.
 - ATLAS collaboration (2018bo). *Search for pair production of up-type vector-like quarks and for four-top-quark events in final states with multiple b -jets with the ATLAS detector.* JHEP **07**, p. 089.
 - ATLAS collaboration (2018bp). *Search for photonic signatures of gauge-mediated supersymmetry in 13 TeV pp collisions with the ATLAS detector.* Phys. Rev. **D97**(9), p. 092006.

- ATLAS collaboration (2018bq). *Search for resonances in the mass distribution of jet pairs with one or two jets identified as b-jets in proton-proton collisions at $\sqrt{s} = 13$ TeV with the ATLAS detector.* Phys. Rev. **D98**, p. 032016.
 - ATLAS collaboration (2018br). *Search for resonant and non-resonant Higgs boson pair production in the $b\bar{b}\tau^+\tau^-$ decay channel in pp collisions at $\sqrt{s} = 13$ TeV with the ATLAS detector.* Phys. Rev. Lett. **121**(19). [Erratum: Phys. Rev. Lett.122,no.8,089901(2019)], p. 191801.
 - ATLAS collaboration (2018bs). *Search for R-parity-violating supersymmetric particles in multi-jet final states produced in p-p collisions at $\sqrt{s} = 13$ TeV using the ATLAS detector at the LHC.* Phys. Lett. **B785**, pp. 136–158.
 - ATLAS collaboration (2018bt). *Search for single production of vector-like quarks decaying into W b in pp collisions at $\sqrt{s} = 13$ TeV with the ATLAS detector.* Submitted to: JHEP.
 - ATLAS collaboration (2019u). *Search for squarks and gluinos in final states with hadronically decaying τ -leptons, jets, and missing transverse momentum using pp collisions at $\sqrt{s} = 13$ TeV with the ATLAS detector.* Phys. Rev. **D99**(1), p. 012009.
 - ATLAS collaboration (2018bu). *Search for supersymmetry in events with four or more leptons in $\sqrt{s} = 13$ TeV pp collisions with ATLAS.* Phys. Rev. **D98**(3), p. 032009.
 - ATLAS collaboration (2018bv). *Search for supersymmetry in final states with charm jets and missing transverse momentum in 13 TeV pp collisions with the ATLAS detector.* JHEP **09**, p. 050.
 - ATLAS collaboration (2018bw). *Search for the production of a long-lived neutral particle decaying within the ATLAS hadronic calorimeter in association with a Z boson from pp collisions at $\sqrt{s} = 13$ TeV.* Submitted to: Phys. Rev. Lett.
 - ATLAS collaboration (2018bx). *Search for top squarks decaying to tau sleptons in pp collisions at $\sqrt{s} = 13$ TeV with the ATLAS detector.* Phys. Rev. **D98**(3), p. 032008.
 - ATLAS collaboration (2018by). *Search for top-quark decays $t \rightarrow Hq$ with 36 fb^{-1} of pp collision data at $\sqrt{s} = 13$ TeV with the ATLAS detector.* Submitted to: JHEP.
 - ATLAS collaboration (2019v). *Search for vector-boson resonances decaying to a top quark and bottom quark in the lepton plus jets final state in pp collisions at $\sqrt{s} = 13$ TeV with the ATLAS detector.* Phys. Lett. **B788**, pp. 347–370.
 - ATLAS collaboration (2018bz). *Search for $W' \rightarrow tb$ decays in the hadronic final state using pp collisions at $\sqrt{s} = 13$ TeV with the ATLAS detector.* Phys. Lett. **B781**, pp. 327–348.
 - ATLAS collaboration (2018ca). *Searches for exclusive Higgs and Z boson decays into $J/\psi\gamma$, $\psi(2S)\gamma$, and $\Upsilon(nS)\gamma$ at $\sqrt{s} = 13$ TeV with the ATLAS detector.* Phys. Lett. **B786**, pp. 134–155.
 - ATLAS collaboration (2019w). *Study of the hard double-parton scattering contribution to inclusive four-lepton production in pp collisions at $\sqrt{s} = 8$ TeV with the ATLAS detector.* Phys. Lett. **B790**. [Phys. Lett.790,595(2019)], pp. 595–614.
 - ATLAS collaboration (2018cb). *Study of the rare decays of B_s^0 and B^0 mesons into muon pairs using data collected during 2015 and 2016 with the ATLAS detector.* Submitted to: JHEP.
- ATLAS Collaboration (2018). *Search for boosted resonances decaying to two b-quarks and produced in association with a jet at $\sqrt{s} = 13$ TeV with the ATLAS detector.* (ATLAS-CONF-2018-052).

FASE2_ATLAS

- Abbot, B. et al., The ATLAS IBL Collaboration (2018). *Production and integration of the ATLAS Insertable B-Layer.* Journal Instrum. **13**, T05008.
- Dalla Betta, G.-F. et al. (2018). “Performance of new radiation tolerant thin n-in-p Silicon pixel sensors for the CMS experiment at High Luminosity LHC”. *2017 IEEE NSS-MIC Conference Record.* Piscataway, NJ, USA: IEEE.
- Dinardo, M. et al. (2018). *The INFN R&D: New pixel detector for the High Luminosity upgrade of the LHC.* Il Nuovo Cimento C **41**, 75 pages.

- Meschini, M. et al. (2018). “Pixel Detector Developments for Tracker Upgrades of the High Luminosity LHC”. *Proceedings of International Conference on Technology and Instrumentation in Particle Physics (TIPP 2017)*. Springer, pp. 349–355.
- Morozzi, A., Moscatelli, F., Passeri, D., Bilei, G. M., Dalla Betta, G.-F., Bomben, M., and Mattiazzo, S. (2018). “Modeling of Radiation Damage Effects at High Luminosity LHC Expected Fluences: Measurements and Simulations”. *2017 IEEE NSS-MIC Conference Record*. Piscataway, NJ, USA: IEEE.
- Sultan, D., Mendicino, R., Boscardin, M., Ronchin, S., Zorzi, N., and Dalla Betta, G.-F. (2018). “A Three-Dimensional Gated Diode Structure for Surface Parameter Characterization in a 3D Sensor Technology”. *2017 IEEE NSS-MIC Conference Record*. Piscataway, NJ, USA: IEEE.
- Zoi, I. et al. (2018). “Beam Test Results of Thin n-in-p 3D and Planar Pixel Sensors for the High Luminosity LHC Tracker Upgrade at CMS”. *Proceedings of Science - EPS HEP 2017*. Trieste, Italy: Sissa, p. 809.

Astroparticle Physics

- Abbrescia, M. et al. (2018a). *Search for long distance correlations between extensive air showers detected by the EEE network*. *Eur. Phys. J. Plus* **133**(2), p. 34.
- (2018b). *The Extreme Energy Events experiment: an overview of the telescopes performance*. *JINST* **13**(08), P08026.
- Nozzoli, F. (2018). ^{146}Nd , ^{144}Sm , and other unexplored 2β -decay isotopes. *Phys. Rev.* **C97**(1), p. 015501.
- Albertsson, K. et al. (2018). *Machine Learning in High Energy Physics Community White Paper*. *J. Phys. Conf. Ser.* **1085**(2), p. 022008.

AMS

- Aguilar, M. et al. (2018a). *Distinctive Properties of High Energy Cosmic Positrons Measured by the Alpha Magnetic Spectrometer*. *Phys. Rev. Lett.* **submitted**.
- (2018b). *Observation of complex time structures in the cosmic-ray electron and positron fluxes with the AMS on the ISS*. *Phys. Rev. Lett.* **121**(5), p. 051102.
- (2018c). *Observation of Fine Time Structures in the Cosmic Proton and Helium Fluxes with the Alpha Magnetic Spectrometer on the International Space Station*. *Phys. Rev. Lett.* **121**(5), p. 051101.
- (2018d). *Observation of New Properties of Secondary Cosmic Rays Lithium, Beryllium, and Boron by the Alpha Magnetic Spectrometer on the International Space Station*. *Phys. Rev. Lett.* **120**(2), p. 021101.
- (2018e). *Precision measurement of cosmic-ray nitrogen and its primary and secondary components with the Alpha Magnetic Spectrometer on the International Space Station*. *Phys. Rev. Lett.* **121**(5), p. 051103.
- Behlmann, M., Delgado, C., Giovacchini, F., and Zuccon, P. (2018). *Identification of isotopes ^3He and ^4He with the AMS detector on the International Space Station*. *PoS ICRC2017*, p. 162.

DarkSide

- Aalseth, C. E., Acerbi, F., et al. (2018). *DarkSide-20k: A 20 tonne two-phase LAr TPC for direct dark matter detection at LNGS*. *Eur. Phys. J. Plus* **133**, p. 131.

FISH

- Colzi, G., Fava, E., Barbiero, M., Mordini, C., Lamporesi, G., and Ferrari, G. (2018). *Production of large Bose-Einstein condensates in a magnetic-shield-compatible hybrid trap*. *Phys. Rev. A* **97** (5), p. 053625.
- Fava, E., Bienaimé, T., Mordini, C., Colzi, G., Qu, C., Stringari, S., Lamporesi, G., and Ferrari, G. (2018). *Observation of Spin Superfluidity in a Bose Gas Mixture*. *Phys. Rev. Lett.* **120** (17), p. 170401.
- Qu, C., Tylutki, M., Stringari, S., and Pitaevskii, L. P. (2017). *Magnetic solitons in Rabi-coupled Bose-Einstein condensates*. *Phys. Rev. A* **95** (3), p. 033614.

HUMOR

- Pontin, A., Bonaldi, M., Borrielli, A., Marconi, L., Marino, F., Pandraud, G., Prodi, G., Sarro, P., Serra, E., and Marin, F. (2018). *Quantum nondemolition measurement of optical field fluctuations by optomechanical interaction*. *PHYSICAL REVIEW A* **97**(033833).
- Rossi, M., Kralj, N., Zippilli, S., Natali, R., Borrielli, A., Pandraud, G., Serra, E., Di Giuseppe, G., and Vitali, D. (2018). *Normal-mode splitting in a weakly coupled optomechanical system*. *PHYSICAL REVIEW LETTERS* **120**(7).
- Serra, E., Morana, B., Borrielli, A., Marin, F., Pandraud, G., Pontin, A., Prodi, G., Sarro, P., and Bonaldi, M. (2018). *Silicon Nitride MOMS Oscillator for Room Temperature Quantum Optomechanics*. *IEEE JOURNAL OF MICROELECTROMECHANICAL SYSTEMS* **27**(6).

LIMADOU

- Ambrosi, G., Bartocci, S., Basara, L., Battiston, R., Burger, W. J., Carfora, L., Castellini, G., Cipollone, P., Conti, L., Contin, A., De Donato, C., De Santis, C., Follega, F. M., Guandalini, C., Ionica, M., Iuppa, R., Laurenti, G., Lazzizzera, I., Lolli, M., Manea, C., Marcelli, L., Masciantonio, G., Mergé, M., Osteria, G., Pacini, L., Palma, F., Palmonari, F., Panico, B., Patrizii, L., Perfetto, F., Picozza, P., Pozzato, M., Puel, M., Rashevskaya, I., Ricci, E., Ricci, M., Ricciarini, S. B., Scotti, V., Sotgiu, A., Sparvoli, R., Spataro, B., and Vitale, V. (2018). *The HEPD particle detector of the CSES satellite mission for investigating seismo-associated perturbations of the Van Allen belts*. *Science China Technological Sciences* **61**(5), pp. 643–652.
- Shen, X., Zhang, X., Yuan, S., Wang, L., Cao, J., Huang, J., Zhu, X., Picozza, P., and Dai, J. (2018). *The state-of-the-art of the China Seismo-Electromagnetic Satellite mission*. *Science China Technological Sciences* **61**(5), pp. 634–642.

LISA Pathfinder

- Anderson, G. et al. (2018). *Experimental results from the ST7 mission on LISA Pathfinder*. *PHYSICAL REVIEW D* **98**(10), p. 102005.
- Armano, M. et al. (2018b). *Beyond the Required LISA Free-Fall Performance: New LISA Pathfinder Results down to 20 μ Hz*. *PHYSICAL REVIEW LETTERS* **120**(6), p. 061101.
- (2018d). *Calibrating the system dynamics of LISA Pathfinder*. *PHYSICAL REVIEW D* **97**(12), p. 122002.
- (2018e). *Characteristics and Energy Dependence of Recurrent Galactic Cosmic-Ray Flux Depressions and of a Forbush Decrease with LISA Pathfinder*. *ASTROPHYSICAL JOURNAL* **854**(2), p. 113.
- (2018f). *Measuring the Galactic Cosmic Ray flux with the LISA Pathfinder radiation monitor*. *ASTROPARTICLE PHYSICS* **98**, pp. 28–37.
- (2018g). *Precision charge control for isolated free-falling test masses: LISA Pathfinder results*. *PHYSICAL REVIEW D* **98**(6), p. 062001.

- Bassan, M. et al. (2018). *Actuation crosstalk in free-falling systems: Torsion pendulum results for the engineering model of the LISA pathfinder gravitational reference sensor*. *ASTROPARTICLE PHYSICS* **97**(6), pp. 19–26.
- Russano, G. et al. (2018). *Measuring fN force variations in the presence of constant nN forces: a torsion pendulum ground test of the LISA Pathfinder free-fall mode*. *CLASSICAL AND QUANTUM GRAVITY* **35**(3), p. 035017.

VIRGO

- Abbott, B. P. et al., LIGO Scientific Collaboration and Virgo Collaboration (2018a). *All-sky search for long-duration gravitational wave transients in the first Advanced LIGO observing run*. *Classical and Quantum Gravity*.
- LIGO Scientific Collaboration and Virgo Collaboration (2018b). *Effects of data quality vetoes on a search for compact binary coalescences in Advanced LIGO's first observing run*. *Classical and Quantum Gravity*.
- LIGO Scientific Collaboration and Virgo Collaboration (2018c). *GWTC-1: A Gravitational-Wave Transient Catalog of Compact Binary Mergers Observed by LIGO and Virgo during the First and Second Observing Runs*. arXiv:1811.12907.
- LIGO Scientific Collaboration and Virgo Collaboration (2018d). *Prospects for observing and localizing gravitational-wave transients with Advanced LIGO, Advanced Virgo and KAGRA*. *Living Reviews in Relativity*.
- Abbott, B. P., Abbott, R., Abbott, T. D., Acernese, F., Ackley, K., Adams, C., Adams, T., Addesso, P., Adhikari, R. X., Adya, V. B., et al., LIGO Scientific Collaboration and Virgo Collaboration (2018e). *Constraints on cosmic strings using data from the first Advanced LIGO observing run*. *Physical Review D* **97**(10), 102002, p. 102002.
- LIGO Scientific Collaboration and Virgo Collaboration (2018f). *First Search for Nontensorial Gravitational Waves from Known Pulsars*. *Physical Review Letters* **120**(3), 031104, p. 031104.
- LIGO Scientific Collaboration and Virgo Collaboration (2018g). *Full band all-sky search for periodic gravitational waves in the O1 LIGO data*. *Physical Review D* **97**(10), 102003, p. 102003.
- LIGO Scientific Collaboration and Virgo Collaboration (2018h). *GW170817: Implications for the Stochastic Gravitational-Wave Background from Compact Binary Coalescences*. *Physical Review Letters* **120**(9), 091101, p. 091101.
- LIGO Scientific Collaboration and Virgo Collaboration (2018i). *GW170817: Measurements of Neutron Star Radii and Equation of State*. *Physical Review Letters* **121**(16), 161101, p. 161101.
- LIGO Scientific Collaboration and Virgo Collaboration (2018j). *Search for Subsolar-Mass Ultracompact Binaries in Advanced LIGO's First Observing Run*. *Physical Review Letters* **121**(23), 231103, p. 231103.
- LIGO Scientific Collaboration and Virgo Collaboration (2018k). *Search for Tensor, Vector, and Scalar Polarizations in the Stochastic Gravitational-Wave Background*. *Physical Review Letters* **120**(20), 201102, p. 201102.
- Acernese, F., Adams, T., Agatsuma, K., Aiello, L., Allocca, A., Aloy, M. A., Amato, A., Antier, S., Arène, M., Arnaud, N., et al., LIGO Scientific Collaboration and Virgo Collaboration (2018). *Calibration of advanced Virgo and reconstruction of the gravitational wave signal $h(t)$ during the observing run O2*. *Classical and Quantum Gravity* **35**(20), 205004, p. 205004.
- Nagano, K., Perreca, A., Arai, K., and Adhikari, R. X. (2018). *External quantum efficiency enhancement by photon recycling with backscatter evasion*. *Applied Optics* **57**(13), p. 3372.

Nuclear Physics

AEGIS

- Aghion, S. et al., The AEGIS Collaboration (2018a). *Antiproton tagging and vertex fitting in a Timepix3 detector*. Journal of Instrumentation **13**(06), P06004–P06004.
- The AEGIS Collaboration (2018b). *Compression of a mixed antiproton and electron non-neutral plasma to high densities*. The European Physical Journal D **72**(4), p. 76.
- The AEGIS Collaboration (2018c). *Producing long-lived 2^3S positronium via 3^3P laser excitation in magnetic and electric fields*. Phys. Rev. A **98**(1), 013402, p. 013402.
- Amsler, C. et al., The AEGIS Collaboration (2019). *Velocity selected production of 2^3S metastable positronium*. Phys. Rev. A **in press**.
- Doser, M. et al., The AEGIS Collaboration (2018). *AEGIS at ELENA: outlook for physics with a pulsed cold antihydrogen beam*. Philosophical transactions. Series A, Mathematical, physical, and engineering sciences **376**(2116).
- Evans, C. et al., The AEGIS Collaboration (2018). *Towards the first measurement of matter-antimatter gravitational interaction*. EPJ Web Conf. **182**, p. 02040.
- Guatieri, F. et al., The AEGIS Collaboration (2018). *AEGIS latest results*. EPJ Web of Conferences **181**, p. 01037.
- Guatieri, F., Mariazzi, S., and Sennen Brusa, R. (2018). *Monte Carlo simulation of the implantation profile of e^+ in nanochanneled silicon*. The European Physical Journal D **72**, p. 198.

FOOT

- Bertazzoni, M. et al. (2019). *Development and characterization of a δE -TOF detector prototype for the FOOT experiment*. Nuclear Instruments and Methods in Physics Research Section A **916**, pp. 116–124.
- Silvestre, G. et al. (2018). *Evaluation of double-sided silicon microstrip sensor for the FOOT experiment*. Nuclear Instruments and Methods in Physics Research Section A.

Theoretical Physics

BELL

- Albeverio, S., Mazzucchi, S., and Canginiotti, N. (2018). *Generalized Feynman path integrals and applications to higher-order heat-type equations*. Expositiones Mathematicae **36**(3), pp. 406–429.
- Ballico, E., A. Bernardi, I. Carusotto, S. Mazzucchi, and V. Moretti, eds. (2019). *Quantum Physics and Geometry*. Springer, DE.
- Khavkine, I., Melati, A., and Moretti, V. (2019). *On Wick polynomials of boson fields in locally covariant algebraic QFT*. Ann. Henri Poincaré **20**, pp. 1000–1030.
- Mazzucchi, S. (2018). *Infinite Dimensional Oscillatory Integrals with Polynomial Phase and Applications to Higher-Order Heat-Type Equations*. Potential Analysis **49**(2), pp. 209–223.
- Moretti, V. and Oppio, M. (2019). *Quantum theory in quaternionic Hilbert space: How Poincaré symmetry reduces the theory to the standard complex one*. Reviews in Mathematical Physics **31**, p. 1950013.
- (2018). *The Correct Formulation of Gleason’s Theorem in Quaternionic Hilbert Spaces*. Annales Henri Poincaré **19**(11), pp. 3321–3355.
- Pastorello, D. (2019). “Entanglement, CP-maps and quantum communications”. Ed. by E. Ballico, A. Bernardi, I. Carusotto, S. Mazzucchi, and V. Moretti. Springer, DE. Chap. 6.

BIOPHYS

- Bartolucci, G., Orioli, S., and Faccioli, P. (2018). *Transition Path Theory from Biased Simulations*. J. Chem. Phys. **149**.
- Garberoglio, G., Jankowski, P., Szalewicz, K., and Harvey, A. H. (2018a). *Fully quantum calculation of the second and third virial coefficients of water and its isotopologues from ab initio potentials*. Faraday Discuss. . **212**, pp. 467–497.
- Garberoglio, G., Vallauri, R., and Bafle, U. (2018b). *Time correlation functions of simple liquids: A new insight on the underlying dynamical processes*. J. Chem. Phys. **148**.
- Heidari, M., Kremer, K., Potestio, R., and Cortes-Huerta, R. (2018a). *Fluctuations, Finite-Size Effects and the Thermodynamic Limit in Computer Simulations: Revisiting the Spatial Block Analysis Method*. Entropy **20**.
- Heidari, M., Kremer, K., Cortes-Huerta, R., and Potestio, R. (2018b). *Concurrent coupling of realistic and ideal models of liquids and solids in Hamiltonian adaptive resolution simulations*. Eur. Phys. J. E **41**.
- (2018c). *Spatially Resolved Thermodynamic Integration: An Efficient Method To Compute Chemical Potentials of Dense Fluids*. J. Chem. Theor. Comput. (**in press**).
- Heidari, M., Kremer, K., Potestio, R., and Cortes-Huerta, R. (2018d). *Finite-size integral equations in the theory of liquids and the thermodynamic limit in computer simulations*. Molecular Physics **116**, pp. 3301–3310.
- Ianeselli, A., Orioli, S., Spagnolli, G., Faccioli, P., Cupellini, L., Jurinovich, S., and Mennucci, B. (2018). *Atomic Detail of Protein Folding Revealed by an Ab Initio Reappraisal of Circular Dichroism*. J. Am. Chem. Soc. **140**.
- Morresi, T., Timpel, M., Pedrielli, A., Garberoglio, G., Tatti, R., Verucchi, R., Pasquali, L., Pugno, N. M., Nardi, M. V., and Taioli, S. (2018c). *A novel combined experimental and multiscale theoretical approach to unravel the structure of SiC/SiOx core/shell nanowires for their optimal design*. Nanoscale **10**.
- Pedrielli, A., Taioli, S., Garberoglio, G., and Pugno, N. M. (2018b). *Gas adsorption and dynamics in Pillared Graphene Frameworks*. Micropor. Mesopor. Mater **257**.
- (2018d). *Mechanical and thermal properties of graphene random nanofoams via Molecular Dynamics simulations*. Carbon **132**.
- Praprotnik, M. and Robinson Cortes-Huerta Raffaello Potestio, L. D. S. (2018). *Adaptive Resolution Molecular Dynamics Technique*. Handbook of Materials Modeling: Methods: Theory and Modeling.
- Segatta, F., Lattanzi, G., and Faccioli, P. (2018b). *Predicting Charge Mobility of Organic Semiconductors with Complex Morphology*. Macromolecules **51**(21), pp. 9060–9068.
- Wang, F., Orioli, S., Ianeselli, A., Spagnolli, G., a Beccara, S., Gershenson, A., Faccioli, P., and Wintrodde, P. L. (2018). *All-Atom Simulations Reveal How Single-Point Mutations Promote Serpin Misfolding*. Biophys. J. **114**.

FBS

- Leidemann, W. (2018). *Ab initio calculations for non-strange and strange few-baryon systems*. J. Phys.: Conf. Ser. **981**, pp. 1–12.
- Rocco, N., Leidemann, W., Lovato, A., and Orlandini, G. (2018a). *Relativistic effects in ab-initio electron-nucleus scattering*. Phys. Rev. C **97**, p. 055501.

FLAG

- Amendola, L. et al. (2018). *Cosmology and fundamental physics with the Euclid satellite*. Living Rev. Rel. **21**(1), p. 2.
- Calzà, M., Rinaldi, M., and Sebastiani, L. (2018). *A special class of solutions in $F(R)$ -gravity*. Eur. Phys. J. **C78**(3), p. 178.
- Casalino, A., Rinaldi, M., Sebastiani, L., and Vagnozzi, S. (2019). *Alive and well: mimetic gravity and a higher-order extension in light of GW170817*. Class. Quant. Grav. **36**(1), p. 017001.
- (2018). *Mimicking dark matter and dark energy in a mimetic model compatible with GW170817*. Phys. Dark Univ. **22**, p. 108.
- Cisterna, A., Erices, C., Kuang, X., and Rinaldi, M. (2018). *Axionic black branes with conformal coupling*. Phys. Rev. **D97**(12), p. 124052.
- Colléaux, A., Chinaglia, S., and Zerbini, S. (2018). *Nonpolynomial Lagrangian approach to regular black holes*. Int. J. Mod. Phys. **D27**(03), p. 1830002.
- Rinaldi, M. (2018). *On the equivalence of Jordan and Einstein frames in scale-invariant gravity*. Eur. Phys. J. Plus **133**(10), p. 408.
- Sebastiani, L. (2018). *Static Spherically Symmetric solutions in a subclass of Horndeski theories of gravity*. Int. J. Geom. Meth. Mod. Phys. **15**(09), p. 1850152.
- Sebastiani, L., Vanzo, L., and Zerbini, S. (2018). *Action growth for black holes in modified gravity*. Phys. Rev. **D97**(4), p. 044009.

MANYBODY

- Baroni, A. et al. (2018). *Local chiral interactions, the tritium Gamow-Teller matrix element, and the three-nucleon contact term*. Phys. Rev. **C98**(4), p. 044003.
- Lovato, A., Gandolfi, S., Carlson, J., Lusk, E., Pieper, S. C., and Schiavilla, R. (2018). *Quantum Monte Carlo calculation of neutral-current ν - ^{12}C inclusive quasielastic scattering*. Phys. Rev. **C97**(2), p. 022502.
- Madeira, L., Lovato, A., Pederiva, F., and Schmidt, K. E. (2018). *Quantum Monte Carlo formalism for dynamical pions and nucleons*. Phys. Rev. **C98**(3), p. 034005.
- Piarulli, M. et al. (2018). *Light-nuclei spectra from chiral dynamics*. Phys. Rev. Lett. **120**(5), p. 052503.
- Riz, L., Pederiva, F., and Gandolfi, S. (2018). *Spin response and neutrino mean free path in neutron matter*.
- Rocco, N., Leidemann, W., Lovato, A., and Orlandini, G. (2018b). *Relativistic effects in ab-initio electron-nucleus scattering*. Phys. Rev. **C97**(5), p. 055501.
- Roggero, A. and Pederiva, F. (2018). *Extension of the Configuration Interaction Monte Carlo Method to Atoms and Molecules*. Advances in Quantum Chemistry **7**, pp. 241–253.
- Sobczyk, J. E., Rocco, N., Lovato, A., and Nieves, J. (2018). *Scaling within the Spectral Function approach*. Phys. Rev. **C97**(3), p. 035506.

NEMESYS

- Azzolini, M., Angelucci, M., Cimino, R., Larciprete, R., Pugno, N. M., Taioli, S., and Dapor, M. (2018a). *Secondary electron emission and yield spectra of metals from Monte Carlo simulations and experiments*. Journal of Physics: Condensed Matter **31**(5), p. 055901.
- Azzolini, M., Morresi, T., Abrams, K., Masters, R., Stehling, N., Rodenburg, C., Pugno, N. M., Taioli, S., and Dapor, M. (2018b). *Anisotropic Approach for Simulating Electron Transport in Layered Materials: Computational and Experimental Study of Highly Oriented Pyrolytic Graphite*. The Journal of Physical Chemistry C **122**(18), pp. 10159–10166.

- Morresi, T., Pedrielli, A., A Beccara, S., Gabbrielli, R., Pugno, N. M., and Taioli, S. (2018a). *Structural, Electronic and Mechanical properties of all- sp^2 graphene allotropes: the specific strength of tilene parent is higher than that of graphene and flakene has the minimal density*. arXiv preprint arXiv:1811.01112.
- Morresi, T., Taioli, S., and Simonucci, S. (2018b). *Nuclear Beta Decay: Relativistic Theory and Ab Initio Simulations of Electroweak Decay Spectra in Medium-Heavy Nuclei and of Atomic and Molecular Electronic Structure*. *Advanced Theory and Simulations* **1**(11), p. 1870030.
- Morresi, T., Timpel, M., Pedrielli, A., Garberoglio, G., Tatti, R., Verucchi, R., Pasquali, L., Pugno, N., Nardi, M. V., and Taioli, S. (2018d). *A novel combined experimental and multiscale theoretical approach to unravel the structure of SiC/SiOx core/shell nanowires for their optimal design*. *Nanoscale* **10**, pp. 13449–13461.
- Nenov, A., Borrego-Varillas, R., Oriana, A., Ganzer, L., Segatta, F., Conti, I., Segarra-Martí, J., Omachi, J., Dapor, M., Taioli, S., et al. (2018). *UV-light induced vibrational coherences, the key to understand Kasha rule violation in trans-azobenzene*. *The journal of physical chemistry letters* **9**, pp. 1534–1541.
- Pedrielli, A., Taioli, S., Garberoglio, G., and Pugno, N. (2018a). *Mechanical and thermal properties of Graphene Random nanofoams via Molecular Dynamics simulations*. *Carbon* **132**, pp. 766–775.
- Pedrielli, A., Taioli, S., Garberoglio, G., and Pugno, N. M. (2018c). *Gas adsorption and dynamics in Pillared Graphene Frameworks*. *Microporous and Mesoporous Materials* **257**, pp. 222–231.
- Segatta, F., Gdor, I., Réhault, J., Taioli, S., Friedman, N., Sheves, M., Rivalta, I., Ruhman, S., Cerullo, G., and Garavelli, M. (2018a). *Ultrafast Carotenoid to Retinal Energy Transfer in Xanthorhodopsin Revealed by the Combination of Transient Absorption and Two-Dimensional Electronic Spectroscopy*. *Chemistry—A European Journal* **24**(46), pp. 12084–12092.

NINPHA

- Rinaldi, M., Scopetta, S., Traini, M., and Vento, V. (2018). *A model calculation of double parton distribution functions of the pion*. *European Physics Journal C* **78**, pp. 781–789.
- Traini, M. and Blaizot, J.-P. (2019). *Diffractive incoherent vector meson production off protons: a quark model approach to gluon fluctuation effects*. *European Physics Journal C* **in print**, 15 pages.

TEONGRAV

- Amati, L. et al. (2018). *The THESEUS space mission concept: science case, design and expected performances*. *Advances in Space Research* **62**, pp. 191–244.
- Ciolfi, R. (2018). *Short gamma-ray burst central engines*. *International Journal of Modern Physics D* **27**, 1842004, p. 1842004.
- Endrizzi, A., Logoteta, D., Giacomazzo, B., Bombaci, I., Kastaun, W., and Ciolfi, R. (2018). *Effects of Chiral Effective Field Theory Equation of State on Binary Neutron Star Mergers*. *Phys. Rev.* **D98**(4), p. 043015.
- Lazzati, D., Perna, R., Morsony, B. J., Lopez-Camara, D., Cantiello, M., Ciolfi, R., Giacomazzo, B., and Workman, J. C. (2018). *Late time afterglow observations reveal a collimated relativistic jet in the ejecta of the binary neutron star merger GW170817*. *Phys. Rev. Lett.* **120**(24), p. 241103.
- Stratta, G., Amati, L., Ciolfi, R., and Vinciguerra, S. (2018a). *THESEUS in the era of multi-messenger astronomy*. *Memorie della Società Astronomica Italiana* **89**, p. 205.
- Stratta, G., Ciolfi, R., Amati, L., Bozzo, E., Ghirlanda, G., Maiorano, E., Nicastro, L., Rossi, A., Vinciguerra, S., Frontera, F., Götz, D., Guidorzi, C., O'Brien, P., Osborne, J. P., Tanvir, N., Branchesi, M., Brocato, E., Dainotti, M. G., De Pasquale, M., Grado, A., Greiner, J., Longo, F., Maio, U., Mereghetti, D., Mignani, R., Piranomonte, S., Rezzolla, L., Salvaterra, R., Starling, R., Willingale, R., Böer, M., Bulgarelli, A., Caruana, J., Colafrancesco, S., Colpi, M., Covino, S., D'Avanzo,

P, D'Elia, V., Drago, A., Fuschino, F., Gendre, B., Hudec, R., Jonker, P., Labanti, C., Malesani, D., Mundell, C. G., Palazzi, E., Patricelli, B., Razzano, M., Campana, R., Rosati, P., Rodic, T., Szécsi, D., Stamerra, A., van Putten, M., Vergani, S., Zhang, B., and Bernardini, M. (2018b). *THESEUS: A key space mission concept for Multi-Messenger Astrophysics*. *Advances in Space Research* **62**, pp. 662–682.

Technological and Interdisciplinary Physics

- Brownstein, J., Wisdom, A., Castle, K., Mowery, Y., Guida, P., Lee, C., Tommasino, F., La Tessa, C., Scifoni, E., Gao, J., Luo, L., Campos, L., Ma, Y., Williams, N., Jung, S., Durante, M., and Kirsch, D. (2018). *Characterizing the Potency and Impact of Carbon Ion Therapy in a Primary Mouse Model of Soft Tissue Sarcoma*. *Mol Cancer Ther* **17**, pp. 858–868.
- Morone, M., Berucci, C., Cipollone, P., De Donato, C., Di Fino, L., Iannilli, M., La Tessa, C., Manea, C., Masciantonio, G., Messi, R., Narici, L., Nobili, G., Pecchi, D., Picozza, P., Reali, E., Rizzo, A., Rovituro, M., Tommasino, F., and Vitali, G. (2018). *A compact Time-Of-Flight detector for radiation measurements in a space habitat: LIDAL-ALTEA*. *Nuclear Instruments and Methods in Physics Research Section A: Accelerators, Spectrometers, Detectors and Associated Equipment* **In press**.
- Rizzo, A., Narici, L., Messi, R., Cipollone, P., De Donato, C., Di Fino, L., Iannilli, M., La Tessa, C., Manea, C., Masciantonio, G., Morone, M., Nobili, G., Pecchi, D., Picozza, P., Reali, E., Rovituro, M., Tommasino, F., and Vitali, G. (2018). *A compact Time-Of-Flight detector for space applications: The LIDAL system*. *Nuclear Instruments and Methods in Physics Research Section A: Accelerators, Spectrometers, Detectors and Associated Equipment* **898**, pp. 98–104.
- Britten, R. A., Jewell, J. S., Duncan, V. D., Hadley, M. M., Macadat, E., Musto, A. E., and La Tessa, C. (2018). *Impaired Attentional Set-Shifting Performance after Exposure to 5 cGy of 600 MeV/n ²⁸Si Particles*. *Radiation Research* **189**(3), pp. 273–282.
- Giraud, M., Schuy, C., Weber, U., Rovituro, M., Santin, G., Norbury, J. W., Tracino, E., Menicucci, A., Bocchini, L., Lobascio, C., Durante, M., and La Tessa, C. (2018). *Accelerator-Based Tests of Shielding Effectiveness of Different Materials and Multilayers using High-Energy Light and Heavy Ions*. *Radiation Research* **190**(5), pp. 526–537.
- Mattiazzo, S., Baruffaldi, F., Bisello, D., Di Ruzza, B., Giubilato, P., Iuppa, R., La Tessa, C., Pantano, D., Pozzobon, N., Ricci, E., Snoeys, W., and Wyss, J. (2018). *iMPACT: An Innovative Tracker and Calorimeter for Proton Computed Tomography*. *IEEE Transactions on Radiation and Plasma Medical Sciences* **2**(4), pp. 345–352.
- Schuy, C., La Tessa, C., Horst, F., Rovituro, M., Durante, M., Giraud, M., Bocchini, L., Baricco, M., Castellero, A., Fioreh, G., and Weber, U. (2019). *Experimental Assessment of Lithium Hydride's Space Radiation Shielding Performance and Monte Carlo Benchmarking*. *Radiation Research* **191**(2), pp. 154–161.

ARDESIA

- Bellotti, G., Butt, A., Carminati, M., Fiorini, C., Bombelli, L., Borghi, G., Piemonte, C., Zorzi, N., and Balerna, A. (2018a). *ARDESIA Detection Module: A Four-Channel Array of SDDs for Mcps X-Ray Spectroscopy in Synchrotron Radiation Applications*. *IEEE Transactions on Nuclear Science* **65**(7), pp. 1355–1364.
- Bellotti, G., Hafizh, I., Butt, A., Carminati, M., Fiorini, C., Balerna, A., Tullio, V., Borghi, G., Piemonte, C., Zorzi, N., Capsoni, A., Coelli, S., Viscione, E., and Bombelli, L. (2018b). “ARDESIA: 4-Channels Fast SDD X-ray Spectrometer for Synchrotron Applications”. *Conference Proceedings of the 2017 IEEE Nuclear Science Symposium and Medical Imaging Conference*. IEEE.

Hafizh, I., Bellotti, G., Carminati, M., Utica, G., Gugiatti, M., Balerna, A., Tullio, V., Borghi, G., Ficorella, F., Picciotto, A., Zorzi, N., Capsoni, A., Coelli, S., Bombelli, L., and Fiorini, C. (2019a). *ARDESIA - a Fast SDD X-ray Spectrometer for Synchrotron Applications*. *Journal of Synchrotron Radiation* **submitted**.

Hafizh, I., Bellotti, G., Carminati, M., Utica, G., Gugiatti, M., Balerna, A., Tullio, V., Borghi, G., Picciotto, A., Ficorella, F., Zorzi, N., Capsoni, A., Coelli, S., Bombelli, L., and Fiorini, C. (2019b). *ARDESIA: a Fast SDD X-ray Spectrometer for Synchrotron Applications*. *X-Ray Spectrometry* **in press**.

ASAP

Ficorella, A., Pancheri, L., Brogi, P., Collazuol, G., Betta, G.-F., Marrocchesi, P., Morsani, F., Ratti, L., and Savoy-Navarro, A. (2018). *Crosstalk Characterization of a Two-Tier Pixelated Avalanche Sensor for Charged Particle Detection*. *IEEE Journal of Selected Topics in Quantum Electronics* **24(2)**.

Marrocchesi, P. S., Brogi, P., Bigongiari, G., Checchia, C., Collazuol, G., Betta, G. F. D., Ficorella, A., Lodola, L., Morsani, F., Musacci, M., Noli, S., Pancheri, L., Savoy-Navarro, A., Silvestrin, L., Stolzi, F., Sulaj, A., Suh, J. E., Ratti, L., Vacchi, C., Zanolini, M., and Zarghami, M. (2018). "APiX: a Geiger-mode Avalanche Digital Sensor for Particle Detection". *2017 IEEE NSS-MIC Conference Record*. Piscataway, U.S.A.: IEEE.

Musacci, M., Bigongiari, G., Brogi, P., Checchia, C., Collazuol, G., Betta, G.-F. D., Ficorella, A., Marrocchesi, P., Mattiazzo, S., Morsani, F., Noli, S., Pancheri, L., Ratti, L., Navarro, A. S., Silvestrin, L., Stolzi, F., Suh, J., Sulaj, A., Vacchi, C., and Zarghami, M. (2018). *Radiation tolerance characterization of Geiger-mode CMOS avalanche diodes for a dual-layer particle detector*. *Nuclear Instruments and Methods in Physics Research Section A: Accelerators, Spectrometers, Detectors and Associated Equipment*.

DEEP_3D

Mendicino, R. and Dalla Betta, G.-F. (2018). *Three-Dimensional detectors for neutron imaging*. *Nucl. Instrum. Methods A* **878**, pp. 129–140.

ELOFLEX

Zanazzi, E., Favaro, M., Ficorella, A., Pancheri, L., Betta, G. D., and Quaranta, A. (2019). *Photoluminescence enhancement of colloidal CdSe/ZnS quantum dots embedded in polyvinyl alcohol after 2 MeV proton irradiation: crucial role of the embedding medium*. *Optical Materials* **88**, pp. 271–276.

— (2018a). *Radiation-induced optical change of ion-irradiated CdSeS/ZnS core-shell quantum dots embedded in polyvinyl alcohol*. *Nuclear Instruments and Methods in Physics Research Section B: Beam Interactions with Materials and Atoms* **435**. International Conference on Radiation Effects in Insulators, July 2-7, 2017 in Versailles, France, pp. 327–330.

Zanazzi, E., Favaro, M., Ficorella, A., Pancheri, L., Dalla Betta, G. F., and Quaranta, A. (2018b). *Proton Irradiation Effects on Colloidal InGaP/ZnS Core-Shell Quantum Dots Embedded in Polydimethylsiloxane: Discriminating Core from Shell Radiation-Induced Defects through Time-Resolved Photoluminescence Analysis*. *The Journal of Physical Chemistry C* **122(38)**, pp. 22170–22177.

MoVe IT

- Boscolo, D., Krämer, M., Durante, M., Fuss, M., and Scifoni, E. (2018). *TRAX-CHEM: A pre-chemical and chemical stage extension of the particle track structure code TRAX in water targets*. *Chemical Physics Letters* **698**, pp. 11–18.
- Buch, T., Scifoni, E., Krämer, M., Durante, M., Scholz, M., and Friedrich, T. (2018). *Modeling Radiation Effects of Ultrasoft X Rays on the Basis of Amorphous Track Structure*. *Radiation research* **189**(1), pp. 32–43.
- Rucinski, A., Battistoni, G., Durante, M., Gajewski, J., Garbacz, M., Krah, N., Olko, P., Patera, V., Rinaldi, I., Skrzypek, A., Tommasino, F., Scifoni, E., and Schiavi, A. (2018). *EP-1848: GPU-accelerated Monte Carlo TPS for treatment plan verification at CCB Krakow proton therapy centre*. *Radiotherapy and Oncology* **127**, S997.
- Sokol, O., Scifoni, E., Hild, S., Durante, M., and Krämer, M. (2018). *216. Biological treatment planning with multiple ion beams*. *Physica Medica: European Journal of Medical Physics* **56**, pp. 193–194.
- Sokol, O., Kraemer, M., Hild, S., Durante, M., and Scifoni, E. (2019). *Kill painting of hypoxic tumors with multiple ion beams*. *Physics in medicine and biology* **64**.
- Taffelli, A., Palma, G., Fellin, F., D'Avino, V., Scartoni, D., Tommasino, F., Scifoni, E., Durante, M., Amichetti, M., Schwarz, M., et al. (2018b). *Modeling the Risk of Radiation Induced Alopecia in Brain Tumor Patients Treated with Active Beam Proton Therapy*. *International Journal of Radiation Oncology Biology Physics* **102**(3), S211.
- Tommasino, F., Rovituso, M., Lorentini, S., La Tessa, C., Petringa, G., Cirrone, P., Romano, F., Scifoni, E., Schwarz, M., and Durante, M. (2018b). *Study For A Passive Scattering Line Dedicated To Radiobiology Experiments At The Trento Proton Therapy Center*. *Radiation protection dosimetry*.
- Tommasino, F., Rovituso, M., Bortoli, E., Tessa, C. L., Petringa, G., Lorentini, S., Verroi, E., Simeonov, Y., Weber, U., Cirrone, P., Schwarz, M., Durante, M., and Scifoni, E. (2019). *A new facility for proton radiobiology at the Trento proton therapy centre: Design and implementation*. *Physica Medica* **58**, pp. 99–106.

NEWREFL

- Bazzanella, N., Burger, W., Cafagna, A., Cestari, C., Iuppa, R., Miotello, A., and Nozzoli, F. “A Systematic Study of Laser Ablation for Space Debris Mitigation”. 21st International Workshop on Laser Ranging, Canberra, Australia, November 2018.
- Terragni, J. (2017/2018). “A computational model of gas-dynamic processes in laser ablation of aluminum and its applicability to space debris reduction”. Supervisor: Prof. Antonio Miotello. Master’s Degree in Physics.

Redsox2

- Bufon, J., Schillani, S., Altissimo, M., Bellutti, P., Bertuccio, G., Billè, F., Borghes, R., Borghi, G., Cautero, G., Cirrincione, D., Fabiani, S., Ficorella, F., Gandola, M., Gianoncelli, A., Giuressi, D., Kourousias, G., Mele, F., Menk, R., Picciotto, A., Rachevski, A., Rashevskaya, I., Sammartini, M., Stofa, A., Zampa, G., Zampa, N., Zorzi, N., and Vacchi, A. (2018b). *A new large solid angle multi-element silicon drift detector system for low energy X-ray fluorescence spectroscopy*. *Journal of Instrumentation* **13**(03), p. C03032.
- Evangelista, Y., Ambrosino, F., Feroci, M., Bellutti, P., Bertuccio, G., Borghi, G., Campana, R., Caselle, M., Cirrincione, D., Ficorella, F., Fiorini, M., Fuschino, F., Gandola, M., Grassi, M., Labanti, C., Malcovati, P., Mele, F., Morbidini, A., Picciotto, A., Rachevski, A., Rashevskaya, I., Sammartini, M., Zampa, G., Zampa, N., Zorzi, N., and Vacchi, A. (2018b). *Characterization of a novel pixelated*

Silicon Drift Detector (PixDD) for high-throughput X-ray astrophysics. *Journal of Instrumentation* **13**(09), P09011.

Hernanz, M., Brandt, S., Feroci, M., Orleanski, P., Santangelo, A., Schanne, S., Wu, X., Zand, J., Zhang, S., Xu, Y., Bozzo, E., Evangelista, Y., Galvez, J. L., Tenzer, C., Zwart, F., Lu, F. J., Zhang, S., Chen, T. X., Ambrosino, F., Argan, A., Monte, E. D., Budtz-Jorgensen, C., Lund, N., Olsen, P., Mansanet, C., Campana, R., Fuschino, F., Labanti, C., Rachevski, A., Vacchi, A., Zampa, G., Zampa, N., Rashevskaya, I., Bellutti, P., Borghi, G., Ficorella, F., Picciotto, A., Zorzi, N., and Limousin, O. (2018). “The wide field monitor onboard the eXTP mission”. *PROCS. SPIE - 2018*, p. 149.

SEED

Panati, S., Olave, J., Rivetti, A., Pancheri, L., Cossio, F., Giubilato, P., Pantano, D., Mattiazzo, S., Rolo, M. D. D. R., and Demaria, N. (2018). “MATISSE: A Versatile Readout Electronics for Monolithic Active Pixel Sensors Characterization”. *2017 IEEE NSS-MIC Conference Record*. Piscataway, U.S.A.: IEEE.

SICILIA

Tudisco, S. et al. (2018). *Silicon Carbide Detectors for Intense Luminosity Investigations and Applications*. *Sensors* **18**(7), p. 2289.

XDET

Ratti, L., Comotti, D., Fabris, L., Grassi, M., Lodola, L., Malcovati, P., Manghisoni, M., Re, V., Traversi, G., Vacchi, C., Batignani, G., Bettarini, S., F. C. F., Morsani, F., Paladino, A., Paoloni, E., Rizzo, G., Benkechache, M., Dalla Betta, G.-F., Mendicino, R., Pancheri, L., Verzellesi, G., and Xu, H. (2018). “The PixFEL front-end for X-ray imaging in the radiation environment of next generation FELs”. *2017 IEEE NSS-MIC Conference Record*. Piscataway, U.S.A.: IEEE.

Seminars

TIFPA Guest Seminars

- Vincenzo Vitagliano, CEICO Central European Institute for Cosmology and Fundamental Physics, Prague, Czech Republic, *Curvature effects on strongly coupled systems*, Jan. 11, 2018.
- Paolo Baldan, Università degli Studi di Roma “La Sapienza”, Rome, Italy, *Study of the landscape of an harmonic spheres glass near jamming*, Feb. 28, 2018.
- Theo Vicente Torres, University of Nottingham, Nottingham, England, *Non-shallow water waves on a vortex: A model for dispersive fields around rotating black holes*, Mar. 13, 2018.
- Gianmassimo Tasinato, Swansea University, Galle, Great Britain, *Probing the Physics of the Early Universe with Gravitational Interferometers*, Apr. 5, 2018.
- Simone Dall’Osso, Stony Brook University, New York, USA, *Newborn magnetars as the brightest multi-messenger sources*, May 3, 2018.
- Sunny Vagnozzi, Oskar Klein Centre, Stockholm University, Sweden, *Neutrino cosmology: measuring the extremely tiny by observing the extremely huge*, May 10, 2018.
- Ilia Musco, Institut de Ciències del Cosmos, University of Barcelona Spain, *Primordial black hole formation and abundance: dependence upon the shape of the inflationary power spectrum*, May 21, 2018.
- Anne Gershenson, University of Massachussets, Amherst, USA, *Folding Metastable Inhibitory Serpins: Insights from Simulations, Cells and Protein Fragments*, May 22, 2018.
- Patrick Lawrence Wintrade, University of Maryland, Baltimore, USA, *Conformational dynamics of neurotransmitter sodium symporters: insights from theory and experiment*, May 23, 2018.
- Mark Edward Tuckerman, New York University and Center for computational chemistry at NYU-Shanghai, New York, USA, *Molecular dynamics based exploration and learning of free energy landscapes of molecular crystals and oligopeptides*, May 25, 2018.
- Valerio Faraoni, Bishop’s University, Sherbrooke, Canada, *General spherical solutions of Einstein and Brans-Dicke gravity: recent progress*, July 10, 2018.
- Andrea Giugno, LMU, Munich, Germany, *a corpuscular model of the gravitational interaction*, Dec. 5, 2018.
- Marco Toppi, Laboratori Nazionali di Frascati, Rome, Italy, *The upgrade of the ALICE inner tracking system-status of the Outer layers production in LNF*, Dec. 12, 2018.
- Walter Tinganelli, GSI, Darmstadt, Germany, *Ibernazione per radioprotezione e radioimmunoterapia*, Dec. 13, 2018.
- Marco Calzà, Università degli Studi di Trento, Trento, Italy, *Reconstructions of $f(R, G)$ and $f(R)$ scenarios at small redshifts through kinematics*, Dec. 17, 2018.
- Jorge Hernandez Armando Rueda, ICRANet, Pescara, Italy, *induced gravitational collapse, binary-driven hypernovae, long gamma-ray bursts and their connection with short gamma-ray burst*, Dec. 21, 2018.

Sensors and detectors

- Lucio Pancheri, invited talk: *Ultra-fast silicon detectors*, At: Frascati Detector School, INFN LNF, Frascati, Italy, Mar. 2018.

Particle Physics

ATLAS

Francesco Maria Follega and Ester Ricci, *Updates On Long-term Alignment Monitoring and diagnostics for ATLAS ID misalignments*, At: 133rd LHCC Meeting, CERN, CERN, Switzerland, Feb. 2018.

Francesco Maria Follega and Ester Ricci, *Updates On Long-term Alignment Monitoring and diagnostics for ATLAS ID misalignments*, At: IFAE, University of Milan Bicocca, Milan, Italy, Apr. 2018.

FASE2_ATLAS

Maurizio Boscardin, *Status of 3D Sensor Developments at FBK*, At: 13th Trento Workshop on Advanced Silicon Radiation Detectors, Max-Planck-Institut für Physik, Munich, Germany, Feb. 2018.

Gian-Franco Dalla Betta, *Characterization and simulation of small-pitch 3D diodes after irradiation up to $3.5 \times 10^{16} n_{eq}cm^{-2}$* , At: 13th Trento Workshop on Advanced Silicon Radiation Detectors, Max-Planck-Institut für Physik, Munich, Germany, Feb. 2018.

Gian-Franco Dalla Betta, *Characterization of FBK small-pitch 3D diodes after neutron irradiation up to $3.5 \times 10^{16} n_{eq}cm^{-2}$* , At: 20th International Workshop on Radiation Imaging Detectors (IWORID2018), Mid Sweden University, Sundsvall, Sweden, June 2018.

Giulio Tiziano Forcolin, invited talk: *Extremely radiation-hard technologies: 3D Sensors*, At: VERTEX 2018 - The 27th International Workshop on Vertex Detectors, Chennai, India, Oct. 2018.

Roberto Mendicino, invited talk: *Characterization and simulation of small-pitch 3D diodes irradiated to HL-LHC fluences*, At: AIDA 2020 Third Annual Meeting, University of Bologna, Bologna, Italy, Apr. 2018.

Roberto Mendicino, *Characterization of SINTEF 3D diodes with different inter-electrode spacings after neutron irradiation up to $2 \times 10^{16} n_{eq}cm^{-2}$* , At: 2018 IEEE Nuclear Science Symposium and Medical Imaging Conference (NSS - MIC'18), Sydney, Australia, Nov. 2018.

Astroparticle Physics

AMS

Laurent Basara, *Misura del flusso di elettroni e positroni nei raggi cosmici con l'esperimento AMS-02*, At: 104° Congresso della Società Italiana di Fisica, Università della Calabria, Rende, Italy, Sept. 2018.

Francesco Dimiccoli, *Misure di Deuterio e 3He con AMS-02*, At: IFAE - Incontri di Fisica delle Alte Energie - 2018, Università di Milano Bicocca, Milan, Italy, Apr. 2018.

Francesco Dimiccoli, *D/P Flux ratio in CR with the AMS-02 experiment*, At: Cosmic Rays International Seminars (CRIS) 2018, Catania and Napoli sections of INFN, Porto Palo, Italy, June 2018.

Francesco Dimiccoli, *Deuteron Flux in CR with the AMS-02 experiment*, At: 104° Congresso della Società Italiana di Fisica, Università della Calabria, Rende, Italy, Sept. 2018.

Francesco Dimiccoli, *Measurements of nuclei and isotopes of secondary origin in CR with AMS-02*, At: ICCPA - International Conference of Particle Physics and Astrophysics - 2018, MePhi, Moscow, Russia, Oct. 2018.

K. Kanishchev, *Misura della composizione isotopica di He, Li, Be nei raggi cosmici con l'esperimento AMS-02*, At: 104° Congresso della Società Italiana di Fisica, Università della Calabria, Rende, Italy, Sept. 2018.

Francesco Nozzoli, *Properties of Elementary Particle Fluxes in Primary Cosmic Rays Measured with the Alpha Magnetic Spectrometer on the International Space Station*, At: 7th Roma International Conference on Astroparticle Physics, Università degli Studi Roma Tre, Rome, Italy, Sept. 2018.

- Francesco Nozzoli, *Mappa e caratteristiche del vento solare misurato dal satellite lunare Chang'e-1*, At: 104° Congresso della Società Italiana di Fisica, Università della Calabria, Rende, Italy, Sept. 2018.
- Francesco Nozzoli, *Futuri rivelatori di anti-deuterio nei raggi cosmici e ricerca di Materia Oscura*, At: 104° Congresso della Società Italiana di Fisica, Università della Calabria, Rende, Italy, Sept. 2018.
- Paolo Zuccon, invited talk: *AMS Isotope studies*, At: AMS Days at La Palma, Istituto Astrofisico de Canarias, La Palma, Spain, Apr. 2018.
- Paolo Zuccon, invited talk: *AMS-02, result and perspectives*, At: Cosmic Rays International Seminars (CRIS) 2018, Catania and Napoli sections of INFN, Porto Palo, Italy, June 2018.
- Paolo Zuccon, invited talk: *AMS-02, result and perspectives*, At: 104° Congresso della Società Italiana di Fisica, Università della Calabria, Rende, Italy, Sept. 2018.

FISH

- Gabriele Ferrari, invited talk: *Observation of Spin Superfluidity in Bose Mixtures*, At: conference INO-CNR symposium, Polo CNR, Pisa, Italy, Mar. 2018.
- Gabriele Ferrari, invited talk: *NAQUAS - Non-equilibrium dynamics in Atomic systems for QUAntum Simulation*, At: QTN seminar, University of Trento, Nov. 2018.
- Giacomo Lamporesi, invited talk: *Statics and dynamics in a miscible quantum mixture*, At: From Quantum Gases to Quantum Optics and Quantum Measurement, Taiwan, Taiwan, Mar. 2018.
- Giacomo Lamporesi, invited talk: *Statics and dynamics of a miscible quantum mixture*, At: 104° Congresso Nazionale SIF, Rende, Italy, Sept. 2018.
- Giacomo Lamporesi, invited talk: *Observation of vortex dynamics in a cigar-shaped BEC*, At: La Laguna 1st international workshop on degenerate quantum gases: Persistent currents, vortices and solitons, La Laguna University, Spain, Dec. 2018.
- Sandro Stringari, invited talk: *Spin Superfluidity of a Mixture of BECs*, At: Quantum Transport with Cold Atoms Conference, Congressi Stefano Franscini, Monte Verità, Svizzera, July 2018.
- Sandro Stringari, invited talk: *Series of lectures on: Superfluidity of Quantum Mixtures*, At: School on Quantum simulation with ultracold atoms, International Institute of Physics, Federal University of Rio Grande do Norte, Natal, Brasil, 2018.
- Sandro Stringari, invited talk: *Synthetic Gauge Fields in Ultracold Atomic Gases*, At: 104° Congresso Nazionale SIF, Rende, Italia, Sept. 2018.

LIMADOU

- Benedetto Di Ruzza, *Un tracciatore per particelle cariche nello spazio basato sul sensore ALPIDE*, At: IFAE2018, Università degli studi Milano Bicocca, Italia, Apr. 2018.
- Francesco Maria Follega, *The High Energy Particle Detector of the CSES mission*, At: 7th International Conference on High Energy Physics in the LHC era, Universidad Tecnica Federico Santa Maria, Valparaiso, Chile, Jan. 2018.
- Roberto Iuppa, invited talk: *The Italian participation in the CSES mission*, At: 4th International Conference for the Decade Memory of the Wenchuan Earthquake, Chinese Earthquake Administration, Chengdu, China, May 2018.
- Roberto Iuppa, invited talk: *Antimatter in cosmic rays*, At: VULCANO Workshop 2018, INFN and INAF, Vulcano, Italy, May 2018.
- Ester Ricci, *Monolithic Active Pixel Sensors for space applications: the case of ALPIDE*, At: 13th "Trento" workshop on advanced silicon radiation detectors, Max Plank Institut fur Physik, Munich, Germany, Feb. 2018.

Ester Ricci, *A novel approach for tracking particles in space*, At: COSPAR2018, Caltech, Pasadena (CA), USA, July 2018.

Ester Ricci, Roberto Iuppa, *Ideas and solutions for a next generation high energy particle detector for the CSES mission*, At: COSPAR2018, Caltech, Pasadena (CA), USA, July 2018.

Ester Ricci, *Monolithic Active Pixel sensors for tracking low energy nuclei: ALPIDE beam test results*, At: 104° Congresso della società italiana di fisica, Università della Calabria, Rende, Italy, Sept. 2018.

LISA Pathfinder

Daniele Bortoluzzi, *Inflight Testing of the Injection of the LISA Pathfinder Test Mass into a Geodesic*, At: LISA Symposium, Chicago, USA, July 2018.

Rita Dolesi, *Achieving the Low End of the LISA Frequency Band*, At: LISA Symposium, Chicago, USA, July 2018.

Roberta Giusteri, *LISA Pathfinder Performance Confirmed Without Force Compensation: Results in Intermittent Actuation Mode*, At: LISA Symposium, Chicago, USA, July 2018.

Roberta Giusteri, *Successful intermittent control confirms the LISA Pathfinder performance: the free-fall experiment results*, At: COSPAR, Pasadena, USA, July 2018.

Giuliana Russano, *LISA Pathfinder results, Measuring femto-g acceleration noise down to 20 μ Hz*, At: COSPAR, Pasadena, USA, July 2018.

Stefano Vitale, *LISA Pathfinder; LISA and the path towards gravitational wave observation from space*, At: Marcel Grossmann conference, Rome, Italy, July 2018.

Stefano Vitale, *The Physics of Free Falling Observers: LISA Pathfinder Results and Legacy*, At: LISA Symposium, Chicago, USA, July 2018.

Stefano Vitale, *Gravitational wave astronomy within ESA Science Programme*, At: Passion for Physics international conference, Varenna, Italy, July 2018.

Stefano Vitale, *LISA Pathfinder; LISA and ESAs gravitational wave astronomy from space*, At: Light Conference 2018, Changchun, China, Sept. 2018.

Daniele Vetrugno, *LISA Pathfinder last results*, At: GRASS 2018, Padua, Italy, Mar. 2018.

Davide Vignotto, At: 4th International Conference and Exhibition on Satellite and Space Mission, Rome, Italy, June 2018.

Nuclear Physics

AEGIS

Roberto S. Brusa, *Influence of Filler Content on Free Volumes Structure and Gas Transport Properties of Biopolymer Nanocomposites*, At: ICPA18 International Conference on Positron Annihilation, Orlando, USA, Aug. 2018.

Sebastiano Mariazzi, *Advances in Ps formation and laser manipulation for pulsed antihydrogen production in the AEGIS experiment*, At: ICPA18 International Conference on Positron Annihilation, Orlando, USA, Aug. 2018.

FOOT

Sofia Colombi, *Fragmentation of 400 MeV/u 12 C ions in bone-like materials*, At: XXX National Seminar on Nuclear & Subnuclear Physics “Francesco Romano”, Otranto, Italy, June 2018.

Sofia Colombi, *Fragmentation of 400 MeV/u 12 C ions in bone-like materials*, At: XVIII Convegno Nazionale della Società Italiana per le Ricerche sulle Radiazioni, SIRR 2018, Dipartimento di Scienze - Università degli Studi Roma Tre, Italy, Sept. 2018.

Theoretical Physics

BELL

- Sonia Mazzucchi, invited talk: *A unified view to infinite dimensional integration with applications to generalized Feynman-Kac formulae*, At: Infinite-dimensional analysis and control theory, Department of Mechanics and Mathematics, Lomonosov Moscow State University, Moscow, Russia, Jan. 2018.
- Sonia Mazzucchi, invited talk: *Infinite dimensional integration techniques and applications to quantum mechanics*, At: Trails in Quantum Mechanics and Surroundings, Politecnico Torino, Turin, Italy, Sept. 2018.
- Valter Moretti, invited talk: *Hadamard states from light-like hypersurfaces*, At: Quantum fields, scattering and spacetime horizons: mathematical challenges, Ecole de Physique des Houches, Les Houches, France, May 2018.
- Valter Moretti, invited talk: *Why does (relativistic) quantum theory needs complex Hilbert spaces?*, At: Trails in Quantum Mechanics and Surroundings, Politecnico Torino, Turin, Italy, Sept. 2018.

BIOPHYS

- Pietro Faccioli, invited talk: *Folding Mechanism Probed by Microscopic Calculation of Time-Resolved CD*, At: Gordon Research Conference on Protein Dynamics, Gavelston, USA, Jan. 2018.
- Gianluca Lattanzi, invited talk: *Computational Biophysics: a new tool for Radiation Research?*, At: 2018 RRS Annual Meeting Speakers, Chicago, USA, Sept. 2018.
- Raffaello Potestio, invited talk: *Fifty shades of coarse-grain: The hot topic of multiple resolution models*, At: CECAM Workshop on New frontiers in particle-based multiscale and coarse-grained modeling, Max Planck Institute for Polymer Physics, Mainz, Germany, Sept. 2018.

FBS

- Giuseppina Orlandini, invited talk: *Electromagnetic reactions from few- to many-body systems*, At: Workshop on Recent advances and challenges in the description of nuclear reactions at the limit of stability, ECT*, Trento, Italy, Mar. 2018.
- Giuseppina Orlandini, invited talk: *Recent developments in integral transform approaches*, At: Program on Fundamental physics with electroweak probes on light nuclei, Institute of Nuclear Theory (INT), Seattle, USA, June 2018.
- Giuseppina Orlandini, *Relativistic effects in non-relativistic calculations of electroweak cross sections*, At: International Conference on Few-Body Problems in Physics (FB22), Caen, France, July 2018.
- Giuseppina Orlandini, invited talk: *Results for Few-Body electromagnetic processes*, At: SFB Workshop on Electromagnetic observables for low-energy nuclear physics, Institut für Kernphysik, Mainz, Germany, Oct. 2018.
- Giuseppina Orlandini, invited talk: *Relativistic Corrections within the Integral Transform Approach*, At: NuInt 18 - 12th International Workshop on Neutrino-Nucleus Interactions in the Few-GeV Region, Gran Sasso Science Institute (GSSI), L'Aquila, Italy, Oct. 2018.
- Winfried Leidemann, invited talk: *Electromagnetic response of light nuclei with the LIT*, At: INT Program INT-18-2a Fundamental Physics with Electroweak Probes of Light Nuclei, Seattle, USA, June 2018.
- Winfried Leidemann, *Hyperspherical harmonics method with particle excitation degrees of freedom*, At: International Conference on Few-Body Problems in Physics (FB22), Caen, France, July 2018.

Winfried Leidemann, invited talk: *Resonant electromagnetic responses with the Lorentz integral transform*, At: ECT* workshop Probing exotic structure of short-lived nuclei by electron scattering, Trento, Italy, July 2018.

Winfried Leidemann, invited talk: *Calculation of astrophysical reactions with the Lorentz integral transform*, At: Fourth National Meeting of Nuclear Physics - INFN 2018, Catania, Italy, Nov. 2018.

FLAG

Alessandro Casalino, *Mimetic Gravity after GW170817*, At: Universum, Bologna, Italy, 2018.

Massimiliano Rinaldi, invited talk: *Higgs Dark Energy*, University of Modena and Reggio Emilia, Italy, Jan. 2018.

Massimiliano Rinaldi, invited talk: *Scale invariant inflation*, CEICO, Czech Republic, July 2018.

Massimiliano Rinaldi, *Scale invariant gravity*, At: SIGRAV2018, S. Margherita di Pula, Cagliari, Italy, Sept. 2018.

Massimiliano Rinaldi, *Scale invariant gravity, black holes and inflation*, At: Modern aspects of gravity and cosmology, Orsay, France, Oct. 2018.

Lorenzo Sebastiani, *Action growth for static black holes in modified gravity*, At: PAFT 2018, University of Modena and Reggio Emilia, Vietri sul Mare, Italy, Mar. 2018.

MANYBODY

Alessandro Lovato, invited talk: *Electromagnetic and neutral-weak responses of light nuclei*, At: Exploring the role of electro-weak currents in Atomic Nuclei, European Center for Theoretical Studies in Nuclear Physics and Related Areas (ECT*), Trento, Italy, Apr. 2018.

Alessandro Lovato, invited talk: *Ab initio Calculations of Electroweak Response Functions*, At: INT Program INT-18-2a Fundamental Physics with Electroweak Probes of Light Nuclei, Institute for Nuclear Theory (INT), Seattle, WA, United States, June 2018.

Alessandro Lovato, invited talk: *Quantum Monte Carlo for neutrino-nucleus scattering*, At: INT Program INT-18-2b Advances in Monte Carlo Techniques for Many-Body Quantum Systems, Institute for Nuclear Theory (INT), Seattle, WA, United States, July 2018.

Alessandro Lovato, invited talk: *Quantum Monte Carlo for neutrino-nucleus scattering*, At: NUFACT 2018 - the 20th International Workshop on Neutrinos from accelerators, Virginia-TECH, Blacksburg, VA, United States, Aug. 2018.

Alessandro Lovato, *Quantum Monte Carlo calculations of dynamical pions and nucleons*, At: Midwest Theory Get-Together, Argonne National Laboratory, Lemont, IL, United States, Sept. 2018.

Alessandro Lovato, invited talk: *Nuclear spectra and weak responses from Quantum Monte Carlo*, At: NSCL/FRIB Theory Seminars, Michigan State University, East Lansing, MI, United States, Oct. 2018.

Alessandro Lovato, invited talk: *Quantum Monte Carlo calculations of Neutrino-Nucleus Interactions*, At: Physics Opportunities in the Near DUNE Detector Hall (PONDD), Fermilab, Batavia, IL, United States, Dec. 2018.

Francesco Pederiva, invited talk: *Pion-full Effective Field Theory in Nuclear Physics with Quantum Monte Carlo Methods*, At: IPN Orsay Theory Group Seminars, Institut de Physique Nucleaire, Université Paris-Sud, Orsay, France, Apr. 2018.

Francesco Pederiva, invited talk: *Perspectives and theoretical challenges in electron scattering experiments on medium mass hypernuclei*, At: Probing exotic structure of short-lived nuclei by electron scattering, European Center for Theoretical Studies in Nuclear Physics and Related Areas (ECT*), Trento, Italy, July 2018.

NEMESYS

- Simone Taioli, invited talk: *First-principles simulations of carbon-based materials*, At: 14th International Conference of Computational Methods in Sciences and Engineering (ICCSME19), Thessaloniki, Greece, Mar. 2018.
- Simone Taioli, invited talk: *The chemistry and physics of carbon from first-principles, multiscale simulations, and experiments*, At: 7th Workshop on Nanocarbon Photonics and Optoelectronics (NPO2018), Savonlinna, Finland, Aug. 2018.

TEONGRAV

- Riccardo Ciolfi, invited talk: *Fireworks from a binary neutron star merger*, At: Four challenges in gravitational wave astronomy with neutron stars, University of Parma, Parma, Italy, Jan. 2018.
- Riccardo Ciolfi, invited talk: *Short GRBs from BNS mergers and the case of GW170817/GRB 170817A*, At: Neutron stars in Lisbon, Instituto Superior Tecnico, Lisbon, Portugal, Apr. 2018.
- Riccardo Ciolfi, invited talk: *Fireworks from a binary neutron star merger*, At: LXII Congress of the Italian Astronomical Society, University of Teramo, Teramo, Italy, May 2018.
- Riccardo Ciolfi, invited talk: *Multimessenger Astrophysics with binary neutron star mergers*, At: XXIII SIGRAV Conference, S. Margherita di Pula (Cagliari), Italy, Sept. 2018.
- Andrea Endrizzi, invited talk: *Numerical Simulations of Binary Neutron Star Mergers: Gravitational Waves and Short Gamma-Ray Bursts*, At: APS April Meeting 2018, Columbus, OH, US, Apr. 2018.
- Andrea Endrizzi, *Effects of a new Equation of State on Binary Neutron Star Mergers*, At: APS April Meeting 2018, Columbus, OH, US, Apr. 2018.
- Andrea Endrizzi, *Investigating Effects of Magnetic Fields and Microphysics in Binary Neutron Star Mergers*, TPI, Friederich-Schiller University, Jena, Germany, July 2018.
- Bruno Giacomazzo, invited talk: *Numerical Simulations of Binary Neutron Star Mergers: Gravitational Waves and Short Gamma-Ray Bursts*, At: MODE Workshop on "Neutron stars and their environments", Montpellier, France, June 2018.
- Bruno Giacomazzo, invited talk: *Review on Numerical Simulations of Binary Neutron Star Mergers*, At: PSI2 Workshop on "GAMMA-RAY BURSTS AND SUPERNOVAE: FROM THE CENTRAL ENGINES TO THE OBSERVER", Orsay, France, June 2018.
- Bruno Giacomazzo, invited talk: *Numerical Relativity Simulations of Gravitational-Wave Sources*, At: Workshop on "GR effects in cosmological large-scale structure", Sexten, Italy, July 2018.

Technological and Interdisciplinary Physics

- Chiara La Tessa, invited talk: *Can nuclear physics take us to Mars?*, At: ENSAR2 - NUSPRASEN Workshop on Nuclear Reactions (Theory and Experiment), Warsaw, Poland, Jan. 2018.
- Chiara La Tessa, invited talk: *How nuclear physics can be used against cancer and space radiation*, At: EUNPC - European Nuclear Physics Conference, Bologna, Italy, Sept. 2018.
- Chiara La Tessa, *Microdosimetry in proton and Helium radiotherapy*, At: 64st Radiation Research Society (RADRES) Annual Meeting, Chicago, MA, USA, Sept. 2018.
- Francesco Tommasino, *Incertezze dosimetriche in protonterapia con pencil beam scanning per tumore alla mammella*, At: X Congresso Nazionale AIFM, Bari, Italy, Apr. 2018.

ARDESIA

- G. Borghi, *Experimental Characterization and Future Sensor Developments for ARDESIA, a 4-Channels Fast SDD X-ray Spectrometer for Synchrotron Applications*, At: 13th "Trento" Workshop on Advanced Silicon Radiation Detectors, Munich, Germany, Feb. 2018.
- M. Carminati, *ARDESIA: a 4-Channels Fast SDD X-ray Spectrometer*, At: European Conference on X-Ray Spectrometry (EXRS - 2018), Ljubljana, Slovenia, June 2018.
- I. Hafizh, *Qualification of ARDESIA SDD X-ray Spectrometer in Synchrotron Measurements*, At: 2018 IEEE Nuclear Science Symposium and Medical Imaging Conference, Sydney, Australia, Nov. 2018.

ASAP

- Lucio Pancheri, invited talk: *APiX: a Geiger-mode avalanche digital sensor for charged particle detection*, At: Front-End Electronics 2018, Jouvence, Canada, May 2018.

MoVe IT

- Elettra V. Bellinzona, *WP1 Updates on TRiP98 side*, At: II MoVe-IT Annual Meeting, MoVe-IT, Trento, Italy, Jan. 2018.
- Elettra V. Bellinzona, *Radiobiological impact of mixed fields from target fragments in proton treatment plan*, At: PTCOG 57, PTCOG, Cincinnati, USA, May 2018.
- Elettra V. Bellinzona, invited talk: *Radiobiological impact of proton target fragments and sensitivity analysis*, At: IV FOOT Collaboration Meeting, INFN Pisa, Isola D'Elba, Italy, June 2018.
- Elettra V. Bellinzona, invited talk: *WP1-task 1.1: target fragmentation*, At: II MoVe-IT Annual Meeting, MoVe-IT, Catania, Italy, June 2018.
- Elettra V. Bellinzona, invited talk: *Radiobiological impact of mixed fields from target fragments in proton treatment plans*, At: XVIII Convegno Nazionale della Società Italiana per le Ricerche sulle Radiazioni, SIRR, Roma, Italy, Sept. 2018.
- Elettra V. Bellinzona, *Radiobiological impact of mixed fields from target fragments in proton treatment plan*, At: Quarto Incontro Nazionale di Fisica Nucleare INFN2018, INFN, Catania, Italy, Nov. 2018.
- Elettra V. Bellinzona, invited talk: *Target Fragmentation and RBE in proton therapy*, At: V FOOT Collaboration Meeting, INFN Torino, Borgomale, Italy, Dec. 2018.
- Emanuele Scifoni, invited talk: *Radiobiological applications of nuclear physics simulations*, At: XV Seminar on Software for Nuclear, Subnuclear and Applied Physics, INFN and University of Sassari, Alghero, Italy, June 2018.
- Emanuele Scifoni, invited talk: *Comparison of treatment plans with different light ions*, At: ENLIGHT 2018, University College London, London, United Kingdom, July 2018.
- Emanuele Scifoni, invited talk: *Monte Carlo simulations and Radiobiological Modeling*, At: VI International Geant4 School, TIFPA, UniTN, Trento Protontherapy Center, Italy, Nov. 2018.
- Emanuele Scifoni, invited talk: *(Energy dependent) Radiosensitization of proton beams: old and new challenges*, At: Towards Proton Boron Capture Therapy, FBK, Trento, Italy, Apr. 2018.
- Emanuele Scifoni, invited talk: *p+19FDG: first experimental tests*, At: NEPTune kickoff meeting, INFN-LNS, Catania, Italy, Dec. 2018.

SEED

- Lucio Pancheri, invited talk: *CMOS Monolithic Active Pixel Sensors*, At: XXVII Giornate di Studio sui Rivelatori - Scuola F. Bonaudi, INFN, Cogne, Italy, Feb. 2018.

TIMESPOT

Gian-Franco Dalla Betta, invited talk: *3D Trenched-Electrode Sensors for Charged Particle Tracking and Timing*, At: ULTIMA 2018 - Ultrafast imaging and tracking instrumentation, methods & applications, Argonne National Laboratory, Chicago, U.S.A. Sept. 2018.

Gian-Franco Dalla Betta, *Fabrication of 3D Trenched-Electrode Pixel Sensors for Tracking and Timing Applications*, At: 2018 IEEE Nuclear Science Symposium and Medical Imaging Conference (NSS - MIC'18), Sydney, Australia, Nov. 2018.

Giulio Tiziano Forcolin, *Development of 3D Trenched-Electrode Pixel Sensors with improved Timing performance*, At: PIXEL 2018 - International Workshop on Semiconductor Pixel Detectors for Particles and Imaging, Academia Sinica, Taipei, Taiwan, Dec. 2018.

① ② ③ ④ ⑤ ⑥ ⑦ ⑧ ⑨ ⑩ ⑪ ⑫ ⑬ ⑭ ⑮ ⑯ ⑰ ⑱ ⑲ ⑳ ㉑ ㉒ ㉓ ㉔ ㉕ ㉖ ㉗ ㉘ ㉙ ㉚ ㉛ ㉜ ㉝ ㉞ ㉟ ㊱ ㊲ ㊳ ㊴ ㊵ ㊶ ㊷ ㊸ ㊹ ㊺ ㊻ ㊼ ㊽ ㊾ ㊿

- | | | | |
|-----------------------|-----------------------|------------------------|---------------------------|
| ① Rita Dolesi | ⑫ Francesco Follega | ⑳ Matteo Favaro | ㉔ Roberto Iuppa |
| ② Christian Manea | ⑬ Alessandro Casalino | ㉑ Giulio Forcolin | ㉕ Federico Cipolletta |
| ③ Chiara La Tessa | ⑭ Maurizio Boscardin | ㉒ Piero Spinnato | ㉖ Matteo Puel |
| ④ Marta Perucci | ⑮ Lorenzo Sebastiani | ㉓ William Burger | ㉗ Sergio Zerbini |
| ⑤ Paolo Zuccon | ⑯ Francesco Pederiva | ㉔ Giuliana Pellizzari | ㉘ Emanuele Scifoni |
| ⑥ Francesco Tommasino | ⑰ Ester Ricci | ㉕ Elettra Bellinzona | ㉙ Stefano Chinaglia |
| ⑦ Graziano Fortuna | ⑱ Bruno Giacomazzo | ㉖ Paolo Falferi | ㉚ Giuseppe Battistoni |
| ⑧ Summit Jalota | ⑲ Luca Penasa | ㉗ Irina Rashevskaya | ㉛ Marco Durante |
| ⑨ Cinzia Boniatti | ⑳ Alexander Helm | ㉘ Valentina Marchesano | ㉜ Giovanni Andrea Prodi |
| ⑩ Francesco Nozzoli | ㉑ Sebastiano Mariazzi | ㉙ Walter Tinganelli | ㉝ Alberto Quaranta |
| ⑪ Giancarlo Pepponi | ㉒ Roberto Mendicino | ㉚ Benedetto di Ruzza | ㉞ Gian-Franco Dalla Betta |



TIFPA group photograph 2018. See previous page for who's who.



Trento Institute for
Fundamental Physics
and Applications

TIFPA - INFN

c/o Dipartimento di Fisica
Università di Trento
Via Sommarive, 14
38123 Povo (Trento), Italy
tel.: +39 0461 281500
fax: +39 0461 282000
email: info@tifpa.infn.it
www.tifpa.infn.it